

CAPITAL UNIVERSITY OF SCIENCE AND
TECHNOLOGY, ISLAMABAD



Unsteady 3D Powell-Eyring Flow of
Copper and
Silicon-Carbide/Methanol for a
Boundary Layer Using
Cattaneo-Christov Model with
Entropy Analysis

by

Atif Ali Zafar

A thesis submitted in partial fulfillment for the
degree of Master of Philosophy

in the

Faculty of Computing

Department of Mathematics

2023

Copyright © 2023 by Atif Ali Zafar

All rights reserved. No part of this thesis may be reproduced, distributed, or transmitted in any form or by any means, including photocopying, recording, or other electronic or mechanical methods, by any information storage and retrieval system without the prior written permission of the author.

*I dedicate my thesis to
my beloved family, friends specially*

My Mother(Tabbassum Noreen),

*A determined and aristocratic embodiment who educate me to belief in ALLAH,
believe in hard work and that so much could be done with little,*

My Father(Zafar Mehmood)

I quote the remarkable words of Hadith,

“A father gives his child nothing better than an education.”



CERTIFICATE OF APPROVAL

**Unsteady 3D Powell-Eyring Flow of Copper and
Silicon-Carbide/Methanol for a Boundary Layer Using
Cattaneo-Christov Model with Entropy Analysis**

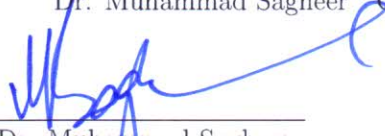
by

Atif Ali Zafar

(MMT203006)

THESIS EXAMINING COMMITTEE

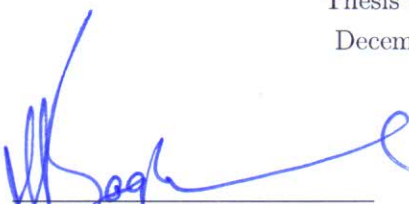
S. No.	Examiner	Name	Organization
(a)	External Examiner	Dr. Muhammad Zubair	MIU, Islamabad
(b)	Internal Examiner	Dr. Abid Kamran	CUST, Islamabad
(c)	Supervisor	Dr. Muhammad Sagheer	CUST, Islamabad



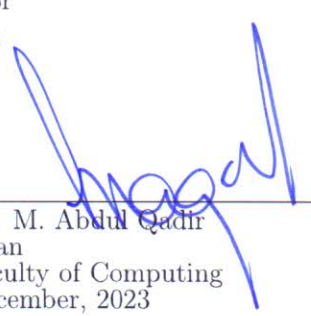
Dr. Muhammad Sagheer

Thesis Supervisor

December, 2023



Dr. Muhammad Sagheer
Head
Dept. of Mathematics
December, 2023



Dr. M. Abdul Qadir
Dean
Faculty of Computing
December, 2023

Author's Declaration

I, **Atif Ali Zafar** hereby state that my MPhil thesis titled “**Unsteady 3D Powell-Eyring Flow of Copper and Silicon-Carbide/Methanol for a Boundary Layer Using Cattaneo-Christov Model with Entropy Analysis**” is my own work and has not been submitted previously by me for taking any degree from Capital University of Science and Technology, Islamabad or anywhere else in the country/abroad.

At any time if my statement is found to be incorrect even after my graduation, the University has the right to withdraw my MPhil Degree.



(**Atif Ali Zafar**)

Registration No: MMT203006

Plagiarism Undertaking

I solemnly declare that research work presented in this thesis titled “**Unsteady 3D Powell-Eyring Flow of Copper and Silicon-Carbide/Methanol for a Boundary Layer Using Cattaneo-Christov Model with Entropy Analysis**” is solely my research work with no significant contribution from any other person. Small contribution/help wherever taken has been duly acknowledged and that complete thesis has been written by me.

I understand the zero tolerance policy of the HEC and Capital University of Science and Technology towards plagiarism. Therefore, I as an author of the above titled thesis declare that no portion of my thesis has been plagiarized and any material used as reference is properly referred/cited.

I undertake that if I am found guilty of any formal plagiarism in the above titled thesis even after award of MPhil Degree, the University reserves the right to withdraw/revoke my MPhil degree and that HEC and the University have the right to publish my name on the HEC/University website on which names of students are placed who submitted plagiarized work.



(Atif Ali Zafar)

Registration No: MMT203006

Acknowledgement

In the name of **ALLAH**, who is the most merciful and beneficent, created the universe and blessed the mankind with intelligence and wisdom to explore its secret. I would like to express my heart felt gratitude and immeasurable respect to my supervisor **Prof. Dr. Muhammad Sagheer HOD** Mathematics Department, Capital University of Science and Technology, for his passionate interest, willingness help, superb guidance and inspiration throughout this investigation. His textural and verbal criticism enabled me in formatting this thesis.

I am extremely grateful to my teacher **Prof. Dr. Shafqat Hussain**, for his continuing belief in my potential, for his encouraging and enthusiastic attitude and for many imparted words of wisdom. I would also like to thank my respectable teachers **Prof. Dr. Rashid Ali, Dr. Abdul Rehman Kashif, Dr. Dur e Shehwar Sagheer, Dr. Samina Rashid, Dr. Muhammad Afzal and Dr. Muhammad Sabeel Khan** for their encouragement and emphasis on striving for excellence when teaching mathematics. I would like to acknowledge the CUST for providing me such a favourable environment to this research.

I must express my very profound gratitude to my dear parents and whole members of my family including my elder brothers **Taimoor Ali Zafar, Haseeb Ali Zafar** and my younger sister **Nosheela Zafar** for providing me with unfailing support and continuous encouragement throughout my years of study and through the process of researching and writing this thesis.

Finally, I want to express my gratitude to my class fellow **Noor ul ain Azam** who encouraged me throughout my MPhil research. I am grateful to my fellow researchers at CUST for valuable discussions on this research. I have enjoyed working alongside them in a pleasant working environment.



(Atif Ali Zafar)

Registration No: MMT203006

Abstract

The aim of this thesis is to investigate the flow, heat transfer and entropy generation characteristics of thermal systems containing non-Newtonian Powell-Eyring nanofluid flow. The present research is devoted to the study of flow, heat transfer and entropy generation of non-Newtonian nanofluid including effects of applied magnetic field, thermal radiation, Joule heating, heat source and variable thermophysical properties. Cattaneo-Christov heat flux model has also been considered to examine the heat transfer. The physical model includes unsteady 3D forced convective flow of an electrically conducting Powell-Eyring nanofluid over a bidirectional stretching surface. The fundamental equations are obtained from the laws of conservation of mass, momentum and energy. The partial differential equations are transformed into a system of coupled nonlinear ordinary differential equations by means of suitable similarity transformation and then solved by an efficient numerical scheme known as the shooting method. Two different nanofluids, copper–methanol (Cu–MeOH) and silicon carbide–methanol (SiC–MeOH), are considered in the analysis. The numerical results are presented in the form of graphs and tables for variation in parameters, for example, non-Newtonian parameter, material parameter, nanoparticle volume fraction parameter, velocity slip parameter, thermal radiation parameter, Biot number, Reynolds number and Brinkman number. The influence of physical parameters on the velocity profile, temperature distribution, skin friction coefficient, Nusselt number and entropy generation are studied. The results obtained reveal that there is an enhancement in the rate of heat transfer with a rise in the nanoparticle volume fraction. The temperature distribution is also influenced by the presence of the relaxation time parameter, Eckert number, thermal radiation and nanoparticle volume fraction. The entropy profile increases as the nanoparticle volume fraction parameter increases. The entropy generation rate of Cu–MeOH nanofluid is higher than that of SiC–MeOH nanofluid. It has been found that increasing the Brinkman number increases the entropy generation.

Contents

Author's Declaration	iv
Plagiarism Undertaking	v
Acknowledgement	vi
Abstract	vii
List of Figures	xi
List of Tables	xiv
Abbreviations	xv
Symbols	xvi
1 Introduction and Literature Survey	1
1.1 Thesis Contributions	9
1.2 Thesis Outline	11
2 Fundamental Concepts and Governing Equations	12
2.1 Basic Definitions	12
2.1.1 Fluid [79]	12
2.1.1.1 Classification of Fluids	13
2.1.2 Fluid Mechanics [79]	13
2.1.2.1 Fluid Kinematics [79]	14
2.1.2.2 Fluid Statics [80]	14
2.1.2.3 Fluid Dynamics [80]	14
2.1.3 Physical Properties of the Fluid	14
2.2 Classification of Fluids	16
2.3 Types of Fluid Flow [79]	17
2.3.1 Steady and unsteady flows	17
2.3.2 Uniform and non-uniform flows	18
2.3.3 One,two and three dimensional flows	19
2.3.4 Rotational and irrotational flows	20
2.3.5 Laminar and Turbulent flows	20

2.3.6	Compressible and incompressible flows	21
2.4	Fundamental Laws [81]	21
2.4.1	Conservation of Mass; the Continuity Equation	21
2.4.2	Conservation of Momentum	22
2.4.3	Conservation of Energy	23
2.5	Heat and Mass Transfer Phenomenon and Related Properties	24
2.6	Dimensionless Numbers	27
2.7	Boundary layer [87]	29
2.8	Entropy Generation	29
2.9	Magnetohydrodynamics	30
2.10	Nanofluids [88]	30
2.11	Material Properties of Nanofluids	31
2.12	Tiwari and Das Model	32
2.13	Cattaneo-Christov Heat Flux Model [61]	32
2.14	Shooting Method	33
3	Computational single phase comparative study of inclined MHD in a Powell-Eyring nanofluid	36
3.1	Introduction	36
3.2	Description of Problem	37
3.2.1	The Governing PDEs	38
3.2.2	Similarity Transformations	39
3.2.3	Physical Quantities of Interest	39
3.2.4	Entropy	40
3.3	Conversion of Mathematical Model into Dimensionless Form	40
3.3.1	The Governing ODEs	40
3.3.2	Physical Quantities of Interest	48
3.3.2.1	Skin Friction Coefficient:	48
3.3.2.2	Nusselt Number:	50
3.3.3	Entropy Generation	51
3.4	Solution Methodology	52
3.5	Numerical Results and Discussions	54
4	Unsteady 3D Powell-Eyring Flow of Cu and SiC/MeOH for a Boundary Layer Using Cattaneo-Christov Model with Entropy Analysis	81
4.1	Introduction	81
4.2	Description of Problem	82
4.2.1	Governing Equations	83
4.2.2	Similarity Transformations	85
4.2.3	Transformation of Physical Quantities	85
4.2.4	Entropy Generation Formulations	86
4.3	PDEs to ODEs Transformation	86
4.3.1	Transformation of the Governing PDEs	86
4.3.2	Non-dimensional Quantities of Interest	99
4.3.2.1	Skin Friction Coefficient	99

4.3.2.2	Nusselt Number	102
4.3.3	Entropy Generation	103
4.4	Solution Methodology	105
4.5	Numerical Results and Discussions	109
4.5.1	Velocity Profile	110
4.5.2	Temperature Profile	128
4.5.3	Entropy Profile	143
5	Conclusion	150
	Bibliography	152

List of Figures

3.1	Physical flow model.	37
3.2	Velocity profile against ω	64
3.3	Temperature profile against ω	64
3.4	Entropy profile against ω	65
3.5	Velocity profile against A	65
3.6	Temperature profile against A	66
3.7	Entropy profile against A	66
3.8	Velocity profile against Δ	67
3.9	Temperature profile against Δ	67
3.10	Entropy profile against Δ	68
3.11	Velocity profile against Γ	68
3.12	Temperature profile against Γ	69
3.13	Entropy profile against Γ	69
3.14	Velocity profile against M	70
3.15	Temperature profile against M	70
3.16	Entropy profile against M	71
3.17	Velocity profile against Φ	71
3.18	Temperature profile against Φ	72
3.19	Entropy profile against Φ	72
3.20	Velocity profile against Λ	73
3.21	Temperature profile against Λ	73
3.22	Entropy profile against Λ	74
3.23	Temperature profile against Nr	74
3.24	Entropy profile against Nr	75
3.25	Temperature profile against Bi	75
3.26	Entropy profile against Bi	76
3.27	Temperature profile against Ec	76
3.28	Entropy profile against Ec	77
3.29	Velocity profile against S	77
3.30	Temperature profile against S	78
3.31	Entropy profile against S	78
3.32	Temperature profile against q	79
3.33	Entropy profile against q	79
3.34	Entropy profile against Re	80
3.35	Entropy profile against Br	80

4.1	The physical geometry of the problem.	82
4.2	Velocity profile against ω	120
4.3	Velocity profile against ω	120
4.4	Velocity profile against Δ_1	121
4.5	Velocity profile against Δ_1	121
4.6	Velocity profile against Δ_2	122
4.7	Velocity profile against Δ_2	122
4.8	Velocity profile against Γ	123
4.9	Velocity profile against Γ	123
4.10	Velocity profile against M	124
4.11	Velocity profile against M	124
4.12	Velocity profile against Φ	125
4.13	Velocity profile against Φ	125
4.14	Velocity profile against Λ_1	126
4.15	Velocity profile against Λ_1	126
4.16	Velocity profile against Λ_2	127
4.17	Velocity profile against Λ_2	127
4.18	Temperature profile against ω	133
4.19	Temperature profile against ω	133
4.20	Temperature profile against A	134
4.21	Temperature profile against A	134
4.22	Temperature profile against Δ_1	135
4.23	Temperature profile against Δ_1	135
4.24	Temperature profile against Δ_2	136
4.25	Temperature profile against Δ_2	136
4.26	Temperature profile against Φ	137
4.27	Temperature profile against Φ	137
4.28	Temperature profile against Λ_1	138
4.29	Temperature profile against Λ_1	138
4.30	Temperature profile against Λ_2	139
4.31	Temperature profile against Λ_2	139
4.32	Temperature profile against ξ	140
4.33	Temperature profile against ξ	140
4.34	Temperature profile against Q	141
4.35	Temperature profile against Q	141
4.36	Temperature profile against q	142
4.37	Temperature profile against q	142
4.38	Entropy profile against Δ_1	144
4.39	Entropy profile against Δ_1	144
4.40	Entropy profile against Δ_2	145
4.41	Entropy profile against Δ_2	145
4.42	Entropy profile against ξ	146
4.43	Entropy profile against ξ	146
4.44	Entropy profile against Q	147
4.45	Entropy profile against Q	147

4.46 Entropy profile against Re	148
4.47 Entropy profile against Re	148
4.48 Entropy profile against Br	149
4.49 Entropy profile against Br	149

List of Tables

2.1	Thermo-physical properties of Nanofluid	31
2.2	Material Properties of Base fluid and Nanoparticles at 293K	31
3.1	Missing conditions of $\frac{d^2 f}{d\chi^2}(0)$ for $Pr = 6.2, q = 3$	60
3.2	Results of $\frac{d^2 f}{d\chi^2}(0)$ for $Pr = 6.2, q = 3$	61
3.3	Missing conditions of $\theta(0)$ for $Pr = 6.2, q = 3$	62
3.4	Results of $\theta(0)$ for $Pr = 6.2, q = 3$	63
4.1	Results of $\frac{d^2 f}{d\chi^2}$ and $\frac{d^2 g}{d\chi^2}$ at $\chi = 0$ for $Pr = 6.2$ and $q = 3$	112
4.1	Results of $\frac{d^2 f}{d\chi^2}$ and $\frac{d^2 g}{d\chi^2}$ at $\chi = 0$ for $Pr = 6.2$ and $q = 3$	113
4.2	Results of $\frac{d^2 f}{d\chi^2}$ and $\frac{d^2 g}{d\chi^2}$ at $\chi = 0$ for $Pr = 6.2$ and $q = 3$	114
4.2	Results of $\frac{d^2 f}{d\chi^2}$ and $\frac{d^2 g}{d\chi^2}$ at $\chi = 0$ for $Pr = 6.2$ and $q = 3$	115
4.3	Results of $\frac{d^2 f}{d\chi^2}$ and $\frac{d^2 g}{d\chi^2}$ at $\chi = 0$ for $Pr = 6.2$ and $q = 3$	116
4.3	Results of $\frac{d^2 f}{d\chi^2}$ and $\frac{d^2 g}{d\chi^2}$ at $\chi = 0$ for $Pr = 6.2$ and $q = 3$	117
4.4	Results of $\frac{d^2 f}{d\chi^2}$ and $\frac{d^2 g}{d\chi^2}$ at $\chi = 0$ for $Pr = 6.2$ and $q = 3$	118
4.4	Results of $\frac{d^2 f}{d\chi^2}$ and $\frac{d^2 g}{d\chi^2}$ at $\chi = 0$ for $Pr = 6.2$ and $q = 3$	119
4.5	Empirical shape factors for different particle shapes	130
4.6	Results of $\theta(0)$ for $Pr = 6.2, q = 3$	131
4.6	Results of $\theta(0)$ for $Pr = 6.2, q = 3$	132

Abbreviations

BVP	Boundary Value Problem
BC	Boundary Condition
BL	Boundary Layer
Cu	Copper
IVPs	Initial Value Problems
MHD	Magnetohydrodynamics
MeOH	Methanol
ODEs	Ordinary Differential Equations
PDEs	Partial Differential Equations
RK	Runge-Kutta
Sic	Silicon-Carbide

Symbols

μ	Dynamic viscosity
ρ	Density
ν	Kinematic viscosity
τ	Dimensionless time
τ_{ij}	Cauchy stress tensor of the Powell-Eyring fluid
C_f	Skin friction coefficient
τ_w	Skin friction or wall shear stress
k_1	Thermal conductivity
α	Thermal diffusivity
σ^*	Electrical conductivity
\bar{f}_1	\bar{x} -component of fluid velocity
\bar{f}_2	\bar{y} -component of fluid velocity
\bar{f}_3	\bar{z} -component of fluid velocity
\mathbf{B}	Inclined magnetic field
B_0	Magnetic field constant
\mathbf{q}	Heat flux across any surface
C_p	Specific heat at constant pressure
$\bar{\xi}$	Unsteadiness parameter
$\hat{\beta}$	Material constant
h^*	Material constant
c^*	Initial stretching rate
\tilde{t}	Time
λ	Thermal relaxation time
\mathbf{V}	Velocity vector

Θ_f	Convective surface temperature
Θ_∞	Ambient temperature
Θ	Fluid temperature
h_t	Wall heat transfer coefficient
h_f	Heat transfer coefficient
a^*, b^*	Positive constants
$\bar{U}_w(\bar{x}, \bar{t}), \bar{V}_w(\bar{x}, \bar{t})$	Stretching velocities
E_G	Entropy generation
ξ	Cattaneo-Christov parameter
ν_f	Kinematic viscosity of the base fluid
q_r	Radiative heat flux
q_w	Heat flux
σ^*	Stefan Boltzmann constant
k^*	Absorption coefficient
ψ	Stream function
θ	Stream function
χ	Similarity variable
$f(\chi)$	Dimensionless stream function
u_w	Velocity of the surface
v_w	Porosity of the stretching surface
$\bar{x}, \bar{y}, \bar{z}$	Cartesian coordinates
Γ	Inclination angle
N	Kinematic viscosity of the fluid
Nu	Nusselt number
$Nu_{\bar{x}}$	Local Nusselt number
$Re_{\bar{x}}, Re_{\bar{y}}$	Local Reynolds number
Φ	Nanoparticle volume concentration coefficient
M	Magnetic parameter
A	Unsteadiness parameter
α_f	Thermal diffusivity
Δ, ω	Material Parameter
Δ_1, Δ_2	Material Parameters

Nr	Thermal radiation parameter
Bi	Biot number
Ec	Eckert number
q	Shape factor
Pr	Prandtl number
S	Mass transfer parameter
S_1, S_2	Mass transfer parameters
Λ	Velocity slip parameter
$\Lambda_1, \Lambda_2, K_1, K_2$	Velocity slip parameters
Q_0	Heat generation/absorption parameter
Re	Reynolds number
Br	Brinkman number
Ω	Dimensionless temperature gradient
P	Density of the fluid
μ_{nf}	Dynamic viscosity of the nanofluid
μ_f	Dynamic viscosity of the base fluid
ρ_{nf}	Density of the nanofluid
ρ_f	Density of the base fluid
ρ_s	Density of Cu and SiC
$(\rho C_p)_{nf}$	Heat capacitance of nanofluid
$(\rho C_p)_f$	Heat capacitance of base fluid
$(\rho C_p)_s$	Heat capacitance of Cu, SiC
κ_{nf}	Thermal conductivity of the nanofluid
κ_f	Thermal conductivity of the base fluid
σ_{nf}^*	Electrical conductivity of the nanofluid
σ_f	Electrical conductivity of the base fluid
σ_s	Electrical conductivity of Cu, SiC
f, g	Dimensionless velocities

Chapter 1

Introduction and Literature Survey

Boundary layer flow has been widely studied in the literature and plays an important role in the field of fluid dynamics. Numerous industrial processes, including food processing, glass fiber production, rubber sheet manufacture and extrusions, metal spinning, wire drawing, and the cooling of large metallic plates like electrolytes, depend on the recognition of boundary layer flows on horizontal surfaces.

The first person to introduce boundary layer theory was Ludwig Prandtl [1]. Using a stretching sheet and the shooting approach based on the 6th order RK integration algorithm, Makinde and Onyejekwe [2] solved a boundary layer flow model with variable electrical conductivity and variable viscosity. They came to the conclusion that the skin friction coefficient and boundary layer convective heat transfer coefficient decrease with an increase in the electrical conductivity parameter. Ibrahim and Makinde [3] investigated the boundary layer flow via a vertically moving sheet with Joule heating and chemical reaction using the numerical shooting approach.

In addition, in a couple of more research papers, Makinde [4] investigated fluid flow and thermal boundary layer over a flat plate. They looked at how fluid flow was affected by viscous dissipation and Newtonian heating for a range of geometries with permeable boundary surfaces. Their research focuses on mathematical models of fluid flows across a stretched surface, both Newtonian and non-Newtonian. Some important studies on boundary layer fluid flow by a stretching sheet are presented in [5–15].

The study of heat transfer and fluid flow is of particular importance because in production processes, the quality of the final product is determined on the basis of the velocity gradient (skin friction) and the rate of transfer of heat by convection. Elbashbeshy [16] numerically studied the flow of heat transfer and viscous fluid by assuming the ascending continuous stretching sheet. In this work, flow occupies the space over an infinite horizontal surface and is induced by the non-linear stretching of the surface.

The results indicated that the suction parameter can be used as means for cooling the continuous moving stretching surface and the thickening level of thermal boundary layer reduced for greater values of suction parameter.

Later, Sanjayanand and Khan [17] extended Elbashbeshy's work to deal with the heat and mass transfer in second-order viscoelastic fluids over exponentially stretching surface. Some recent developments that highlight heat and mass transfer can be found in [18–22].

Choi and Eastman [23] floated the idea of nanofluids by mixing additive solids with conventional fluids that were smaller than 100 nm. Typically, oxide ceramics, metal oxides, metal nitrides, etc., make up the nanoparticles. The transport and heat conduction characteristics of base fluids, such as water, methanol, and ethylene glycol, are altered by the metallic particles. Among the significant characteristics of nanofluids, a significant one is an enhanced thermal conductivity. Because they have the ability to accelerate heat transfer, nanofluids are used in industrial processes as heat flow controllers in heat valves and coolants in nuclear reactors, among other things.

In the field of medicine, iron-based nanofluids can be used to treat cancer patients in addition to medications and radiation [24–26]. Copper-ethylene glycol nanofluids with enhanced thermal conductivity were studied by Eastman et al. [27]. Furthermore, they found that Cu-EG is a superior thermal conductor than CuO-EG after comparing copper-ethylene glycol with copperoxide-ethylene glycol. The physical characteristics of nanofluids, particularly heat transmission and boundary layer flow, have been extensively studied.

The research papers of Wang et al. [28] and Keblinski et al. [29] can also be considered for further knowledge in this area. According to Buongiorno [30], nanofluids have superior stability compared to regular fluids, exhibiting superior wetting, spreading, and dispersion characteristics on solid surfaces. Some more articles that highlight the nanofluids' capability of transferring heat and mass in different physical situations are [31–36].

Important industrial applications for MHD's involvement in improving heat transfer of nanofluids beyond a stretched surface include liquid metal flow, optical switches, geothermal energy extraction, plasma flow, MHD generators, and MHD flow meters, among others. Many researchers intended to discuss MHD flow their flow models. Hakeem et al. [37] examined the effects of MHD on the second order partial slip flow of nanofluids on a shrinking/stretching sheet with thermal radiation. They came to the conclusion that, in both the shrinking and stretching scenarios, the skin friction factor was highest for $Al - H_2O$ and lowest for $Au - H_2O$ using the analytical hypergeometric function and numerical shooting approach. Furthermore, they observed that increasing the value of the magnetic field parameter caused the lower branch solution of shrinking sheet.

Using Buongiorno's mathematical model, Hsiao [38] investigated the impact of Lorentz force and viscous dissipation of micropolar nanofluids flowing over a stretched surface. It is found that the temperature profile increment as the Eckert and Prandtl numbers increase.

In addition, the heat transfer rate also increased for increasing the values of these numbers. Qayyum et al. [39] studied the magneto flow of 3rd grade nanofluids on an stretching surface with different thicknesses and convection boundary conditions. They discovered that as the values of the third-grade fluid and thermal conjugate parameters increased, the velocity and temperature distributions increased correspondingly.

The numerical solutions of inclined magnetohydrodynamic Williamson fluid flow on

a nonlinear stretching sheet with the cumulative impact of increasing viscosity in the presence of nanoparticles were obtained by Khan et al. [40] using the shooting approach. They came to the conclusion that a decrease in the velocity profile was demonstrated by raising the values of the Hartmann number, variable viscosity, and angle of inclination. Conversely, when the Hartmann number grows, it also increases the velocity gradient.

The two-dimensional MHD flow of a Casson nanofluid moving over a permeable stretching surface with thermal radiation was examined by Eid et al. [41]. They talked about how various physical characteristics affected the flow and heat transmission and used the shooting technique for the numerical findings. They discovered that when the concentration of nanoparticle volume fraction in the base fluid increases, the thermal boundary layer thickens. In order to solve the Casson nanofluid flow caused on by the stretching sheet with the effects of Lorentz forces, permeability, and thermal radiation, Kho et al. [42] employed the numerical shooting approach. They discovered that as the fluid's Casson and magnetic properties increase, the velocity gradient and the rate of heat transfer decrease near the boundary surface.

It is well known, that the particles used in the preparation of nanofluids have impact on heat transfer of the system. However, little attention is given to study the effect of nanoparticles shapes on heat transfer characteristics of nanofluids. It was noted by Choi [23] that spherical nanoparticles increase heat transmission. Because spherical particles have a bigger surface area than non-spherical particles, he explains why there is greater heat transmission.

The effect of nanoparticles shape on thermodynamic efficiency of tube and shell shaped heat exchangers are exhibited by Elias et al. [43]. They observed a better heat transfer rate for the cylindrical shaped nanoparticles. On the other hand, entropy generation rate is also higher for cylindrical shaped nanoparticles.

Mahian et al. [44] scrutinized the influence of nanoparticles shape and tube material on the performance of a plate mini-channel thermal solar system. Xu and Chen [45]

presented the heat exchange of Marangoni boundary layer flow for Cattaneo-Christov heat flux theory. In their results, spherical shaped nanoparticles provide the greatest performance for heat exchange enhancement. The analysis is based on sphere, hexahedron, tetrahedron, cylinder and lamina shaped nanoparticles and $Cu - H_2O$ nanofluid.

Sheikholeslami [46] used the control volume finite element method (CVFEM) and scrutinized the impact of Lorentz forces on $Cu - H_2O$ nanofluid convective flow in a porous cavity considering common geometrical shapes for nanoparticles.

The Cattaneo heat flux model for Maxwell viscoelastic nanofluids on a vertical sheet with natural convection and five distinct nanoparticle shapes sphere, hexahedron, tetrahedron, column, and lamina was introduced by Shen et al. [47]. To get the answer, they used the L_1 -algorithm in conjunction with the numerical finite difference method. The findings indicate that the spherical nanoparticles exhibit the lowest convective heat exchange rate and the maximum heat transfer rate. The skin friction factor and convective heat exchange was observed to reduce with an increase in the magnetic parameter whereas the temperature fractional parameter was noticed to have an opposite impact. Some more contributions regarding wall-slip condition and nanoparticle-shapes are presented in [48–53].

In every industrial process, minimizing entropy is an essential requirement. The scientists examine how entropy is created and try to identify ways to lessen it. The development of entropy emphasizes the significance of irreversible elements in non-ideal processes such as heat transmission, friction, and others within a system [54]. Qing et al. [55] investigated the volumetric total entropy production for a Casson nanofluid flow passing through a permeable stretching sheet with magnetic effects. Using sequential numerical linearization, they discovered that entropy production increased with increases in the Hartmann number, permeability parameter, Reynolds number, and Brinkman number.

Bhatti et al. [56] examined the entropy production of MHD Powell-Eyring nanofluid across a porous stretched sheet using the Chebyshev spectral collocation numerical

technique. They came to the conclusion that as Hartmann's number and radiation parameter values rise, so does the entropy distribution. The finite volume technique was utilized by Akbarzadeh et al. [57] to investigate the thermo-hydraulic efficiency and entropy production of a wavy channel including three distinct corrugation profiles: sinusoidal, trapezoidal, and triangular forms.

Sithole et al. [58] examined the impact of nonlinear thermal radiation and MHD on the entropy and chemical reaction of second-grade nanofluids on heated stretching surfaces. The findings demonstrate that when the temperature difference ratio parameter grows, the system's entropy reduces and increases with larger Hartmann, Reynolds, and Brinkmann numbers.

For the past two decades, the heat transmission processes have been studied using Fourier's law of heat conduction [59]. The instantaneous reaction to initial disturbances in the system under study is described by this rule. Fourier's law was enhanced by Cattaneo [60] by adding a relaxation time. Furthermore, by attaching the Oldroyd upper convected derivatives rather than the material derivative, Christov [61] enhanced this model. The Cattaneo-Christov heat and mass flow model for a stretchable sheet under the combined action of upper convected Maxwell nanofluids was published by Sui et al. [62]. According to the study's findings, the temperature profile gets smaller as the temperature relaxation parameter rises.

Cattaneo-Christov double diffusion for 3 D nanofluid flow on linear stretching sheet was described by Hayat et al. [63]. It was demonstrated that as thermal and concentration relaxation parameters are increased, temperature and concentration drop. Muhammad et al. [64] has developed a mathematical model for squeezed nanofluid flow with double diffusion.

The findings demonstrated that when the thermal and solutal relaxation parameters increased, correspondingly increased the concentration and temperature gradients. Dogonchi and Ganji [65] examined the MHD nanofluid flow using the Daun-Rach method. Rather than Fourier's law, the data demonstrate the low temperature distribution for

the Cattaneo-Christov model. Using the Keller-box approach, Akmal et al. [66] investigated the Cattaneo-Christov model for squeezing flow of nanofluids. Observations showed that the entropy of the bottom plate is larger than that of the top plate.

Dogonchi et al. [67] have suggested the squeezing nanofluid for unsteady flows. By using the Duan-Rach method, they were able to acquire data that demonstrated an inverse connection for the stretching parameter and a direct link between the Nusselt number and the shrinking parameter. Dianchen et al. [68] looked at Cattaneo-Christov and the combined impacts of homogeneous and heterogeneous responses to unsteady squeezing flow. They found that skin friction and Nusselt number behave differently when considering the squeezing parameter.

In squeezing nanofluid flow, Zubair et al. [69] described the Cattaneo-Christov model. This study showed that when the squeezing parameter and Eckert number increased correspondingly increased the temperature gradient. Ramadevi et al. [70] examined the influence of Carreau fluid submitted to the squeezing flow.

The findings demonstrated that temperature and concentration profiles decreased as the thermal relaxation parameter was increased. In the case of an unsteady Casson fluid, Shankar et al. [71] discussed the flow characteristics between parallel plates. The study's findings demonstrate that, in contrast to traditional Fourier's rule, the temperature and concentration distributions are smaller for double diffusivity.

For the convective transport of nanofluids, Newtonian fluid models are taken into consideration in the majority of the previously stated research. However, in practical settings, nanofluids behave differently from Newtonian fluids. For nanofluids, it would therefore be more reasonable to take into account a non-Newtonian fluid model.

Ellahi et al. [72] used Brinkman's nanofluid model to obtain the precise solution of Power law nanofluids containing copper nanoparticles using an optimal homotopy asymptotic method (OHAM). They discovered that when the volume fraction of the nanoparticles increased, the velocity characteristics of shear thinning fluids reduced.

Furthermore, the temperature and heat flux of shear thinning fluid enlarged by improvement of particle volume concentration (PVC) while enhancement in temperature with small size of particle is detected.

The two-dimensional MHD flow of Carreau nanofluids via a nonlinear surface permeable to heat radiation was examined by Eid et al. [41]. They investigated the effects of various physical factors on heat transfer and nanofluid flow using the shooting method. They came to the conclusion that when thermal radiation increased, the rate of heat transfer reduced, and when the value of the magnetic parameter increased, the opposite behavior was seen.

Sravanthi et al. [73] analyzed Maxwell's nanofluid flow calculations, including Lorentz force effects on porous surfaces that extend exponentially in the presence of a homogeneous-heterogeneous heat source. The temperature profile raises and lowers the convective heat exchange capacity in order to raise the value of the heat source rate. The temperature of the nanofluid drops and convective heat exchange intensity increases as a result of increased heat dissipation.

In order to address the Casson nanofluid flow caused by the stretched porous media and the impact of thermal radiation, Kho et al. [42] used the shooting approach. The problem of mixed convective flow of Powell-eyring nanofluids on an inclined sheet was addressed by Khan and colleagues [74].

It is well known fact that the viscosity and thermal conductivity are not constants when the temperature of the nanofluid is very high. Irfan et al. [75] numerically investigated the problem of 3-dimensional convective flow of Carreau nanofluid over a bidirectional stretching sheet in the existence of heat absorption and temperature dependent thermal conductivity. In their research, influence of variable thermal conductivity parameter was opposite to unsteadiness parameter on concentration and temperature profiles for both $n < 1$ and $n > 1$ (n is power law index).

Reddy et al. [76] presented the effects of Lorentz forces on the Williamson nanofluid

over a stretching surface with thermal radiation, variable thickness and temperature dependent thermal conductivity. They used the spectral quasilinearization method (SQLM) and found that the influence of variable thermal conductivity parameter reduces the temperature gradient at the boundary surface.

Furthermore, they noticed that velocity distribution reduces for higher values of Williamson parameter and its also decrease the thinking level of momentum boundary layer. Khan et al. [77] discussed 3-dimensional flow of sisko magneto-nanofluid past a stretching sheet with the impact of heat source and variable thermal conductivity. They used the Buongiorno nanofluid model and detected that for increasing values of temperature dependent thermal conductivity the local Nusselt number increase for thinning fluids and shear thickening.

Based on the above studies and a detailed review of the literature on nanofluid flow and heat transfer, the authors conclude that only limited studies have been conducted to investigate the non-Newtonian model and variable thermophysical properties of nanofluids. Keeping the above in mind, this thesis presents analysis of flow, heat transfer and volumetric entropy generation for a thermal system consisting of non-Newtonian Powell-Eyring nanofluids. The solution of the mathematical model is obtained through a numerical scheme called the shooting method. Graphical interpretations were used to study the numerical solution.

1.1 Thesis Contributions

It turns out that the present study is unique and no such study has yet been reviewed in the literature. Therefore, the aim of this study is to investigate the influence of Cu and SiC-MeOH on the unstable three-dimensional flow of Eyring-Powell nanofluids. The Cattaneo-Christov heat flow model is used to study the heat transfer process. We have significant investigated the effect of entropy generation on heat transfer. The PDEs are converted to ODEs using the similarity transformation.

Furthermore, a numerical solution can be obtained by the shooting method. The ODEs decrease with the boundary condition being resolved by the shooting method. The skin friction and mass transport values under the influence of the new parameters are analyzed by the use of tables. Graphs of temperature and velocity are shown versus the new research parameters. The present survey is focused on the numerical analysis of Cattaneo-Christov based study of three-dimensional unsteady, laminar, incompressible flow of non-Newtonian Powell-Eyring nanofluid flow. The governing equations of flow, heat transfer and volumetric entropy generation analysis are modeled under boundary layer approximations using Tiwari and Das model [78] for non-Newtonian nanofluids. The analysis is carried out considering the following physical effects of interest:

- Uniform applied magnetic field (MHD).
- Porous medium.
- Variable thermal physical properties.
- Thermal radiation.
- Cattaneo-Christov heat flux model.
- Different types of nanoparticles.
- Nanoparticle shape factor.
- Single phase model.

Similarity transformations are used to transform the provided nonlinear PDEs into a system of ODEs. Moreover, the numerical solutions of nonlinear ODEs are obtained using the shooting method. The numerically obtained results are calculated using MATLAB. Graphs and tables have been used to illustrate the effects of significant parameters on the velocity distribution $\frac{df}{d\chi}$, temperature distribution $\theta(\chi)$, skin friction coefficient C_f , and local Nusselt number $Nu_{\bar{x}}$.

1.2 Thesis Outline

The following chapters comprise the division of this work.

- A brief literature survey in **Chapter 1** relating nanofluids, types of nanofluids and solution methodology have been discussed. The recent trends in nanofluid research have also been cited.
- **Chapter 2** provides basic definitions related to nanofluid, flow and heat transfer. The thermophysical properties of different nanomaterials are also presented. The mathematical model used in this study has been discussed in detail as well as the solution methodology.
- The entropy analysis of a Powell-Eyring nanofluid flowing across a stretched surface with temperature-dependent thermal radiation and thermal conductivity is presented in **Chapter 3**. The impacts of various nanoparticle shapes are also included in the mathematical model. Using the shooting approach, numerical results are obtained for the governing flow equations.
- The entropy based analysis of Cu and SiC-MeOH of unsteady three-dimensional Powell-Eyring magneto-nanofluid flow by utilizing Cattaneo-Christov heat flux model past over a bidirectional stretching surface is carried out in **Chapter 4**.
- **Chapter 5** contains the conclusion of this work.

The work's references are enumerated in **Bibliography**.

Chapter 2

Fundamental Concepts and Governing Equations

Basic ideas, definitions, and governing laws related to fluid dynamics have been discussed in this chapter. In particular, some important dimensionless quantities have been described, which appear to be useful in the next chapters. In addition, a brief review of the numerical method used to solve the governing equations has been conducted.

2.1 Basic Definitions

2.1.1 Fluid [79]

“A fluid is a substance which deforms continuously when subjected to external shearing force.”

A fluid has the following characteristics:

1. It follows the shape of the containing vessel rather than having a distinct shape of its own.
2. A liquid or fluid will experience a deformation as long as shear force is applied, even at very low levels.

2.1.1.1 Classification of Fluids

(i) **Liquid:**

“A liquid is a fluid which possesses a definite volume (which varies only slightly with temperature and pressure).”

(ii) **Gas:**

“It possesses no definite volume and is compressible.”

(iii) **Vapour:**

“It is a gas whose temperature and pressure are such that it is very near the liquid state.”

(iv) **Ideal fluids:**

“An ideal fluid is one which has no viscosity and surface tension and is incompressible. In true sense no such fluid exists in nature. However fluids which have low viscosities such as water and air can be treated as ideal fluids under certain conditions.”

(v) **Real fluids:**

“A real fluid is one which has viscosity, surface tension and compressibility in addition to the density. The real fluids are actually available in nature.”

2.1.2 Fluid Mechanics [79]

“Fluid mechanics may be defined as that branch of science which deals with the behaviour of fluids under the conditions of rest and motion.”

2.1.2.1 Fluid Kinematics [79]

“Fluid Kinematics is a branch of ‘Fluid mechanics’ which deals with the study of velocity and acceleration of the particles of fluids in motion and their distribution in space without considering any force or energy involved.”

2.1.2.2 Fluid Statics [80]

“The study of fluids at rest is called fluid statics.”

2.1.2.3 Fluid Dynamics [80]

“The study of fluid if the pressure forces are considered for the fluids in motion, is called fluid dynamics.”

2.1.3 Physical Properties of the Fluid

- **Mass Density or Density [80]**

“Density or Mass Density of a fluid is defined as the ratio of the mass of a fluid to its volume. Thus mass per unit volume of a fluid is called density. It is denoted by ρ . The unit of mass density in SI unit is Kg per cubic metre, i.e., Kg/m³.

Mathematically, mass density is written as:

$$\rho = \frac{\text{Mass of fluid}}{\text{Volume of fluid}}.$$

The value of density of water is 1 gm/cm³ or 1000 Kg/m³.”

- **Specific Volume [80]**

“Specific Volume of a fluid occupied by a unit mass or volume per unit mass of a fluid is called specific volume. Mathematically, it is expressed as:

$$\text{Specific volume} = \frac{\text{Volume of fluid}}{\text{Mass of fluid}} = \frac{1}{\frac{\text{Mass of fluid}}{\text{Volume of fluid}}}.$$

Thus, specific volume is the reciprocal of mass density.”

- **Pressure [79]**

“When a fluid is contained in a vessel, it exerts force at all points on the sides and bottom and top of the container. The force per unit area is called pressure.

If,

P = The force, and

A = Area on which the force acts; then intensity of pressure,

$$p = \frac{P}{A}$$

The pressure of a fluid on a surface will always act normal to the surface.”

- **Viscosity [79]**

“Viscosity is defined as the property of a fluid which offers resistance to the movement of one layer of fluid over another adjacent layer of the fluid.” It is denoted by τ (called Tau).

Mathematically,

$$\tau \propto \frac{du}{dy}$$

or

$$\tau = \mu \frac{du}{dy},$$

where, μ = constant of proportionality and $\frac{du}{dy}$ = Rate of shear stress or rate of shear deformation or velocity gradient.

$$\mu = \frac{\tau}{\left[\frac{du}{dy} \right]}$$

Therefore, the shear stress needed to generate a unit rate of shear strain may also be used to describe viscosity.

- **Kinematic Viscosity [79]**

“It is defined as the ratio between the dynamic viscosity and density of fluid. It is denoted by symbol ν read as “**nu**”.

Mathematically,

$$\nu = \frac{\mu}{\rho}.”$$

- **Newton’s Law of Viscosity [79]**

“This law states that the shear stress (τ) on a fluid element layer is directly proportional to the rate of shear strain. The constant of proportionality is called the co-efficient of viscosity. The fluids which follow this law are known as Newtonian fluids.”

- **Thermal Conductivity [81]**

“The Fourier heat conduction law states that the heat flow is proportional to the temperature gradient. The coefficient of proportionality is a material parameter known as the thermal conductivity, which may be a function of several variables.”

2.2 Classification of Fluids

Fluids can be classified into five types:

- **Ideal Fluid or Inviscid Fluid [80]**

“A fluid, which is incompressible and has no viscosity, is known as an ideal fluid. Ideal fluid is only an imaginary fluid as all the fluids, which exist, have some viscosity.”

- **Real Fluid or Viscous Fluid [80]**

“A fluid, which possesses viscosity, is known as a real fluid. In actual practice, all the fluids are real fluids.”

- **Newtonian Fluid [82]**

“Fluids for which the applied shear stress and the rate of deformation are linearly proportional to each other are termed as Newtonian fluids.

In the case of Newtonian fluids, mathematical expression of τ_{xy} is given by expression enumerated underneath.

$$\tau_{xy} = \mu \frac{du}{dy},$$

where, μ represents dynamic viscosity and $\frac{du}{dy}$ is the rate of deformation. The SI unit of shear stress τ_{xy} is $\text{N}\cdot\text{s}\cdot\text{m}^{-2}$.”

- **Non-Newtonian Fluid [83]**

“A non-Newtonian fluid is one whose properties are different from Newtonian fluids i.e. apparent viscosity changes with applied stress or forces. In non-Newtonian fluid the correlation between the shear stress and the rate of strain is non-linear. For these types of fluids, the constant of proportionality, viscosity, may change with time. Many salt solution, solution of polymers as well as liquids in which fine particles are suspended, are non-Newtonian, as are most commonly found substances in our everyday life such as ketchup, toothpaste, paint, blood and shampoo.”

- **Ideal Plastic Fluid [80]**

“A fluid, in which shear stress is more than the yield value and shear stress is proportional to the rate of shear strain (or velocity gradient), is known as ideal plastic fluid.”

2.3 Types of Fluid Flow [79]

2.3.1 Steady and unsteady flows

- **Steady flow**

“The type of flow in which the fluid characteristics like velocity, pressure, density, etc. at a point do not change with time is called steady flow. Mathematically,

we have:

$$\left(\frac{\partial u}{\partial t}\right)_{x_0, y_0, z_0} = 0; \left(\frac{\partial v}{\partial t}\right)_{x_0, y_0, z_0} = 0; \left(\frac{\partial w}{\partial t}\right)_{x_0, y_0, z_0} = 0;$$

$$\left(\frac{\partial p}{\partial t}\right)_{x_0, y_0, z_0} = 0; \left(\frac{\partial \rho}{\partial t}\right)_{x_0, y_0, z_0} = 0; \text{ and so on}$$

where (x_0, y_0, z_0) is a fixed point in a fluid field where these variables are being measured w.r.t. time.”

Example: Flow through a prismatic or non-prismatic conduit at a constant flow

rate Qm^3/s is steady. (A prismatic conduit has a constant size shape and has a velocity equation in the form $u = ax^2 + bx + c$, which is independent of time t).

- **Unsteady flow**

“It is that type of flow in which the velocity, pressure or density at a point change w.r.t. time. Mathematically, we have:

$$\left(\frac{\partial u}{\partial t}\right)_{x_0, y_0, z_0} \neq 0; \left(\frac{\partial v}{\partial t}\right)_{x_0, y_0, z_0} \neq 0; \left(\frac{\partial w}{\partial t}\right)_{x_0, y_0, z_0} \neq 0;$$

$$\left(\frac{\partial p}{\partial t}\right)_{x_0, y_0, z_0} \neq 0; \left(\frac{\partial \rho}{\partial t}\right)_{x_0, y_0, z_0} \neq 0 \text{ and so on”}$$

Example: The flow in a pipe whose valve is being opened or closed gradually (velocity equation is in the form $u = ax^2 + bx(t)$).

2.3.2 Uniform and non-uniform flows

- **Uniform flow**

“The type of flow, in which the velocity at any given time does not change with respect to space is called uniform flow. Mathematically, we have:

$$\left(\frac{\partial V}{\partial s}\right)_{t=\text{constant}} = 0$$

where ∂V = Change in velocity, and ∂s = Displacement in any direction.”

Example: Flow through a straight prismatic conduit (i.e. flow through a straight pipe of constant diameter).

- **Non-uniform flow**

“It is that type of flow in which the velocity at any given time changes with respect to space.

Mathematically,

$$\left(\frac{\partial V}{\partial s}\right)_{t=\text{constant}} \neq 0.”$$

Examples: (i) Flow through a non-prismatic conduit.

(ii) Flow around a uniform diameter pipe-bend or a canal bend.

2.3.3 One,two and three dimensional flows

- **One dimensional flow**

“It is that type of flow in which the flow parameter such as velocity is a function of time and one space co-ordinate only. Mathematically:

$$u = f(x),$$

$$v = 0, \quad w = 0.$$

where u, v and w are velocity components in x, y and z directions respectively.”

Example:

Flow in a pipe where average flow parameters are considered for analysis.

- **Two dimensional flow**

“The flow in which the velocity is a function of time and two rectangular space coordinates is called two dimensional flow. Mathematically:

$$u = f_1(x, y),$$

$$v = f_2(x, y),$$

$$w = 0.”$$

Examples:

- (i) Flow between parallel plates of infinite extent.
- (ii) Flow in the main stream of a wide river.

- **Three dimensional flow**

“It is that type of flow in which the velocity is a function of time and three mutually perpendicular directions. Mathematically:

$$u = f_1(x, y, z),$$

$$v = f_2(x, y, z),$$

$$w = f_3(x, y, z).”$$

Examples:

- (i) Flow in a converging or diverging pipe or channel.
- (ii) Flow in a prismatic open channel in which the width and the water depth are of the same order of magnitude.

2.3.4 Rotational and irrotational flows

- **Rotational flow**

“A flow is said to be rotational if the fluid particles while moving in the direction of flow rotate about their mass centres. Flow near the solid boundaries is rotational.”

Example: Motion of liquid in a rotating tank.

- **Irrotational flow**

“A flow is said to be irrotational if the fluid particles while moving in the direction of flow do not rotate about their mass centres. Flow outside the boundary layer is generally considered irrotational.”

Example: Flow above a drain hole of a stationary tank or a wash basin.

2.3.5 Laminar and Turbulent flows

- **Laminar flow**

“A laminar flow is one in which paths taken by the individual particles do not cross one another and move along well defined paths.”

Examples:

- (i) Flow through a capillary tube.
- (ii) Flow of blood in veins and arteries.
- (iii) Ground water flow.

- **Turbulent flow**

“A turbulent flow is that flow in which fluid particles move in a zig zag way.”

Example: High velocity flow in a conduit of large size. The majority of fluid flow issues that arise in engineering practice are turbulent in nature.

2.3.6 Compressible and incompressible flows

- **Compressible flow**

“It is that type of flow in which the density ρ of the fluid changes from point to point (or in other words density is not constant for this flow). Mathematically:

$$\rho \neq \text{constant.}”$$

Example: Flow of gases through orifices, nozzles, gas turbines, etc.

- **Incompressible flow**

“It is that type of flow in which density is constant for the fluid flow. Liquids are generally considered flowing incompressibly. Mathematically:

$$\rho = \text{constant.}”$$

Example: Subsonic aerodynamics.

2.4 Fundamental Laws [81]

2.4.1 Conservation of Mass; the Continuity Equation

“The principle of conservation of mass can be stated as the time rate of change of mass in a fixed volume is equal to the net rate of flow of mass across the surface. The mathematical statement of the principle results in the following equation, known as the continuity (of mass) equation

$$\frac{\partial \rho}{\partial t} + \nabla \cdot (\rho \mathbf{v}) = 0 \quad (2.1)$$

where ρ is the density of the medium, \mathbf{v} the velocity vector, and ∇ is the nabla or del operator. The continuity equation in (2.1) is in conservation (or divergence) form since it can be derived directly from an integral statement of mass conservation. By

introducing the material derivative or Eulerian derivative operator $\frac{D}{Dt}$

$$\frac{D}{Dt} = \frac{\partial}{\partial t} + \mathbf{v} \cdot \nabla, \quad (2.2)$$

the continuity equation (2.1) can be expressed in the alternate, non-conservation (or advective) form

$$\frac{\partial \rho}{\partial t} + \mathbf{v} \cdot \nabla \rho + \rho \nabla \cdot \mathbf{v} = \frac{D\rho}{Dt} + \rho \nabla \cdot \mathbf{v} = 0 \quad (2.3)$$

For steady-state conditions, the continuity equation becomes

$$\nabla \cdot (\rho \mathbf{v}) = 0 \quad (2.4)$$

When the density changes following a fluid particle are negligible, the continuum is termed incompressible and we have $\frac{D\rho}{Dt} = 0$. The continuity equation (2.3) then becomes

$$\nabla \cdot \mathbf{v} = 0 \quad (2.5)$$

which is often referred to as the incompressibility condition or incompressibility constraint.”

2.4.2 Conservation of Momentum

“The principle of conservation of linear momentum (or Newton’s Second Law of motion) states that the time rate of change of linear momentum of a given set of particles is equal to the vector sum of all the external forces acting on the particles of the set, provided Newton’s Third Law of action and reaction governs the internal forces. Newton’s Second Law can be written as

$$\frac{\partial \rho \mathbf{v}}{\partial t} + \nabla \cdot (\rho \mathbf{v} \otimes \mathbf{v}) = \nabla \cdot \boldsymbol{\sigma} + \rho \mathbf{f} \quad (2.6)$$

where \otimes is the tensor (or dyadic) product of two vectors, $\boldsymbol{\sigma}$ is the Cauchy stress tensor (N/m^2) and \mathbf{f} is the body force vector, measured per unit mass and normally taken to be the gravity vector. Equation (2.6) describes the motion of a continuous medium, and in fluid mechanics they are also known as the Navier equations. The form of the

momentum equation shown in (2.6) is the conservation (divergence) form that is most often utilized for compressible flows. This equation may be simplified to a form more commonly used with incompressible flows. Expanding the first two derivatives and collecting terms

$$\rho \left(\frac{\partial \mathbf{v}}{\partial t} + \mathbf{v} \nabla \cdot \mathbf{v} \right) + \mathbf{v} \left(\frac{\partial \rho}{\partial t} + \nabla \cdot \rho \mathbf{v} \right) = \nabla \cdot \sigma + \rho \mathbf{f} \quad (2.7)$$

The second term in parentheses is the continuity equation (2.1) and neglecting this term allows (2.7) to reduce to the non-conservation (advective) form

$$\rho \frac{D\mathbf{v}}{Dt} = \nabla \cdot \sigma + \rho \mathbf{f} \quad (2.8)$$

where the material derivative (2.2) has been employed.

The principle of conservation of angular momentum can be stated as the time rate of change of the total moment of momentum of a given set of particles is equal to the vector sum of the moments of the external forces acting on the system. In the absence of distributed couples, the principle leads to the symmetry of the stress tensor:

$$\sigma = (\sigma)^T \quad (2.9)$$

where the superscript T denotes the transpose of the enclosed quantity.”

2.4.3 Conservation of Energy

“The law of conservation of energy (or the First Law of Thermodynamics) states that the time rate of change of the total energy is equal to the sum of the rate of work done by applied forces and the change of heat content per unit time. In the general case, the First Law of Thermodynamics can be expressed in conservation form as

$$\frac{\partial \rho e^t}{\partial t} + \nabla \cdot \rho \mathbf{v} e^t = -\nabla \cdot \mathbf{q} + \nabla \cdot (\sigma \cdot \mathbf{v}) + Q + \rho \mathbf{f} \cdot \mathbf{v} \quad (2.10)$$

where $e^t = e + 1/2 \mathbf{v} \cdot \mathbf{v}$ is the total energy (J/m^3), e is the internal energy, \mathbf{q} is the heat flux vector (W/m^2) and Q is the internal heat generation (W/m^3). The total energy

equation (2.10) is useful for high speed compressible flows where the kinetic energy is significant. For incompressible flows, an internal energy equation is more appropriate and can be derived from (2.10) with use of the momentum equation (2.6). Taking the dot product of the velocity vector with the momentum equation produces an equation for the kinetic energy; this equation is subtracted from the total energy equation (2.10) to produce the conservation (divergence) form of the internal energy equation

$$\frac{\partial \rho e}{\partial t} + \nabla \cdot \rho \mathbf{v} e = -\nabla \cdot \mathbf{q} + Q + \Phi \quad (2.11)$$

where Φ is a dissipation function that is defined by

$$\Phi = \sigma : \nabla \mathbf{v} \quad (2.12)$$

In Eq. (2.12) $\nabla \mathbf{v}$ is the velocity gradient tensor which will be defined more completely in the following sections. The thermal energy equation in (2.11) can be simplified further by expanding the derivatives on the left-hand side of the equation and using the continuity equation. The resulting equation is the non-conservative (advective) form of the energy equation

$$\rho \frac{De}{Dt} = -\nabla \cdot \mathbf{q} + Q + \Phi \quad (2.13)$$

which is the standard form used for incompressible flows. Constitutive relations for e and \mathbf{q} will be defined in the next sections and allowed (2.13) to be expressed in terms of the temperature T .”

2.5 Heat and Mass Transfer Phenomenon and Related Properties

Heat transfer is the phenomenon of transferring energy and entropy from one place to another. The formal definition of heat transfer and its different types are given below.

- **Heat Transfer** [81]

“Heat transfer is a branch of engineering that deals with the transfer of thermal energy from one point to another within a medium or from one medium to another due to the occurrence of a temperature difference. Heat transfer may take place in one or more of its three basic forms: conduction, convection, and radiation.”

- **Mass Transfer** [84]

“Mass transfer is the flow of molecules from one body to another when these bodies are in contact or within a system consisting of two components when the distribution of materials is not uniform. When a copper plate is placed on a steel plate, some molecules from either side will diffuse into the otherside. When salt is placed in a glass and water poured over it, after sufficient time the salt molecules will diffuse into the water body. A more common example is drying of clothes or the evaporation of water spilled on the floor when water molecules diffuse into the air surrounding it. Usually, mass transfer takes place from a location where the particular component is proportionately high to a location where the component is proportionately low. Mass transfer may also take place due to potentials other than concentration difference.”

- **Conduction** [85]

“Conduction is the transfer of heat from one part of a body at a higher temperature to another part of the same body at a lower temperature, or from one body at a higher temperature to another body in physical contact with it at a lower temperature. The conduction process takes place at the molecular level and involves the transfer of energy from the more energetic molecules to those with a lower energy level. This can be easily visualized within gases, where we note that the average kinetic energy of molecules in the higher-temperature regions is greater than that of those in the lower-temperature regions. The more energetic molecules, being in constant and random motion, periodically collide with molecules of a lower energy level and exchange energy and momentum. In this manner, there is a continuous transport of energy from the high-temperature regions to those of lower temperature. In liquids, the molecules are more closely

spaced than in gases, but the molecular energy exchange process is qualitatively similar to that in gases. In the solids that are nonconductors of electricity (dielectrics), heat is conducted by lattice waves caused by atomic motion. In the solids that are good conductors of electricity, this lattice vibration mechanism is only a small contribution to the energy transfer process, the principal contribution being that due to the motion of free electrons, which move in a similar way to molecules in a gas.”

- **Convection** [84]

“The process of heat transfer between a surface and a fluid flowing in contact with it is called convection.”

Types of Convection:

(i) Natural Convection or Free Convection

(ii) Forced Convection

(iii) Mixed Convection

- **Natural Convection or Free Convection** [84]

“If the flow is caused by the buoyant forces generated by heating or cooling of the fluid the process is called as natural or free convection.”

- **Forced Convection** [84]

“If the flow is caused by an external device like a pump or blower, it is termed as forced convection.”

- **Radiation** [85]

“Radiation, or more correctly thermal radiation, is electromagnetic radiation emitted by a body by virtue of its temperature and at the expense of its internal energy. Thus thermal radiation is of the same nature as visible light, x -rays, and radio waves, the difference between them being in their wavelengths and the source of generation. The eye is sensitive to electromagnetic radiation in the region from 0.39 to $0.78\mu m$; this is identified as the visible region of the spectrum. Radio waves have a wavelength of 1×10^3 to $2 \times 10^{10}\mu m$, and x -rays have wavelengths of 1×10^{-5} to $2 \times 10^{-2}\mu m$, while the bulk of thermal radiation

occurs in rays from approximately 0.1 to $100\mu m$. All heated solids and liquids, as well as some gases, emit thermal radiation. The transfer of energy by conduction requires the presence of a material medium, while radiation does not. In fact, radiation transfer occurs most efficiently in a vacuum. On the macroscopic level, the calculation of thermal radiation is based on the Stefan- Boltzmann law, which relates the energy flux emitted by an ideal radiator (or blackbody) to the fourth power of the absolute temperature.”

2.6 Dimensionless Numbers

The following dimensionless numbers will appear in the discussion given in the next chapters.

Prandtl Number [86]

“This number expresses the ratio of the momentum diffusivity (viscosity) to the thermal diffusivity. It characterizes the physical properties of a fluid with convective and diffusive heat transfers. It describes, for example, the phenomena connected with the energy transfer in a boundary layer. It expresses the degree of similarity between velocity and diffusive thermal fields or, alternatively, between hydrodynamic and thermal boundary layers. With $Pr = 1$ and $\text{grad } p = 0$, the thermal and hydrodynamic fields are similar. For example, if diverse molten materials have equal Prandtl numbers, they have similar velocity and temperature fields in crystallization.

$$Pr = \frac{\eta c_p}{\lambda}$$

where, η represents the dynamic viscosity, c_p denotes the specific heat capacity and λ stands for thermal conductivity.”

Nusselt Number [86]

“It expresses the ratio of the total heat transfer in a system to the heat transfer by conduction. It characterizes the heat transfer by convection between a fluid and the environment close to it or, alternatively, the connection between the heat transfer

intensity and the temperature field in a flow boundary layer. It expresses the dimensionless thermal transference. The physical significance is based on the idea of a fluid boundary layer in which the heat is transferred by conduction. If it is not so, the criterion loses its significance. In the expression $\alpha (\lambda/L)^{-1}$, it expresses the ratio of the heat transfer intensity to heat conduction intensity in a boundary layer. In the expression $L (\lambda/\alpha)^{-1}$, it represents the ratio of the characteristic length to the boundary layer thickness. In the expression $L/\lambda (1/\alpha)^{-1}$, it expresses the ratio of thermal resistances by conduction to those by convection in a boundary layer.

$$Nu = \frac{\alpha L}{\lambda}$$

where, $\alpha (W/m^2k)$ – heat transfer coefficient; $L (m)$ – characteristic length; $\lambda (W/mk)$ – thermal conductivity.”

Biot Number [86]

“This number expresses the ratio of the heat flow transferred by convection on a body surface to the heat flow transferred by conduction in a body. It characterizes the third-type boundary condition. The equation $Bi = L (\lambda\alpha^{-1})^{-1}$ expresses the ratio of a characteristic body length to an equivalent environmental thickness adhering to the surface. With $Bi \geq 100$ in the heat transfer on the surface, the thermal resistance is slight in comparison to the heat transfer by conduction. The temperature field is characterized by considerable non-uniformity. On the contrary, with $Bi \leq 0.1$, difference ($T_P - T_S$) is great on the body surface and slight inside the body and the field is uniform. With the general shape of body, the ratio $L = VS^{-1}$ is inserted for the characteristic length.”

Brinkmann Number [86]

“It expresses the ratio of the heat arising due to viscous friction of a fluid to the heat transferred by molecular conduction. It characterizes the heat conduction in viscous fluid flow. For high fluid viscosity values and low thermal conductivity values (e.g. molten polymers), the value is $Br \gg 1$.”

Skin Friction Coefficient [86]

“It expresses the dynamic friction resistance originating in viscous fluid flow around

a fixed wall. The expression $C_f = \frac{0.664}{\sqrt{Re_x}}$ is valid for laminar flow along a flat plate (Blasius' boundary layer) and the expression $C_f = 0.0576\sqrt[5]{Re_x}$ holds for turbulent flow.

$$C_f = \frac{\tau_w}{\frac{1}{2}\rho w_\infty^2}, \quad \text{where } \tau_w = \eta \left. \frac{dw}{dy} \right|_{y=0}.$$

where, τ_w (Pa) – shear stress on the wall ($y = 0$); ρ (kg/m) – fluid density;

w_∞ (m/s) – free fluid flow; η (Pas) – dynamic viscosity;

y (m) – coordinate perpendicular to the wall surface; Re_x – Reynolds number.”

2.7 Boundary layer [87]

The idea of boundary layer was first introduced by Ludwig Prandtl in 1904. Ludwig Prandtl gave the basic idea of the boundary layer for moving fluid over a surface. It is the close layer of fluid flow near solid region where the viscosity effects are significant. The flow in this layer is usually laminar. The boundary layer thickness is the measure of the distance apart from the surface.

2.8 Entropy Generation

A system's entropy is a measure of its disorder. This means that the system is unable to use 100% of useful energy. The entropy of a system is zero in an ideal system where we are able to preserve the energy contained in the system precisely, however this is not the case in the real world. Energy is lost in some way, which causes entropy to continuously increase. The goal here is to identify strategies for reducing this entropy loss. Entropy reduction is therefore a crucial problem in every industrial setting. The scientists have been studying the formation of entropy and trying to find ways to lower it.

2.9 Magnetohydrodynamics

The study of electrically conducting fluid motion in the presence of a magnetic field, such as that of liquid metals and plasmas, is known as magnetohydrodynamics. Magnetohydrodynamics' central premise is that current may be produced by magnetic fields in conductive fluids in motion, which in turn exerts force on the fluid and modifies the magnetic field itself.

Hannes Alfvén, who understood the significance of the electric currents carried by a plasma and the magnetic field they create, established the fundamental equations of magnetohydrodynamics.

Alfvén combined the fluid dynamics equations with Ampère and Faraday's electrodynamics rules to create a revolutionary mathematical theory. The physics of the sun, solar wind, and stellar atmospheres, as well as space plasmas in earth and planetary magnetospheres, were all explained by this theory.

2.10 Nanofluids [88]

Nanofluid is a suspension or combination of a base fluid with nanosized particles with sizes ranging from 1 to 100 nanometers. The goal of the science involved in creating the nanofluids is to increase the basic fluids' thermal capacity.

Commonly used solid additives in the form of nanoparticles are made of downsized metals and their oxides, as well as ceramics and oxides, carbides, and metal composites with extremely high thermal conductivity. Water is the most often used base fluid, while other options include kerosene oil, engine oil, ethylene glycol, and mixtures of water and motor oil.

Heat transfer mechanisms may be examined in relation to nanofluids. The primary characteristic of nanofluids is their improved thermal characteristics.

TABLE 2.1: Thermo-physical properties of Nanofluid

Properties	Nanofluid
Dynamic Viscosity	$\mu_{nf} = \mu_f(1 - \Phi)^{-2.5}$
Density	$\rho_{nf} = (1 - \Phi)\rho_f + \Phi\rho_s$
Heat Capacity	$(\rho C_p)_{nf} = (1 - \Phi)(\rho C_p)_f + \Phi(\rho C_p)_s$
Thermal conductivity	$\frac{\kappa_{nf}}{\kappa_f} = \left[\frac{(\kappa_s + (q-1)\kappa_f) - (q-1)\Phi(\kappa_f - \kappa_s)}{(\kappa_s + (q-1)\kappa_f) + \Phi(\kappa_f - \kappa_s)} \right]$
Electrical conductivity	$\frac{\sigma_{nf}^*}{\sigma_f} = \left[1 + \frac{3(\frac{\sigma_s}{\sigma_f} - 1)\Phi}{(\frac{\sigma_s}{\sigma_f} + 2) - (\frac{\sigma_s}{\sigma_f} - 1)\Phi} \right]$

The thermophysical characteristics of nanofluids are displayed in Table (2.1), (for further information, see, for example, [89, 90]).

2.11 Material Properties of Nanofluids

The following table lists the material characteristics of the base fluid and several nanoparticles that were employed in this thesis.

TABLE 2.2: Material Properties of Base fluid and Nanoparticles at 293K

Thermophysical	Cu	SiC	MeOH
$\rho(\text{kg}/\text{m}^3)$	8933	3160	792
$C_p(\text{J}/\text{kgK})$	385.0	1340	2545
$k(\text{W}/\text{m})$	401.00	350	0.2035
$\sigma(\text{S}/\text{m})$	5.96×10^7	0.7×10^2	0.5×10^{-6}

2.12 Tiwari and Das Model

Two different kinds of models are utilized in mathematics to address issues pertaining to nanofluids. One type of single phase model is the Tiwari and Das model. The fluid, velocity, and temperature are assumed to be the same in a single phase model. In the case of the two-phase model, the temperature and the fluid velocity as well as the nanoparticles are measured differently. The benefit of the single phase model is that because we ignore the slip mechanisms so the model is simplified one and it is easily to solve numerically. However, this method's drawback is that, occasionally, the numerical findings don't match the experimental results. The volume concentration of nanoparticles in the Tiwari and Das model varies from 3% – 20%.

2.13 Cattaneo-Christov Heat Flux Model [61]

Fourier's concept of heat conduction remained valid for a century. A shortcoming of the Fourier's interpretation of heat transport was that a disturbance in the temperature gradient at the boundary is felt instantly through the medium which means that heat energy travels at an infinite speed which is not possible physically. This drawback of Fourier's law was addressed by Cattaneo. Cattaneo's modification to the Fourier's law is given as:

$$\left(1 + \lambda_0 \frac{\partial}{\partial t}\right) \mathbf{q} = -k \nabla T.$$

Here, λ_0 is termed as thermal relaxation time. It is the time lag involved in achieving the steady state solution once a temperature gradient is applied across a volume element. Cattaneo's modification addressed the drawback of the Fourier's law but resulted in a coupled system to be solved in order to get knowledge about the energy distribution in the system. Christov, further modified the Cattaneo's concept by considering a material Oldroyds' upper-convected derivative instead of the ordinary time derivative. With the help of this modification, a single energy equation was achieved.

Hence, in terms of Christov's theory the heat conduction law is written as:

$$\mathbf{q} + \lambda_0 \left(\frac{\partial \mathbf{q}}{\partial t} + \mathbf{V} \cdot \nabla \mathbf{q} - \mathbf{q} \cdot \nabla \mathbf{V} + (\nabla \cdot \mathbf{V}) \mathbf{q} \right) = -\kappa \nabla T.$$

2.14 Shooting Method

Consider the following fourth order boundary value problem.

$$g'''' - (1 - x^2)g'' + 5g^2 = 0, \quad (2.14)$$

with boundary condition

$$g(0) = 1, \quad g'(0) = 0, \quad g''(1) = -2, \quad g'''(1) = -3. \quad (2.15)$$

Equation (2.14) can be transformed into a system of first-order equations by introducing the following notations.

$$g = g_1, \quad g' = g_2, \quad g'' = g_3, \quad g''' = g_4. \quad (2.16)$$

Next, the given BVP is transformed into the subsequent form.

$$\begin{aligned} g_1' &= g_2, & g_1(0) &= 1, \\ g_2' &= g_3, & g_2(0) &= 0, \\ g_3' &= g_4, & g_3(1) &= -2, \\ g_4' &= (1 - x^2)g_3^2 - 5g_1^2, & g_4(1) &= -3. \end{aligned} \quad (2.17)$$

To obtain the following IVP, denote the missing initial conditions $g_3(0)$ and $g_4(0)$ by p and q , respectively.

$$\left. \begin{aligned} g_1' &= g_2, & g_1(0) &= 1, \\ g_2' &= g_3, & g_2(0) &= 0, \\ g_3' &= g_4, & g_3(0) &= p, \\ g_4' &= (1-x^2)g_3^2 - 5g_1^2, & g_4(0) &= q. \end{aligned} \right\} \quad (2.18)$$

Now solve the given IVP across the interval $[0, 1]$ using the RK-4 approach. The RK-4 solution is then examined for $g''(1)$ and $g'''(1)$. The issue is resolved if these solutions satisfy the boundary condition specified in Eq. (2.15).

But typically, this doesn't occur on the first try. As a result, we must repeatedly improve the first estimations. For this, we solve the following system of non-linear algebraic equations using Newton's technique.

$$\left. \begin{aligned} g_3(x, p, q) + 2 &= 0, \\ g_4(x, p, q) + 3 &= 0, \end{aligned} \right\} \quad (2.19)$$

Newton's approach for the system of non-linear equations Eq.(2.18) has an iterative strategy that is as follows.

$$\begin{bmatrix} p_{n+1} \\ q_{n+1} \end{bmatrix} = \begin{bmatrix} p_n \\ q_n \end{bmatrix} - \begin{bmatrix} \frac{\partial}{\partial p} g_3(1, p_n, q_n) & \frac{\partial}{\partial q} g_3(1, p_n, q_n) \\ \frac{\partial}{\partial p} g_4(1, p_n, q_n) & \frac{\partial}{\partial q} g_4(1, p_n, q_n) \end{bmatrix}^{-1} \begin{bmatrix} g_3(x, p, q) + 2 \\ g_4(x, p, q) + 3 \end{bmatrix} \quad (2.20)$$

For simplification, use the following notations,

$$\left. \begin{aligned} \frac{\partial g_1}{\partial p} &\equiv g_5, & \frac{\partial g_2}{\partial p} &\equiv g_6, & \frac{\partial g_3}{\partial p} &\equiv g_7, & \frac{\partial g_4}{\partial p} &\equiv g_8, \\ \frac{\partial g_1}{\partial q} &\equiv g_9, & \frac{\partial g_2}{\partial q} &\equiv g_{10}, & \frac{\partial g_3}{\partial q} &\equiv g_{11}, & \frac{\partial g_4}{\partial q} &\equiv g_{12} \end{aligned} \right\} \quad (2.21)$$

By differentiating the system of Eq. (2.18) first with respect to p and then with respect to q and utilizing the new notations, we can determine the Jacobian matrix.

$$\left. \begin{aligned} g'_5 &= g_6, & g_5(0) &= 0, \\ g'_6 &= g_7, & g_6(0) &= 0, \\ g'_7 &= g_8, & g_7(0) &= 1, \\ g'_8 &= 2(1-x^2)g_3g_7 - 10g_1g_5, & g_8(0) &= 0, \\ g'_9 &= g_{10}, & g_9(0) &= 0, \\ g'_{10} &= g_{11}, & g_{10}(0) &= 0, \\ g'_{11} &= g_{12}, & g_{11}(0) &= 0, \\ g'_{12} &= 2(1-x^2)g_3g_{11} - 10g_1g_9, & g_{12}(0) &= 1. \end{aligned} \right\} \quad (2.22)$$

Utilizing the RK-4 technique, solve the aforementioned system of equations (2.22) and enter the computed values for g_7 , g_{11} , g_8 , and g_{12} in eq. (2.20). This provides updated first guesses. Until we have the necessary precision in our solutions, we repeat this process.

Chapter 3

Computational single phase comparative study of inclined MHD in a Powell-Eyring nanofluid

3.1 Introduction

A comprehensive review of [91] has been conducted by using the shooting method. Powell-Eyring non-Newtonian fluid has been considered as a nanofluid. The non-linear PDEs are converted into dimensionless ODEs using similarity transformation. Using the shooting approach and the computational software MATLAB, the ODEs have been solved.

Results are discussed to study the impact of governing physical parameters on velocity, temperature, entropy, velocity gradient (skin friction coefficient) and the strength of convective heat exchange (Nusselt number) of nanofluid made up of Cu-MeOH and SiC-MeOH.

In addition to this, empirical values of five different nanoparticle shapes have been utilized to look at their impact on the heat transfer rate as well as the temperature distribution in the boundary layer.

fluid is as follows:

$$\tau_{ij} = \mu_{nf} \left(\frac{\partial \bar{f}_{1i}}{\partial \bar{x}_j} \right) + \frac{1}{\hat{\beta}} \sinh^{-1} \left(\frac{1}{h^*} \frac{\partial \bar{f}_{1i}}{\partial \bar{x}_j} \right), \quad (3.1)$$

where, μ_{nf} is the dynamic viscosity of the non-Newtonian fluid, whereas $\hat{\beta}$ and h^* are the material constants. A uniformly distributed inclined magnetic field of strength $B(\tilde{t}) = \frac{B_0}{\sqrt{1-\xi\tilde{t}}}$ is assumed in the present model and the induced magnetic field is seen as insignificant in comparison to the applied \mathbf{B} . The stretching speed and porous surface temperature are

$$\bar{U}_w(\bar{x}, \tilde{t}) = \frac{c^* \bar{x}}{1 - \xi \tilde{t}}, \quad \Theta_f(\bar{x}, \tilde{t}) = \Theta_\infty + \frac{c^* \bar{x}}{1 - \xi \tilde{t}}. \quad (3.2)$$

3.2.1 The Governing PDEs

Under the boundary layer assumption and appropriate boundary conditions for Powell-Eyring nanofluid, the constitutive equations for conservation of mass, momentum, and energy can be written as [93]:

$$\frac{\partial \bar{f}_1}{\partial \bar{x}} + \frac{\partial \bar{f}_2}{\partial \bar{y}} = 0, \quad (3.3)$$

$$\begin{aligned} \frac{\partial \bar{f}_1}{\partial \tilde{t}} + \bar{f}_1 \frac{\partial \bar{f}_1}{\partial \bar{x}} + \bar{f}_2 \frac{\partial \bar{f}_1}{\partial \bar{y}} &= \left(\nu_{nf} + \frac{1}{\rho_{nf} \hat{\beta} h^*} \right) \frac{\partial^2 \bar{f}_1}{\partial \bar{y}^2} - \frac{1}{2 \hat{\beta} h^{*3} \rho_{nf}} \left(\frac{\partial \bar{f}_1}{\partial \bar{y}} \right)^2 \frac{\partial^2 \bar{f}_1}{\partial \bar{y}^2} \\ &\quad - \frac{\sigma_{nf}^* B^2(\tilde{t}) \bar{f}_1}{\rho_{nf}} \sin^2(\Gamma), \end{aligned} \quad (3.4)$$

$$\begin{aligned} \frac{\partial \Theta}{\partial \tilde{t}} + \bar{f}_1 \frac{\partial \Theta}{\partial \bar{x}} + \bar{f}_2 \frac{\partial \Theta}{\partial \bar{y}} &= \frac{k_{nf}}{(\rho C_p)_{nf}} \left(\frac{\partial^2 \Theta}{\partial \bar{y}^2} \right) - \frac{1}{(\rho C_p)_{nf}} \left(\frac{\partial q_r}{\partial \bar{y}} \right) + \frac{\nu_{nf}}{(\rho C_p)_{nf}} \left(\frac{\partial \bar{f}_1}{\partial \bar{y}} \right)^2 \\ &\quad + \frac{\sigma_{nf}^* B^2(\tilde{t}) \bar{f}_1^2}{(\rho C_p)_{nf}} \sin^2(\Gamma). \end{aligned} \quad (3.5)$$

The BCs' for the contemporary model are:

$$\left. \begin{aligned} \bar{f}_1(\bar{x}, 0) &= \bar{U}_w + \mu_{nf} \left(\frac{\partial \bar{f}_1}{\partial \bar{y}} \right), \quad \bar{f}_2(\bar{x}, 0) = \bar{V}_w, \\ -k_0 \left(\frac{\partial \Theta}{\partial \bar{y}} \right) &= h_f (\Theta_f - \Theta) \quad \text{at} \quad \bar{y} = 0, \\ \bar{f}_1 &\longrightarrow 0, \quad \Theta \longrightarrow \Theta_\infty, \quad \text{as} \quad \bar{y} \longrightarrow \infty. \end{aligned} \right\} \quad (3.6)$$

The radiative heat flux is given by

$$q_r = -\frac{4\sigma^*}{3k^*} \frac{\partial \Theta^4}{\partial \bar{y}} = -\frac{16\sigma^*}{3k^*} \Theta^3 \frac{\partial \Theta}{\partial \bar{y}}, \quad (3.7)$$

If the temperature difference is very small, then the temperature Θ^4 can be expanded about Θ_∞ using Taylor series, as follows.

$$\Theta^4 = \Theta_\infty^4 + 4\Theta_\infty^3(\Theta - \Theta_\infty) + 6\Theta_\infty^2(\Theta - \Theta_\infty)^2 + \dots$$

Ignoring the higher order terms, we have

$$\begin{aligned} \Theta^4 &= \Theta_\infty^4 + 4\Theta_\infty^3(\Theta - \Theta_\infty) = \Theta_\infty^4 + 4\Theta_\infty^3\Theta - 4\Theta_\infty^4 \\ &= -3\Theta_\infty^4 + 4\Theta_\infty^3\Theta = 4\Theta_\infty^3\Theta - 3\Theta_\infty^4. \end{aligned}$$

3.2.2 Similarity Transformations

The nonlinear Partial differential equations will be converted into a system of dimensionless Ordinary differential equations using the following analogies [94]:

$$\left. \begin{aligned} \bar{f}_1 &= \frac{c^*}{1 - \xi \bar{t}} \bar{x} \frac{df}{d\chi}, & \bar{f}_2 &= -\sqrt{\frac{\nu_f c^*}{1 - \xi \bar{t}}} f(\chi), \\ \chi(\bar{x}, \bar{y}) &= \sqrt{\frac{c^*}{\nu_f(1 - \xi \bar{t})}} \bar{y}, & \psi(\bar{x}, \bar{y}) &= \sqrt{\frac{\nu_f c^*}{1 - \xi \bar{t}}} \bar{x} f(\chi), \\ \theta(\chi) &= \frac{\Theta - \Theta_\infty}{\Theta_f - \Theta_\infty}. \end{aligned} \right\} \quad (3.8)$$

3.2.3 Physical Quantities of Interest

The dimensional forms of the skin friction coefficient, Nusselt number are shown below [95]. The dimensionless forms of these parameters will be produced and used in the subsequent section of this chapter, which will elaborate the solution to our current situation,

$$\left. \begin{aligned} C_{f\bar{x}} &= \frac{\tau_w}{\rho_f \bar{U}_w^2}, & Nu_{\bar{x}} &= \frac{\bar{x} q_w}{k_f(\Theta_f - \Theta_\infty)}. \end{aligned} \right\} \quad (3.9)$$

3.2.4 Entropy

Entropy is a disorder of a system and its surroundings from a physical perspective. Entropy often arises in a number of systems, particularly those involving fluid viscous force, Joule heating, and flow-driven force. Therefore, entropy is also known as the number of irreversibilities. As a result, heat cannot entirely be converted into work. The entropy generation is expressed as follows in the dimensional form [96]:

$$E_G = \frac{k_{nf}}{\Theta_\infty^2} \left[\left(\frac{\partial \Theta}{\partial \bar{y}} \right)^2 + \frac{16}{3} \frac{\sigma^* \Theta_\infty^3}{k^* \nu_f (\rho C_p)_f} \left(\frac{\partial \Theta}{\partial \bar{y}} \right)^2 \right] + \frac{\mu_{nf}}{\Theta_\infty} \left(\frac{\partial \bar{f}_1}{\partial \bar{y}} \right)^2 + \frac{\sigma_{nf}^* B^2(\tilde{t}) \sin^2(\Gamma) \bar{f}_1^2}{\Theta_\infty}. \quad (3.10)$$

3.3 Conversion of Mathematical Model into Dimensionless Form

3.3.1 The Governing ODEs

To get a solution to a problem, we first need a system of equations (3.3), (3.4) and (3.5), along with boundary conditions (3.6), is converted into a system of ODEs. We use the transformations (3.11), where ψ be the stream function satisfying the continuity equation, in the sense:

$$\left. \begin{aligned} \bar{f}_1 &= \frac{\partial \psi}{\partial \bar{y}}, & \bar{f}_2 &= -\frac{\partial \psi}{\partial \bar{x}}. \end{aligned} \right\} \quad (3.11)$$

To convert equations (3.3)-(3.5) into the dimensionless form, different derivatives are required which have been computed in the upcoming part of this sub-section.

$$\frac{\partial \chi}{\partial \bar{x}} = 0. \quad (3.12)$$

$$\frac{\partial \chi}{\partial \bar{y}} = \sqrt{\frac{c^*}{\nu_f (1 - \xi \tilde{t})}}. \quad (3.13)$$

$$\bar{f}_1 = \frac{\partial \psi}{\partial \bar{y}} = \frac{\partial \psi}{\partial \chi} \frac{\partial \chi}{\partial \bar{y}} = \frac{c^*}{1 - \xi \tilde{t}} \bar{x} \frac{d\psi}{d\chi}. \quad (3.14)$$

$$\frac{\partial \bar{f}_1}{\partial \bar{x}} = \frac{c^*}{1 - \bar{\xi}\bar{t}} \frac{df}{d\chi}. \quad \left(\because \frac{\partial \chi}{\partial \bar{x}} = 0 \right) \quad (3.15)$$

$$\bar{f}_2 = -\frac{\partial \psi}{\partial \bar{x}} = -\sqrt{\frac{\nu_f c^*}{1 - \bar{\xi}\bar{t}}} f(\chi). \quad (3.16)$$

$$\frac{\partial \bar{f}_2}{\partial \bar{y}} = -\frac{c^*}{1 - \bar{\xi}\bar{t}} \frac{df}{d\chi}. \quad (3.17)$$

$$\bar{f}_1 \frac{\partial \bar{f}_1}{\partial \bar{x}} = \frac{c^{*2}}{(1 - \bar{\xi}\bar{t})^2} \bar{x} \left(\frac{df}{d\chi} \right)^2. \quad (3.18)$$

$$\frac{\partial \bar{f}_1}{\partial \bar{y}} = \frac{c^*}{1 - \bar{\xi}\bar{t}} \sqrt{\frac{c^*}{\nu_f (1 - \bar{\xi}\bar{t})}} \bar{x} \frac{d^2 f}{d\chi^2}. \quad (3.19)$$

$$\bar{f}_2 \frac{\partial \bar{f}_1}{\partial \bar{y}} = -\frac{c^{*2}}{(1 - \bar{\xi}\bar{t})^2} \bar{x} f(\chi) \frac{d^2 f}{d\chi^2}. \quad (3.20)$$

$$\frac{\partial \chi}{\partial \bar{t}} = \frac{\bar{y}}{2} \sqrt{\frac{\nu_f (1 - \bar{\xi}\bar{t})}{c^*}} \left[\frac{c^* \bar{\xi}}{\nu_f (1 - \bar{\xi}\bar{t})^2} \right]. \quad (3.21)$$

$$\frac{\partial \bar{f}_1}{\partial \bar{t}} = \frac{c^* \bar{\xi} \bar{x}}{(1 - \bar{\xi}\bar{t})^2} \frac{df}{d\chi} + \frac{c^* \bar{\xi}}{2(1 - \bar{\xi}\bar{t})^2} \sqrt{\frac{c^*}{\nu_f (1 - \bar{\xi}\bar{t})}} \bar{x} \bar{y} \frac{d^2 f}{d\chi^2}. \quad (3.22)$$

$$\left(\frac{\partial \bar{f}_1}{\partial \bar{y}} \right)^2 = \frac{c^{*3} \bar{x}^2}{\nu_f (1 - \bar{\xi}\bar{t})^3} \left(\frac{d^2 f}{d\chi^2} \right)^2. \quad (3.23)$$

$$\frac{\partial^2 \bar{f}_1}{\partial \bar{y}^2} = \frac{c^{*2}}{\nu_f (1 - \bar{\xi}\bar{t})^2} \bar{x} \frac{d^3 f}{d\chi^3}. \quad (3.24)$$

$$\theta(\chi) = \frac{\Theta - \Theta_\infty}{\Theta_f - \Theta_\infty}$$

$$\Rightarrow \Theta - \Theta_\infty = (\Theta_f - \Theta_\infty) \theta(\chi)$$

$$\Rightarrow \Theta = (\Theta_f - \Theta_\infty) \theta(\chi) + \Theta_\infty$$

$$\Rightarrow \Theta = \left(\Theta_\infty + \frac{c^* \bar{x}}{1 - \bar{\xi}\bar{t}} - \Theta_\infty \right) \theta(\chi) + \Theta_\infty$$

$$\Rightarrow \Theta = \left(\frac{c^* \bar{x}}{1 - \bar{\xi}\bar{t}} \right) \theta(\chi) + \Theta_\infty$$

$$\frac{\partial \Theta}{\partial \bar{x}} = \left[\frac{c^*}{1 - \bar{\xi}\bar{t}} \right] \theta(\chi). \quad (3.25)$$

$$\frac{\partial \Theta}{\partial \bar{y}} = \left[\frac{c^* \bar{x}}{1 - \bar{\xi}\bar{t}} \right] \frac{d\theta}{d\chi} \sqrt{\frac{c^*}{\nu_f (1 - \bar{\xi}\bar{t})}}. \quad (3.26)$$

$$\left(\frac{\partial\Theta}{\partial\bar{y}}\right)^2 = \frac{c^{*3}\bar{x}^2}{\nu_f(1-\bar{\xi}\bar{t})^3} \left(\frac{d\theta}{d\chi}\right)^2. \quad (3.27)$$

$$\frac{\partial^2\Theta}{\partial\bar{x}^2} = 0. \quad (3.28)$$

$$\frac{\partial^2\Theta}{\partial\bar{y}^2} = \frac{c^{*2}\bar{x}}{\nu_f(1-\bar{\xi}\bar{t})^2} \frac{d^2\theta}{d\chi^2}. \quad (3.29)$$

$$\bar{f}_1 \frac{\partial\Theta}{\partial\bar{x}} = \frac{c^{*2}}{(1-\bar{\xi}\bar{t})^2} \bar{x} \frac{d\theta}{d\chi}(\chi). \quad (3.30)$$

$$\bar{f}_2 \frac{\partial\Theta}{\partial\bar{y}} = -\left[\frac{c^{*2}\bar{x}}{(1-\bar{\xi}\bar{t})^2}\right] f(\chi) \frac{d\theta}{d\chi}. \quad (3.31)$$

$$\frac{\partial\Theta}{\partial\bar{t}} = \frac{c^*\bar{x}\bar{\xi}}{(1-\bar{\xi}\bar{t})^2} \theta(\chi) + \frac{c^{*2}\bar{x}\bar{\xi}}{\nu_f(1-\bar{\xi}\bar{t})^3} \frac{\bar{y}}{2} \sqrt{\frac{\nu_f(1-\bar{\xi}\bar{t})}{c^*}} \frac{d\theta}{d\chi}. \quad (3.32)$$

$$\frac{\partial q_r}{\partial\bar{y}} = -\frac{16\Theta_\infty^3 \sigma^*}{3k^*} \frac{\partial^2\Theta}{\partial\bar{y}^2}. \quad (3.33)$$

$$\begin{aligned} \frac{\mu_{nf}}{\rho_f} &= \frac{\mu_f(1-\Phi)^{-2.5}}{(1-\Phi)\rho_f + \Phi\rho_s} \\ \frac{\rho_{nf}}{\rho_f} &= \frac{\mu_f}{\rho_f} \\ &= \frac{\mu_f(1-\Phi)^{-2.5}}{\mu_f \left[(1-\Phi) + \Phi \left(\frac{\rho_s}{\rho_f} \right) \right]} \\ &= \frac{1}{(1-\Phi)^{2.5} \left[(1-\Phi) + \Phi \left(\frac{\rho_s}{\rho_f} \right) \right]} = \frac{1}{N_1 N_2}, \end{aligned}$$

$$\begin{aligned} \rho_{nf} \frac{\mu_f}{\rho_f} &= \left[(1-\Phi)\rho_f + \Phi\rho_s \right] \times \frac{\mu_f}{\rho_f} \\ &= \left[(1-\Phi) + \Phi \frac{\rho_s}{\rho_f} \right] \times \mu_f = N_2 \times \mu_f \\ \frac{\sigma_{nf}^*}{\sigma_f} &= \left[1 + \frac{3\left(\frac{\sigma_s}{\sigma_f} - 1\right)\Phi}{\left(\frac{\sigma_s}{\sigma_f} + 2\right) - \left(\frac{\sigma_s}{\sigma_f} - 1\right)\Phi} \right] \\ \sigma_{nf}^* &= \left[1 + \frac{3\left(\frac{\sigma_s}{\sigma_f} - 1\right)\Phi}{\left(\frac{\sigma_s}{\sigma_f} + 2\right) - \left(\frac{\sigma_s}{\sigma_f} - 1\right)\Phi} \right] \times \sigma_f \\ \sigma_{nf}^* &= N_5 \times \sigma_f \\ \rho_{nf} &= \left[(1-\Phi)\rho_f + \Phi\rho_s \right] \times \frac{\rho_f}{\rho_f} \\ \rho_{nf} &= \left[(1-\Phi) + \Phi \frac{\rho_s}{\rho_f} \right] \times \rho_f \\ \rho_{nf} &= N_2 \times \rho_f, \\ \frac{k_{nf}}{k_f} &= \left[\frac{(k_s + (q-1)k_f) - (q-1)\Phi(k_f - k_s)}{(k_s + (q-1)k_f) + \Phi(k_f - k_s)} \right], \end{aligned}$$

$$k_{nf} = \left[\frac{(k_s + (q-1)k_f) - (q-1)\Phi(k_f - k_s)}{(k_s + (q-1)k_f) + \Phi(k_f - k_s)} \right] \times k_f,$$

$$k_{nf} = N_4 \times k_f.$$

$$(\rho C_p)_{nf} = (1 - \Phi)(\rho C_p)_f + \Phi(\rho C_p)_s,$$

$$\frac{(\rho C_p)_{nf}}{(\rho C_p)_f} = (1 - \Phi) + \Phi \frac{(\rho C_p)_s}{(\rho C_p)_f},$$

$$(\rho C_p)_{nf} = \left[(1 - \Phi) + \Phi \frac{(\rho C_p)_s}{(\rho C_p)_f} \right] \times (\rho C_p)_f,$$

$$(\rho C_p)_{nf} = N_3 \times (\rho C_p)_f.$$

For convenience, the following notations have been introduced :

$$N_1 = (1 - \Phi)^{2.5}. \quad (3.34)$$

$$N_2 = \left[(1 - \Phi) + \Phi \left(\frac{\rho_s}{\rho_f} \right) \right]. \quad (3.35)$$

$$N_3 = \left[(1 - \Phi) + \Phi \frac{(\rho C_p)_s}{(\rho C_p)_f} \right]. \quad (3.36)$$

$$N_4 = \left[\frac{(k_s + (q-1)k_f) - (q-1)\Phi(k_f - k_s)}{(k_s + (q-1)k_f) + \Phi(k_f - k_s)} \right]. \quad (3.37)$$

$$N_5 = \left[1 + \frac{3 \left(\frac{\sigma_s}{\sigma_f} - 1 \right) \Phi}{\left(\frac{\sigma_s}{\sigma_f} + 2 \right) - \left(\frac{\sigma_s}{\sigma_f} - 1 \right) \Phi} \right]. \quad (3.38)$$

By the choice of the stream function ψ in (3.11), the continuity equation is already satisfied. It can again be verified using (3.15) and (3.17), in (3.3) as follows.

$$\frac{\partial \bar{f}_1}{\partial \bar{x}} + \frac{\partial \bar{f}_2}{\partial \bar{y}} = \frac{c^*}{1 - \bar{\xi} \bar{t}} \frac{df}{d\chi} - \frac{c^*}{1 - \bar{\xi} \bar{t}} \frac{df}{d\chi} = 0.$$

Hence continuity equation (3.3) is identically satisfied.

Now, the dimensionless form of the momentum equation (3.4) can be obtained by using

equations (3.18)- (3.24), (3.34), (3.35) and (3.38) as follows,

$$\Rightarrow \frac{c^* \bar{\xi}}{(1 - \bar{\xi} \bar{t})^2} \bar{x} \frac{df}{d\chi} + \frac{c^* \bar{\xi}}{2(1 - \bar{\xi} \bar{t})^2} \sqrt{\frac{c^*}{\nu_f(1 - \bar{\xi} \bar{t})}} \bar{x} \bar{y} \frac{d^2 f}{d\chi^2} + \frac{c^{*2}}{(1 - \bar{\xi} \bar{t})^2} \bar{x} \left(\frac{df}{d\chi} \right)^2 - \frac{c^{*2}}{(1 - \bar{\xi} \bar{t})^2} \bar{x}$$

$$f(\chi) \frac{d^2 f}{d\chi^2} = \left(\nu_{nf} + \frac{1}{\rho_{nf} \hat{\beta} h^*} \right) \frac{c^{*2}}{\nu_f(1 - \bar{\xi} \bar{t})^2} \bar{x} \frac{d^3 f}{d\chi^3} - \frac{1}{2 \hat{\beta} h^{*3} \rho_{nf}} \frac{c^{*3} \bar{x}^2}{\nu_f(1 - \bar{\xi} \bar{t})^3} \left(\frac{d^2 f}{d\chi^2} \right)^2$$

$$\frac{c^{*2}}{\nu_f(1 - \bar{\xi} \bar{t})^2} \bar{x} \frac{d^3 f}{d\chi^3} - \frac{\sigma_{nf}^*}{\rho_{nf}} \frac{B_0^2}{(\sqrt{(1 - \bar{\xi} \bar{t})})^2} \frac{c^* \bar{x}}{(1 - \bar{\xi} \bar{t})} \frac{df}{d\chi} \sin^2(\Gamma).$$

$$\begin{aligned}
&\Rightarrow \frac{\bar{\xi}}{c^*} \frac{df}{d\chi} + \frac{1}{2} \frac{\bar{\xi}}{c^*} \sqrt{\frac{c^*}{\nu_f(1-\bar{\xi}\tilde{t})}} \bar{y} \frac{d^2f}{d\chi^2} + \left(\frac{df}{d\chi}\right)^2 - f(\chi) \frac{d^2f}{d\chi^2} = \left(\nu_{nf} + \frac{1}{\rho_{nf}\hat{\beta}h^*}\right) \frac{1}{\nu_f} \frac{d^3f}{d\chi^3} \\
&\quad - \frac{1}{2\hat{\beta}h^{*3}\rho_{nf}} \frac{c^{*3}\bar{x}^2}{\nu_f(1-\bar{\xi}\tilde{t})^3} \left(\frac{d^2f}{d\chi^2}\right)^2 \frac{1}{\nu_f} \frac{d^3f}{d\chi^3} - \frac{\sigma_{nf}^* B_0^2}{\rho_{nf} c^*} \frac{df}{d\chi} \sin^2(\Gamma). \\
&\Rightarrow \frac{\bar{\xi}}{c^*} \left[\frac{df}{d\chi} + \frac{1}{2} \sqrt{\frac{c^*}{\nu_f(1-\bar{\xi}\tilde{t})}} \bar{y} \frac{d^2f}{d\chi^2} \right] + \left(\frac{df}{d\chi}\right)^2 - f(\chi) \frac{d^2f}{d\chi^2} = \left(\frac{\nu_{nf}}{\nu_f} + \frac{1}{\rho_{nf}\nu_f\hat{\beta}h^*}\right) \frac{d^3f}{d\chi^3} \\
&\quad - \left[\frac{c^{*3}\bar{x}^2\bar{x}}{(1-\bar{\xi}\tilde{t})^3} \right] \left(\frac{d^2f}{d\chi^2}\right)^2 \frac{d^3f}{d\chi^3} - \frac{\sigma_{nf}^* B_0^2}{\rho_{nf} c^*} \frac{df}{d\chi} \sin^2(\Gamma). \\
&\Rightarrow A \left[\frac{df}{d\chi} + \frac{\chi}{2} \frac{d^2f}{d\chi^2} \right] + \left(\frac{df}{d\chi}\right)^2 - f(\chi) \frac{d^2f}{d\chi^2} = \left(\frac{\mu_{nf}}{\rho_f} + \frac{1}{\mu_f \rho_{nf} \hat{\beta} h^*}\right) \frac{d^3f}{d\chi^3} \\
&\quad - \left[\frac{\bar{U}_w^3 \bar{x}}{(2\nu_f h^{*2})(\rho_{nf} \frac{\mu_f}{\rho_f} \hat{\beta} h^*)} \right] \left(\frac{d^2f}{d\chi^2}\right)^2 \frac{d^3f}{d\chi^3} - \frac{\sigma_{nf}^* B_0^2}{\rho_{nf} c^*} \frac{df}{d\chi} \sin^2(\Gamma).
\end{aligned}$$

The dimensionless momentum equation gets the following form :

$$\begin{aligned}
&A \left[\frac{df}{d\chi} + \frac{\chi}{2} \frac{d^2f}{d\chi^2} \right] + \left(\frac{df}{d\chi}\right)^2 - f(\chi) \frac{d^2f}{d\chi^2} \\
&= \left(\frac{1}{N_1 N_2} + \frac{1}{N_2 \mu_f \hat{\beta} h^*}\right) \frac{d^3f}{d\chi^3} - \left[\frac{\Delta}{N_2 \mu_f \hat{\beta} h^*} \right] \left(\frac{d^2f}{d\chi^2}\right)^2 \frac{d^3f}{d\chi^3} - \frac{N_5 \times \sigma_f B_0^2}{N_2 \times \rho_f c^*} \frac{df}{d\chi} \sin^2(\Gamma). \\
&\left(\frac{1}{N_1 N_2} + \frac{w}{N_2}\right) \frac{d^3f}{d\chi^3} - A \left[\frac{df}{d\chi} + \frac{\chi}{2} \frac{d^2f}{d\chi^2} \right] - \left(\frac{df}{d\chi}\right)^2 + f \frac{d^2f}{d\chi^2} - \frac{\Delta w}{N_2} \left(\frac{d^2f}{d\chi^2}\right)^2 \frac{d^3f}{d\chi^3} \\
&- \frac{N_5}{N_2} M \frac{df}{d\chi} \sin^2(\Gamma) = 0. \tag{3.39}
\end{aligned}$$

Now, the dimensionless form of the energy equation (3.5) can be obtained by using equations (3.25)- (3.33), (3.34), (3.36), (3.37) and (3.38) as follows,

$$\begin{aligned}
&\frac{\partial \Theta}{\partial \tilde{t}} + \bar{f}_1 \frac{\partial \Theta}{\partial \bar{x}} + \bar{f}_2 \frac{\partial \Theta}{\partial \bar{y}} = \frac{k_{nf}}{(\rho C_p)_{nf}} \left(\frac{\partial^2 \Theta}{\partial \bar{y}^2}\right) - \frac{1}{(\rho C_p)_{nf}} \left(\frac{\partial q_r}{\partial \bar{y}}\right) + \frac{\nu_{nf}}{(\rho C_p)_{nf}} \left(\frac{\partial \bar{f}_1}{\partial \bar{y}}\right)^2 \\
&\quad + \frac{\sigma_{nf}^* B^2(\tilde{t}) \bar{f}_1^2}{(\rho C_p)_{nf}} \sin^2(\Gamma). \\
&\Rightarrow \frac{c^* \bar{x} \bar{\xi}}{(1-\bar{\xi}\tilde{t})^2} \theta(\chi) + \frac{c^{*2} \bar{x} \bar{\xi}}{\nu_f(1-\bar{\xi}\tilde{t})^3} \frac{\bar{y}}{2} \sqrt{\frac{\nu_f(1-\bar{\xi}\tilde{t})}{c^*}} \frac{d\theta}{d\chi} + \frac{c^{*2}}{(1-\bar{\xi}\tilde{t})^2} \bar{x} \frac{df}{d\chi} \theta(\chi) - \frac{c^{*2} \bar{x}}{(1-\bar{\xi}\tilde{t})^2} f(\chi) \\
&\quad \frac{d\theta}{d\chi} = \frac{k_{nf}}{(\rho C_p)_{nf}} \frac{c^{*2} \bar{x}}{\nu_f(1-\bar{\xi}\tilde{t})^2} \frac{d^2\theta}{d\chi^2} - \frac{1}{(\rho C_p)_{nf}} \left[\frac{-16\Theta_\infty^3 \sigma^*}{3k^*} \left(\frac{\partial^2 \Theta}{\partial \bar{y}^2}\right) \right] + \frac{\nu_{nf}}{(\rho C_p)_{nf}} \\
&\quad \frac{c^{*3} \bar{x}^2}{\nu_f(1-\bar{\xi}\tilde{t})^3} \left(\frac{d^2f}{d\chi^2}\right)^2 + \frac{\sigma_{nf}^*}{(\rho C_p)_{nf}} \frac{B_0^2}{(\sqrt{(1-\bar{\xi}\tilde{t})^2} (1-\bar{\xi}\tilde{t})^2)} \left(\frac{df}{d\chi}\right)^2 \sin^2(\Gamma).
\end{aligned}$$

$$\begin{aligned}
&\Rightarrow \frac{c^* \bar{x} \bar{\xi}}{(1 - \bar{\xi} \bar{t})^2} \theta(\chi) + \frac{c^* \bar{\xi}}{2(1 - \bar{\xi} \bar{t})^2} \sqrt{\frac{\nu_f c^{*2} (1 - \bar{\xi} \bar{t})}{\nu_f^2 c^* (1 - \bar{\xi} \bar{t})^2}} \bar{x} \bar{y} \frac{d\theta}{d\chi} + \frac{c^{*2}}{(1 - \bar{\xi} \bar{t})^2} \bar{x} \frac{df}{d\chi} \theta(\chi) - \frac{c^{*2} \bar{x}}{(1 - \bar{\xi} \bar{t})^2} \\
&f(\chi) \frac{d\theta}{d\chi} = \frac{k_{nf}}{(\rho C_p)_{nf}} \frac{c^{*2} \bar{x}}{\nu_f (1 - \bar{\xi} \bar{t})^2} \frac{d^2 \theta}{d\chi^2} + \frac{16\Theta_\infty^3 \sigma^*}{(\rho C_p)_{nf} 3k^*} \frac{c^{*2} \bar{x}}{\nu_f (1 - \bar{\xi} \bar{t})^2} \frac{d^2 \theta}{d\chi^2} + \frac{\nu_{nf}}{(\rho C_p)_{nf}} \\
&\frac{c^{*3} \bar{x}^2}{\nu_f (1 - \bar{\xi} \bar{t})^3} \left(\frac{d^2 f}{d\chi^2} \right)^2 + \frac{\sigma_{nf}^*}{(\rho C_p)_{nf}} \frac{B_0^2}{(\sqrt{(1 - \bar{\xi} \bar{t})})^2} \frac{(c^* \bar{x})^2}{(1 - \bar{\xi} \bar{t})^2} \left(\frac{df}{d\chi} \right)^2 \sin^2(\Gamma). \\
&\Rightarrow \frac{c^* \bar{x} \bar{\xi}}{(1 - \bar{\xi} \bar{t})^2} \theta(\chi) + \frac{c^* \bar{\xi}}{2(1 - \bar{\xi} \bar{t})^2} \sqrt{\frac{c^*}{\nu_f (1 - \bar{\xi} \bar{t})}} \bar{x} \bar{y} \frac{d\theta}{d\chi} + \frac{c^{*2}}{(1 - \bar{\xi} \bar{t})^2} \bar{x} \frac{df}{d\chi} \theta(\chi) - \frac{c^{*2} \bar{x}}{(1 - \bar{\xi} \bar{t})^2} \\
&f(\chi) \frac{d\theta}{d\chi} = \frac{k_{nf}}{(\rho C_p)_{nf}} \frac{c^{*2} \bar{x}}{\nu_f (1 - \bar{\xi} \bar{t})^2} \frac{d^2 \theta}{d\chi^2} + \frac{16\Theta_\infty^3 \sigma^*}{(\rho C_p)_{nf} 3k^*} \frac{c^{*2} \bar{x}}{\nu_f (1 - \bar{\xi} \bar{t})^2} \frac{d^2 \theta}{d\chi^2} + \frac{\nu_{nf}}{(\rho C_p)_{nf}} \\
&\frac{c^{*3} \bar{x}^2}{\nu_f (1 - \bar{\xi} \bar{t})^3} \left(\frac{d^2 f}{d\chi^2} \right)^2 + \frac{\sigma_{nf}^*}{(\rho C_p)_{nf}} \frac{B_0^2}{(\sqrt{(1 - \bar{\xi} \bar{t})})^2} \frac{(c^* \bar{x})^2}{(1 - \bar{\xi} \bar{t})^2} \left(\frac{df}{d\chi} \right)^2 \sin^2(\Gamma). \\
&\Rightarrow \frac{\bar{\xi}}{c^*} \theta(\chi) + \frac{\bar{\xi}}{c^*} \frac{\chi}{2} \frac{d\theta}{d\chi} + \frac{df}{d\chi} \theta(\chi) - f(\chi) \frac{d\theta}{d\chi} = \frac{k_{nf}}{(\rho C_p)_{nf}} \frac{1}{\nu_f} \frac{d^2 \theta}{d\chi^2} + \frac{16\Theta_\infty^3 \sigma^*}{(\rho C_p)_{nf} 3k^*} \frac{1}{\nu_f} \frac{d^2 \theta}{d\chi^2} \\
&+ \frac{\nu_{nf}}{(\rho C_p)_{nf}} \frac{c^* \bar{x}}{\nu_f (1 - \bar{\xi} \bar{t})} \left(\frac{d^2 f}{d\chi^2} \right)^2 + \frac{\sigma_{nf}^*}{(\rho C_p)_{nf}} \frac{B_0^2 \bar{x}}{(1 - \bar{\xi} \bar{t})} \left(\frac{df}{d\chi} \right)^2 \sin^2(\Gamma). \\
&\Rightarrow A \left[\theta(\chi) + \frac{\chi}{2} \frac{d\theta}{d\chi} \right] + \frac{df}{d\chi} \theta(\chi) - f(\chi) \frac{d\theta}{d\chi} = \frac{k_{nf}}{(\rho C_p)_{nf}} \frac{1}{\nu_f} \frac{d^2 \theta}{d\chi^2} + \frac{16\Theta_\infty^3 \sigma^*}{(\rho C_p)_{nf} 3k^*} \frac{1}{\nu_f} \frac{d^2 \theta}{d\chi^2} \\
&+ \frac{\nu_{nf}}{(\rho C_p)_{nf}} \frac{\bar{U}_w}{\nu_f} \left(\frac{d^2 f}{d\chi^2} \right)^2 + \frac{\sigma_{nf}^*}{(\rho C_p)_{nf}} \frac{B_0^2}{c^*} \frac{c^* \bar{x}}{(1 - \bar{\xi} \bar{t})} \left(\frac{df}{d\chi} \right)^2 \sin^2(\Gamma). \\
&\Rightarrow A \left[\theta(\chi) + \frac{\chi}{2} \frac{d\theta}{d\chi} \right] + \frac{df}{d\chi} \theta(\chi) - f(\chi) \frac{d\theta}{d\chi} = \frac{N_4 \times k_f}{N_3 \times (\rho C_p)_f} \frac{1}{\nu_f} \frac{d^2 \theta}{d\chi^2} + \frac{16\Theta_\infty^3 \sigma^*}{N_3 (\rho C_p)_f 3k^*} \frac{1}{\nu_f} \frac{d^2 \theta}{d\chi^2} \\
&+ \frac{\frac{\mu_f}{N_1}}{\frac{\mu_f}{N_3} (\rho C_p)_f} \frac{\bar{U}_w}{\nu_f} \left(\frac{d^2 f}{d\chi^2} \right)^2 + \frac{N_5 \sigma_f}{N_3 (\rho C_p)_f} \frac{B_0^2 \bar{U}_w}{c^*} \left(\frac{df}{d\chi} \right)^2 \sin^2(\Gamma). \\
&\Rightarrow A \left[\theta(\chi) + \frac{\chi}{2} \frac{d\theta}{d\chi} \right] + \frac{df}{d\chi} \theta(\chi) - f(\chi) \frac{d\theta}{d\chi} = \frac{N_4}{N_3 Pr} \frac{d^2 \theta}{d\chi^2} + \frac{Nr}{N_3} \frac{d^2 \theta}{d\chi^2} + \frac{E_c}{N_1 N_3} \left(\frac{d^2 f}{d\chi^2} \right)^2 \\
&+ \frac{N_5}{N_3} M \frac{\bar{U}_w}{(C_p)_f} \left(\frac{df}{d\chi} \right)^2 \sin^2(\Gamma). \\
&\Rightarrow \frac{N_3 Pr}{N_4} \left[A \left[\theta(\chi) + \frac{\chi}{2} \frac{d\theta}{d\chi} \right] + \frac{df}{d\chi} \theta(\chi) - f(\chi) \frac{d\theta}{d\chi} \right] = \frac{d^2 \theta}{d\chi^2} + \frac{Pr Nr}{N_4} \frac{d^2 \theta}{d\chi^2} + \frac{E_c Pr}{N_1 N_4} \left(\frac{d^2 f}{d\chi^2} \right)^2 + \\
&\frac{Pr N_5}{N_4} E_c M \left(\frac{df}{d\chi} \right)^2 \sin^2(\Gamma). \\
&\Rightarrow \frac{d^2 \theta}{d\chi^2} + \frac{Pr Nr}{N_4} \frac{d^2 \theta}{d\chi^2} - \frac{N_3 Pr}{N_4} \left[A \left[\theta(\chi) + \frac{\chi}{2} \frac{d\theta}{d\chi} \right] + \frac{df}{d\chi} \theta(\chi) - f(\chi) \frac{d\theta}{d\chi} \right] + \frac{E_c Pr}{N_1 N_4} \left(\frac{d^2 f}{d\chi^2} \right)^2 + \\
&\frac{Pr N_5}{N_4} E_c M \left(\frac{df}{d\chi} \right)^2 \sin^2(\Gamma) = 0.
\end{aligned}$$

$$\begin{aligned}
&\Rightarrow \left(1 + \frac{PrNr}{N_4}\right) \frac{d^2\theta}{d\chi^2} - \frac{N_3Pr}{N_4} \left[A \left[\theta(\chi) + \frac{\chi}{2} \frac{d\theta}{d\chi} \right] + \frac{df}{d\chi} \theta(\chi) - f(\chi) \frac{d\theta}{d\chi} - \frac{E_c}{N_1N_3} \left(\frac{d^2f}{d\chi^2} \right)^2 \right. \\
&\quad \left. - \frac{N_5}{N_3} ME_c \left(\frac{df}{d\chi} \right)^2 \sin^2(\Gamma) \right] = 0. \\
&\Rightarrow \left(1 + \frac{PrNr}{N_4}\right) \frac{d^2\theta}{d\chi^2} + \frac{N_3Pr}{N_4} \left[f \frac{d\theta}{d\chi} - \frac{df}{d\chi} \theta - A \left[\theta + \frac{\chi}{2} \frac{d\theta}{d\chi} \right] + \frac{E_c}{N_1N_3} \left(\frac{d^2f}{d\chi^2} \right)^2 + \frac{N_5}{N_3} \right. \\
&\quad \left. ME_c \left(\frac{df}{d\chi} \right)^2 \sin^2(\Gamma) \right] = 0. \tag{3.40}
\end{aligned}$$

The boundary conditions corresponding to PDEs have been transformed into the dimensionless form through the following procedure:

$$\begin{aligned}
&\bar{f}_2(\bar{x}, 0) = \bar{V}_w, && \text{at } \bar{y} = 0. \\
&\Rightarrow \bar{V}_w = -\sqrt{\frac{\nu_f c^*}{1 - \bar{\xi}\bar{t}}} f(\chi), && \text{at } \chi = 0. \\
&\Rightarrow f(\chi) = -\bar{V}_w \sqrt{\frac{1 - \bar{\xi}\bar{t}}{\nu_f c^*}}, && \text{at } \chi = 0. \\
&\Rightarrow f(0) = S. \\
&\bar{f}_1(\bar{x}, 0) = \bar{U}_w + \mu_{nf} \left(\frac{\partial \bar{f}_1}{\partial \bar{y}} \right), && \text{at } \bar{y} = 0. \\
&\Rightarrow \frac{c^* \bar{x}}{1 - \bar{\xi}\bar{t}} \frac{df}{d\chi} = \frac{c^* \bar{x}}{1 - \bar{\xi}\bar{t}} + \frac{c^* \bar{x}}{1 - \bar{\xi}\bar{t}} \sqrt{\frac{c^*}{\nu_f (1 - \bar{\xi}\bar{t})}} \frac{\mu_f}{N_1} \frac{d^2f}{d\chi^2}, && \text{at } \chi = 0. \\
&\Rightarrow \frac{c^* \bar{x}}{1 - \bar{\xi}\bar{t}} \frac{df}{d\chi} = \frac{c^* \bar{x}}{1 - \bar{\xi}\bar{t}} \left(1 + \sqrt{\frac{c^*}{\nu_f (1 - \bar{\xi}\bar{t})}} \frac{\mu_f}{N_1} \frac{d^2f}{d\chi^2} \right), && \text{at } \chi = 0. \\
&\Rightarrow \frac{df}{d\chi} = 1 + \frac{\Lambda}{N_1} \frac{d^2f}{d\chi^2}, && \text{at } \chi = 0. \\
&\Rightarrow \frac{df}{d\chi}(0) = 1 + \frac{\Lambda}{N_1} \frac{d^2f}{d\chi^2}(0). \\
&\quad -k_0 \left(\frac{\partial \Theta}{\partial \bar{y}} \right) = h_f (\Theta_f - \Theta), && \text{at } \bar{y} = 0. \\
&\Rightarrow -k_0 \frac{c^* \bar{x}}{1 - \bar{\xi}\bar{t}} \sqrt{\frac{c^*}{\nu_f (1 - \bar{\xi}\bar{t})}} \frac{d\theta}{d\chi} = h_f \left(\Theta_\infty + \frac{c^* \bar{x}}{1 - \bar{\xi}\bar{t}} - \Theta \right), && \text{at } \chi = 0. \\
&\Rightarrow \frac{c^* \bar{x}}{1 - \bar{\xi}\bar{t}} \frac{d\theta}{d\chi} = \frac{-h_f}{k_0} \sqrt{\frac{\nu_f (1 - \bar{\xi}\bar{t})}{c^*}} \left(\Theta_\infty + \frac{c^* \bar{x}}{1 - \bar{\xi}\bar{t}} - \frac{c^* \bar{x}}{1 - \bar{\xi}\bar{t}} \theta(\chi) - \Theta_\infty \right), && \text{at } \chi = 0. \\
&\Rightarrow \frac{c^* \bar{x}}{1 - \bar{\xi}\bar{t}} \frac{d\theta}{d\chi} = -\frac{h_f}{k_0} \sqrt{\frac{\nu_f (1 - \bar{\xi}\bar{t})}{c^*}} \left(\frac{c^* \bar{x}}{1 - \bar{\xi}\bar{t}} - \frac{c^* \bar{x}}{1 - \bar{\xi}\bar{t}} \theta(\chi) \right), && \text{at } \chi = 0. \\
&\Rightarrow \frac{c^* \bar{x}}{1 - \bar{\xi}\bar{t}} \frac{d\theta}{d\chi} = -\frac{h_f}{k_0} \sqrt{\frac{\nu_f (1 - \bar{\xi}\bar{t})}{c^*}} \frac{c^* \bar{x}}{1 - \bar{\xi}\bar{t}} (1 - \theta(\chi)), && \text{at } \chi = 0. \\
&\Rightarrow \frac{d\theta}{d\chi} = -Bi(1 - \theta(\chi)), && \text{at } \chi = 0. \\
&\Rightarrow \frac{d\theta}{d\chi}(0) = -Bi(1 - \theta(0)).
\end{aligned}$$

$$\begin{aligned}
& \bar{f}_1 \rightarrow 0, & \text{as } \bar{y} \rightarrow \infty. \\
\Rightarrow & \frac{c^* \bar{x}}{1 - \bar{\xi} \bar{t}} \frac{df}{d\chi} \rightarrow 0, & \text{as } \bar{y} \rightarrow \infty. \\
\Rightarrow & \frac{df}{d\chi} \rightarrow 0, & \text{as } \chi \rightarrow \infty. \\
& \Theta \rightarrow \Theta_\infty, & \text{as } \bar{y} \rightarrow \infty. \\
\Rightarrow & \Theta_\infty + \frac{c^* \bar{x}}{1 - \bar{\xi} \bar{t}} \theta(\chi) \rightarrow \Theta_\infty, & \text{as } \bar{y} \rightarrow \infty. \\
\Rightarrow & \theta(\chi) \rightarrow 0, & \text{as } \chi \rightarrow \infty.
\end{aligned}$$

By combining (3.39) and (3.40),

$$\begin{aligned}
& \left(\frac{1}{N_1 N_2} + \frac{w}{N_2} \right) \frac{d^3 f}{d\chi^3} - A \left[\frac{df}{d\chi} + \frac{\chi}{2} \frac{d^2 f}{d\chi^2} \right] - \left(\frac{df}{d\chi} \right)^2 + f \frac{d^2 f}{d\chi^2} - \frac{\Delta w}{N_2} \left(\frac{d^2 f}{d\chi^2} \right)^2 \frac{d^3 f}{d\chi^3} \\
& - \frac{N_5}{N_2} M \frac{df}{d\chi} \sin^2(\Gamma) = 0, \tag{3.41}
\end{aligned}$$

$$\begin{aligned}
& \left(1 + \frac{Pr Nr}{N_4} \right) \frac{d^2 \theta}{d\chi^2} + \frac{N_3 Pr}{N_4} \left[f \frac{d\theta}{d\chi} - \frac{df}{d\chi} \theta - A \left[\theta + \frac{\chi}{2} \frac{d\theta}{d\chi} \right] + \frac{E_c}{N_1 N_3} \left(\frac{d^2 f}{d\chi^2} \right)^2 \right. \\
& \left. + \frac{N_5}{N_3} M E_c \left(\frac{df}{d\chi} \right)^2 \sin^2(\Gamma) \right] = 0. \tag{3.42}
\end{aligned}$$

The dimensionless form of BCs corresponding to (3.6), are given below:

$$\left. \begin{aligned}
f(0) = S, \quad \frac{df}{d\chi}(0) = 1 + \frac{\Lambda}{N_1} \frac{d^2 f}{d\chi^2}(0), \quad \frac{df}{d\chi}(\chi) \rightarrow 0, \quad \text{as } \chi \rightarrow \infty, \\
\frac{d\theta}{d\chi}(0) = -Bi(1 - \theta(0)), \quad \theta(\chi) \rightarrow 0, \quad \text{as } \chi \rightarrow \infty
\end{aligned} \right\} \tag{3.43}$$

Moreover, $A = \frac{\bar{\xi}}{c^*}$ is the unsteady flow parameter, $w = \frac{1}{\mu_f \hat{\beta} h^*}$ and $\Delta = \frac{\bar{U}_w^3 \bar{x}}{2h^{*2} \nu_f}$ are

the material parameter, $M = \frac{\sigma_f B_0^2}{c^* \rho_f}$ is the magnetic parameter, and $Pr = \frac{\nu_f}{\alpha_f}$ is the Prandtl number, $\alpha_f = \frac{k_f}{(\rho C_p)_f}$ is the thermal diffusivity parameter, $N_r =$

$\frac{16}{3} \frac{\sigma^* T_\infty^3}{k^* \nu_f (\rho C_p)_f}$ is the thermal radiation parameter, $S = -\bar{V}_w \sqrt{\frac{(1 - \bar{\xi} \bar{t})}{\nu_f c^*}}$ is the mass

transfer parameter, $\Lambda = \sqrt{\frac{c^*}{\nu_f (1 - \bar{\xi} \bar{t})}} \mu_f$ is the velocity slip parameter, $E_c = \frac{\bar{U}_w}{(C_p)_f}$ is

the Eckert number and $B_i = \frac{h_f}{k_0} \sqrt{\frac{\nu_f (1 - \bar{\xi} \bar{t})}{c^*}}$ is the Biot number.

3.3.2 Physical Quantities of Interest

The local Nusselt number $Nu_{\bar{x}}$ and the skin friction coefficient $C_{f\bar{x}}$ are of significance to us at this point. These physical quantities have the following descriptions:

3.3.2.1 Skin Friction Coefficient:

The dimensional form of coefficient of skin friction is given as:

$$C_f = \frac{\tau_w}{\rho_f \bar{U}_w^2}. \quad (3.44)$$

In order to obtain the dimensionless form of C_f , the following procedure will be adopted:

$$\tau_w = \left[\left(\mu_{nf} + \frac{1}{\hat{\beta}h^*} \right) \left(\frac{\partial \bar{f}_1}{\partial \bar{y}} \right) - \frac{1}{6\hat{\beta}h^{*3}} \left(\frac{\partial \bar{f}_1}{\partial \bar{y}} \right)^3 \right] \Bigg|_{\bar{y}=0}. \quad (3.45)$$

By using (3.19) in (3.45), we get

$$\tau_w = - \left[\left(\mu_{nf} + \frac{1}{\hat{\beta}h^*} \right) \frac{c^*}{1-\xi\bar{t}} \sqrt{\frac{c^*}{\nu_f(1-\xi\bar{t})}} \bar{x} \frac{d^2 f}{d\chi^2} - \frac{1}{6\hat{\beta}h^{*3}} \left(\frac{c^*}{1-\xi\bar{t}} \sqrt{\frac{c^*}{\nu_f(1-\xi\bar{t})}} \bar{x} \frac{d^2 f}{d\chi^2} \right)^3 \right] \Bigg|_{\bar{y}=0}.$$

Putting τ_w in (3.44), we get

$$\begin{aligned} C_f &= \frac{- \left[\left(\mu_{nf} + \frac{1}{\hat{\beta}h^*} \right) \frac{c^*}{1-\xi\bar{t}} \sqrt{\frac{c^*}{\nu_f(1-\xi\bar{t})}} \bar{x} \frac{d^2 f}{d\chi^2} - \frac{1}{6\hat{\beta}h^{*3}} \left(\frac{c^*}{1-\xi\bar{t}} \sqrt{\frac{c^*}{\nu_f(1-\xi\bar{t})}} \bar{x} \frac{d^2 f}{d\chi^2} \right)^3 \right] \Bigg|_{\bar{y}=0}}{\rho_f \bar{U}_w^2} \\ &= \frac{- \left[\left(\frac{\mu_f}{N_1} + \frac{1}{\hat{\beta}h^*} \right) \frac{c^*}{1-\xi\bar{t}} \sqrt{\frac{c^*}{\nu_f(1-\xi\bar{t})}} \bar{x} \frac{d^2 f}{d\chi^2} - \frac{1}{6\hat{\beta}h^{*3}} \frac{c^{*3}}{(1-\xi\bar{t})^3} \left(\sqrt{\frac{c^*}{\nu_f(1-\xi\bar{t})}} \bar{x} \frac{d^2 f}{d\chi^2} \right)^3 \right] \Bigg|_{\bar{y}=0}}{\rho_f \bar{U}_w^2} \\ &= \frac{- \left[\left(\frac{\mu_f}{N_1} + \frac{1}{\hat{\beta}h^*} \right) \bar{U}_w \sqrt{\frac{c^*}{\nu_f(1-\xi\bar{t})}} \bar{x} \frac{d^2 f}{d\chi^2} - \frac{1}{6\hat{\beta}h^{*3}} \bar{U}_w^3 \left(\sqrt{\frac{c^*}{\nu_f(1-\xi\bar{t})}} \bar{x} \frac{d^2 f}{d\chi^2} \right)^3 \right] \Bigg|_{\bar{y}=0}}{\rho_f \bar{U}_w^2} \\ &= \frac{- \left[\left(\frac{\mu_f}{N_1 \mu_f} + \frac{1}{\hat{\beta}h^* \mu_f} \right) \bar{U}_w \sqrt{\frac{c^*}{\nu_f(1-\xi\bar{t})}} \bar{x} \frac{d^2 f}{d\chi^2} - \frac{1}{6\hat{\beta}h^{*3} \mu_f} \bar{U}_w^3 \left(\sqrt{\frac{c^*}{\nu_f(1-\xi\bar{t})}} \bar{x} \frac{d^2 f}{d\chi^2} \right)^3 \right] \Bigg|_{\bar{y}=0}}{\frac{\rho_f \bar{U}_w^2}{\mu_f}} \end{aligned}$$

$$\begin{aligned}
&= \frac{- \left[\left(\frac{1}{N_1} + \frac{1}{\hat{\beta}h^*\mu_f} \right) \frac{d^2f}{d\chi^2}(0) - \frac{1}{6\hat{\beta}h^{*3}\mu_f} \bar{U}_w^2 \frac{c^*\bar{x}^2}{\nu_f(1-\xi\bar{t})} \left(\frac{d^2f}{d\chi^2} \right)^3(0) \right] \sqrt{\frac{c^*}{\nu_f(1-\xi\bar{t})} \bar{x}}}{\frac{\bar{U}_w\bar{x}}{\nu_f}} \\
&= \frac{- \left[\left(\frac{1}{N_1} + \frac{1}{\hat{\beta}h^*\mu_f} \right) \frac{d^2f}{d\chi^2}(0) - \frac{1}{6\hat{\beta}h^{*3}\mu_f} \bar{U}_w^2 \frac{c^*\bar{x}\cdot\bar{x}}{\nu_f(1-\xi\bar{t})} \left(\frac{d^2f}{d\chi^2} \right)^3(0) \right] \sqrt{\frac{c^*}{\nu_f(1-\xi\bar{t})} \bar{x}}}{\frac{\bar{U}_w\bar{x}}{\nu_f}} \\
&= \frac{- \left[\left(\frac{1}{N_1} + \frac{1}{\hat{\beta}h^*\mu_f} \right) \frac{d^2f}{d\chi^2}(0) - \frac{1}{3} \frac{1}{\hat{\beta}h^*\mu_f} \frac{\bar{U}_w\bar{x}}{2h^{*2}\nu_f} \left(\frac{d^2f}{d\chi^2} \right)^3(0) \right] \sqrt{\frac{c^*\bar{x}}{\nu_f\bar{x}(1-\xi\bar{t})} \bar{x}}}{\frac{\bar{U}_w\bar{x}}{\nu_f}} \\
&= \frac{- \left[\left(\frac{1}{N_1} + \frac{1}{\hat{\beta}h^*\mu_f} \right) \frac{d^2f}{d\chi^2}(0) - \frac{1}{3} \frac{1}{\hat{\beta}h^*\mu_f} \frac{\bar{U}_w^3\bar{x}}{2h^{*2}\nu_f} \left(\frac{d^2f}{d\chi^2} \right)^3(0) \right] \sqrt{\frac{\bar{U}_w\bar{x}^2}{\nu_f\bar{x}}}}{\frac{\bar{U}_w\bar{x}}{\nu_f}} \\
&= \frac{- \left[\left(\frac{1}{N_1} + \omega \right) \frac{d^2f}{d\chi^2}(0) - \frac{1}{3} \omega \Delta \left(\frac{d^2f}{d\chi^2} \right)^3(0) \right] \sqrt{\frac{\bar{U}_w\bar{x}}{\nu_f}}}{Re_{\bar{x}}} \\
&= \frac{- \left[\left(\frac{1}{N_1} + \omega \right) \frac{d^2f}{d\chi^2}(0) - \frac{\omega\Delta}{3} \left(\frac{d^2f}{d\chi^2} \right)^3(0) \right] \sqrt{Re_{\bar{x}}}}{Re_{\bar{x}}} \\
&= \frac{- \left[\left(\frac{1}{N_1} + \omega \right) \frac{d^2f}{d\chi^2}(0) - \frac{\omega\Delta}{3} \left(\frac{d^2f}{d\chi^2} \right)^3(0) \right]}{\sqrt{Re_{\bar{x}}}}.
\end{aligned}$$

Hence, the dimensionless form of the coefficient of skin friction is

$$C_f Re_{\bar{x}}^{\frac{1}{2}} = - \left[\left(\frac{1}{N_1} + \omega \right) \frac{d^2f}{d\chi^2}(0) - \frac{\omega\Delta}{3} \left(\frac{d^2f}{d\chi^2} \right)^3(0) \right], \quad (3.46)$$

where $Re_{\bar{x}}$ represents the Reynolds number defined as $Re_{\bar{x}} = \frac{\bar{U}_w\bar{x}}{\nu_f}$.

3.3.2.2 Nusselt Number:

The dimensional form of the local Nusselt number is defined as:

$$Nu_{\bar{x}} = \frac{\bar{x}q_w}{k_f(\Theta_f - \Theta_\infty)}, \quad (3.47)$$

where q_w is formulated as

$$q_w = -k_{nf} \left(1 + \frac{16}{3} \frac{\sigma^* \Theta_\infty^3}{k^* \nu_f (\rho C_p)_f} \right) \left(\frac{\partial \Theta}{\partial \bar{y}} \right) \Big|_{\bar{y}=0}. \quad (3.48)$$

Using (3.26) in (3.48), we get

$$q_w = -k_{nf} \left(1 + \frac{16}{3} \frac{\sigma^* \Theta_\infty^3}{k^* \nu_f (\rho C_p)_f} \right) \left(\frac{c^* \bar{x}}{1 - \bar{\xi} \bar{t}} \frac{d\theta}{d\chi} \sqrt{\frac{c^*}{\nu_f (1 - \bar{\xi} \bar{t})}} \right) \Big|_{\bar{y}=0}.$$

Putting q_w in (3.47), we get

$$\begin{aligned} Nu_{\bar{x}} &= - \frac{\bar{x} k_{nf} \left(1 + \frac{16}{3} \frac{\sigma^* \Theta_\infty^3}{k^* \nu_f (\rho C_p)_f} \right) \left(\frac{c^* \bar{x}}{1 - \bar{\xi} \bar{t}} \frac{d\theta}{d\chi} \sqrt{\frac{c^*}{\nu_f (1 - \bar{\xi} \bar{t})}} \right) \Big|_{\bar{y}=0}}{k_f (\Theta_w - \Theta_\infty)} \\ &= - \frac{\bar{x} k_{nf} \left(1 + \frac{4(4)}{3} \frac{\sigma^* \Theta_\infty^3}{k^* \nu_f (\rho C_p)_f} \right) \left(\frac{c^* \bar{x}}{1 - \bar{\xi} \bar{t}} \frac{d\theta}{d\chi} (0) \sqrt{\frac{c^*}{\nu_f (1 - \bar{\xi} \bar{t})}} \right)}{k_f \frac{c^* \bar{x}}{1 - \bar{\xi} \bar{t}}} \\ &= - \frac{\bar{x} k_{nf} \left(1 + \frac{4(4)}{3} \frac{\sigma^* \Theta_\infty^3}{k^* \nu_f (\rho C_p)_f} \right) \frac{d\theta}{d\chi} (0) \sqrt{\frac{c^*}{\nu_f (1 - \bar{\xi} \bar{t})}}}{k_f} \\ &= - \frac{k_{nf}}{k_f} \left(1 + \frac{4(4)}{3} \frac{\sigma^* \Theta_\infty^3}{k^* \nu_f (\rho C_p)_f} \right) \frac{d\theta}{d\chi} (0) \sqrt{\frac{c^* \bar{x}}{\nu_f \bar{x} (1 - \bar{\xi} \bar{t})}} \bar{x} \\ &= - \frac{k_{nf}}{k_f} (1 + Nr) \frac{d\theta}{d\chi} (0) \sqrt{\frac{\bar{U}_w \bar{x}^2}{\nu_f \bar{x}}} \\ &= - \frac{k_{nf}}{k_f} (1 + Nr) \frac{d\theta}{d\chi} (0) \sqrt{Re_{\bar{x}}}. \\ &\Rightarrow \frac{Nu_{\bar{x}}}{Re_{\bar{x}}^{\frac{1}{2}}} = - \frac{k_{nf}}{k_f} (1 + Nr) \frac{d\theta}{d\chi} (0). \\ &\Rightarrow Nu_{\bar{x}} Re_{\bar{x}}^{-\frac{1}{2}} = - \frac{k_{nf}}{k_f} (1 + Nr) \frac{d\theta}{d\chi} (0). \end{aligned} \quad (3.49)$$

Finally,

$$\left. \begin{aligned} C_f Re_{\bar{x}}^{\frac{1}{2}} &= - \left[\left(\frac{1}{N_1} + \omega \right) \frac{d^2 f}{d\chi^2}(0) - \frac{\omega \Delta}{3} \left(\frac{d^2 f}{d\chi^2} \right)^3(0) \right], \\ Nu_{\bar{x}} Re_{\bar{x}}^{-\frac{1}{2}} &= - \frac{k_{nf}}{k_f} (1 + Nr) \frac{d\theta}{d\chi}(0). \end{aligned} \right\} \quad (3.50)$$

3.3.3 Entropy Generation

Using (3.23), (3.27), (3.34) (3.37) and (3.38), the dimensionless form of E_G , is:

$$\begin{aligned} E_G &= \frac{k_{nf}}{\Theta_{\infty}^2} \left[(1 + Nr) \frac{c^{*3} \bar{x}^2}{\nu_f (1 - \bar{\xi} \bar{t})^3} \left(\frac{d\theta}{d\chi} \right)^2 \right] + \frac{\mu_{nf}}{\Theta_{\infty}} \frac{c^{*3} \bar{x}^2}{\nu_f (1 - \bar{\xi} \bar{t})^3} \left(\frac{d^2 f}{d\chi^2} \right)^2 + \frac{\sigma_{nf}^* B_0^2}{\Theta_{\infty}} \\ &\quad \frac{\sin^2(\Gamma)}{(\sqrt{(1 - \bar{\xi} \bar{t})})^2} \left[\frac{c^* \bar{x}}{(1 - \bar{\xi} \bar{t})} \frac{df}{d\chi} \right]^2. \\ \Rightarrow E_G &= \frac{N_4 k_f}{\Theta_{\infty}^2} \left[(1 + Nr) \frac{c^{*2} \bar{x}^2}{(1 - \bar{\xi} \bar{t})^2} \left(\frac{d\theta}{d\chi} \right)^2 \right] \frac{c^* \bar{x}}{\nu_f \bar{x} (1 - \bar{\xi} \bar{t})} + \frac{\mu_{nf}}{\Theta_{\infty}} \frac{c^{*2} \bar{x}^2}{(1 - \bar{\xi} \bar{t})^2} \frac{c^* \bar{x}}{\nu_f \bar{x} (1 - \bar{\xi} \bar{t})} \\ &\quad \left(\frac{d^2 f}{d\chi^2} \right)^2 + \frac{N_5 \sigma_f B_0^2 \sin^2(\Gamma)}{\Theta_{\infty} (1 - \bar{\xi} \bar{t})} \frac{c^{*2} \bar{x}^2}{(1 - \bar{\xi} \bar{t})^2} \left(\frac{df}{d\chi} \right)^2. \\ \Rightarrow E_G &= \frac{N_4 k_f}{\Theta_{\infty}^2} \left[(1 + Nr) (\Theta_f - \Theta_{\infty})^2 \left(\frac{d\theta}{d\chi} \right)^2 \right] \frac{\bar{U}_w}{\nu_f \bar{x}} + \frac{\mu_{nf}}{\Theta_{\infty}} \bar{U}_w^2 \frac{\bar{U}_w}{\nu_f \bar{x}} \left(\frac{d^2 f}{d\chi^2} \right)^2 + \frac{N_5 \sigma_f B_0^2}{\Theta_{\infty}} \\ &\quad \frac{\sin^2(\Gamma)}{(1 - \bar{\xi} \bar{t})} \bar{U}_w^2 \left(\frac{df}{d\chi} \right)^2. \\ \Rightarrow E_G &= \frac{N_4 k_f}{\Theta_{\infty}^2} \left[(1 + Nr) (\Theta_f - \Theta_{\infty})^2 \left(\frac{d\theta}{d\chi} \right)^2 \right] \frac{\bar{U}_w}{\nu_f \bar{x}} + \frac{\mu_f}{\Theta_{\infty}} \bar{U}_w^2 \frac{\bar{U}_w}{\nu_f \bar{x}} \left(\frac{d^2 f}{d\chi^2} \right)^2 + \frac{N_5 \sigma_f B_0^2}{\Theta_{\infty}} \\ &\quad \frac{\sin^2(\Gamma)}{(1 - \bar{\xi} \bar{t})} \bar{U}_w^2 \left(\frac{df}{d\chi} \right)^2. \end{aligned}$$

The dimensionless entropy generation is denoted by NG and is defined as:

$$NG = \frac{\Theta_{\infty}^2 c^{*2} E_G}{k_f (\Theta_f - \Theta_{\infty})^2}. \quad (3.51)$$

$$\begin{aligned} NG &= \frac{\Theta_{\infty}^2 c^{*2}}{k_f (\Theta_f - \Theta_{\infty})^2} \left[\frac{N_4 k_f}{\Theta_{\infty}^2} \left[(1 + Nr) (\Theta_f - \Theta_{\infty})^2 \left(\frac{d\theta}{d\chi} \right)^2 \right] \frac{\bar{U}_w}{\nu_f \bar{x}} + \frac{\mu_f}{\Theta_{\infty}} \bar{U}_w^2 \frac{\bar{U}_w}{\nu_f \bar{x}} \left(\frac{d^2 f}{d\chi^2} \right)^2 \right. \\ &\quad \left. + \frac{N_5 \sigma_f B_0^2 \sin^2(\Gamma)}{\Theta_{\infty} (1 - \bar{\xi} \bar{t})} \bar{U}_w^2 \left(\frac{df}{d\chi} \right)^2 \right]. \end{aligned}$$

$$\begin{aligned}
&= \left[N_4(1 + Nr) \left(\frac{d\theta}{d\chi} \right)^2 + \frac{1}{N_1} \frac{\Theta_\infty}{(\Theta_f - \Theta_\infty)} \frac{\mu_f \bar{U}_w^2}{k_f(\Theta_f - \Theta_\infty)} \left(\frac{d^2 f}{d\chi^2} \right)^2 \right] \frac{\bar{U}_w c^{*2}}{\nu_f \bar{x}} + \\
&\quad \frac{\Theta_\infty \bar{U}_w^2}{k_f(\Theta_f - \Theta_\infty)^2} \frac{N_5 \sigma_f B_0^2 \sin^2(\Gamma) c^{*2}}{(1 - \xi \tilde{t})} \left(\frac{df}{d\chi} \right)^2 \\
&= \left[N_4(1 + Nr) \left(\frac{d\theta}{d\chi} \right)^2 + \frac{1}{N_1} \frac{Br}{\Omega} \left(\frac{d^2 f}{d\chi^2} \right)^2 \right] Re + \frac{\Theta_\infty N_5}{(\Theta_f - \Theta_\infty)} \frac{\bar{U}_w^2}{k_f(\Theta_f - \Theta_\infty)} \frac{\sigma_f B_0^2}{\rho_f c^*} \rho_f c^* \\
&\quad \frac{\sin^2(\Gamma) c^{*2} \bar{x}}{(1 - \xi \tilde{t}) \bar{x}} \left(\frac{df}{d\chi} \right)^2 \\
&= \left[N_4(1 + Nr) \left(\frac{d\theta}{d\chi} \right)^2 + \frac{1}{N_1} \frac{Br}{\Omega} \left(\frac{d^2 f}{d\chi^2} \right)^2 \right] Re + \frac{N_5}{\Omega} \frac{\bar{U}_w^2 \mu_f}{k_f(\Theta_f - \Theta_\infty)} \frac{\sigma_f B_0^2}{c^* \rho_f} \frac{c^* \bar{x}}{(1 - \xi \tilde{t})} \\
&\quad \sin^2(\Gamma) \frac{c^{*2}}{\nu_f \bar{x}} \left(\frac{df}{d\chi} \right)^2 \\
&= \left[N_4(1 + Nr) \left(\frac{d\theta}{d\chi} \right)^2 + \frac{1}{N_1} \frac{Br}{\Omega} \left(\frac{d^2 f}{d\chi^2} \right)^2 \right] Re + \frac{N_5}{\Omega} Br M \frac{\bar{U}_w c^{*2}}{\nu_f \bar{x}} \sin^2(\Gamma) \left(\frac{df}{d\chi} \right)^2 \\
&= \left[N_4(1 + Nr) \left(\frac{d\theta}{d\chi} \right)^2 + \frac{1}{N_1} \frac{Br}{\Omega} \left(\frac{d^2 f}{d\chi^2} \right)^2 \right] Re + \frac{N_5 Br M R \sin^2(\Gamma)}{\Omega} \left(\frac{df}{d\chi} \right)^2 \\
&= Re \left[N_4(1 + Nr) \left(\frac{d\theta}{d\chi} \right)^2 + \frac{1}{N_1} \frac{Br}{\Omega} \left(\left(\frac{d^2 f}{d\chi^2} \right)^2 + N_1 N_5 M \sin^2(\Gamma) \left(\frac{df}{d\chi} \right)^2 \right) \right],
\end{aligned}$$

where $Re = \frac{\bar{U}_w c^2}{\nu_f \bar{x}}$, $Br = \frac{\mu_f \bar{U}_w^2}{k_f(\Theta_f - \Theta_\infty)}$ and $\Omega = \frac{\Theta_\infty}{(\Theta_f - \Theta_\infty)}$.

3.4 Solution Methodology

To find a numerical solution for the system of ODEs (3.41) and (3.42), subject to boundary conditions (3.43), the shooting method has been used. From equations (3.41) and (3.42),

$$\frac{d^3 f}{d\chi^3} = \frac{A \left[\frac{df}{d\chi} + \frac{\chi}{2} \frac{d^2 f}{d\chi^2} \right] + \left(\frac{df}{d\chi} \right)^2 - f \frac{d^2 f}{d\chi^2} + \frac{N_5}{N_2} M \frac{df}{d\chi} \sin^2(\Gamma)}{\left(\frac{1}{N_1 N_2} + \frac{w}{N_2} - \frac{\Delta w}{N_2} \left(\frac{d^2 f}{d\chi^2} \right)^2 \right)}, \quad (3.52)$$

$$\frac{d^2 \theta}{d\chi^2} = \frac{-\frac{N_3 Pr}{N_4} \left[f \frac{d\theta}{d\chi} - \frac{df}{d\chi} \theta - A \left[\theta + \frac{\chi}{2} \frac{d\theta}{d\chi} \right] + \frac{E_c}{N_1 N_3} \left(\frac{d^2 f}{d\chi^2} \right)^2 + \frac{N_5}{N_3} M E_c \left(\frac{df}{d\chi} \right)^2 \sin^2(\Gamma) \right]}{\left(1 + \frac{Pr Nr}{N_4} \right)}. \quad (3.53)$$

First, the equation (3.52), is solved numerically, and then the calculation results are obtained for f , $\frac{df}{d\chi}$ and $\frac{d^2f}{d\chi^2}$ will be used in (3.53), as a known input. To apply shooting method, we first convert the equations (3.52) and (3.53) into a system of first-order ordinary differential equations by using the following new variables:

$$f = y_1, \quad \frac{df}{d\chi} = y_1' = y_2, \quad \frac{d^2f}{d\chi^2} = y_2' = y_3, \quad \frac{d^3f}{d\chi^3} = y_3' = y_4 = y_5.$$

The momentum equation is therefore transformed into the system of first order ODEs that follows:

$$\begin{aligned} y_1' &= y_2, & y_1(0) &= S, \\ y_2' &= y_3, & y_2(0) &= 1 + \frac{\Lambda}{N_1} y_3(0), \\ y_3' &= \frac{A \left[y_2 + \frac{\chi}{2} y_3 \right] + y_2^2 - y_1 y_3 + \frac{N_5}{N_2} M y_2 \sin^2(\Gamma)}{\left(\frac{1}{N_1 N_2} + \frac{w}{N_2} - \frac{\Delta w}{N_2} y_3^2 \right)}, & y_3(0) &= \gamma. \end{aligned}$$

Here, γ is the assumed missing condition $\frac{d^2f}{d\chi^2}(0) = y_3(0)$. To solve the initial value problem above, we use the fourth-order Runge-Kutta method. An approximate solution to (3.52), can be obtained by converting the unbounded domain $[0, \infty)$ to the bounded domain $[0, \chi_\infty]$, where χ_∞ is a suitable finite positive real number. The missing condition γ must be chosen such that the component y_2 satisfies the following boundary condition:

$$y_2(\chi_\infty, \gamma) = 0.$$

Newton's technique was applied in the following iterative phases to solve the previous equation.

$$\gamma^{(n+1)} = \gamma^{(n)} - \left(\frac{y_2(\chi_\infty, \gamma)}{\frac{\partial}{\partial \gamma}(y_2(\chi_\infty, \gamma))} \right) \Big|_{r=r_n}.$$

In order to obtain the derivatives w.r.t. γ , following new notations will be used:

$$\frac{\partial y_1}{\partial \gamma} = y_4, \quad \frac{\partial y_2}{\partial \gamma} = y_5, \quad \frac{\partial y_3}{\partial \gamma} = y_6.$$

Consequently, the Newton's iterative technique takes on the subsequent form:

$$\gamma^{(n+1)} = \gamma^{(n)} - \left(\frac{y_2(\chi_\infty, \gamma)}{y_5(\chi_\infty, \gamma)} \right)^{(n)}.$$

Now differentiating the system of first order ordinary differential equations with respect to γ , three more equations will be appeared, which are:

$$\begin{aligned} y_4' &= y_5, & y_4(0) &= 0, \\ y_5' &= y_6, & y_5(0) &= \frac{\Lambda}{N_1}, \\ y_6' &= \frac{1}{\left(\frac{1}{N_1 N_2} + \frac{w}{N_2} - \frac{\Delta w}{N_2} y_3^2 \right)^2} \left[\left(\frac{1}{N_1 N_2} + \frac{w}{N_2} - \frac{\Delta w}{N_2} y_3^2 \right) \left(A \left[y_5 + \frac{\chi}{2} y_6 \right] \right. \right. \\ &+ 2y_2 y_5 - y_1 y_6 - y_4 y_3 + \frac{N_5}{N_2} M y_5 \sin^2(\Gamma) \left. \right) - \left(A \left[y_2 + \frac{\chi}{2} y_3 \right] + y_2^2 - y_1 y_3 \right. \\ &\left. \left. + \frac{N_5}{N_2} M y_2 \sin^2(\Gamma) \right) \left(- \frac{\Delta w}{N_2} 2y_3 y_6 \right) \right]. & y_6(0) &= 1. \end{aligned}$$

The stopping criteria for the Newton's iterative technique is given below:

$$|y_2(\chi_\infty, \gamma)| < \epsilon,$$

where $\epsilon > 0$ is an arbitrarily small positive number. The value of ϵ has been taken as 10^{-9} . Equation (3.53) will be treated in a similar way.

3.5 Numerical Results and Discussions

In this section, the impact of the dimensionless parameters of interest on the skin friction coefficient $C_f Re_x^{\frac{1}{2}}$, nusselt number $Nu_x Re_x^{-\frac{1}{2}}$ and entropy generation N_G has been thoroughly discussed through different graphs and tables. In Table 3.3, T_{f_1} and T_{f_2} are the intervals for the choice of missing condition γ and Table 3.3 shows the intervals I_{θ_1} and I_{θ_2} for the choice of missing condition β while computing the skin friction coefficient and Nusselt number respectively. Tables 3.2 and 3.4 explain the

effect of the material parameters ω and Δ , unsteady parameter A , magnetic parameter M , nanoparticle volume fraction Φ , velocity slip parameter Λ , thermal radiation parameter Nr , Eckert number Ec , Biot number Bi and mass transfer parameter S with fixed Prandtl number $Pr = 6.2$ and $q = 3$ on the fluid motion, temperature fluctuation and total volumetric entropy generation in Powell-Eyring nanofluids.

Figures 3.2–3.4 illustrate how the material fluid parameter ω affects the temperature, velocity, and entropy production profiles of non-Newtonian Powell-Eyring nanofluids, SiC-MeOH and Cu-MeOH. Computations were performed with $\omega = 0.1, 0.3, 0.5$ at a uniform nanoparticle concentration $\Phi = 0.2$. The velocity profile in Figure 3.2 increases as the value of ω increases and thus leads to an increase in the thickness of the momentum boundary layer. Moreover, the BL thickness of the SiC-MeOH nanofluid is comparatively greater than that of the Cu-MeOH nanofluid, with a fixed value of $\omega = 0.1$.

A reduction in the fluid's resistance is the cause of the upward shift in the velocity profile. At the border, this likewise translates into a higher skin friction coefficient. From Figure 3.3, we can observe that the temperature of the nanofluid decreases as the value of the parameter ω increments. This decreasing trend indicates that the thermal boundary layer thickness is decreasing and the heat transfer coefficient is increasing. The reason behind this temperature profile is due to the reduced elastic stress parameter.

The heat transfer rate increases for SiC-MeOH and Cu based nanofluids. Finally, Figure 3.4 shows the effect of the material parameter ω on the entropy of the system. We found that as the material parameters increase, the entropy of the system decreases. The irreversibility of the system peaks near the surface and decreases to zero away from the surface. Also, the irreversibility of Cu-MeOH nanofluid is higher than that of SiC-MeOH nanofluid.

Figures 3.5–3.7 show the impact of the unsteady parameter A on the velocity, temperature and entropy generation profiles of Powell-Eyring nanofluids. Note that the fluid

flows slowly, as in Figure 3.5, and the temperature of the boundary layer decreases as the value of parameter A increases in Figure 3.6. This is due to the fact that unsteadiness parameter A is inversely proportional to stretching rate, so increasing A reduces the stretching of the surface and less stretching means less velocity. Increasing the value of parameter A reduces the thickness of both the momentum and thermal boundary layers.

Figure 3.7 shows the effect of variation of unsteadiness parameter A on entropy generation. The changeover point for the entropy profile is estimated at about $\chi = 0.3$. In other words, the thermal process is converging towards the case of reversible process. From Table 3.2 and 3.4, we see a tendency for the velocity and temperature gradients at the boundary to increase. The unsteadiness absorbs boundary layer energy and increases heat transfer at the boundary surface.

The behavior of temperature distribution, entropy production, and nanofluid motion with increasing material-fluid parameter Δ are depicted in Figures 3.8–3.10. Δ has the opposite effect on fluid velocity and boundary layer thickness as ω . As Δ grows, the momentum boundary layer thickness drops and the velocity profile in Figure 3.8 diminishes. Figure 3.9 shows that the temperature of the nanofluid increases as the value of the fluid parameter Δ increases. This increasing trend suggests that the thermal boundary layer thickness is increasing and the heat transfer coefficient is decreasing. Additionally, Figure 3.10 shows the influence of the fluid parameter Δ on the entropy of the system. It is evident that raising the fluid parameters causes the system's entropy to rise.

The effects of the inclination angle Γ of the magnetic field on the velocity, temperature, and entropy profiles are shown in Figures 3.11–3.13 respectively. It is observed that as the values of the Γ increases, the flow resistance tends to increase, resulting in a decrease in the boundary layer velocity and an increase in temperature. The effects of Γ on the entropy of the system is depicted in Figure 3.13. Based on observation, the added Γ tends to increase entropy. From a physical point of view, the greater the Γ of the magnetic field, the greater the Lorentz force and the greater the energy dissipation

in the fluid. This clearly shows the effect on entropy. Furthermore, at the boundary, increasing and decreasing trends in velocity and temperature gradients are recognized with increasing Γ Table 3.2 and 3.4.

Figures 3.14-3.16 show the motion, temperature distribution and entropy generation behavior of the nanofluid as the strength of the applied transverse magnetic field increases. Similar behavior is observed in the velocity, temperature, and entropy profiles as the value of the parameter M increases. When a magnetic field is applied perpendicular to the direction of flow, it creates a drag force known as the Lorentz force, which reduces the movement of the fluid within the boundary layer.

The influence of the Lorentz force in the form of a decreasing trend in the velocity profile can be clearly seen in Figure 3.14. Since the parameter M is inversely proportional to the density of the nanofluid, increasing the applied magnetic field decreases the density and consequently increases the temperature profile in the boundary layer Figure 3.15. This increases the thermal boundary layer thickness and reduces the Nusselt number. As the strength of the parameter M increases, the velocity gradient increases but the rate of heat transfer decreases. Figure 3.15 shows that the entropy of the system increases with increasing magnetic field.

By changing the nanoparticle volume concentration parameter Φ , Figures 3.17-3.19 display the dynamics of fluid motion, temperature distribution, and entropy formation in the boundary layer of Powell-Eyring nanofluids. The parameter Φ corresponds to the volume of solid particles in the basefluid. Solid particles are known to have higher thermal conductivity than fluids. Therefore, increasing Φ decreases the velocity of the fluid and increases the temperature in the boundary layer region, as shown in Figure 3.17. The temperature and thickness of the thermal boundary layer rise as the overall thermal conductivity of the nanofluid increases, as shown in Figure 3.18. Nusselt number and velocity gradient patterns show increasing and declining trends with increasing Φ parameter. Figure 3.19 shows that the entropy profile increases as the nanoparticle volume fraction parameter increases. The entropy generation rate is higher for Cu-MeOH nanofluids than for SiC-MeOH nanofluids.

Figures 3.20-3.22 showed that a positive value of the slip parameter Λ reduces fluid motion and entropy generation in Powell-Eyring nanofluids. In contrast, the temperature of Powell-Eyring nanofluids increases as the value of the Λ parameter increases. In Figure 3.20 the decrease in velocity is consistent with the fact that slip velocity slows down the motion of the boundary surface. In other words, velocity slip act opposite to stretching pull of the surface and resists its transmission to the fluid. As a result, as the parameter Λ increases, the momentum boundary layer decreases. Figure 3.21 shows the boundary layer temperature distribution for the parameter Λ .

Since the temperature distribution and velocity slip are inversely correlated, raising the parameter Λ results in a thicker thermal boundary layer and a lower Nusselt number. Table 3.2 and 3.4 show that the positive increase in velocity slip affects the velocity gradient and heat transfer coefficient of both Cu-MeOH and SiC-MeOH nanofluids. It shows that it leads to a decrease. Boundary slip lowers the friction at the solid-fluid contact, which lowers the heat transfer coefficient and causes the desired effect.

From Figure 3.22 it is easy to see that the entropy decreases as the value of Λ increases. Larger values of Λ slow down the boundary layer. This reduction in velocity reduces frictional forces within the fluid. Reducing friction also reduces the irreversibility of friction. As a result, the contribution to entropy within entropy becomes weaker, reducing the entropy of the system.

Figures 3.23-3.28 show temperature profiles of methanol-based nanofluids with different thermal radiation parameters Nr , Biot number Bi , and Eckert number Ec . Physically, the fluid receives more heat as the Nr value is raised, thickening the thermal boundary layer. The ratio of conduction in a fluid to convection at its surface is expressed as the Biot number, also known as the sheet convective parameter. A rise in the sheet convective parameter indicates that conduction-based heat transfer is more important at the fluid surface than the convective coefficient. The stretched surface is heated by the hot fluid in the boundary layer, which raises the temperature of the thermal system, as indicated by the increase in Bi . Consequently, the rise in

the Nusselt number at the boundary is closely correlated with the increases in the parameters Nr and Bi .

Figures 3.24 and 3.26 show the entropy increase with increasing thermal radiation parameter Nr and Biot number Bi . In Figures 3.24 and 3.26 the intersection of the entropy profiles is estimated around $\chi = 0.3$. Before this behavior occurs, entropy increases and then begins to decrease. In other words, the thermal process approaches that of a reversible process. Moreover, the ratio of the boundary layer's kinetic energy to its enthalpy difference, or Ec , describes the dissipation of heat transmission. Greater kinetic energy is indicated by Ec values. As a result, frictional heating raises the liquid's temperature at the surface. Figure 3.27 illustrates how the fluid temperature rises as Ec does. The growing Nr and Ec parameters of NG are seen in Figures 3.24 and 3.28, respectively. Additionally, a crossover point was visible in the entropy profile at $\chi = 0.3$. The entropy generation increased before this behavior, but started to decrease after the behavior.

Figures 3.29-3.31 show the influence of the parameter S on the fluid velocity, temperature, and entropy. An increase in the mass transfer parameter $S > 0$ shows a decreasing trend in velocity and temperature profiles, leading to a contraction of the boundary layer.

During suction, more fluid flows to the outside of the wall, slowing the movement and reducing the thickness of both boundary layer. Both velocity and temperature gradients were observed to increase with increasing values of S and are listed in tables 3.2 and 3.4. Increasing the suction impact, will increase the entropy of the system as more fluid will be displaced.

The influence of $\Phi = 0.2$ is seen in Figure 3.32, which displays the heat transfer characteristics of boundary layer flow in Cu and SiC-MeOH nanofluids at nanoparticle concentrations with varying nanoparticle shapes (sphere, hexahedron, tetrahedron, column, and lamina).

The dimensionless temperature of the nanofluid rises as the form factor q rises, as this graphical illustration demonstrates. Spherical nanoparticles have the lowest dimensionless temperature at the border, followed by tetrahedron, hexahedron, column, and lamina. Because spherical particles have a larger surface area, they tend to remove more heat from the boundary layer. Spherical particles exhibit the greatest temperature reduction in the boundary layer, since this impact is less noticeable for other forms. Furthermore, Figure 3.33 showed that the entropy of the system increased, with the lowest entropy production rate observed for spherical particles.

The effects of the Reynolds number Re and the Brinkman number Br on the entropy generation profile are shown in this section. Higher values of Re are associated with an increase in entropy, as indicated by numerical computations. Physically, this means that inertial forces dominate viscous effects See Figure 3.34. Figure 3.35 discussed the effect of Br on the entropy. Increasing the Brinkmann number is known to increase entropy generation. This is due to the fact that the Brinkmann number is the ratio of heat dissipation to heat conduction at a surface. An increase in Br value therefore means that more heat is dissipated at the surface compared to conduction, resulting in an increase in entropy.

TABLE 3.1: Missing conditions of $\frac{d^2 f}{d\chi^2}(0)$ for $Pr = 6.2$, $q = 3$.

ω	A	Δ	Γ	M	Φ	Λ	S	T_{f_1} (Cu-MeOH)	T_{f_2} (SiC-MeOH)
0.1	0.2	0.2	$\pi/2$	0.1	0.2	0.3	0.1	[-0.77, -0.69]	[-0.66, -0.50]
0.3								[-0.75, -0.70]	[-0.64, -0.50]
0.5								[-0.73, -0.70]	[-0.62, -0.49]
	0.0							[-0.73, -0.52]	[-0.63, -0.35]
	0.1							[-0.75, -0.60]	[-0.64, -0.41]
		5						[-0.78, -0.75]	[-0.66, -0.60]
		10						[-0.80, -0.78]	[-0.68, -0.62]
			$\pi/4$					[-0.76, -0.67]	[-0.64, -0.47]
			$\pi/6$					[-0.75, -0.67]	[-0.64, -0.45]
				0.0				[-0.75, -0.66]	[-0.63, -0.43]
				0.2				[-0.78, -0.71]	[-0.68, -0.52]
					0.1			[-0.84, -0.74]	[-0.74, -0.55]
					0.15			[-0.81, -0.72]	[-0.70, -0.54]
						0.0		[-1.53, -1.33]	[-1.13, -0.82]
						0.1		[-1.13, -1.0]	[-0.90, -0.67]
							0.3	[-0.83, -0.69]	[-0.70, -0.48]
							0.4	[-0.87, -0.69]	[-0.72, -0.46]

TABLE 3.2: Results of $\frac{d^2f}{d\chi^2}(0)$ for $Pr = 6.2$, $q = 3$.

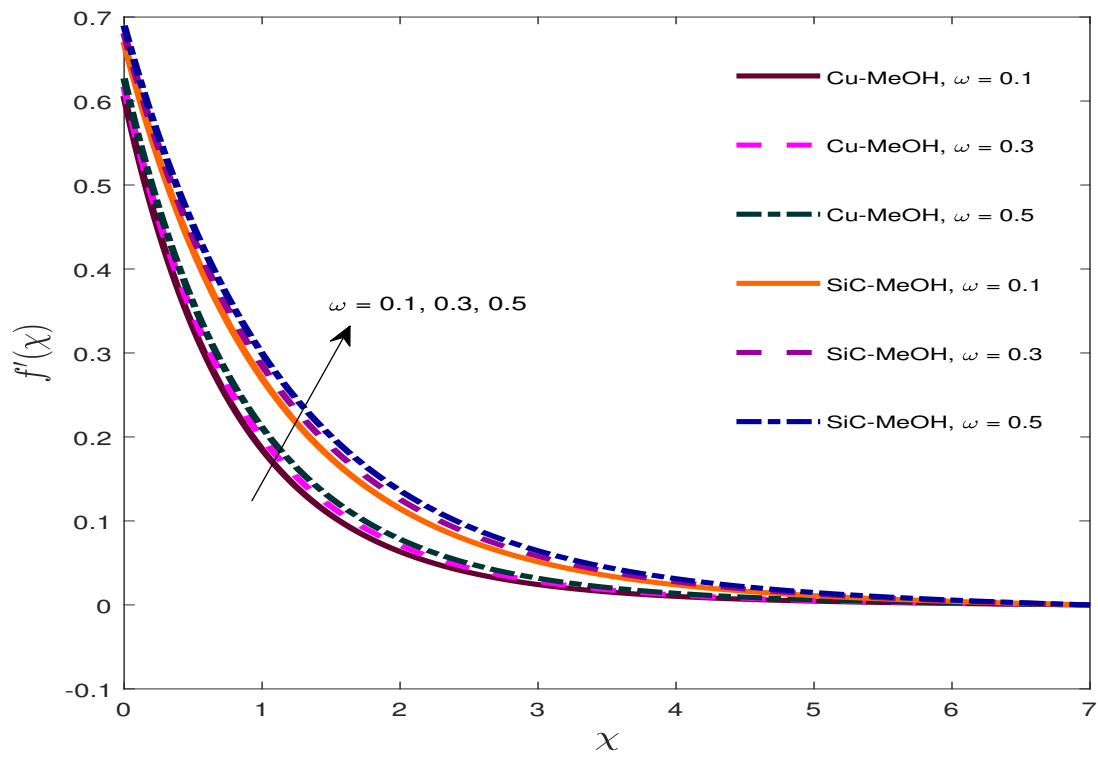
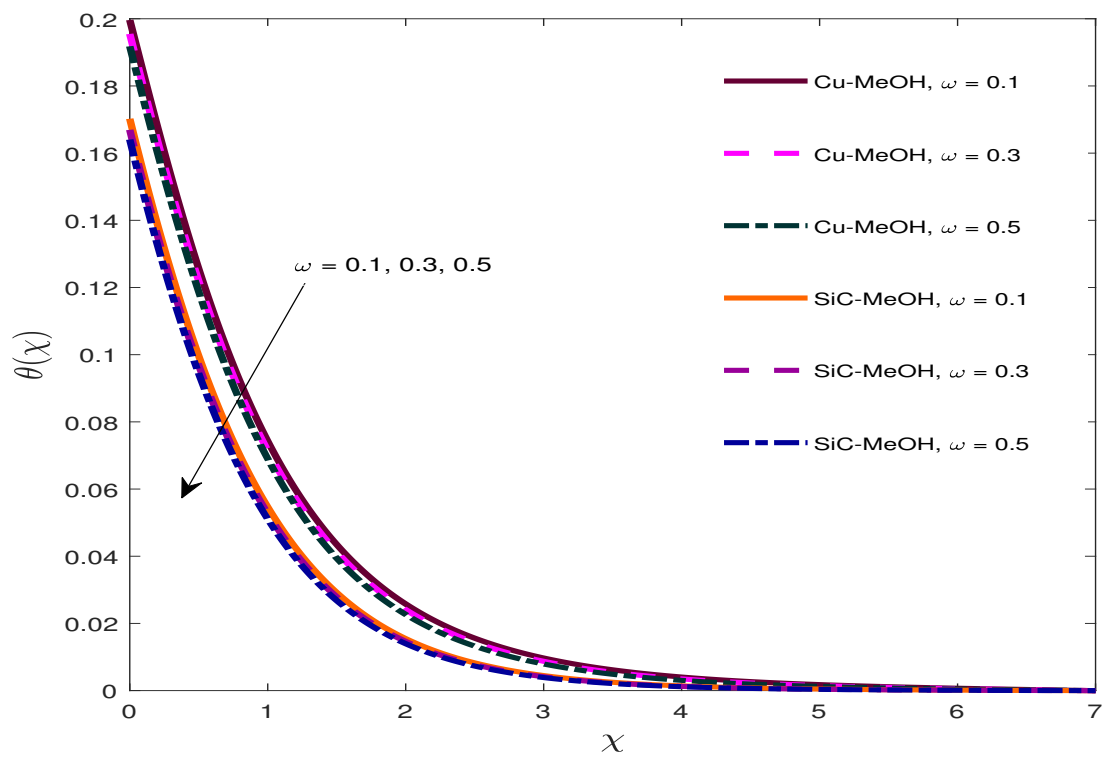
ω	A	Δ	Γ	M	Φ	Λ	S	$C_f Re_x^{\frac{1}{2}}$	$C_f Re_x^{\frac{1}{2}}$
								(Cu-MeOH)	(SiC-MeOH)
0.1	0.2	0.2	$\pi/2$	0.1	0.2	0.3	0.1	1.3854	1.1599
0.3								1.4879	1.2427
0.5								1.5873	1.3227
	0.0							1.3223	1.1064
	0.1							1.3543	1.1335
		5						1.3425	1.1370
		10						1.2925	1.1112
			$\pi/4$					1.3729	1.1396
			$\pi/6$					1.3665	1.1291
				0.0				1.3600	1.1184
				0.2				1.4095	1.1981
					0.1			1.1473	1.0014
					0.15			1.2708	1.0797
						0.0		2.7489	1.9996
						0.1		2.0416	1.5962
							0.3	1.4899	1.2268
							0.4	1.5435	1.2612

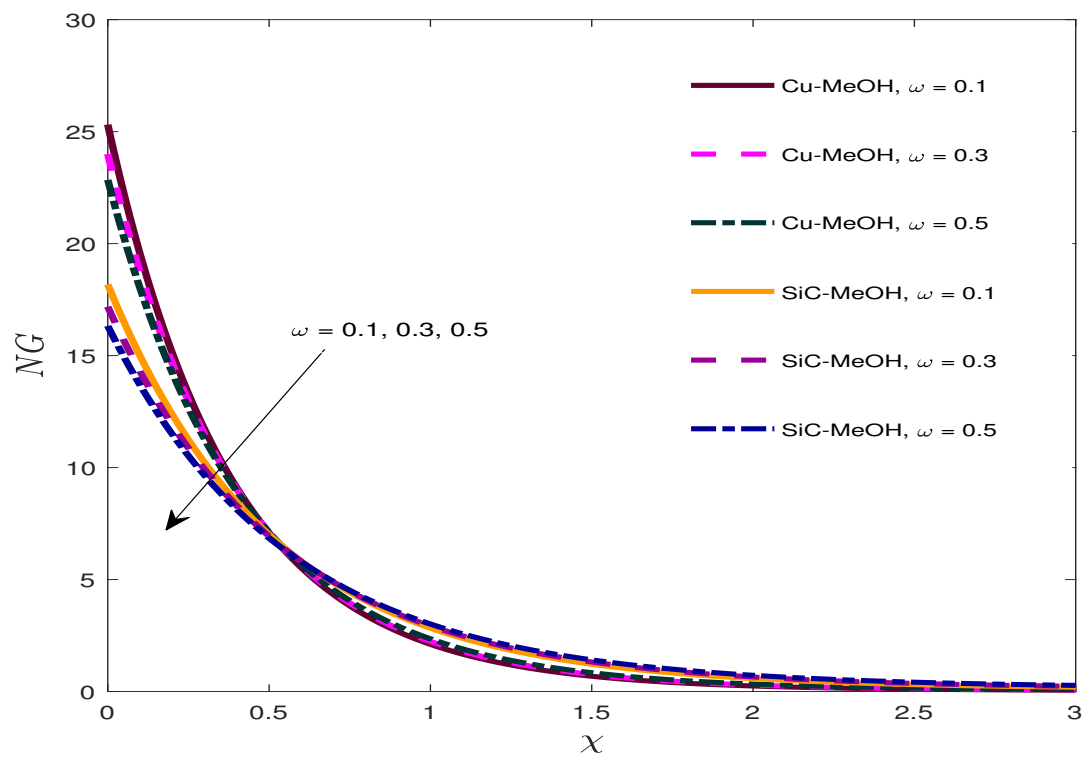
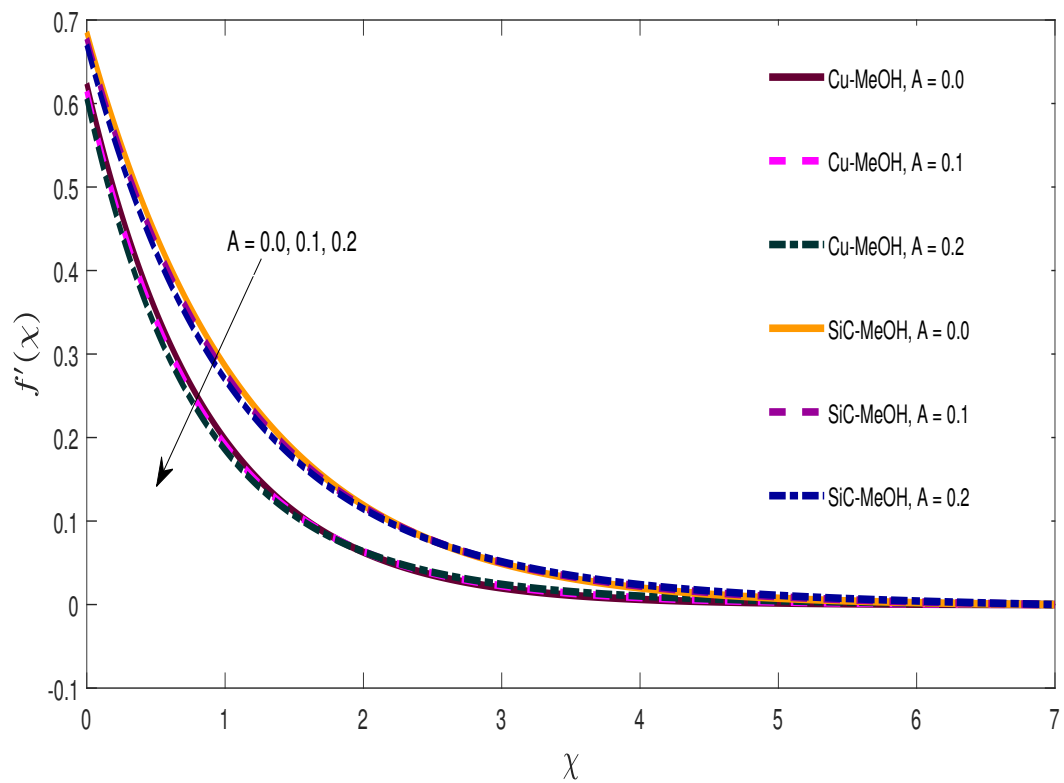
TABLE 3.3: Missing conditions of $\theta(0)$ for $Pr = 6.2$, $q = 3$.

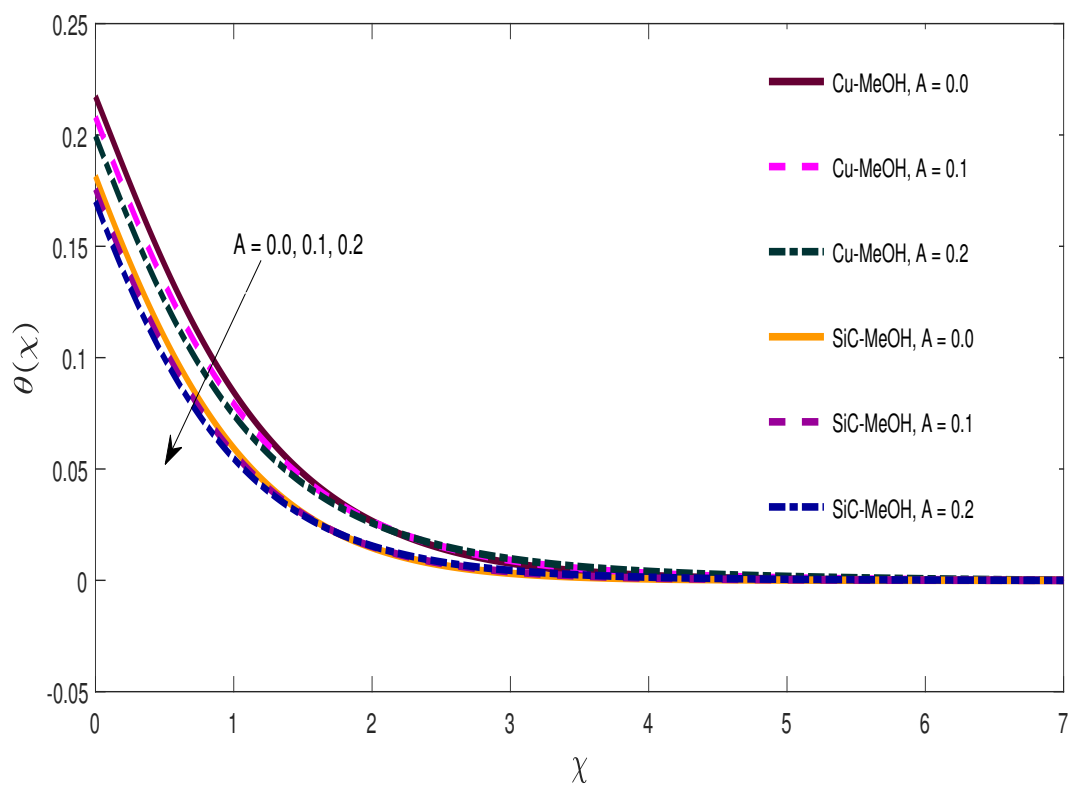
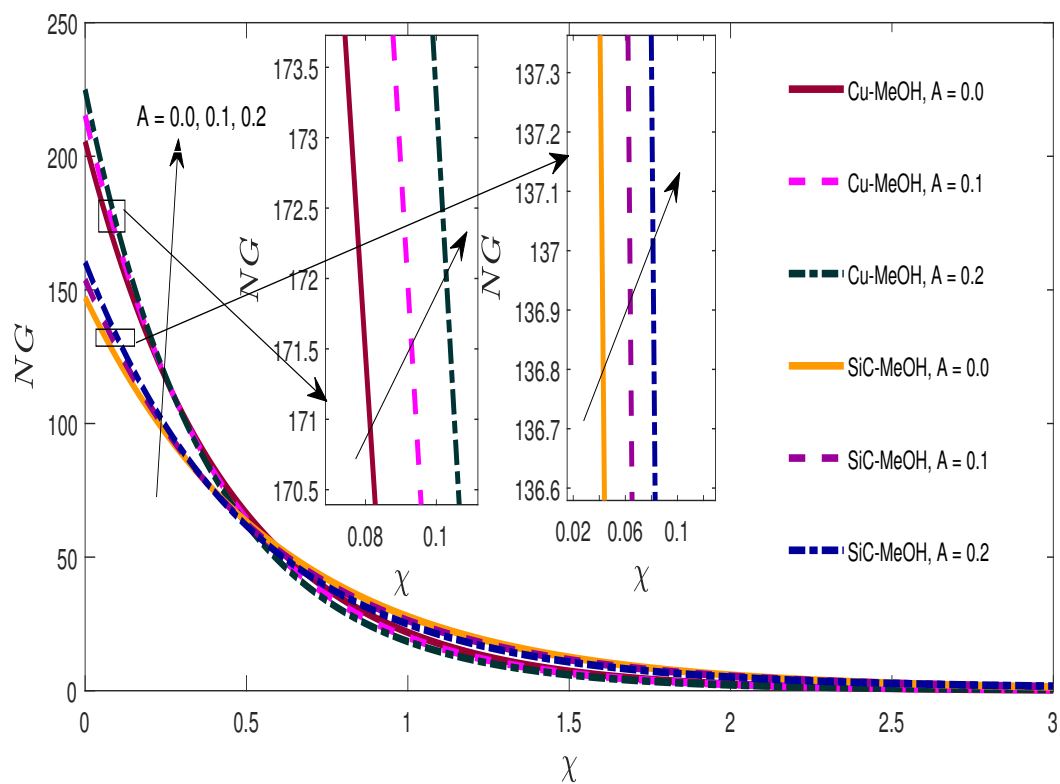
ω	A	Δ	Γ	M	Φ	Λ	Nr	Bi	Ec	S	I_{θ_1}	I_{θ_2}
											(Cu-MeOH)	(SiC-MeOH)
0.1	0.2	0.2	$\pi/2$	0.1	0.2	0.3	0.3	0.2	0.2	0.1	[-1.0, 0.83]	[-1.0, 1.1]
0.3											[-1.0, 0.88]	[-1.0, 1.1]
0.5											[-1.0, 0.89]	[-1.0, 1.2]
	0.0										[-1.0, 0.86]	[-1.0, 2.0]
	0.1										[-1.0, 0.85]	[-1.0, 2.0]
		5.0									[-1.0, 0.81]	[-1.0, 1.0]
		10.0									[-1.0, 0.80]	[-1.0, 1.0]
			$\pi/4$								[-1.0, 0.84]	[-1.0, 1.1]
			$\pi/6$								[-1.0, 0.82]	[-1.0, 1.1]
				0.0							[-1.0, 0.86]	[-1.0, 1.1]
				0.2							[-1.0, 0.80]	[-1.0, 1.0]
				0.1							[-1.0, 0.93]	[-1.0, 1.0]
					0.15						[-1.0, 0.85]	[-1.0, 1.1]
						0.0					[-1.0, 1.1]	[-1.0, 1.4]
						0.1					[-1.0, 0.89]	[-1.0, 1.3]
							0.5				[-1.0, 0.89]	[-1.0, 1.1]
							0.8				[-1.0, 0.99]	[-1.0, 1.2]
								0.1			[-1.0, 0.77]	[-1.0, 1.0]
								0.6			[-1.0, 1.0]	[-1.0, 1.3]
									0.4		[-1.0, 0.84]	[-1.0, 1.1]
									0.6		[-1.0, 0.90]	[-1.0, 1.1]
										0.3	[-1.0, 1.1]	[-1.0, 1.5]
										0.4	[-1.0, 1.3]	[-1.0, 1.9]

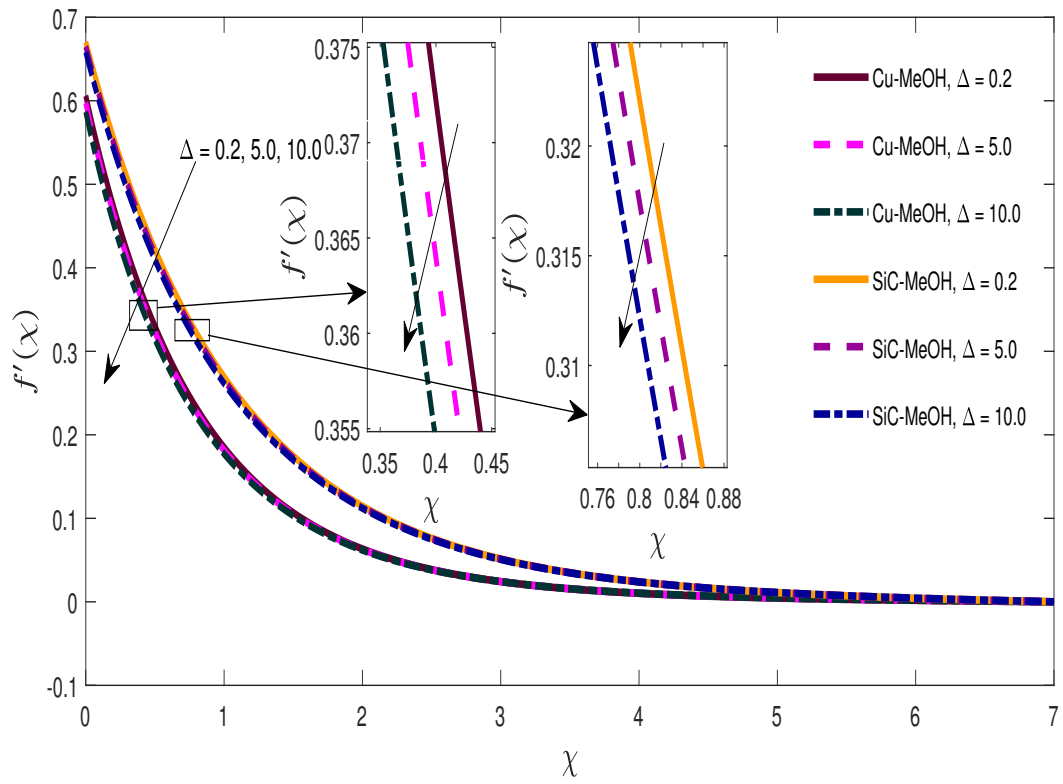
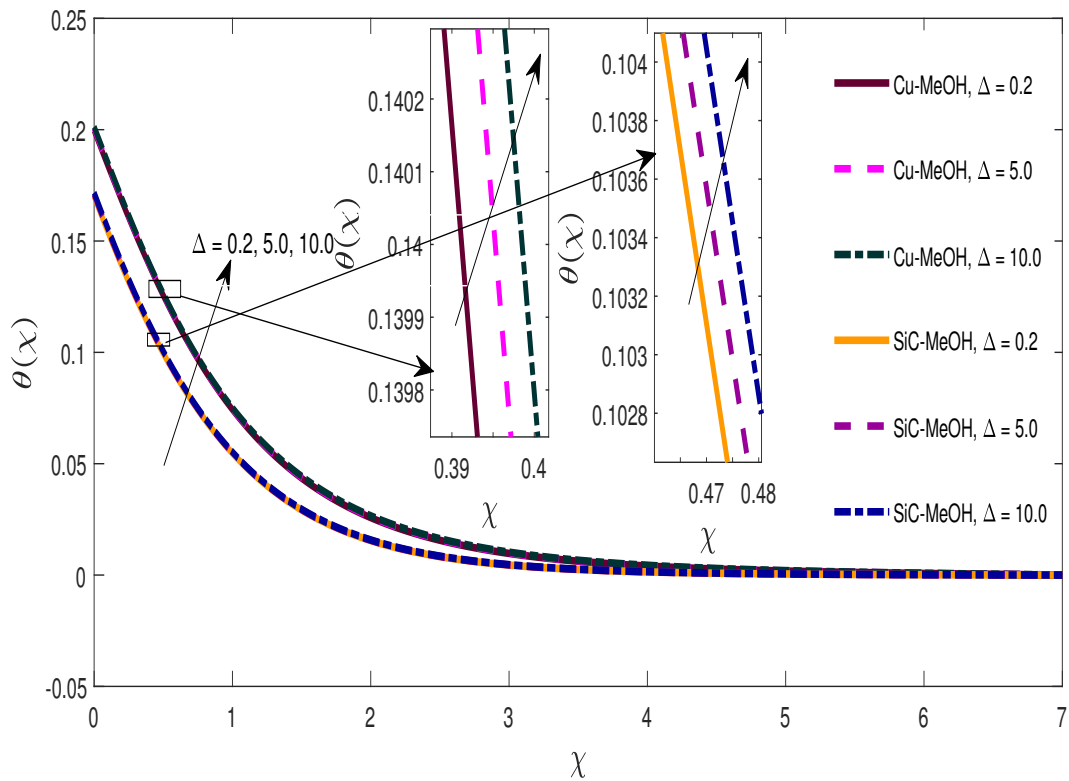
TABLE 3.4: Results of $\theta(0)$ for $Pr = 6.2$, $q = 3$.

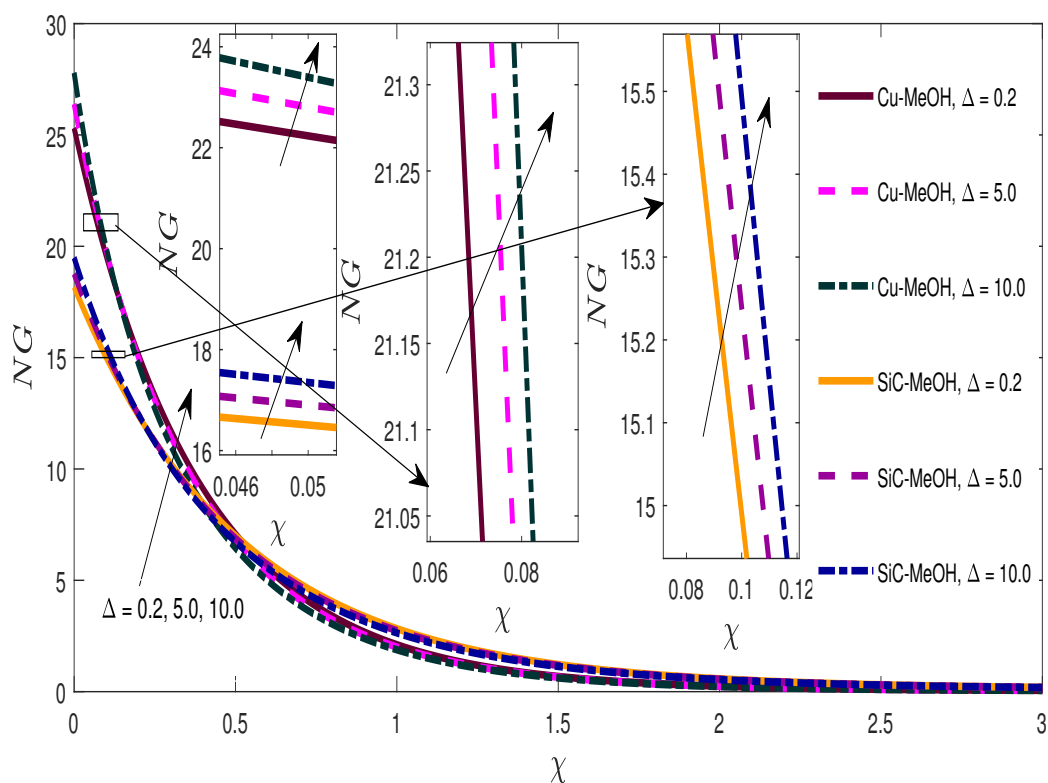
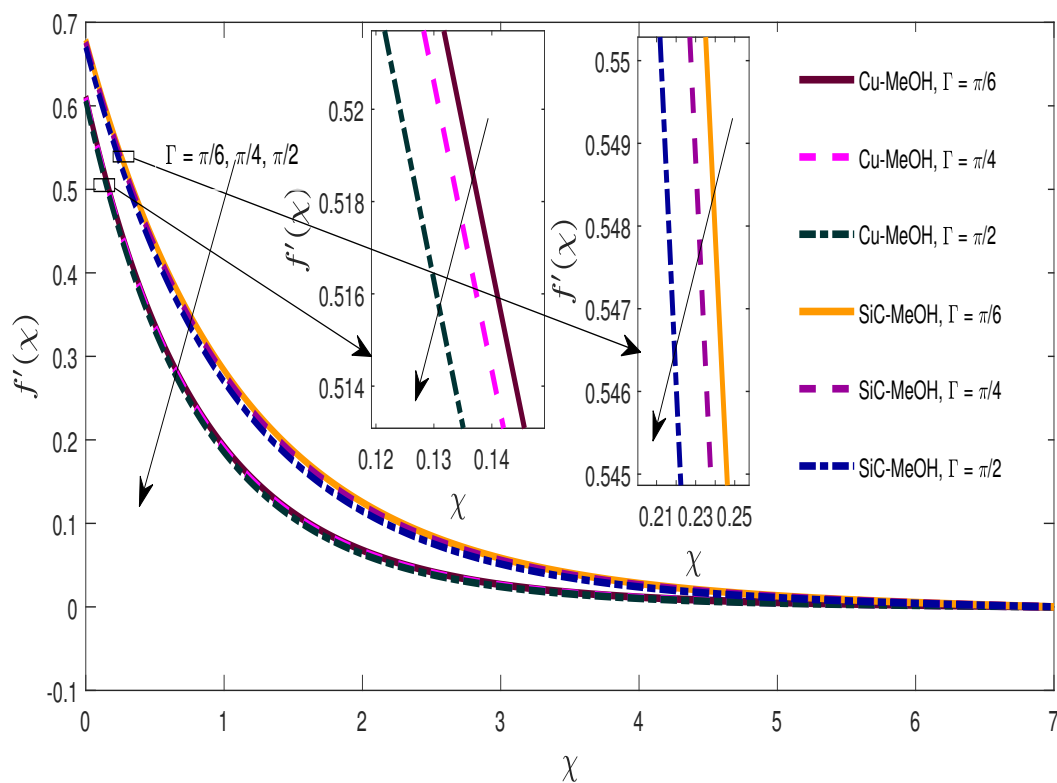
ω	A	Δ	Γ	M	Φ	Λ	Nr	Bi	Ec	S	$Nu_x Re_x^{-\frac{1}{2}}$	$Nu_x Re_x^{-\frac{1}{2}}$
											(Cu-MeOH)	(SiC-MeOH)
0.1	0.2	0.2	$\pi/2$	0.1	0.2	0.3	0.3	0.2	0.2	0.1	0.3638	0.3771
											0.3657	0.3786
											0.3674	0.3800
										0.0	0.3558	0.3720
										0.1	0.3600	0.3746
										5.0	0.3634	0.3768
										10.0	0.3631	0.3765
										$\pi/4$	0.3655	0.3793
										$\pi/6$	0.3664	0.3805
										0.0	0.3672	0.3816
										0.2	0.3606	0.3730
										0.1	0.2825	0.2891
										0.15	0.3206	0.3306
										0.0	0.3201	0.3567
										0.1	0.3456	0.3678
										0.5	0.4111	0.4270
										0.8	0.4792	0.4993
										0.1	0.1947	0.2003
										0.6	0.8644	0.9161
										0.4	0.3328	0.3532
										0.6	0.3018	0.3292
										0.3	0.3719	0.3845
										0.4	0.3759	0.3879

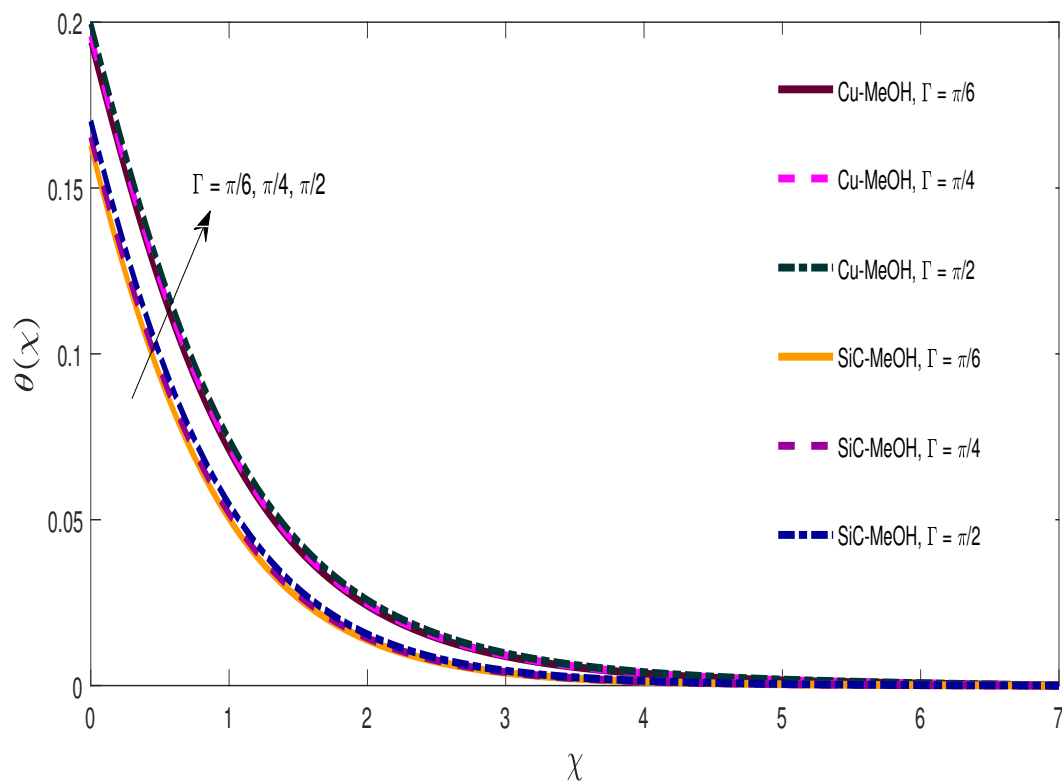
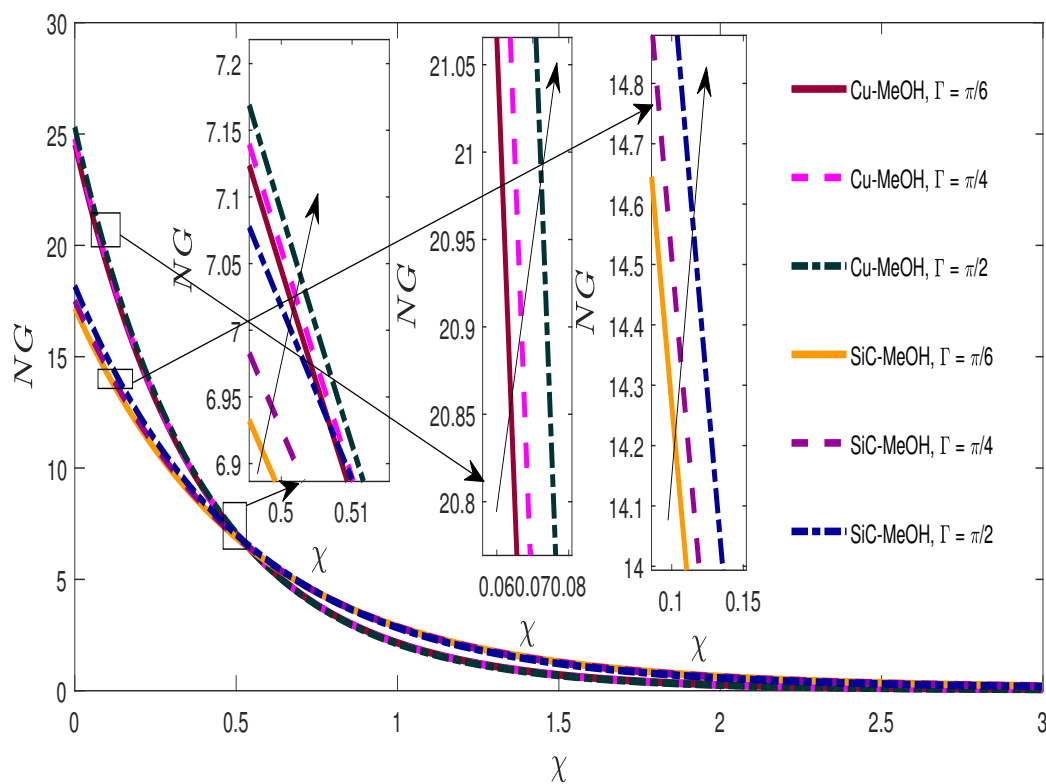
FIGURE 3.2: Velocity profile against ω FIGURE 3.3: Temperature profile against ω

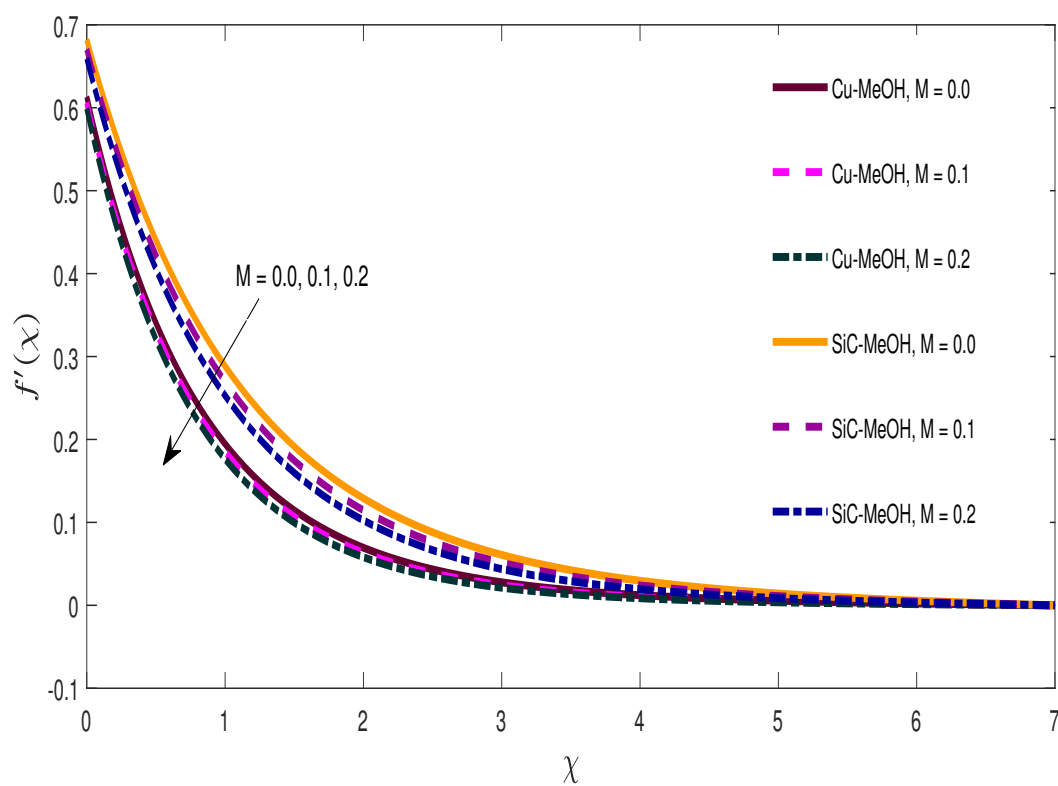
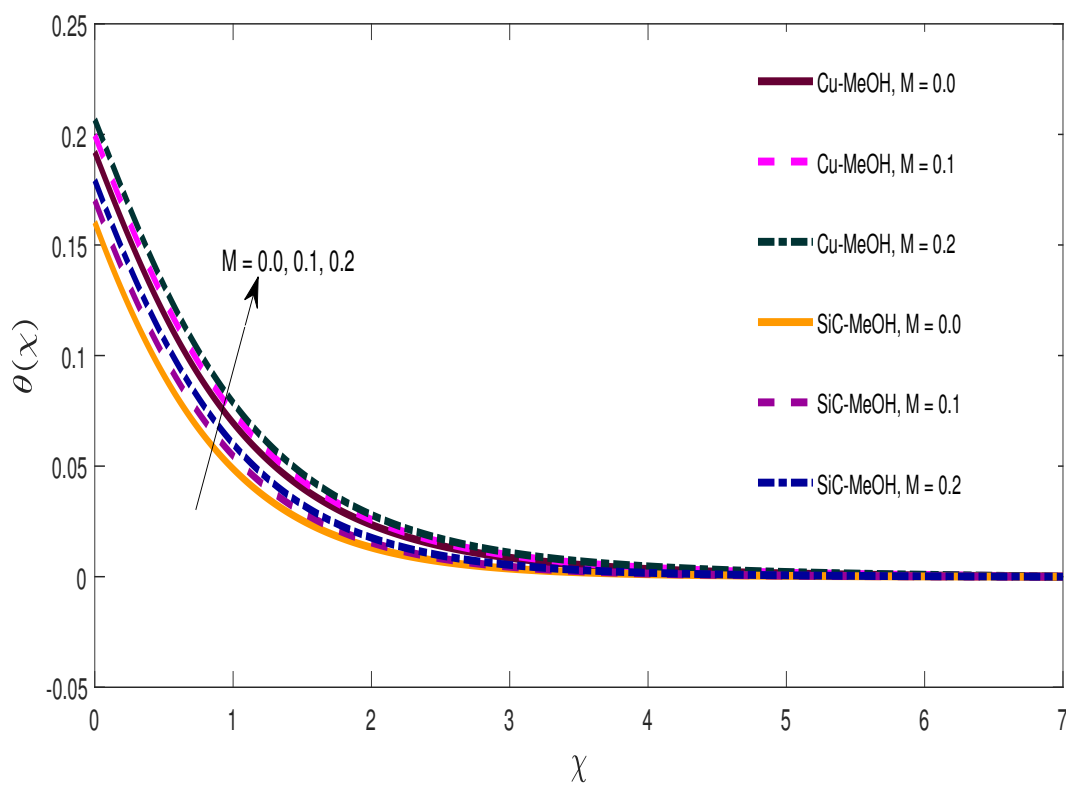
FIGURE 3.4: Entropy profile against ω FIGURE 3.5: Velocity profile against A

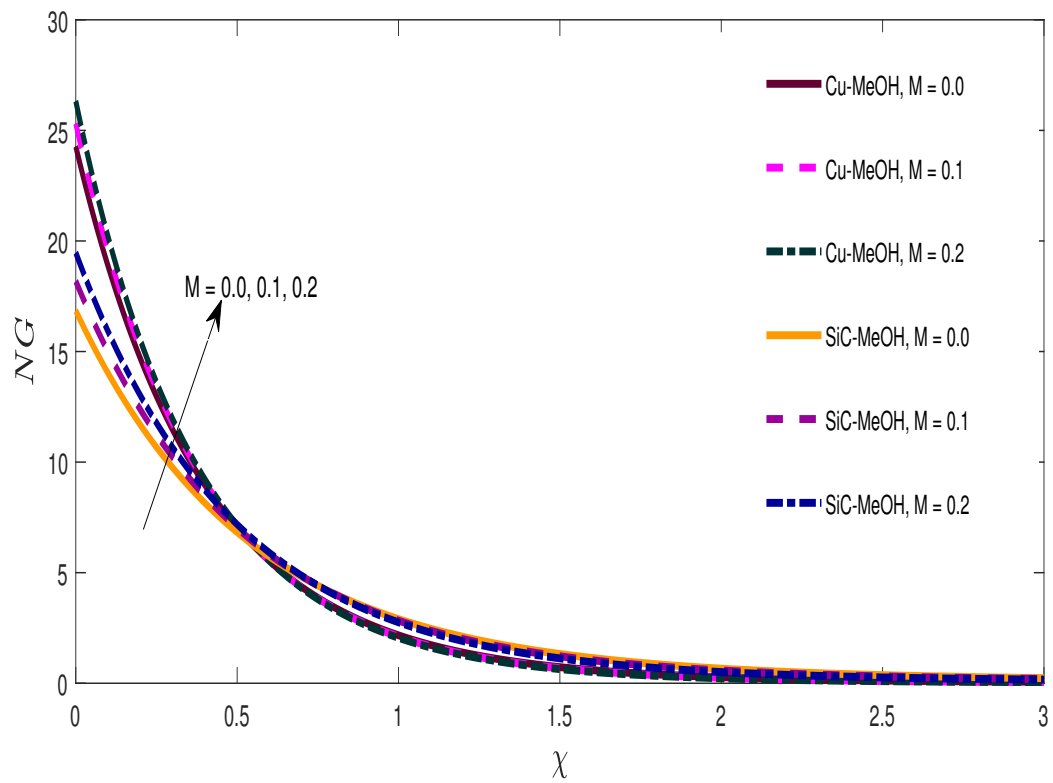
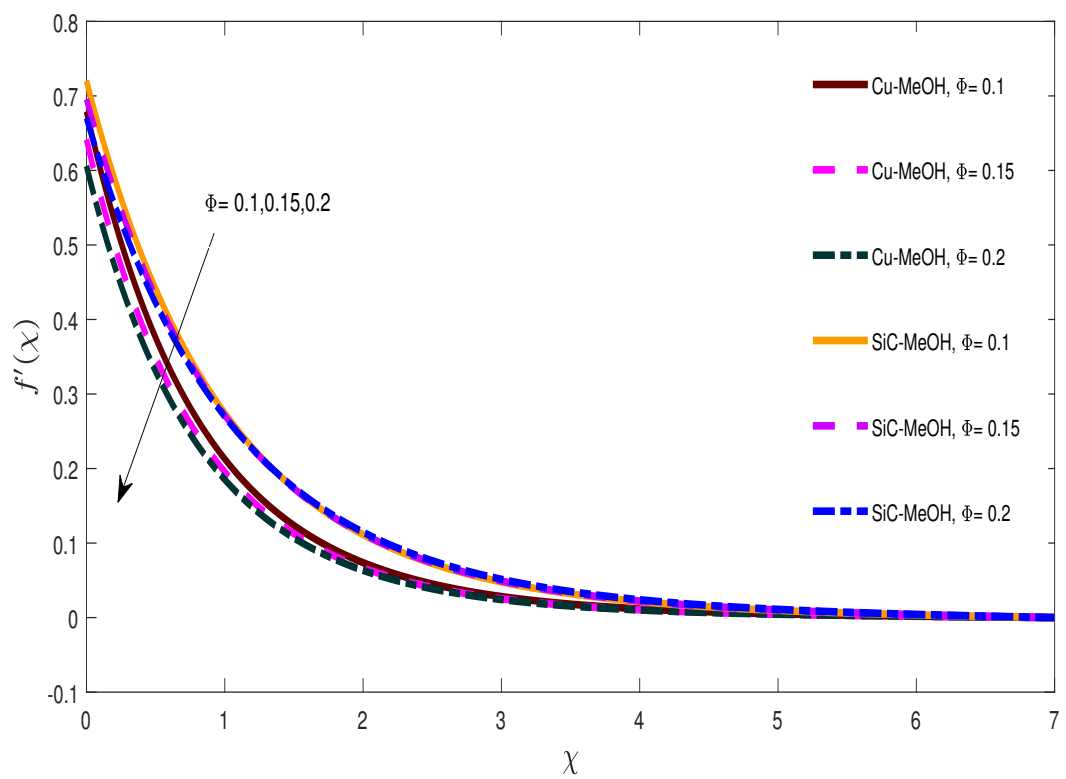
FIGURE 3.6: Temperature profile against A FIGURE 3.7: Entropy profile against A

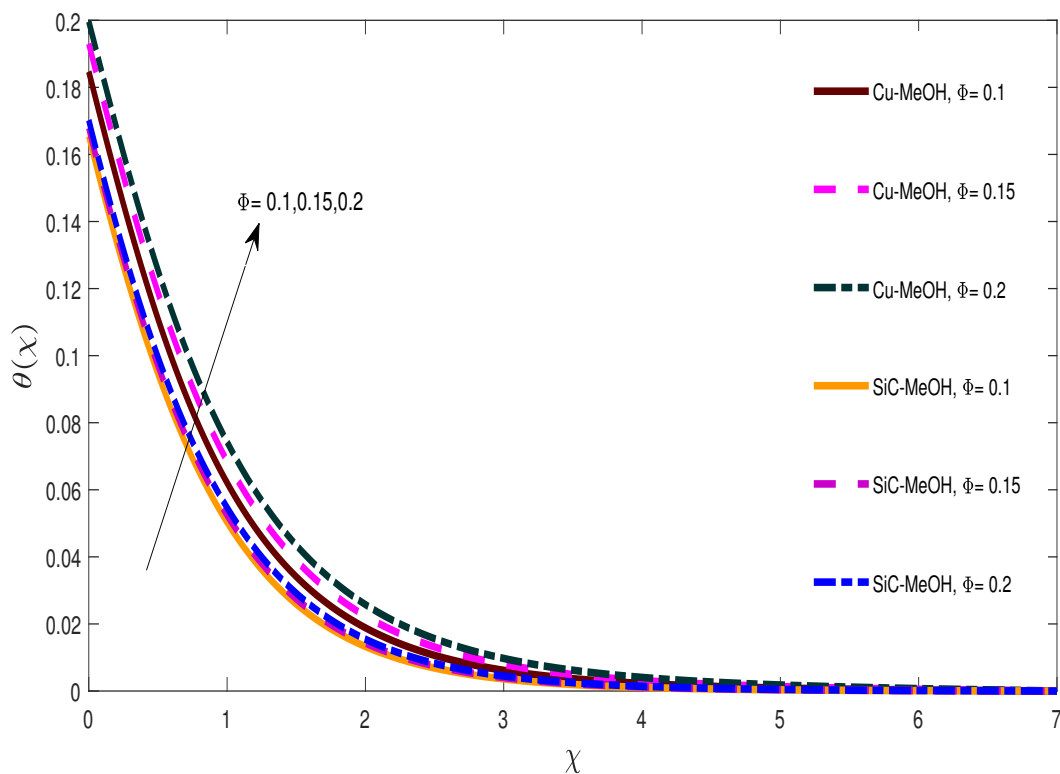
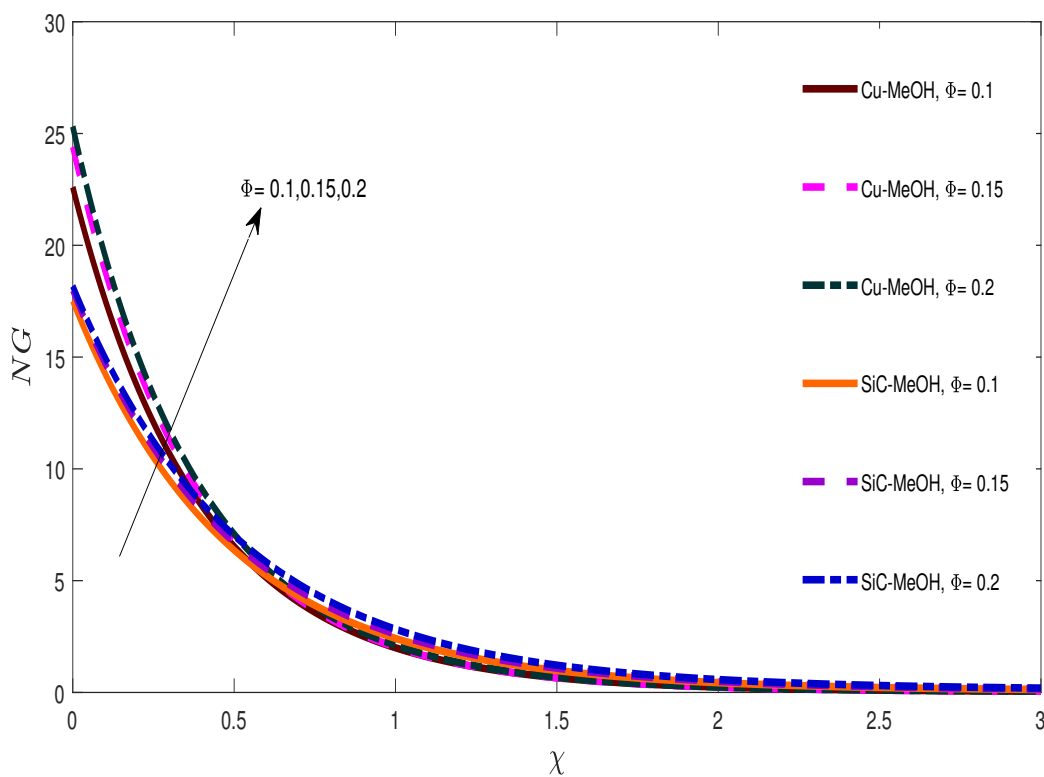
FIGURE 3.8: Velocity profile against Δ FIGURE 3.9: Temperature profile against Δ

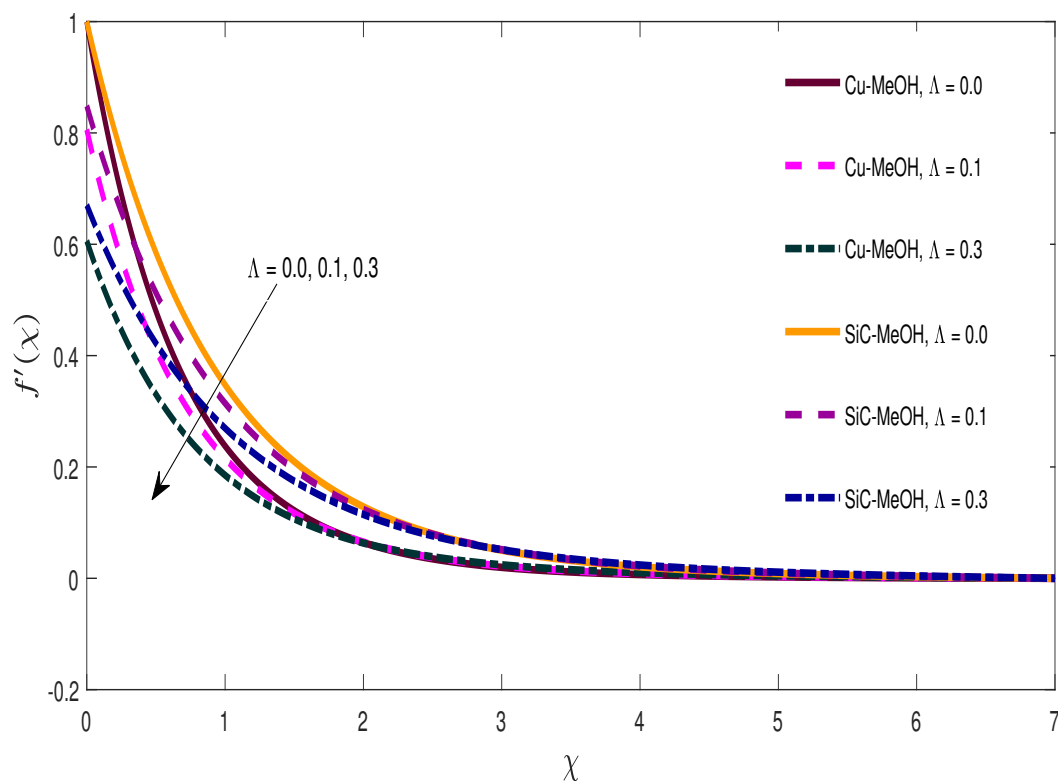
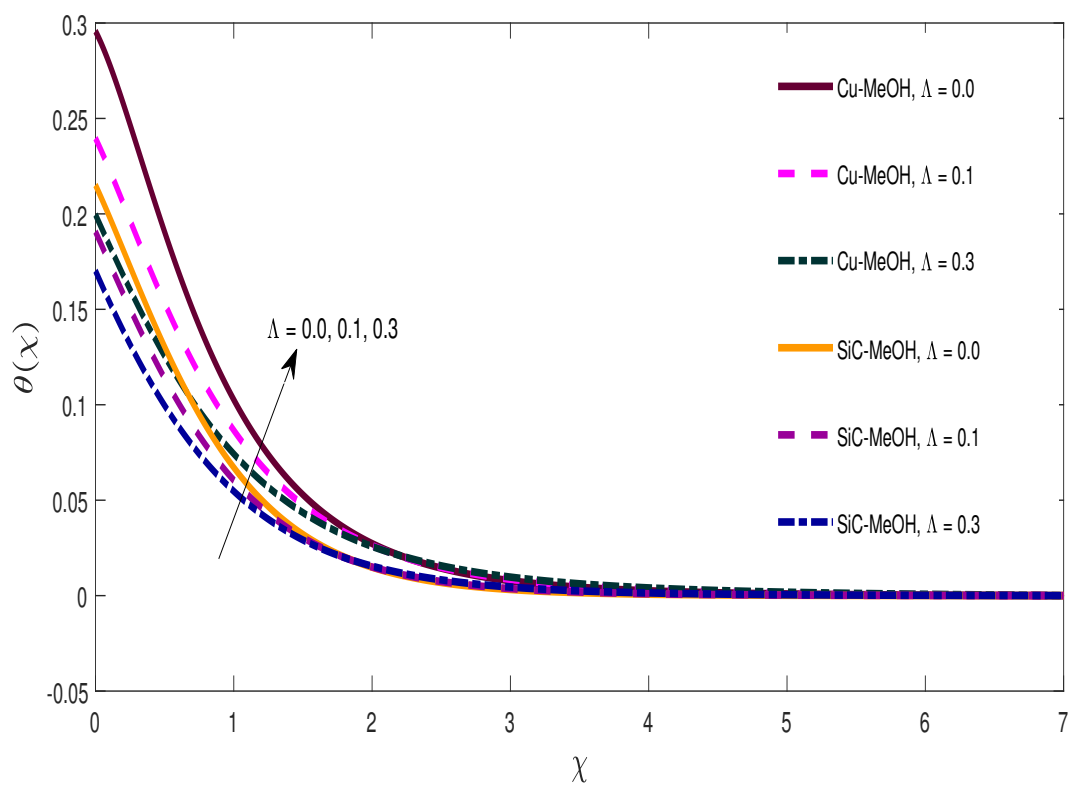
FIGURE 3.10: Entropy profile against Δ FIGURE 3.11: Velocity profile against Γ

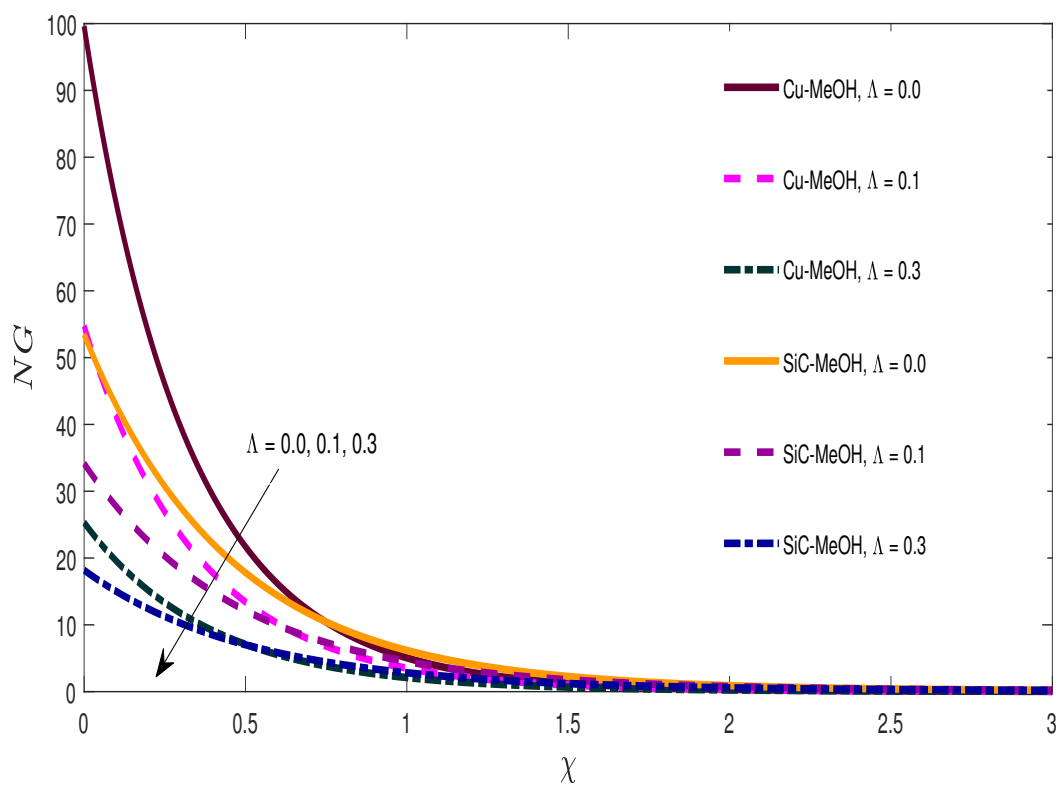
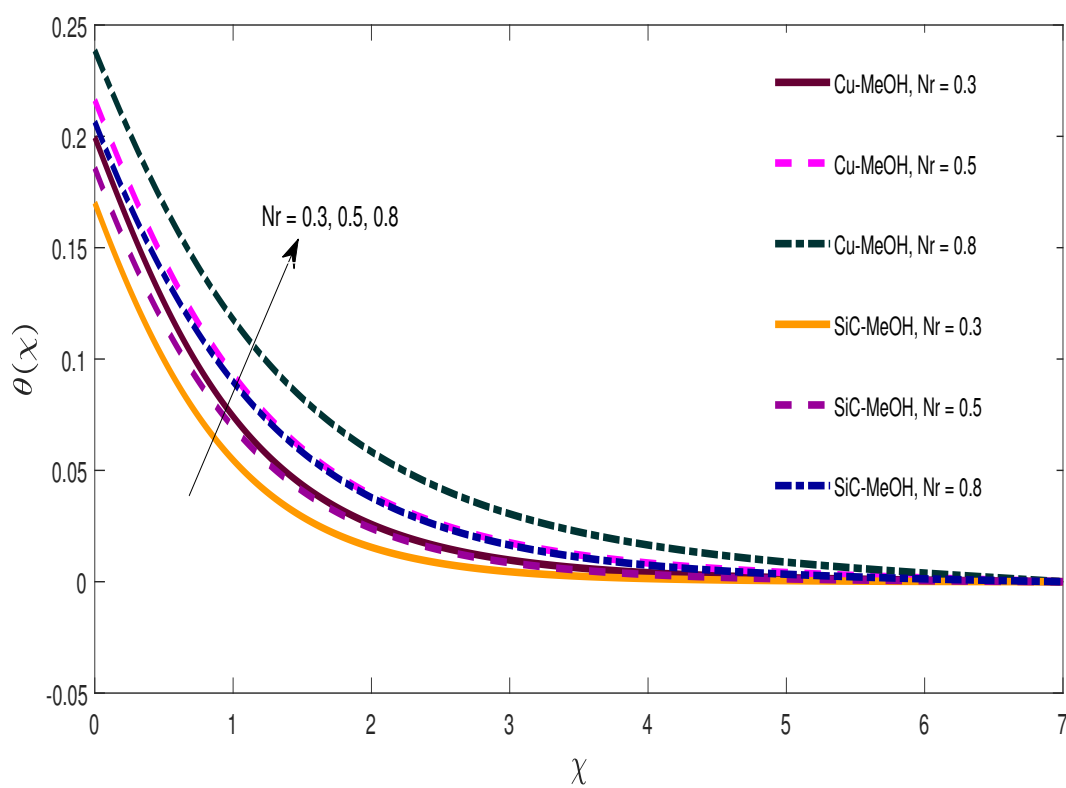
FIGURE 3.12: Temperature profile against Γ FIGURE 3.13: Entropy profile against Γ

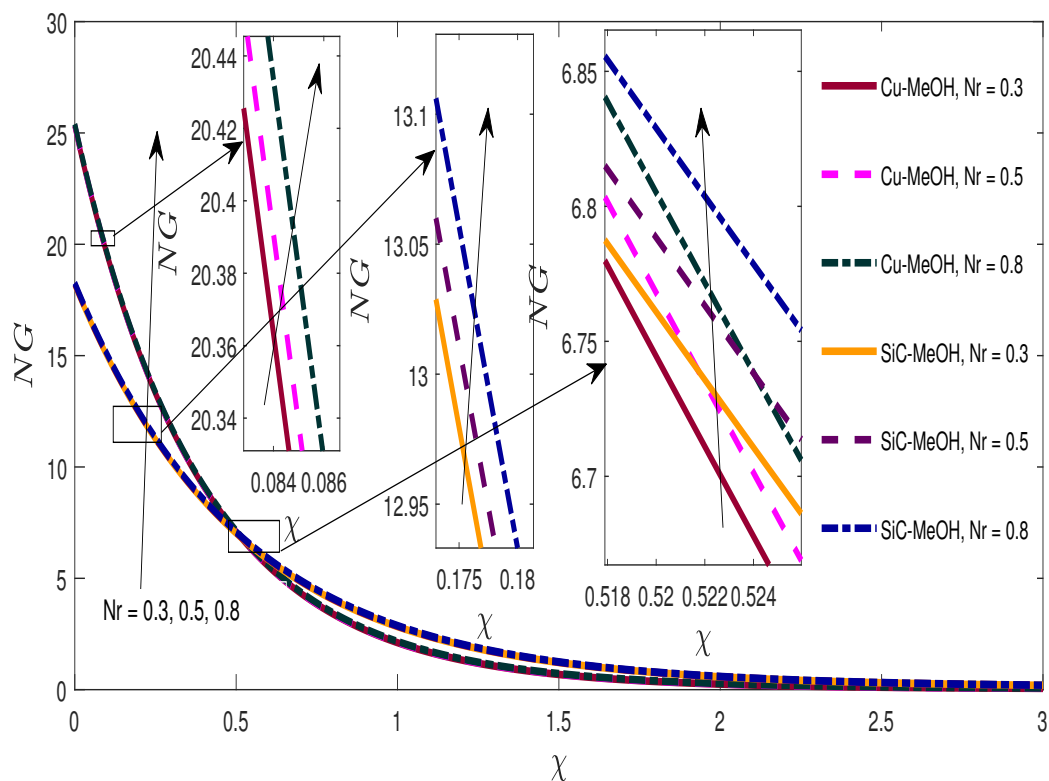
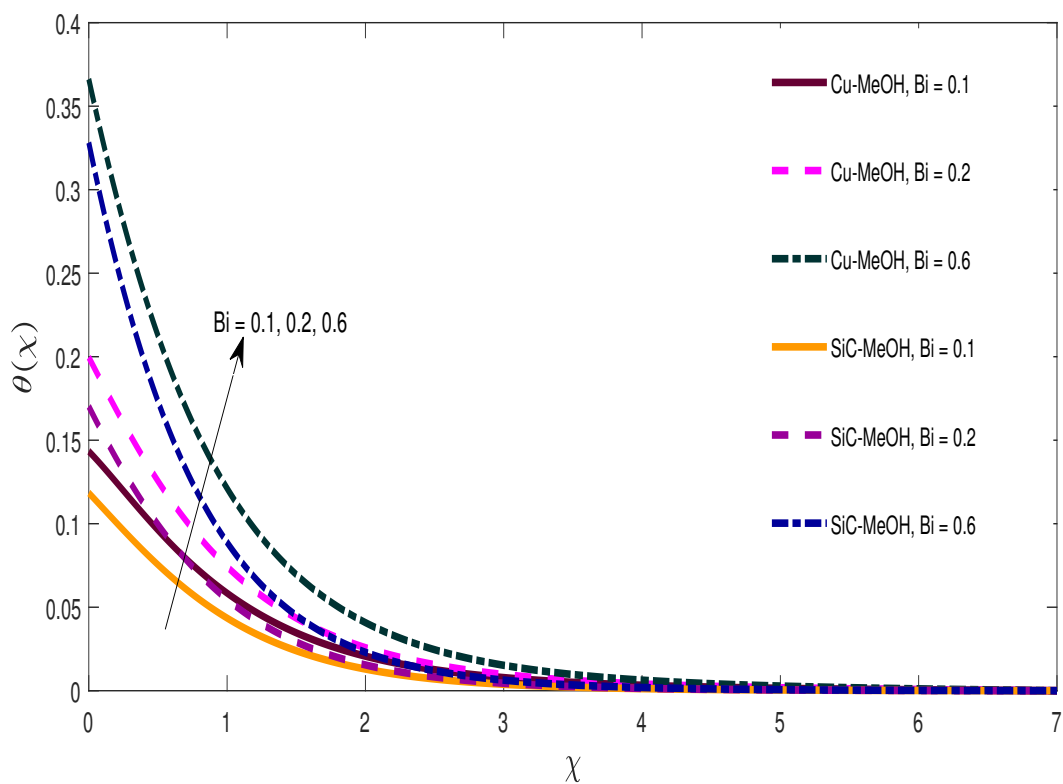
FIGURE 3.14: Velocity profile against M FIGURE 3.15: Temperature profile against M

FIGURE 3.16: Entropy profile against M FIGURE 3.17: Velocity profile against Φ

FIGURE 3.18: Temperature profile against Φ FIGURE 3.19: Entropy profile against Φ

FIGURE 3.20: Velocity profile against Λ FIGURE 3.21: Temperature profile against Λ

FIGURE 3.22: Entropy profile against Λ FIGURE 3.23: Temperature profile against Nr

FIGURE 3.24: Entropy profile against Nr FIGURE 3.25: Temperature profile against Bi

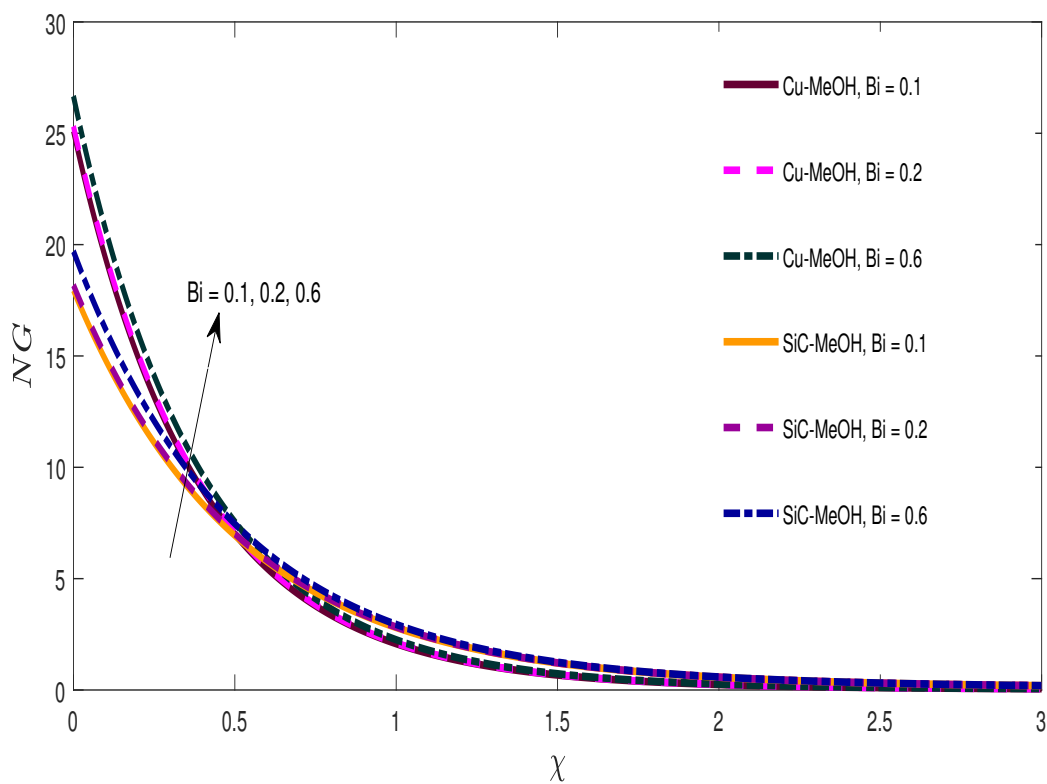


FIGURE 3.26: Entropy profile against Bi

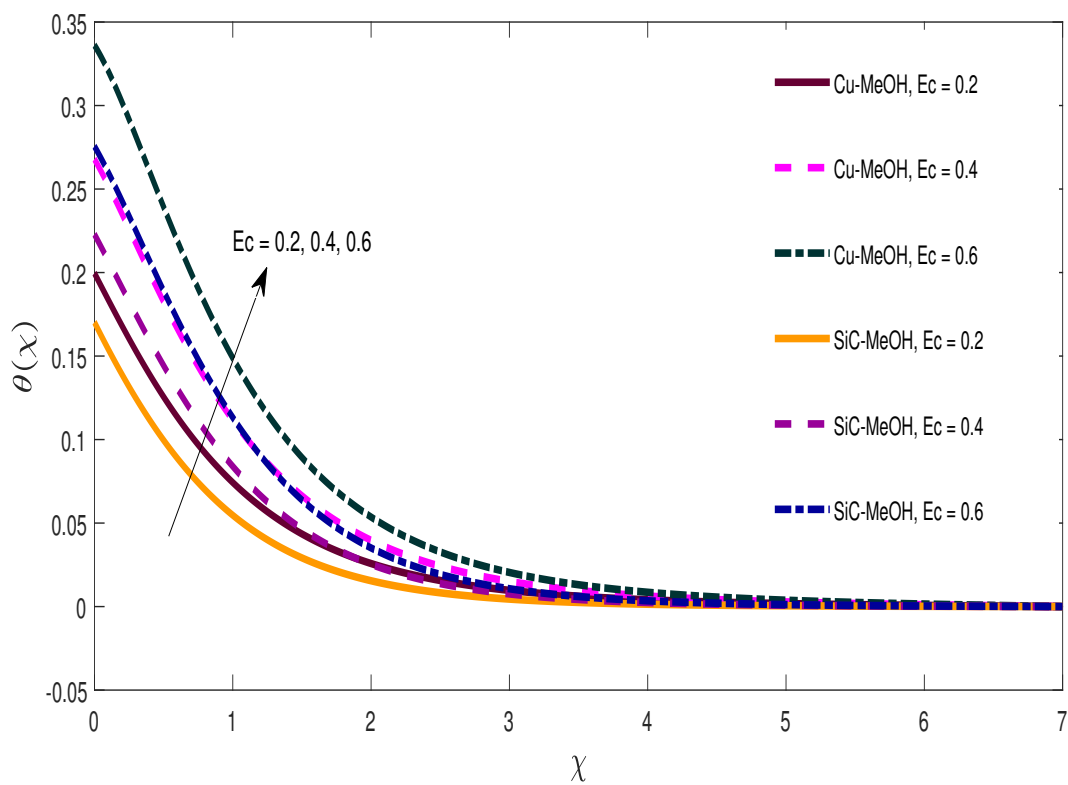
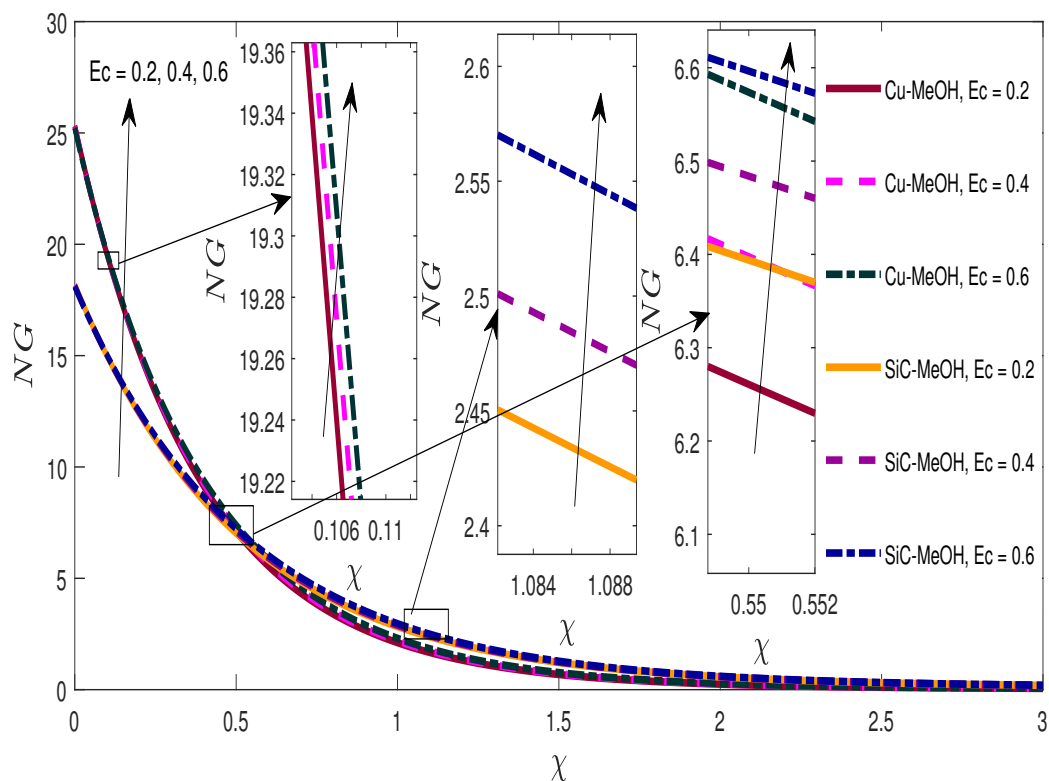
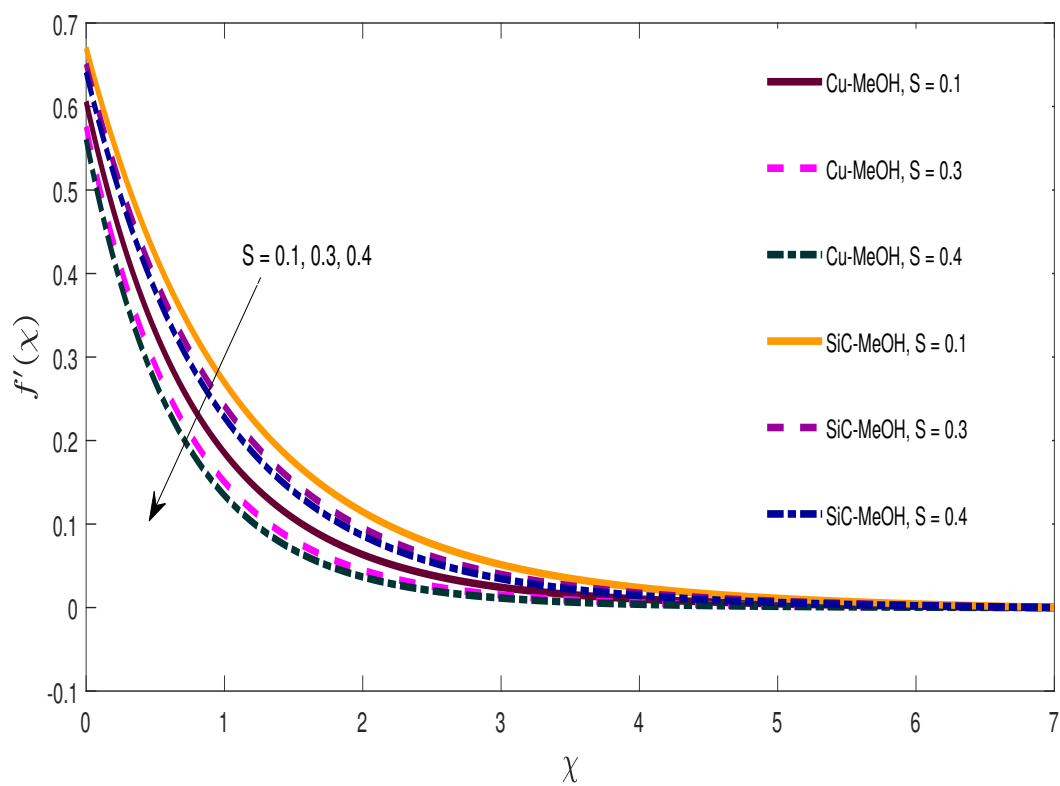


FIGURE 3.27: Temperature profile against Ec

FIGURE 3.28: Entropy profile against Ec FIGURE 3.29: Velocity profile against S

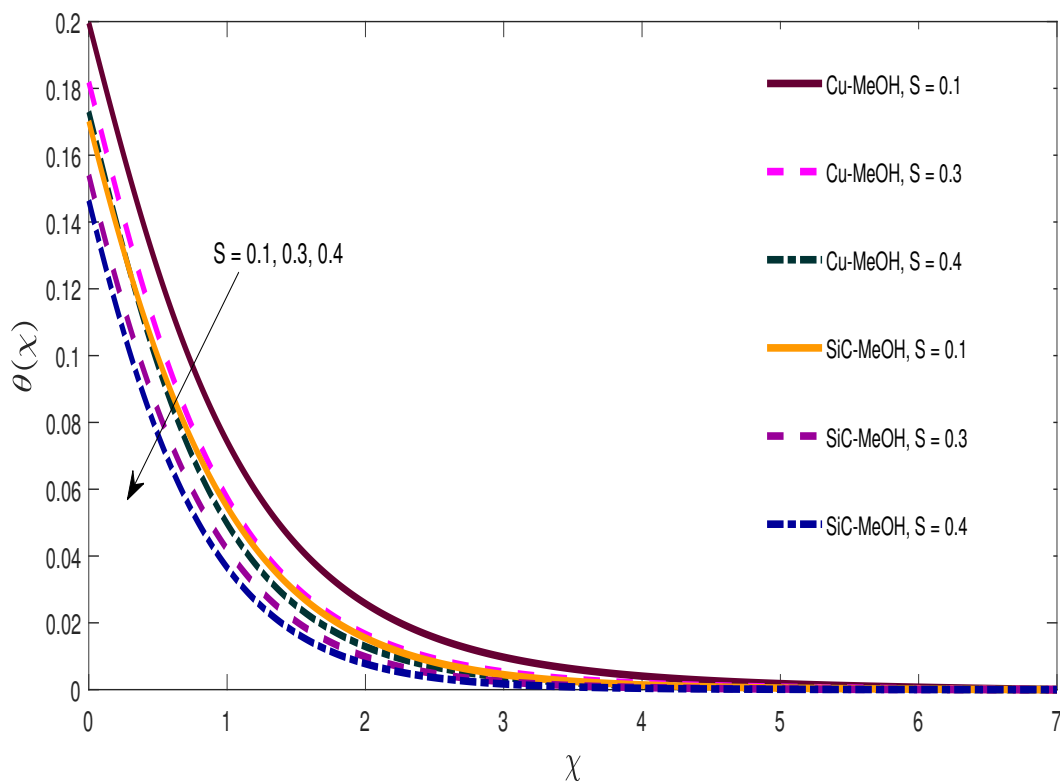


FIGURE 3.30: Temperature profile against S

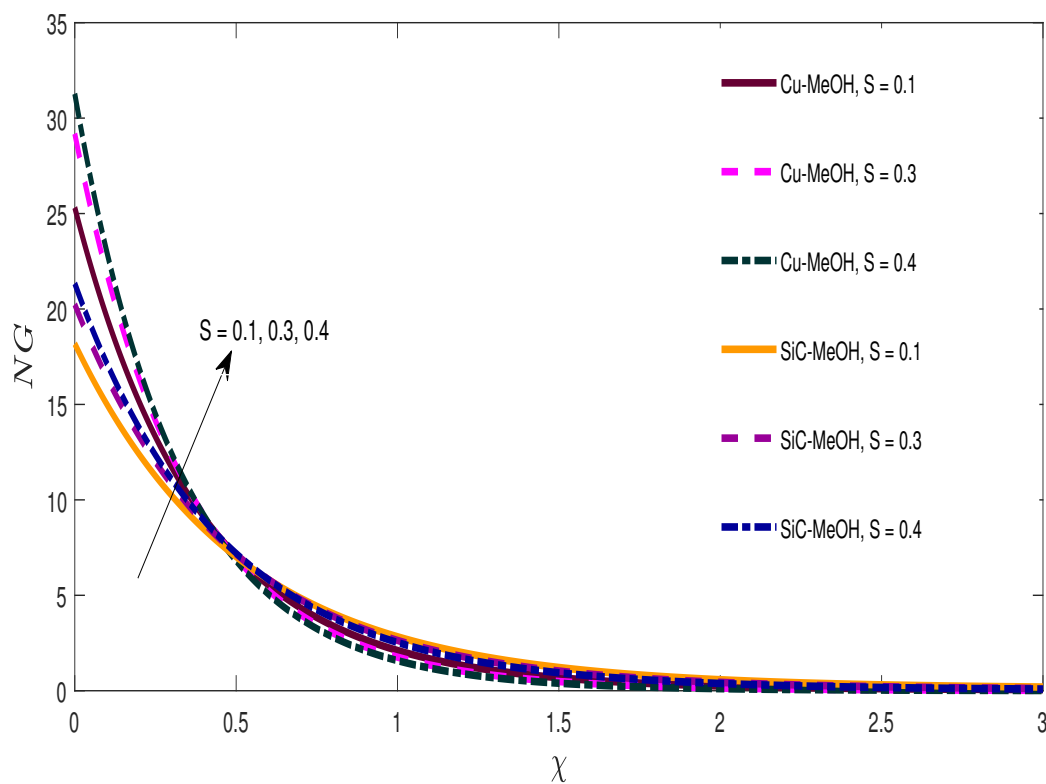
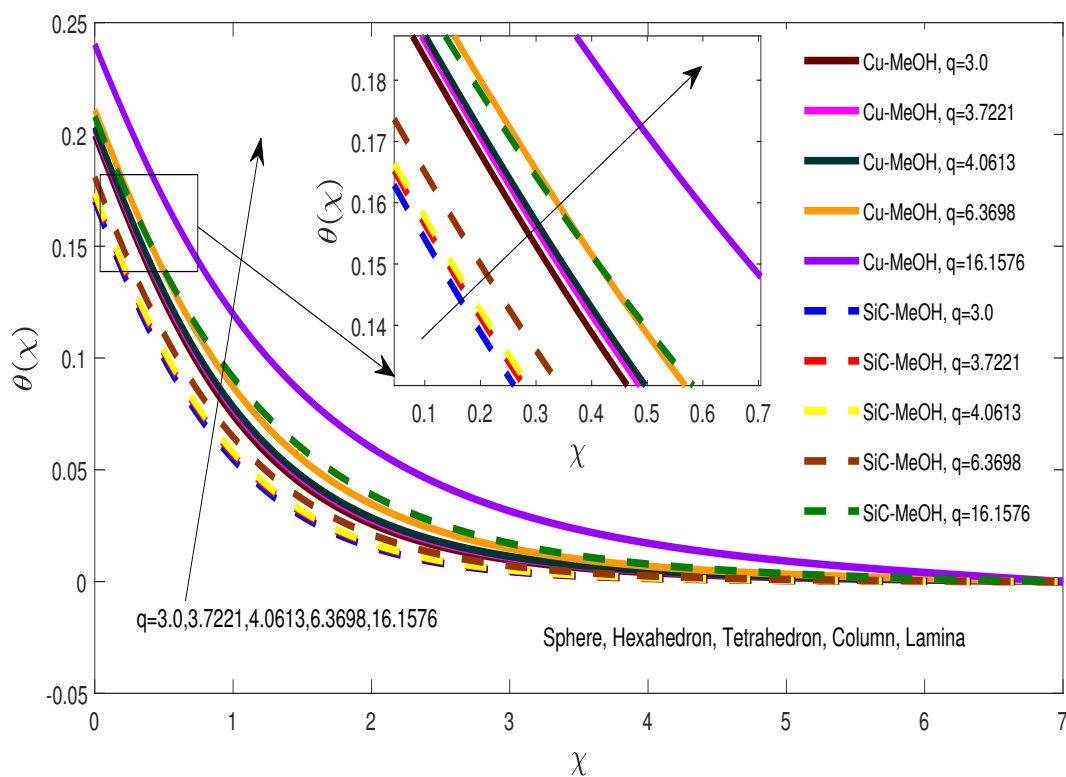
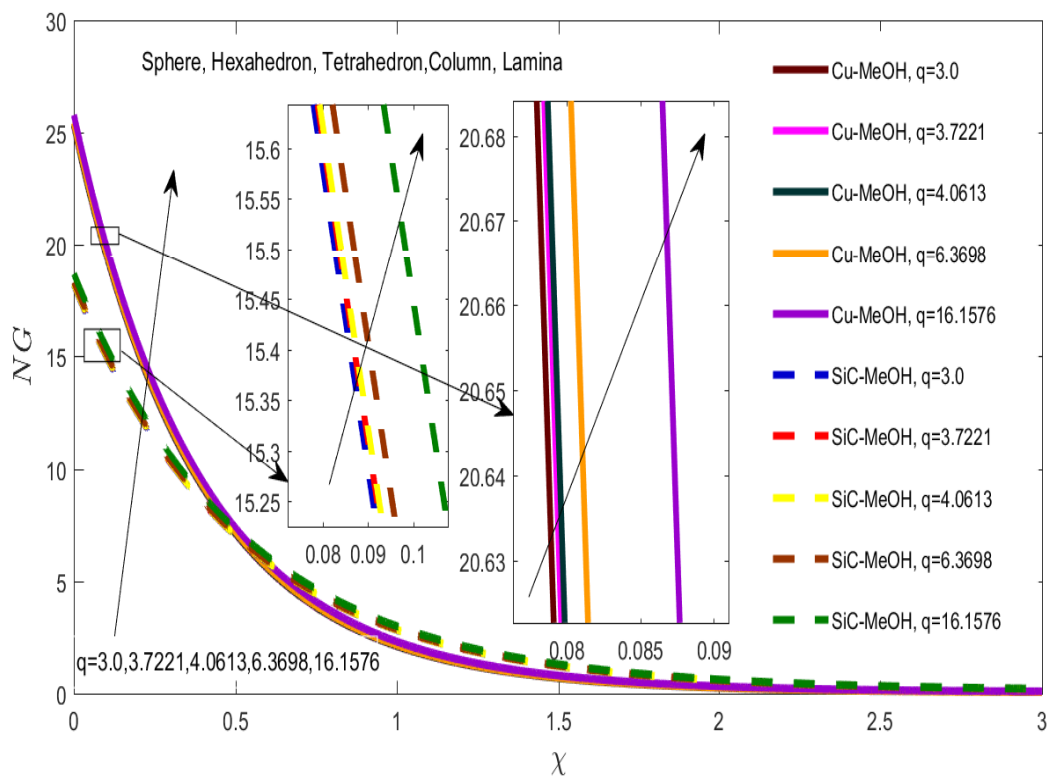
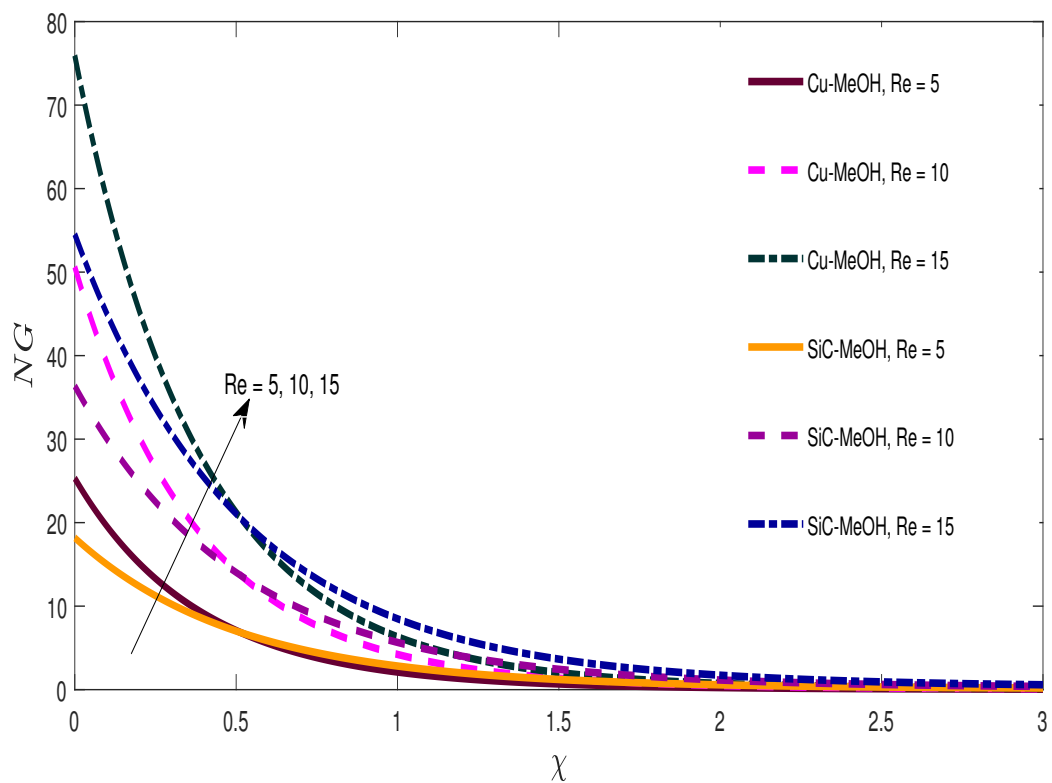
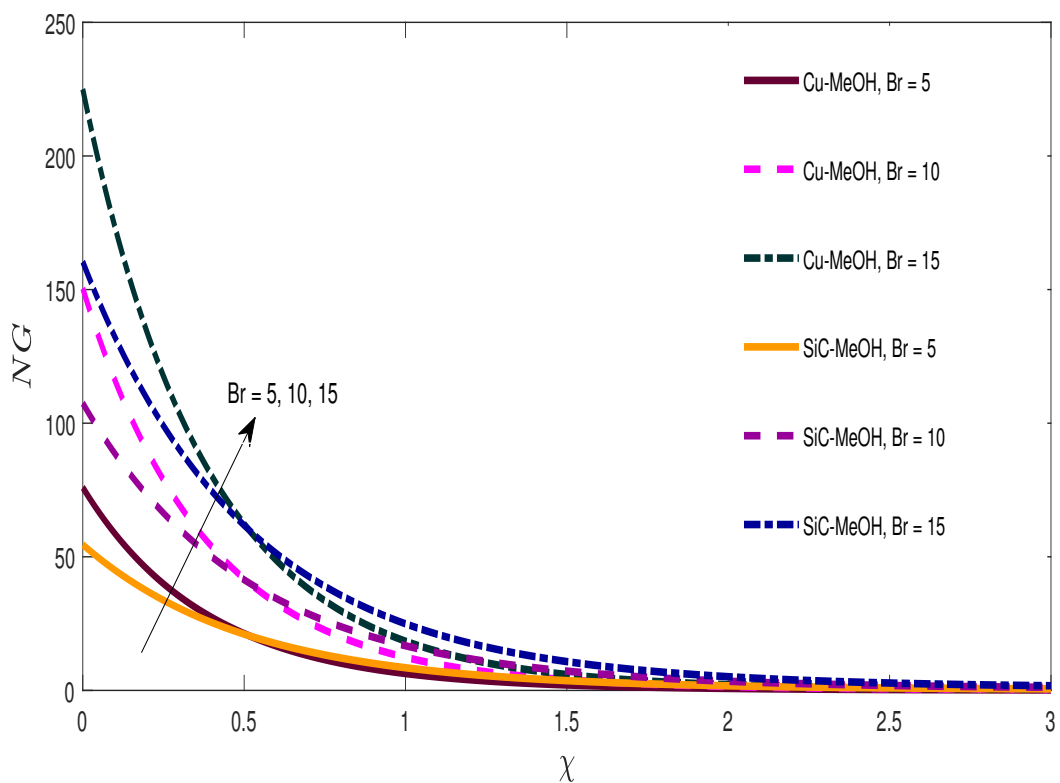


FIGURE 3.31: Entropy profile against S

FIGURE 3.32: Temperature profile against q FIGURE 3.33: Entropy profile against q

FIGURE 3.34: Entropy profile against Re FIGURE 3.35: Entropy profile against Br

Chapter 4

Unsteady 3D Powell-Eyring Flow of Cu and SiC/MeOH for a Boundary Layer Using Cattaneo-Christov Model with Entropy Analysis

4.1 Introduction

The objective of the present study is to explore the numerical simulations performed for Copper-Methanol (Cu-MeOH) and Silicon Carbide-Methanol (SiC-MeOH) nanofluids. The mathematical results are presented for considering velocity slip at the boundary and inducing the effect of thermal radiation for optically thick nanofluid. A uniformly distributed inclined magnetic field of strength is also assumed in the present model. To study the heat transfer, the Cattaneo-Christov heat flux model was considered. The influence of entropy generation on heat transfer was investigated numerically. Similarity transformations' utilization is carried out to reduce governing PDEs to ODEs and then numerical simulations are performed using the shooting technique to approximate the solutions for the velocity, temperature and entropy profiles. Additionally, the velocity gradient and heat exchange rate at the boundary were calculated and discussed graphically.

4.2 Description of Problem

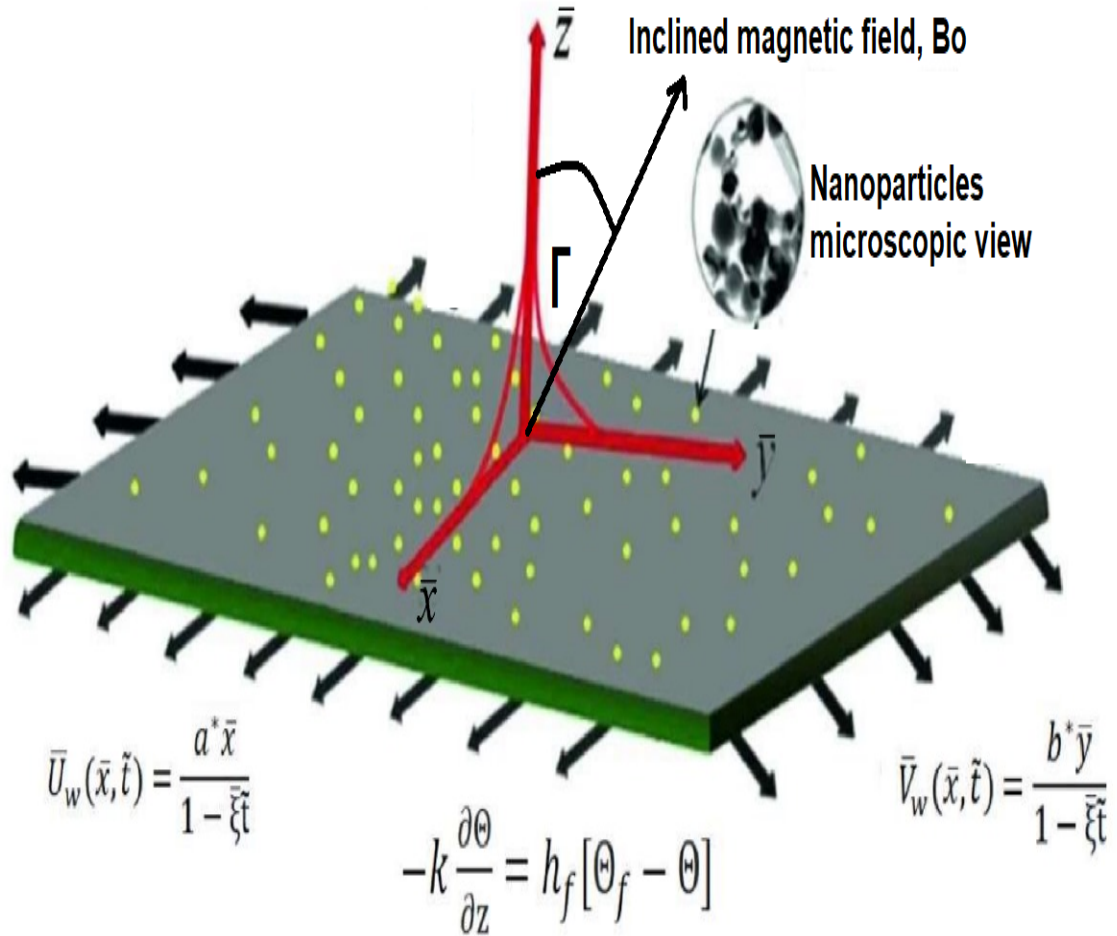


FIGURE 4.1: The physical geometry of the problem.

Consider an unsteady magnetohydrodynamics (MHD) three dimensional boundary layer flow of an incompressible Powell-Eyring nanofluid past a bidirectional stretching surface. It is assumed that the sheet is stretched along \bar{x} and \bar{y} directions with velocities $\bar{f}_1 = \bar{U}_w(\bar{x}, \bar{t}) = \frac{a^* \bar{x}}{(1 - \xi \bar{t})}$ and $\bar{f}_2 = \bar{V}_w(\bar{x}, \bar{t}) = \frac{b^* \bar{y}}{(1 - \xi \bar{t})}$ respectively, where a^* and b^* are positive constants relating to the stretching speed and \bar{t} is the time. The \bar{x} and \bar{y} axes are directed along the continuous stretching sheet and the \bar{z} axis normal to it. The sheet coincides with the plane $\bar{z} = 0$ and the flow takes place in the domain $\bar{z} > 0$. A uniform inclined magnetic field of strength B_0 is applied in \bar{z} -direction. In addition, the heat transfer analysis is carried out in the presence of nonlinear thermal radiation and heat generation. Heat transfer phenomenon is taken into account by incorporating the Cattaneo-Christov heat flux model. The surface temperature is maintained at a

certain value Θ_f such that $\Theta_f > \Theta_\infty$, where Θ_∞ is the ambient temperature. The Cauchy stress tensor Θ in the Powell-Eyring fluid model is given as [97]:

$$\Theta = -pI + \tau, \quad (4.1)$$

$$\rho_f a_i = -\nabla p + \nabla \cdot (\tau_{ij}) + \sigma^*(J \times B). \quad (4.2)$$

Here, p is the pressure, I is the identity tensor, σ^* is the electrical conductivity of the fluid, and τ_{ij} is extra stress tensor of the Eyring–Powell fluid model and is defined as:

$$\tau_{ij} = \mu \left(\frac{\partial \bar{f}_{1i}}{\partial \bar{x}_j} \right) + \left(\frac{1}{\hat{\beta}} \right) \sinh^{-1} \left[\left(\frac{1}{\gamma} \right) \left(\frac{\partial \bar{f}_{1i}}{\partial \bar{x}_j} \right) \right],$$

where μ is the viscosity coefficient, and $\hat{\beta}$ and γ are characteristics of the Eyring–Powell fluid such that:

$$\sinh^{-1} \left(\frac{1}{\gamma} \frac{\partial \bar{f}_{1i}}{\partial \bar{x}_j} \right) \cong \frac{1}{\gamma} \left(\frac{\partial \bar{f}_{1i}}{\partial \bar{x}_j} \right) - \frac{1}{6\gamma} \left(\frac{\partial \bar{f}_{1i}}{\partial \bar{x}_j} \right)^3 \quad \text{and} \quad \left| \frac{1}{\gamma} \frac{\partial \bar{f}_{1i}}{\partial \bar{x}_j} \right| < 1. \quad (4.3)$$

4.2.1 Governing Equations

The governing equations for the conservation of mass, momentum, and energy under the boundary layer assumption and appropriate boundary conditions for Powell-Eyring nanofluid can be expressed as [98, 99]:

$$\frac{\partial \bar{f}_1}{\partial \bar{x}} + \frac{\partial \bar{f}_2}{\partial \bar{y}} + \frac{\partial \bar{f}_3}{\partial \bar{z}} = 0, \quad (4.4)$$

$$\begin{aligned} \frac{\partial \bar{f}_1}{\partial \bar{t}} + \bar{f}_1 \frac{\partial \bar{f}_1}{\partial \bar{x}} + \bar{f}_2 \frac{\partial \bar{f}_1}{\partial \bar{y}} + \bar{f}_3 \frac{\partial \bar{f}_1}{\partial \bar{z}} = & \left(\nu_{nf} + \frac{1}{\rho_{nf} \hat{\beta} h^*} \right) \frac{\partial^2 \bar{f}_1}{\partial \bar{z}^2} - \frac{1}{2 \hat{\beta} h^{*3} \rho_{nf}} \left(\frac{\partial \bar{f}_1}{\partial \bar{z}} \right)^2 \frac{\partial^2 \bar{f}_1}{\partial \bar{z}^2} \\ & - \frac{\sigma_{nf}^* B^2(\bar{t}) \bar{f}_1}{\rho_{nf}} \sin^2(\Gamma), \end{aligned} \quad (4.5)$$

$$\begin{aligned} \frac{\partial \bar{f}_2}{\partial \bar{t}} + \bar{f}_1 \frac{\partial \bar{f}_2}{\partial \bar{x}} + \bar{f}_2 \frac{\partial \bar{f}_2}{\partial \bar{y}} + \bar{f}_3 \frac{\partial \bar{f}_2}{\partial \bar{z}} &= \left(\nu_{nf} + \frac{1}{\rho_{nf} \hat{\beta} h^*} \right) \frac{\partial^2 \bar{f}_2}{\partial \bar{z}^2} - \frac{1}{2 \hat{\beta} h^* \rho_{nf}} \left(\frac{\partial \bar{f}_2}{\partial \bar{z}} \right)^2 \frac{\partial^2 \bar{f}_2}{\partial \bar{z}^2} \\ &\quad - \frac{\sigma_{nf}^* B^2(\bar{t}) \bar{f}_2}{\rho_{nf}} \sin^2(\Gamma), \end{aligned} \quad (4.6)$$

$$\begin{aligned} \frac{\partial \Theta}{\partial \bar{t}} + \bar{f}_1 \frac{\partial \Theta}{\partial \bar{x}} + \bar{f}_2 \frac{\partial \Theta}{\partial \bar{y}} + \bar{f}_3 \frac{\partial \Theta}{\partial \bar{z}} &= \frac{k_{nf}}{(\rho C_p)_{nf}} \left(\frac{\partial^2 \Theta}{\partial \bar{z}^2} \right) - \frac{1}{(\rho C_p)_{nf}} \left(\frac{\partial q_r}{\partial \bar{z}} \right) + \frac{\nu_{nf}}{(\rho C_p)_{nf}} \\ &\quad \left(\frac{\partial \bar{f}_1}{\partial \bar{z}} \right)^2 + \frac{Q_0}{(\rho C_p)_{nf}} (\Theta - \Theta_\infty) - \lambda \left[\bar{f}_1 \frac{\partial \bar{f}_1}{\partial \bar{x}} \frac{\partial \Theta}{\partial \bar{x}} \right. \\ &\quad + \bar{f}_2 \frac{\partial \bar{f}_1}{\partial \bar{y}} \frac{\partial \Theta}{\partial \bar{x}} + \bar{f}_3 \frac{\partial \bar{f}_1}{\partial \bar{z}} \frac{\partial \Theta}{\partial \bar{x}} + \bar{f}_1 \frac{\partial \bar{f}_2}{\partial \bar{x}} \frac{\partial \Theta}{\partial \bar{y}} + \bar{f}_2 \frac{\partial \bar{f}_2}{\partial \bar{y}} \frac{\partial \Theta}{\partial \bar{y}} \\ &\quad + \bar{f}_3 \frac{\partial \bar{f}_2}{\partial \bar{z}} \frac{\partial \Theta}{\partial \bar{y}} + \bar{f}_1 \frac{\partial \bar{f}_3}{\partial \bar{x}} \frac{\partial \Theta}{\partial \bar{z}} + \bar{f}_2 \frac{\partial \bar{f}_3}{\partial \bar{y}} \frac{\partial \Theta}{\partial \bar{z}} + \bar{f}_3 \frac{\partial \bar{f}_3}{\partial \bar{z}} \frac{\partial \Theta}{\partial \bar{z}} \\ &\quad + \bar{f}_1^2 \frac{\partial^2 \Theta}{\partial \bar{x}^2} + \bar{f}_2^2 \frac{\partial^2 \Theta}{\partial \bar{y}^2} + \bar{f}_3^2 \frac{\partial^2 \Theta}{\partial \bar{z}^2} + 2 \bar{f}_1 \bar{f}_2 \frac{\partial^2 \Theta}{\partial \bar{x} \partial \bar{y}} \\ &\quad \left. + 2 \bar{f}_1 \bar{f}_3 \frac{\partial^2 \Theta}{\partial \bar{y} \partial \bar{z}} + 2 \bar{f}_1 \bar{f}_3 \frac{\partial^2 \Theta}{\partial \bar{x} \partial \bar{z}} \right] + \frac{\sigma_{nf}^* B^2(\bar{t}) \bar{f}_1^2}{(\rho C_p)_{nf}} \sin^2(\Gamma). \end{aligned} \quad (4.7)$$

The associated BCs of the governing PDEs are [97]:

$$\left. \begin{aligned} \bar{f}_1 &= \bar{U}_w(\bar{x}) + K_1 \left(\frac{\partial \bar{f}_1}{\partial \bar{z}} \right), \quad \bar{f}_2 = \bar{V}_w(\bar{y}) + K_2 \left(\frac{\partial \bar{f}_2}{\partial \bar{z}} \right), \\ \bar{f}_3 &= 0, \quad -k \left(\frac{\partial \Theta}{\partial \bar{z}} \right) = h_f (\Theta_f - \Theta) \\ \bar{f}_1 &\longrightarrow 0, \bar{f}_2 \longrightarrow 0, \Theta \longrightarrow \Theta_\infty \quad \text{as } \bar{z} \longrightarrow \infty. \end{aligned} \right\} \text{at } \bar{z} = 0, \quad (4.8)$$

where \bar{f}_1 , \bar{f}_2 and \bar{f}_3 are velocities in \bar{x} , \bar{y} and \bar{z} directions, \bar{t} is the time, Θ is the fluid temperature, Γ is the inclination angle of the magnetic field. The radiative heat flux q_r is given by

$$q_r = -\frac{4\sigma^*}{3k^*} \frac{\partial \Theta^4}{\partial \bar{z}} = -\frac{16\sigma^*}{3k^*} \Theta^3 \frac{\partial \Theta}{\partial \bar{z}}. \quad (4.9)$$

where σ^* is the Stefan-Boltzman constant and k^* is the mean absorption coefficient. If the temperature difference is very small, then the temperature Θ^4 can be expanded

about Θ_∞ using the Taylor series, as follows:

$$\Theta^4 = \Theta_\infty^4 + 4\Theta_\infty^3(\Theta - \Theta_\infty) + 6\Theta_\infty^2(\Theta - \Theta_\infty)^2 + \dots$$

Ignoring the higher order terms, we have

$$\begin{aligned}\Theta^4 &= \Theta_\infty^4 + 4\Theta_\infty^3(\Theta - \Theta_\infty) \\ &= -3\Theta_\infty^4 + 4\Theta_\infty^3\Theta \\ &= 4\Theta_\infty^3\Theta - 3\Theta_\infty^4.\end{aligned}$$

4.2.2 Similarity Transformations

The nonlinear partial differential equations are converted to dimensionless ordinary differential equations using the following analogy:

$$\left. \begin{aligned}\bar{f}_1 &= \frac{c^*}{1 - \xi\bar{t}}\bar{x}\frac{df}{d\chi}, & \bar{f}_2 &= \frac{c^*}{1 - \xi\bar{t}}\bar{y}\frac{dg}{d\chi}, \\ \bar{f}_3 &= -\sqrt{\frac{c^*\nu_f}{1 - \xi\bar{t}}}[f(\chi) + g(\chi)], \\ \chi(\bar{x}, \bar{y}) &= \sqrt{\frac{c^*}{\nu_f(1 - \xi\bar{t})}}\bar{z}, & \theta(\chi) &= \frac{\Theta - \Theta_\infty}{\Theta_f - \Theta_\infty}.\end{aligned}\right\} \quad (4.10)$$

4.2.3 Transformation of Physical Quantities

The dimensional forms of the skin friction coefficient, Nusselt number are shown below. The dimensionless form of these parameters will be produced and used in the subsequent section of this chapter, which will examine the solution to our current problem.

$$\left. \begin{aligned}C_{f\bar{x}} &= \frac{\tau_w}{\rho_f \bar{U}_w^2}, & C_{f\bar{y}} &= \frac{\tau_w}{\rho_f \bar{U}_w^2}, & Nu_{\bar{x}} &= \frac{\bar{x}q_w}{k_f(\Theta_f - \Theta_\infty)}.\end{aligned}\right\} \quad (4.11)$$

4.2.4 Entropy Generation Formulations

Entropy is a disorder of a system and its surroundings from a physical perspective. Entropy often arises in a number of systems, particularly those involving fluid viscous force, Joule heating, and flow-driven force. Therefore, entropy is also known as the number of irreversibilities. As a result, heat cannot entirely be converted into work. The dimensional form of entropy generation is expressed as follows:

$$E_G = \frac{k_{nf}}{\Theta_\infty^2} \left[\left(\frac{\partial \Theta}{\partial \bar{z}} \right)^2 + \frac{16}{3} \frac{\sigma^* \Theta_\infty^3}{k^* \nu_f (\rho C_p)_f} \left(\frac{\partial \Theta}{\partial \bar{z}} \right)^2 \right] + \frac{\mu_{nf}}{\Theta_\infty} \left(\frac{\partial \bar{f}_1}{\partial \bar{z}} \right)^2 + \frac{\sigma_{nf}^* B^2(\tilde{t}) \sin^2(\Gamma) \bar{f}_1^2}{\Theta_\infty}. \quad (4.12)$$

4.3 PDEs to ODEs Transformation

4.3.1 Transformation of the Governing PDEs

To solve the governing system of PDEs (4.4)-(4.7) into a system of ODEs, we introduce similarity variables which are given in equation (4.10).

$$\frac{\partial \chi}{\partial \bar{x}} = 0. \quad (4.13)$$

$$\frac{\partial \chi}{\partial \bar{y}} = 0. \quad (4.14)$$

$$\frac{\partial \chi}{\partial \bar{z}} = \sqrt{\frac{c^*}{\nu_f (1 - \xi \tilde{t})}}. \quad (4.15)$$

$$\frac{\partial \bar{f}_1}{\partial \bar{x}} = \frac{c^*}{1 - \xi \tilde{t}} \frac{df}{d\chi}. \quad (4.16)$$

$$\frac{\partial \bar{f}_2}{\partial \bar{y}} = \frac{c^*}{1 - \xi \tilde{t}} \frac{dg}{d\chi}. \quad (4.17)$$

$$\frac{\partial \bar{f}_3}{\partial \bar{z}} = -\frac{c^*}{1 - \xi \tilde{t}} \left[\frac{df}{d\chi} + \frac{dg}{d\chi} \right]. \quad (4.18)$$

$$\bar{f}_1 \frac{\partial \bar{f}_1}{\partial \bar{x}} = \frac{c^{*2}}{(1 - \xi \tilde{t})^2} \bar{x} \left(\frac{df}{d\chi} \right)^2. \quad (4.19)$$

$$\frac{\partial \bar{f}_1}{\partial \bar{y}} = 0. \quad (4.20)$$

$$\frac{\partial \chi}{\partial \bar{t}} = \frac{\bar{z}}{2} \sqrt{\frac{\nu_f(1-\bar{\xi}\bar{t})}{c^*}} \left[\frac{c^*\bar{\xi}}{\nu_f(1-\bar{\xi}\bar{t})^2} \right]. \quad (4.21)$$

$$\frac{\partial \bar{f}_1}{\partial \bar{t}} = \frac{c^*\bar{\xi}\bar{x}}{(1-\bar{\xi}\bar{t})^2} \frac{df}{d\chi} + \frac{c^*\bar{\xi}}{2(1-\bar{\xi}\bar{t})^2} \sqrt{\frac{c^*}{\nu_f(1-\bar{\xi}\bar{t})}} \bar{x}\bar{z} \frac{d^2f}{d\chi^2}. \quad (4.22)$$

$$\frac{\partial \bar{f}_1}{\partial \bar{z}} = \frac{c^*\bar{x}}{1-\bar{\xi}\bar{t}} \frac{d^2f}{d\chi^2} \sqrt{\frac{c^*}{\nu_f(1-\bar{\xi}\bar{t})}}. \quad (4.23)$$

$$\bar{f}_3 \frac{\partial \bar{f}_1}{\partial \bar{z}} = -\frac{c^{*2}\bar{x}}{(1-\bar{\xi}\bar{t})^2} [f(\chi) + g(\chi)] \frac{d^2f}{d\chi^2}. \quad (4.24)$$

$$\left(\frac{\partial \bar{f}_1}{\partial \bar{z}} \right)^2 = \frac{c^{*3}\bar{x}^2}{\nu_f(1-\bar{\xi}\bar{t})^3} \left(\frac{d^2f}{d\chi^2} \right)^2. \quad (4.25)$$

$$\frac{\partial^2 \bar{f}_1}{\partial \bar{z}^2} = \frac{c^{*2}}{\nu_f(1-\bar{\xi}\bar{t})^2} \bar{x} \frac{d^3f}{d\chi^3}. \quad (4.26)$$

$$\frac{\partial \bar{f}_2}{\partial \bar{x}} = 0. \quad (4.27)$$

$$\bar{f}_2 \frac{\partial \bar{f}_2}{\partial \bar{y}} = \frac{c^{*2}}{(1-\bar{\xi}\bar{t})^2} \bar{y} \left(\frac{dg}{d\chi} \right)^2. \quad (4.28)$$

$$\frac{\partial \bar{f}_2}{\partial \bar{t}} = \frac{c^*\bar{\xi}\bar{y}}{(1-\bar{\xi}\bar{t})^2} \frac{dg}{d\chi} + \frac{c^*\bar{\xi}}{2(1-\bar{\xi}\bar{t})^2} \sqrt{\frac{c^*}{\nu_f(1-\bar{\xi}\bar{t})}} \bar{y}\bar{z} \frac{d^2g}{d\chi^2}. \quad (4.29)$$

$$\frac{\partial \bar{f}_2}{\partial \bar{z}} = \frac{c^*\bar{y}}{1-\bar{\xi}\bar{t}} \frac{d^2g}{d\chi^2} \sqrt{\frac{c^*}{\nu_f(1-\bar{\xi}\bar{t})}}. \quad (4.30)$$

$$\bar{f}_3 \frac{\partial \bar{f}_2}{\partial \bar{z}} = -\frac{c^{*2}\bar{y}}{(1-\bar{\xi}\bar{t})^2} [f(\chi) + g(\chi)] \frac{d^2g}{d\chi^2}. \quad (4.31)$$

$$\left(\frac{\partial \bar{f}_2}{\partial \bar{z}} \right)^2 = \frac{c^{*3}\bar{y}^2}{\nu_f(1-\bar{\xi}\bar{t})^3} \left(\frac{d^2g}{d\chi^2} \right)^2. \quad (4.32)$$

$$\frac{\partial^2 \bar{f}_2}{\partial \bar{z}^2} = \frac{c^{*2}}{\nu_f(1-\bar{\xi}\bar{t})^2} \bar{y} \frac{d^3g}{d\chi^3}. \quad (4.33)$$

$$\theta(\chi) = \frac{\Theta - \Theta_\infty}{\Theta_f - \Theta_\infty}$$

$$\Rightarrow \Theta - \Theta_\infty = (\Theta_f - \Theta_\infty)\theta(\chi)$$

$$\Rightarrow \Theta = (\Theta_f - \Theta_\infty)\theta(\chi) + \Theta_\infty$$

$$\Rightarrow \Theta = \left(\Theta_\infty + \frac{c^*\bar{x}}{1-\bar{\xi}\bar{t}} - \Theta_\infty \right) \theta(\chi) + \Theta_\infty$$

$$\Rightarrow \Theta = \left(\frac{c^* \bar{x}}{1 - \bar{\xi} \bar{t}} \right) \theta(\chi) + \Theta_\infty$$

$$\frac{\partial \Theta}{\partial \bar{x}} = \left[\frac{c^*}{1 - \bar{\xi} \bar{t}} \right] \theta(\chi). \quad (4.34)$$

$$\frac{\partial \Theta}{\partial \bar{y}} = 0. \quad (4.35)$$

$$\frac{\partial \Theta}{\partial \bar{z}} = \left[\frac{c^* \bar{x}}{1 - \bar{\xi} \bar{t}} \right] \frac{d\theta}{d\chi} \sqrt{\frac{c^*}{\nu_f (1 - \bar{\xi} \bar{t})}}. \quad (4.36)$$

$$\frac{\partial^2 \Theta}{\partial \bar{x}^2} = 0. \quad (4.37)$$

$$\frac{\partial^2 \Theta}{\partial \bar{z}^2} = \frac{c^{*2} \bar{x}}{\nu_f (1 - \bar{\xi} \bar{t})^2} \frac{d^2 \theta}{d\chi^2}. \quad (4.38)$$

$$\bar{f}_1 \frac{\partial \Theta}{\partial \bar{x}} = \frac{c^{*2}}{(1 - \bar{\xi} \bar{t})^2} \bar{x} \frac{df}{d\chi} \theta(\chi). \quad (4.39)$$

$$\bar{f}_3 \frac{\partial \Theta}{\partial \bar{z}} = - \frac{c^{*2} \bar{x}}{(1 - \bar{\xi} \bar{t})^2} f(\chi) \frac{d\theta}{d\chi} - \frac{c^{*2} \bar{x}}{(1 - \bar{\xi} \bar{t})^2} g(\chi) \frac{d\theta}{d\chi}. \quad (4.40)$$

$$\frac{\partial \Theta}{\partial \bar{t}} = \frac{c^* \bar{x} \bar{\xi}}{(1 - \bar{\xi} \bar{t})^2} \theta(\chi) + \frac{c^{*2} \bar{x} \bar{\xi}}{\nu_f (1 - \bar{\xi} \bar{t})^3} \frac{\bar{z}}{2} \sqrt{\frac{\nu_f (1 - \bar{\xi} \bar{t})}{c^*}} \frac{d\theta}{d\chi}. \quad (4.41)$$

$$\frac{\partial q_r}{\partial \bar{y}} = - \frac{16 \Theta_\infty^3 \sigma^*}{3 k^*} \frac{\partial^2 \Theta}{\partial \bar{z}^2}. \quad (4.42)$$

$$\frac{\partial \bar{f}_3}{\partial \bar{x}} = 0. \quad (4.43)$$

$$\frac{\partial \bar{f}_3}{\partial \bar{y}} = 0. \quad (4.44)$$

$$\bar{f}_1 \frac{\partial \bar{f}_1}{\partial \bar{x}} \frac{\partial \Theta}{\partial \bar{x}} = \frac{c^{*3} \times \bar{x}}{(1 - \bar{\xi} \bar{t})^3} \left(\frac{df}{d\chi} \right)^2 \theta(\chi). \quad (4.45)$$

$$\bar{f}_3 \frac{\partial \bar{f}_1}{\partial \bar{z}} \frac{\partial \Theta}{\partial \bar{x}} = - \frac{c^{*3} \bar{x}}{(1 - \bar{\xi} \bar{t})^3} f(\chi) \frac{d^2 f}{d\chi^2} \theta(\chi) - \frac{c^{*3} \bar{x}}{(1 - \bar{\xi} \bar{t})^3} g(\chi) \frac{d^2 f}{d\chi^2} \theta(\chi). \quad (4.46)$$

$$\bar{f}_3 \frac{\partial \bar{f}_3}{\partial \bar{z}} \frac{\partial \Theta}{\partial \bar{z}} = \frac{c^{*3} \bar{x}}{(1 - \bar{\xi} \bar{t})^3} [f(\chi) + g(\chi)] \left[\frac{df}{d\chi} + \frac{dg}{d\chi} \right] \frac{d\theta}{d\chi}. \quad (4.47)$$

$$\bar{f}_3^2 \frac{\partial^2 \Theta}{\partial \bar{z}^2} = \frac{c^{*3} \bar{x}}{(1 - \bar{\xi} \bar{t})^3} [f(\chi) + g(\chi)]^2 \frac{d^2 \theta}{d\chi^2}. \quad (4.48)$$

$$\begin{aligned}
\frac{\mu_{nf}}{\rho_f} &= \frac{\mu_f(1-\Phi)^{-2.5}}{\frac{(1-\Phi)\rho_f + \Phi\rho_s}{\mu_f}} \\
&= \frac{\mu_f(1-\Phi)^{-2.5}}{\mu_f \left[(1-\Phi) + \Phi \left(\frac{\rho_s}{\rho_f} \right) \right]} \\
&= \frac{1}{(1-\Phi)^{2.5} \left[(1-\Phi) + \Phi \left(\frac{\rho_s}{\rho_f} \right) \right]}. \tag{4.49}
\end{aligned}$$

$$\begin{aligned}
\rho_{nf} \frac{\mu_f}{\rho_f} &= \left[(1-\Phi)\rho_f + \Phi\rho_s \right] \times \frac{\mu_f}{\rho_f} \\
&= \left[(1-\Phi) + \Phi \frac{\rho_s}{\rho_f} \right] \times \mu_f. \tag{4.50}
\end{aligned}$$

$$\begin{aligned}
\frac{\sigma_{nf}^*}{\sigma_f} &= \left[1 + \frac{3\left(\frac{\sigma_s}{\sigma_f} - 1\right)\Phi}{\left(\frac{\sigma_s}{\sigma_f} + 2\right) - \left(\frac{\sigma_s}{\sigma_f} - 1\right)\Phi} \right] \\
\sigma_{nf}^* &= \left[1 + \frac{3\left(\frac{\sigma_s}{\sigma_f} - 1\right)\Phi}{\left(\frac{\sigma_s}{\sigma_f} + 2\right) - \left(\frac{\sigma_s}{\sigma_f} - 1\right)\Phi} \right] \times \sigma_f. \tag{4.51}
\end{aligned}$$

$$\begin{aligned}
\rho_{nf} &= \left[(1-\Phi)\rho_f + \Phi\rho_s \right] \times \frac{\rho_f}{\rho_f} \\
\rho_{nf} &= \left[(1-\Phi) + \Phi \frac{\rho_s}{\rho_f} \right] \times \rho_f. \tag{4.52}
\end{aligned}$$

$$\begin{aligned}
\frac{k_{nf}}{k_f} &= \left[\frac{(k_s + (q-1)k_f) - (q-1)\Phi(k_f - k_s)}{(k_s + (q-1)k_f) + \Phi(k_f - k_s)} \right] \\
k_{nf} &= \left[\frac{(k_s + (q-1)k_f) - (q-1)\Phi(k_f - k_s)}{(k_s + (q-1)k_f) + \Phi(k_f - k_s)} \right] \times k_f. \tag{4.53}
\end{aligned}$$

$$\begin{aligned}
(\rho C_p)_{nf} &= (1-\Phi)(\rho C_p)_f + \Phi(\rho C_p)_s \\
\frac{(\rho C_p)_{nf}}{(\rho C_p)_f} &= (1-\Phi) + \Phi \frac{(\rho C_p)_s}{(\rho C_p)_f} \\
(\rho C_p)_{nf} &= \left[(1-\Phi) + \Phi \frac{(\rho C_p)_s}{(\rho C_p)_f} \right] \times (\rho C_p)_f. \tag{4.54}
\end{aligned}$$

By using (4.16), (4.17) and (4.18), in (4.4) as follows.

$$\frac{\partial \bar{f}_1}{\partial \bar{x}} + \frac{\partial \bar{f}_2}{\partial \bar{y}} + \frac{\partial \bar{f}_3}{\partial \bar{z}} = \frac{c^*}{1 - \bar{\xi} \bar{t}} \frac{df}{d\chi} + \frac{c^*}{1 - \bar{\xi} \bar{t}} \frac{dg}{d\chi} - \frac{c^*}{1 - \bar{\xi} \bar{t}} \frac{df}{d\chi} - \frac{c^*}{1 - \bar{\xi} \bar{t}} \frac{dg}{d\chi} = 0.$$

Hence continuity Equation (4.4) is identically satisfied.

Now, the dimensionless form of the momentum equation (4.5) can be obtained by using equations (4.19)-(4.26) and (4.49)-(4.52) as follows,

$$\begin{aligned} \frac{\partial \bar{f}_1}{\partial \bar{t}} + \bar{f}_1 \frac{\partial \bar{f}_1}{\partial \bar{x}} + \bar{f}_2 \frac{\partial \bar{f}_1}{\partial \bar{y}} + \bar{f}_3 \frac{\partial \bar{f}_1}{\partial \bar{z}} &= \left(\nu_{nf} + \frac{1}{\rho_{nf} \hat{\beta} h^*} \right) \frac{\partial^2 \bar{f}_1}{\partial \bar{z}^2} - \frac{1}{2 \hat{\beta} h^{*3} \rho_{nf}} \left(\frac{\partial \bar{f}_1}{\partial \bar{z}} \right)^2 \frac{\partial^2 \bar{f}_1}{\partial \bar{z}^2} \\ &\quad - \frac{\sigma_{nf}^* B^2(\bar{t}) \bar{f}_1}{\rho_{nf}} \sin^2(\Gamma), \end{aligned}$$

$$\begin{aligned} \Rightarrow \frac{c^* \bar{\xi}}{(1 - \bar{\xi} \bar{t})^2} \bar{x} \frac{df}{d\chi} + \frac{c^* \bar{\xi}}{2(1 - \bar{\xi} \bar{t})^2} \sqrt{\frac{c^*}{\nu_f(1 - \bar{\xi} \bar{t})}} \bar{x} \bar{z} \frac{d^2 f}{d\chi^2} + \frac{c^{*2}}{(1 - \bar{\xi} \bar{t})^2} \bar{x} \left(\frac{df}{d\chi} \right)^2 + 0 \\ - \frac{c^{*2}}{(1 - \bar{\xi} \bar{t})^2} \bar{x} f(\chi) \frac{d^2 f}{d\chi^2} - \frac{c^{*2}}{(1 - \bar{\xi} \bar{t})^2} \bar{x} g(\chi) \frac{d^2 f}{d\chi^2} = \left(\nu_{nf} + \frac{1}{\rho_{nf} \hat{\beta} h^*} \right) \frac{c^{*2}}{\nu_f(1 - \bar{\xi} \bar{t})^2} \\ \bar{x} \frac{d^3 f}{d\chi^3} - \frac{1}{2 \hat{\beta} h^{*3} \rho_{nf}} \frac{c^{*3} \bar{x}^2}{\nu_f(1 - \bar{\xi} \bar{t})^3} \left(\frac{d^2 f}{d\chi^2} \right)^2 - \frac{c^{*2}}{\nu_f(1 - \bar{\xi} \bar{t})^2} \bar{x} \frac{d^3 f}{d\chi^3} - \frac{\sigma_{nf}^*}{\rho_{nf}} \frac{B_0^2}{(\sqrt{(1 - \bar{\xi} \bar{t})})^2} \\ \frac{c^* \bar{x}}{(1 - \bar{\xi} \bar{t})} \frac{df}{d\chi} \sin^2(\Gamma). \end{aligned}$$

$$\begin{aligned} \Rightarrow \frac{\bar{\xi}}{c^*} \frac{df}{d\chi} + \frac{1}{2} \frac{\bar{\xi}}{c^*} \sqrt{\frac{c^*}{\nu_f(1 - \bar{\xi} \bar{t})}} \bar{z} \frac{d^2 f}{d\chi^2} + \left(\frac{df}{d\chi} \right)^2 - f(\chi) \frac{d^2 f}{d\chi^2} - g(\chi) \frac{d^2 f}{d\chi^2} = \left(\nu_{nf} + \right. \\ \left. \frac{1}{\rho_{nf} \hat{\beta} h^*} \right) \frac{1}{\nu_f} \frac{d^3 f}{d\chi^3} - \frac{1}{2 \hat{\beta} h^{*3} \rho_{nf}} \frac{c^{*3} \bar{x}^2}{\nu_f(1 - \bar{\xi} \bar{t})^3} \left(\frac{d^2 f}{d\chi^2} \right)^2 - \frac{1}{\nu_f} \frac{d^3 f}{d\chi^3} - \frac{\sigma_{nf}^*}{\rho_{nf}} \frac{B_0^2}{c^*} \frac{df}{d\chi} \sin^2(\Gamma). \end{aligned}$$

$$\begin{aligned} \Rightarrow \frac{\bar{\xi}}{c^*} \left[\frac{df}{d\chi} + \frac{1}{2} \sqrt{\frac{c^*}{\nu_f(1 - \bar{\xi} \bar{t})}} \bar{z} \frac{d^2 f}{d\chi^2} \right] + \left(\frac{df}{d\chi} \right)^2 - f(\chi) \frac{d^2 f}{d\chi^2} - g(\chi) \frac{d^2 f}{d\chi^2} = \left(\frac{\nu_{nf}}{\nu_f} + \right. \\ \left. \frac{1}{\rho_{nf} \nu_f \hat{\beta} h^*} \right) \frac{d^3 f}{d\chi^3} - \left[\frac{\frac{c^{*3} \bar{x}^2 \bar{x}}{(1 - \bar{\xi} \bar{t})^3}}{2 \nu_f^2 \hat{\beta} h^{*3} \rho_{nf} \bar{x}} \right] \left(\frac{d^2 f}{d\chi^2} \right)^2 \frac{d^3 f}{d\chi^3} - \frac{\sigma_{nf}^*}{\rho_{nf}} \frac{B_0^2}{c^*} \frac{df}{d\chi} \sin^2(\Gamma). \end{aligned}$$

$$\begin{aligned}
&\Rightarrow A \left[\frac{df}{d\chi} + \frac{\chi}{2} \frac{d^2 f}{d\chi^2} \right] + \left(\frac{df}{d\chi} \right)^2 - f(\chi) \frac{d^2 f}{d\chi^2} - g(\chi) \frac{d^2 f}{d\chi^2} = \left(\frac{\mu_{nf}}{\rho_{nf}} + \frac{1}{\frac{\mu_f}{\rho_f} \rho_{nf} \hat{\beta} h^*} \right) \frac{d^3 f}{d\chi^3} \\
&\quad - \left[\frac{\bar{U}_w^3 \bar{x}}{(2\nu_f h^{*2}) (\rho_{nf} \frac{\mu_f}{\rho_f} \hat{\beta} h^*)} \right] \left(\frac{d^2 f}{d\chi^2} \right)^2 \frac{d^3 f}{d\chi^3} - \frac{\sigma_{nf}^* B_0^2}{\rho_{nf} c^*} \frac{df}{d\chi} \sin^2(\Gamma). \\
&\Rightarrow A \left[\frac{df}{d\chi} + \frac{\chi}{2} \frac{d^2 f}{d\chi^2} \right] + \left(\frac{df}{d\chi} \right)^2 - f(\chi) \frac{d^2 f}{d\chi^2} - g(\chi) \frac{d^2 f}{d\chi^2} = \left(\frac{1}{(1-\Phi)^{2.5} [(1-\Phi) + \Phi \frac{\rho_s}{\rho_f}]} \right. \\
&\quad + \left. \frac{1}{[(1-\Phi) + \Phi \frac{\rho_s}{\rho_f}] \mu_f \hat{\beta} h^*} \right) \frac{d^3 f}{d\chi^3} - \left[\frac{\Delta_1}{[(1-\Phi) + \Phi \frac{\rho_s}{\rho_f}] \mu_f \hat{\beta} h^*} \right] \left(\frac{d^2 f}{d\chi^2} \right)^2 \frac{d^3 f}{d\chi^3} \\
&\quad - \frac{\left[1 + \frac{3(\frac{\sigma_s}{\sigma_f} - 1)\Phi}{(\frac{\sigma_s}{\sigma_f} + 2) - (\frac{\sigma_s}{\sigma_f} - 1)\Phi} \right] \sigma_f B_0^2}{[(1-\Phi) + \Phi \frac{\rho_s}{\rho_f}] \rho_f} \frac{df}{d\chi} \sin^2(\Gamma). \\
&\Rightarrow \left(\frac{1}{(1-\Phi)^{2.5} [(1-\Phi) + \Phi \frac{\rho_s}{\rho_f}]} + \frac{w}{[(1-\Phi) + \Phi \frac{\rho_s}{\rho_f}]} \right) \frac{d^3 f}{d\chi^3} - A \left[\frac{df}{d\chi} + \frac{\chi}{2} \frac{d^2 f}{d\chi^2} \right] - \left(\frac{df}{d\chi} \right)^2 \\
&\quad + f \frac{d^2 f}{d\chi^2} + g \frac{d^2 f}{d\chi^2} - \left[\frac{\Delta_1 w}{[(1-\Phi) + \Phi \frac{\rho_s}{\rho_f}]} \right] \left(\frac{d^2 f}{d\chi^2} \right)^2 \frac{d^3 f}{d\chi^3} - \frac{\left[1 + \frac{3(\frac{\sigma_s}{\sigma_f} - 1)\Phi}{(\frac{\sigma_s}{\sigma_f} + 2) - (\frac{\sigma_s}{\sigma_f} - 1)\Phi} \right]}{[(1-\Phi) + \Phi \frac{\rho_s}{\rho_f}]} M \\
&\quad \frac{df}{d\chi} \sin^2(\Gamma) = 0.
\end{aligned}$$

Now, the dimensionless form of the momentum equation (4.6) can be obtained by using equations (4.27)-(4.33) and (4.49)-(4.52) as follows:

$$\begin{aligned}
\frac{\partial \bar{f}_2}{\partial \bar{t}} + \bar{f}_1 \frac{\partial \bar{f}_2}{\partial \bar{x}} + \bar{f}_2 \frac{\partial \bar{f}_2}{\partial \bar{y}} + \bar{f}_3 \frac{\partial \bar{f}_2}{\partial \bar{z}} &= \left(\nu_{nf} + \frac{1}{\rho_{nf} \hat{\beta} h^*} \right) \frac{\partial^2 \bar{f}_2}{\partial \bar{z}^2} - \frac{1}{2\hat{\beta} h^{*3} \rho_{nf}} \left(\frac{\partial \bar{f}_2}{\partial \bar{z}} \right)^2 \frac{\partial^2 \bar{f}_2}{\partial \bar{z}^2} \\
&\quad - \frac{\sigma_{nf}^* B^2(\bar{t}) \bar{f}_2}{\rho_{nf}} \sin^2(\Gamma). \\
\Rightarrow \frac{c^* \bar{\xi}}{(1-\bar{\xi} \bar{t})^2} \bar{y} \frac{dg}{d\chi} + \frac{c^* \bar{\xi}}{2(1-\bar{\xi} \bar{t})^2} \sqrt{\frac{c^*}{\nu_f (1-\bar{\xi} \bar{t})}} \bar{y} \bar{z} \frac{d^2 g}{d\chi^2} + 0 + \frac{c^{*2}}{(1-\bar{\xi} \bar{t})^2} \bar{y} \left(\frac{dg}{d\chi} \right)^2 \\
&\quad - \frac{c^{*2}}{(1-\bar{\xi} \bar{t})^2} \bar{y} f(\chi) \frac{d^2 g}{d\chi^2} - \frac{c^{*2}}{(1-\bar{\xi} \bar{t})^2} \bar{y} g(\chi) \frac{d^2 g}{d\chi^2} = \left(\nu_{nf} + \frac{1}{\rho_{nf} \hat{\beta} h^*} \right) \frac{c^{*2}}{\nu_f (1-\bar{\xi} \bar{t})^2} \\
&\quad \bar{y} \frac{d^3 g}{d\chi^3} - \frac{1}{2\hat{\beta} h^{*3} \rho_{nf}} \frac{c^{*3} \bar{y}^2}{\nu_f (1-\bar{\xi} \bar{t})^3} \left(\frac{d^2 g}{d\chi^2} \right)^2 \frac{c^{*2}}{\nu_f (1-\bar{\xi} \bar{t})^2} \bar{y} \frac{d^3 g}{d\chi^3} - \frac{\sigma_{nf}^* B_0^2}{\rho_{nf} (\sqrt{(1-\bar{\xi} \bar{t})})^2} \\
&\quad \frac{c^* \bar{y}}{(1-\bar{\xi} \bar{t})} \frac{dg}{d\chi} \sin^2(\Gamma).
\end{aligned}$$

$$\Rightarrow \frac{\bar{\xi}}{c^*} \frac{dg}{d\chi} + \frac{1}{2} \frac{\bar{\xi}}{c^*} \sqrt{\frac{c^*}{\nu_f(1-\bar{\xi}\bar{t})}} \bar{z} \frac{d^2g}{d\chi^2} + \left(\frac{dg}{d\chi}\right)^2 - f(\chi) \frac{d^2g}{d\chi^2} - g(\chi) \frac{d^2g}{d\chi^2} = \left(\nu_{nf} + \frac{1}{\rho_{nf}\hat{\beta}h^*} \right) \frac{1}{\nu_f} \frac{d^3g}{d\chi^3} - \frac{1}{2\hat{\beta}h^{*3}\rho_{nf}} \frac{c^{*3}\bar{y}^2}{\nu_f(1-\bar{\xi}\bar{t})^3} \left(\frac{d^2g}{d\chi^2}\right)^2 \frac{1}{\nu_f} \frac{d^3g}{d\chi^3} - \frac{\sigma_{nf}^* B_0^2}{\rho_{nf} c^*} \frac{dg}{d\chi} \sin^2(\Gamma).$$

$$\Rightarrow \frac{\bar{\xi}}{c^*} \left[\frac{dg}{d\chi} + \frac{1}{2} \sqrt{\frac{c^*}{\nu_f(1-\bar{\xi}\bar{t})}} \bar{z} \frac{d^2g}{d\chi^2} \right] + \left(\frac{dg}{d\chi}\right)^2 - f(\chi) \frac{d^2g}{d\chi^2} - g(\chi) \frac{d^2g}{d\chi^2} = \left(\frac{\nu_{nf}}{\nu_f} + \frac{1}{\rho_{nf}\nu_f\hat{\beta}h^*} \right) \frac{d^3g}{d\chi^3} - \left[\frac{c^{*3}\bar{y}^2\bar{y}}{(1-\bar{\xi}\bar{t})^3} \right] \frac{\left(\frac{d^2g}{d\chi^2}\right)^2}{2\nu_f^2\hat{\beta}h^{*3}\rho_{nf}\bar{y}} \frac{d^3g}{d\chi^3} - \frac{\sigma_{nf}^* B_0^2}{\rho_{nf} c^*} \frac{dg}{d\chi} \sin^2(\Gamma).$$

$$\Rightarrow A \left[\frac{dg}{d\chi} + \frac{\chi}{2} \frac{d^2g}{d\chi^2} \right] + \left(\frac{dg}{d\chi}\right)^2 - f(\chi) \frac{d^2g}{d\chi^2} - g(\chi) \frac{d^2g}{d\chi^2} = \left(\frac{\mu_{nf}}{\rho_{nf}} + \frac{1}{\frac{\mu_f}{\rho_f} \rho_{nf}\hat{\beta}h^*} \right) \frac{d^3g}{d\chi^3} - \left[\frac{\bar{U}_w^3\bar{y}}{(2\nu_f h^{*2})(\rho_{nf} \frac{\mu_f}{\rho_f} \hat{\beta}h^*)} \right] \left(\frac{d^2g}{d\chi^2}\right)^2 \frac{d^3g}{d\chi^3} - \frac{\sigma_{nf}^* B_0^2}{\rho_{nf} c^*} \frac{dg}{d\chi} \sin^2(\Gamma).$$

$$\Rightarrow A \left[\frac{dg}{d\chi} + \frac{\chi}{2} \frac{d^2g}{d\chi^2} \right] + \left(\frac{dg}{d\chi}\right)^2 - f(\chi) \frac{d^2g}{d\chi^2} - g(\chi) \frac{d^2g}{d\chi^2} = \left(\frac{1}{(1-\Phi)^{2.5}[(1-\Phi) + \Phi \frac{\rho_s}{\rho_f}] + \frac{1}{[(1-\Phi) + \Phi \frac{\rho_s}{\rho_f}]\mu_f\hat{\beta}h^*}} \right) \frac{d^3g}{d\chi^3} - \left[\frac{\Delta_2}{[(1-\Phi) + \Phi \frac{\rho_s}{\rho_f}]\mu_f\hat{\beta}h^*} \right] \left(\frac{d^2g}{d\chi^2}\right)^2 \frac{d^3g}{d\chi^3} - \frac{\left[1 + \frac{3(\frac{\sigma_s}{\sigma_f}-1)\Phi}{(\frac{\sigma_s}{\sigma_f}+2)-(\frac{\sigma_s}{\sigma_f}-1)\Phi} \right] \sigma_f B_0^2}{[(1-\Phi) + \Phi \frac{\rho_s}{\rho_f}]\rho_f} \frac{dg}{d\chi} \sin^2(\Gamma).$$

$$\Rightarrow \left(\frac{1}{(1-\Phi)^{2.5}[(1-\Phi) + \Phi \frac{\rho_s}{\rho_f}]} + \frac{w}{[(1-\Phi) + \Phi \frac{\rho_s}{\rho_f}]} \right) \frac{d^3g}{d\chi^3} - A \left[\frac{dg}{d\chi} + \frac{\chi}{2} \frac{d^2g}{d\chi^2} \right] - \left(\frac{dg}{d\chi}\right)^2 + f \frac{d^2g}{d\chi^2} + g \frac{d^2g}{d\chi^2} - \left[\frac{\Delta_2 w}{[(1-\Phi) + \Phi \frac{\rho_s}{\rho_f}]} \right] \left(\frac{d^2g}{d\chi^2}\right)^2 \frac{d^3g}{d\chi^3} - \frac{\left[1 + \frac{3(\frac{\sigma_s}{\sigma_f}-1)\Phi}{(\frac{\sigma_s}{\sigma_f}+2)-(\frac{\sigma_s}{\sigma_f}-1)\Phi} \right]}{[(1-\Phi) + \Phi \frac{\rho_s}{\rho_f}]} M \frac{dg}{d\chi} \sin^2(\Gamma) = 0.$$

Now, the dimensionless form of the energy equation (4.7) can be obtained by using equations (4.41)-(4.48), and (4.53),(4.54) as follows:

$$\begin{aligned}
\frac{\partial \Theta}{\partial \bar{t}} + \bar{f}_1 \frac{\partial \Theta}{\partial \bar{x}} + \bar{f}_2 \frac{\partial \Theta}{\partial \bar{y}} + \bar{f}_3 \frac{\partial \Theta}{\partial \bar{z}} &= \frac{k_{nf}}{(\rho C_p)_{nf}} \left(\frac{\partial^2 \Theta}{\partial \bar{z}^2} \right) - \frac{1}{(\rho C_p)_{nf}} \left(\frac{\partial q_r}{\partial \bar{z}} \right) + \frac{\nu_{nf}}{(\rho C_p)_{nf}} \\
&\quad \left(\frac{\partial \bar{f}_1}{\partial \bar{z}} \right)^2 + \frac{Q_0}{(\rho C_p)_{nf}} (\Theta - \Theta_\infty) - \lambda \left[\bar{f}_1 \frac{\partial \bar{f}_1}{\partial \bar{x}} \frac{\partial \Theta}{\partial \bar{x}} \right. \\
&\quad + \bar{f}_2 \frac{\partial \bar{f}_1}{\partial \bar{y}} \frac{\partial \Theta}{\partial \bar{x}} + \bar{f}_3 \frac{\partial \bar{f}_1}{\partial \bar{z}} \frac{\partial \Theta}{\partial \bar{x}} + \bar{f}_1 \frac{\partial \bar{f}_2}{\partial \bar{x}} \frac{\partial \Theta}{\partial \bar{y}} + \bar{f}_2 \frac{\partial \bar{f}_2}{\partial \bar{y}} \frac{\partial \Theta}{\partial \bar{y}} \\
&\quad + \bar{f}_3 \frac{\partial \bar{f}_2}{\partial \bar{z}} \frac{\partial \Theta}{\partial \bar{y}} + \bar{f}_1 \frac{\partial \bar{f}_3}{\partial \bar{x}} \frac{\partial \Theta}{\partial \bar{z}} + \bar{f}_2 \frac{\partial \bar{f}_3}{\partial \bar{y}} \frac{\partial \Theta}{\partial \bar{z}} + \bar{f}_3 \frac{\partial \bar{f}_3}{\partial \bar{z}} \frac{\partial \Theta}{\partial \bar{z}} \\
&\quad + \bar{f}_1^2 \frac{\partial^2 \Theta}{\partial \bar{x}^2} + \bar{f}_2^2 \frac{\partial^2 \Theta}{\partial \bar{y}^2} + \bar{f}_3^2 \frac{\partial^2 \Theta}{\partial \bar{z}^2} + 2\bar{f}_1 \bar{f}_2 \frac{\partial^2 \Theta}{\partial \bar{x} \partial \bar{y}} \\
&\quad \left. + 2\bar{f}_1 \bar{f}_3 \frac{\partial^2 \Theta}{\partial \bar{y} \partial \bar{z}} + 2\bar{f}_1 \bar{f}_3 \frac{\partial^2 \Theta}{\partial \bar{x} \partial \bar{z}} \right] + \frac{\sigma_{nf}^* B^2(\bar{t}) \bar{f}_1^2}{(\rho C_p)_{nf}} \sin^2(\Gamma).
\end{aligned}$$

$$\begin{aligned}
\Rightarrow \frac{c^* \bar{x} \bar{\xi}}{(1 - \bar{\xi} \bar{t})^2} \theta(\chi) + \frac{c^{*2} \bar{x} \bar{\xi}}{\nu_f (1 - \bar{\xi} \bar{t})^3} \frac{\bar{z}}{2} \sqrt{\frac{\nu_f (1 - \bar{\xi} \bar{t})}{c^*}} \frac{d\theta}{d\chi} + \frac{c^{*2} \bar{x}}{(1 - \bar{\xi} \bar{t})^2} \bar{x} \frac{df}{d\chi} \theta(\chi) - \frac{c^{*2} \bar{x}}{(1 - \bar{\xi} \bar{t})^2} f(\chi) \\
\frac{d\theta}{d\chi} - \frac{c^{*2} \bar{x}}{(1 - \bar{\xi} \bar{t})^2} g(\chi) \frac{d\theta}{d\chi} = \frac{k_{nf}}{(\rho C_p)_{nf}} \frac{c^{*2} \bar{x}}{\nu_f (1 - \bar{\xi} \bar{t})^2} \frac{d^2 \theta}{d\chi^2} - \frac{1}{(\rho C_p)_{nf}} \left[\frac{-16\Theta_\infty^3 \sigma^*}{3k^*} \left(\frac{\partial^2 \Theta}{\partial \bar{z}^2} \right) \right] \\
+ \frac{\nu_{nf}}{(\rho C_p)_{nf}} \frac{c^{*3} \bar{x}^2}{\nu_f (1 - \bar{\xi} \bar{t})^3} \left(\frac{d^2 f}{d\chi^2} \right)^2 + \frac{Q_0}{(\rho C_p)_{nf}} (\Theta - \Theta_\infty) - \lambda \left[\frac{c^{*3} \bar{x}}{(1 - \bar{\xi} \bar{t})^3} \left(\frac{df}{d\chi} \right)^2 \theta(\chi) - \right. \\
\left. \frac{c^{*3} \bar{x}}{(1 - \bar{\xi} \bar{t})^3} f(\chi) \frac{d^2 f}{d\chi^2} \theta(\chi) - \frac{c^{*3} \bar{x}}{(1 - \bar{\xi} \bar{t})^3} g(\chi) \frac{d^2 f}{d\chi^2} \theta(\chi) + \frac{c^{*3} \bar{x}}{(1 - \bar{\xi} \bar{t})^3} [f(\chi) + g(\chi)] \left[\frac{df}{d\chi} + \frac{dg}{d\chi} \right] \right. \\
\left. \frac{d\theta}{d\chi} + \frac{c^{*3} \bar{x}}{(1 - \bar{\xi} \bar{t})^3} [f(\chi) + g(\chi)]^2 \frac{d^2 \theta}{d\chi^2} \right] + \frac{\sigma_{nf}^*}{(\rho C_p)_{nf}} \frac{B_0^2}{(\sqrt{(1 - \bar{\xi} \bar{t})})^2} \frac{(c^* \bar{x})^2}{(1 - \bar{\xi} \bar{t})^2} \left(\frac{df}{d\chi} \right)^2 \sin^2(\Gamma).
\end{aligned}$$

$$\begin{aligned}
\Rightarrow \frac{c^* \bar{x} \bar{\xi}}{(1 - \bar{\xi} \bar{t})^2} \theta(\chi) + \frac{c^* \bar{\xi}}{2(1 - \bar{\xi} \bar{t})^2} \sqrt{\frac{\nu_f c^{*2} (1 - \bar{\xi} \bar{t})}{\nu_f^2 c^* (1 - \bar{\xi} \bar{t})^2}} \bar{x} \bar{z} \frac{d\theta}{d\chi} + \frac{c^{*2}}{(1 - \bar{\xi} \bar{t})^2} \bar{x} \frac{df}{d\chi} \theta(\chi) - \frac{c^{*2} \bar{x}}{(1 - \bar{\xi} \bar{t})^2} \\
f(\chi) \frac{d\theta}{d\chi} - \frac{c^{*2} \bar{x}}{(1 - \bar{\xi} \bar{t})^2} g(\chi) \frac{d\theta}{d\chi} = \frac{k_{nf}}{(\rho C_p)_{nf}} \frac{c^{*2} \bar{x}}{\nu_f (1 - \bar{\xi} \bar{t})^2} \frac{d^2 \theta}{d\chi^2} + \frac{16\Theta_\infty^3 \sigma^*}{(\rho C_p)_{nf} 3k^*} \frac{c^{*2} \bar{x}}{\nu_f (1 - \bar{\xi} \bar{t})^2} \frac{d^2 \theta}{d\chi^2} \\
+ \frac{\nu_{nf}}{(\rho C_p)_{nf}} \frac{c^{*3} \bar{x}^2}{\nu_f (1 - \bar{\xi} \bar{t})^3} \left(\frac{d^2 f}{d\chi^2} \right)^2 + \frac{Q_0}{(\rho C_p)_{nf}} (\Theta - \Theta_\infty) - \lambda \left[\frac{c^{*3} \bar{x}}{(1 - \bar{\xi} \bar{t})^3} \left(\frac{df}{d\chi} \right)^2 \theta(\chi) - \right. \\
\left. \frac{c^{*3} \bar{x}}{(1 - \bar{\xi} \bar{t})^3} f(\chi) \frac{d^2 f}{d\chi^2} \theta(\chi) - \frac{c^{*3} \bar{x}}{(1 - \bar{\xi} \bar{t})^3} g(\chi) \frac{d^2 f}{d\chi^2} \theta(\chi) + \frac{c^{*3} \bar{x}}{(1 - \bar{\xi} \bar{t})^3} [f(\chi) + g(\chi)] \left[\frac{df}{d\chi} + \frac{dg}{d\chi} \right] \right. \\
\left. \frac{d\theta}{d\chi} + \frac{c^{*3} \bar{x}}{(1 - \bar{\xi} \bar{t})^3} [f(\chi) + g(\chi)]^2 \frac{d^2 \theta}{d\chi^2} \right] + \frac{\sigma_{nf}^*}{(\rho C_p)_{nf}} \frac{B_0^2}{(1 - \bar{\xi} \bar{t})} \frac{c^{*2} \bar{x}^2}{(1 - \bar{\xi} \bar{t})^2} \left(\frac{df}{d\chi} \right)^2 \sin^2(\Gamma).
\end{aligned}$$

$$\begin{aligned}
&\Rightarrow \frac{c^* \bar{x} \bar{\xi}}{(1 - \bar{\xi} \bar{t})^2} \theta(\chi) + \frac{c^* \bar{\xi}}{2(1 - \bar{\xi} \bar{t})^2} \sqrt{\frac{c^*}{\nu_f(1 - \bar{\xi} \bar{t})}} \bar{x} \bar{z} \frac{d\theta}{d\chi} + \frac{c^{*2}}{(1 - \bar{\xi} \bar{t})^2} \bar{x} \frac{df}{d\chi} \theta(\chi) - \frac{c^{*2} \bar{x}}{(1 - \bar{\xi} \bar{t})^2} f(\chi) \\
&\frac{d\theta}{d\chi} - \frac{c^{*2} \bar{x}}{(1 - \bar{\xi} \bar{t})^2} g(\chi) \frac{d\theta}{d\chi} = \frac{k_{nf}}{(\rho C_p)_{nf}} \frac{c^{*2} \bar{x}}{\nu_f(1 - \bar{\xi} \bar{t})^2} \frac{d^2\theta}{d\chi^2} + \frac{16\Theta_\infty^3 \sigma^*}{(\rho C_p)_{nf} 3k^*} \frac{c^{*2} \bar{x}}{\nu_f(1 - \bar{\xi} \bar{t})^2} \frac{d^2\theta}{d\chi^2} + \\
&\frac{\nu_{nf}}{(\rho C_p)_{nf}} \frac{c^{*3} \bar{x}^2}{\nu_f(1 - \bar{\xi} \bar{t})^3} \left(\frac{d^2f}{d\chi^2} \right)^2 + \frac{Q_0}{(\rho C_p)_{nf}} (\Theta - \Theta_\infty) - \lambda \left[\frac{c^{*3} \bar{x}}{(1 - \bar{\xi} \bar{t})^3} \left(\frac{df}{d\chi} \right)^2 \theta(\chi) - \right. \\
&\left. \frac{c^{*3} \bar{x}}{(1 - \bar{\xi} \bar{t})^3} f(\chi) \frac{d^2f}{d\chi^2} \theta(\chi) - \frac{c^3 \bar{x}}{(1 - \bar{\xi} \bar{t})^3} g(\chi) \frac{d^2f}{d\chi^2} \theta(\chi) + \frac{c^{*3} \bar{x}}{(1 - \bar{\xi} \bar{t})^3} [f(\chi) + g(\chi)] \left[\frac{df}{d\chi} + \frac{dg}{d\chi} \right] \right. \\
&\left. \frac{d\theta}{d\chi} + \frac{c^{*3} \bar{x}}{(1 - \bar{\xi} \bar{t})^3} [f(\chi) + g(\chi)]^2 \frac{d^2\theta}{d\chi^2} \right] + \frac{\sigma_{nf}^*}{(\rho C_p)_{nf}} \frac{B_0^2}{(1 - \bar{\xi} \bar{t})} \frac{c^{*2} \bar{x}^2}{(1 - \bar{\xi} \bar{t})^2} \left(\frac{df}{d\chi} \right)^2 \sin^2(\Gamma). \\
&\Rightarrow \frac{\bar{\xi}}{c^*} \theta(\chi) + \frac{\bar{\xi}}{c^*} \frac{\chi}{2} \frac{d\theta}{d\chi} + \frac{df}{d\chi} \theta(\chi) - f(\chi) \frac{d\theta}{d\chi} - g(\chi) \frac{d\theta}{d\chi} = \frac{k_{nf}}{(\rho C_p)_{nf}} \frac{1}{\nu_f} \frac{d^2\theta}{d\chi^2} + \frac{4(4)\Theta_\infty^3 \sigma^*}{(\rho C_p)_{nf} 3k^*} \frac{1}{\nu_f} \\
&\frac{d^2\theta}{d\chi^2} + \frac{\nu_{nf}}{(\rho C_p)_{nf}} \frac{c^* \bar{x}}{\nu_f(1 - \bar{\xi} \bar{t})} \left(\frac{d^2f}{d\chi^2} \right)^2 + \frac{Q_0}{(\rho C_p)_{nf}} (\Theta - \Theta_\infty) \theta(\chi) - \lambda \left[\frac{c^*}{(1 - \bar{\xi} \bar{t})} \left(\frac{df}{d\chi} \right)^2 \right. \\
&\theta(\chi) - \frac{c^*}{(1 - \bar{\xi} \bar{t})} f(\chi) \frac{d^2f}{d\chi^2} \theta(\chi) - \frac{c^*}{(1 - \bar{\xi} \bar{t})} g(\chi) \frac{d^2f}{d\chi^2} \theta(\chi) + \frac{c^*}{(1 - \bar{\xi} \bar{t})} [f(\chi) + g(\chi)] \\
&\left. \left[\frac{df}{d\chi} + \frac{dg}{d\chi} \right] \frac{d\theta}{d\chi} + \frac{c^*}{(1 - \bar{\xi} \bar{t})} [f(\chi) + g(\chi)]^2 \frac{d^2\theta}{d\chi^2} \right] + \frac{\sigma_{nf}^*}{(\rho C_p)_{nf}} \frac{B_0^2}{c^*} \frac{c^* \bar{x}}{(1 - \bar{\xi} \bar{t})} \left(\frac{df}{d\chi} \right)^2 \sin^2(\Gamma).
\end{aligned}$$

$$\begin{aligned}
&\Rightarrow A \left[\theta(\chi) + \frac{\chi}{2} \frac{df}{d\chi} \right] + \frac{df}{d\chi} \theta(\chi) - f(\chi) \frac{d\theta}{d\chi} - g(\chi) \frac{d\theta}{d\chi} = \frac{k_{nf}}{(\rho C_p)_{nf}} \frac{1}{\nu_f} \frac{d^2\theta}{d\chi^2} + \frac{4(4)\Theta_\infty^3 \sigma^*}{(\rho C_p)_{nf} 3k^*} \frac{1}{\nu_f} \\
&\frac{d^2\theta}{d\chi^2} + \frac{\nu_{nf}}{(\rho C_p)_{nf}} \frac{\bar{U}_w}{\nu_f} \left(\frac{d^2f}{d\chi^2} \right)^2 + \frac{Q_0}{(\rho C_p)_{nf}} (\Theta - \Theta_\infty) \theta(\chi) - \lambda_0 (1 - \bar{\xi} \bar{t}) \frac{c^*}{(1 - \bar{\xi} \bar{t})} \left[\left(\frac{df}{d\chi} \right)^2 \right. \\
&\theta(\chi) - f(\chi) \frac{d^2f}{d\chi^2} \theta(\chi) - g(\chi) \frac{d^2f}{d\chi^2} \theta(\chi) + [f(\chi) + g(\chi)] \left[\frac{df}{d\chi} + \frac{dg}{d\chi} \right] \frac{d\theta}{d\chi} + [f(\chi) + g(\chi)]^2 \\
&\left. \frac{d^2\theta}{d\chi^2} \right] + \frac{\sigma_{nf}^*}{(\rho C_p)_{nf}} \frac{B_0^2}{c^*} \bar{U}_w \left(\frac{df}{d\chi} \right)^2 \sin^2(\Gamma).
\end{aligned}$$

$$\begin{aligned}
&\Rightarrow A \left[\theta(\chi) + \frac{\chi}{2} \frac{d^2\theta}{d\chi^2} \right] + \frac{df}{d\chi} \theta(\chi) - f(\chi) \frac{d\theta}{d\chi} - g(\chi) \frac{d\theta}{d\chi} = \frac{\left[\frac{(k_s + (q-1)k_f) - (q-1)\Phi(k_f - k_s)}{(k_s + (q-1)k_f) + \Phi(k_f - k_s)} \right] \times k_f}{\left[(1 - \Phi) + \Phi \frac{(\rho C_p)_s}{(\rho C_p)_f} \right] \times (\rho C_p)_f} \frac{1}{\nu_f} \\
&\frac{d^2\theta}{d\chi^2} + \frac{4(4)\Theta_\infty^3 \sigma^*}{\left[(1 - \Phi) + \Phi \frac{(\rho C_p)_s}{(\rho C_p)_f} \right] (\rho C_p)_f 3k^*} \frac{1}{\nu_f} \frac{d^2\theta}{d\chi^2} + \frac{\frac{\mu_f}{(1 - \Phi)^{2.5}}}{\frac{\mu_f}{\rho_f}} \frac{\bar{U}_w}{\left[(1 - \Phi) + \Phi \frac{(\rho C_p)_s}{(\rho C_p)_f} \right] (\rho C_p)_f} \\
&\left(\frac{d^2f}{d\chi^2} \right)^2 + \frac{Q_0}{\left[(1 - \Phi) + \Phi \frac{(\rho C_p)_s}{(\rho C_p)_f} \right] \times (\rho C_p)_f} (\Theta_f - \Theta_\infty) \theta(\chi) - \xi \left[\left(\frac{df}{d\chi} \right)^2 \theta(\chi) - \right. \\
&\left. f(\chi) \frac{d^2f}{d\chi^2} \theta(\chi) - g(\chi) \frac{d^2f}{d\chi^2} \theta(\chi) + [f(\chi) + g(\chi)] \left[\frac{df}{d\chi} + \frac{dg}{d\chi} \right] \frac{d\theta}{d\chi} + [f(\chi) + g(\chi)]^2 \frac{d^2\theta}{d\chi^2} \right] +
\end{aligned}$$

$$\begin{aligned}
& \frac{\left[1 + \frac{3(\frac{\sigma_s}{\sigma_f} - 1)\Phi}{(\frac{\sigma_s}{\sigma_f} + 2) - (\frac{\sigma_s}{\sigma_f} - 1)\Phi}\right] \sigma_f}{\left[(1 - \Phi) + \Phi \frac{(\rho C_p)_s}{(\rho C_p)_f}\right] \times (\rho C_p)_f} \frac{B_0^2 \bar{U}_w}{c^*} \left(\frac{df}{d\chi}\right)^2 \sin^2(\Gamma). \\
\Rightarrow & A \left[\theta(\chi) + \frac{\chi}{2} \frac{d\theta}{d\chi} \right] + \frac{df}{d\chi} \theta(\chi) - f(\chi) \frac{d\theta}{d\chi} - g(\chi) \frac{d\theta}{d\chi} = \frac{\frac{k_{nf}}{k_f}}{\left[(1 - \Phi) + \Phi \frac{(\rho C_p)_s}{(\rho C_p)_f}\right] Pr} \frac{d^2\theta}{d\chi^2} + \\
& \frac{Nr}{\left[(1 - \Phi) + \Phi \frac{(\rho C_p)_s}{(\rho C_p)_f}\right]} \frac{d^2\theta}{d\chi^2} + \frac{Ec}{(1 - \Phi)^{2.5} \left[(1 - \Phi) + \Phi \frac{(\rho C_p)_s}{(\rho C_p)_f}\right]} \left(\frac{d^2f}{d\chi^2}\right)^2 + \\
& \frac{Q}{\left[(1 - \Phi) + \Phi \frac{(\rho C_p)_s}{(\rho C_p)_f}\right]} \theta(\chi) - \xi \left[\left(\frac{df}{d\chi}\right)^2 \theta(\chi) - f(\chi) \frac{d^2f}{d\chi^2} \theta(\chi) - g(\chi) \frac{d^2f}{d\chi^2} \theta(\chi) + \right. \\
& \left. [f(\chi) + g(\chi)] \left[\frac{df}{d\chi} + \frac{dg}{d\chi} \right] \frac{d\theta}{d\chi} + [f(\chi) + g(\chi)]^2 \frac{d^2\theta}{d\chi^2} \right] + \frac{\left[1 + \frac{3(\frac{\sigma_s}{\sigma_f} - 1)\Phi}{(\frac{\sigma_s}{\sigma_f} + 2) - (\frac{\sigma_s}{\sigma_f} - 1)\Phi}\right]}{\left[(1 - \Phi) + \Phi \frac{(\rho C_p)_s}{(\rho C_p)_f}\right]} \\
& M \frac{\bar{U}_w}{(C_p)_f} \left(\frac{df}{d\chi}\right)^2 \sin^2(\Gamma).
\end{aligned}$$

Multiplying by $\frac{k_f \left[(1 - \Phi) + \Phi \frac{(\rho C_p)_s}{(\rho C_p)_f}\right] Pr}{k_{nf}}$ on both sides, we get

$$\begin{aligned}
\Rightarrow & \frac{k_f \left[(1 - \Phi) + \Phi \frac{(\rho C_p)_s}{(\rho C_p)_f}\right] Pr}{k_{nf}} \left[A \left[\theta(\chi) + \frac{\chi}{2} \frac{d\theta}{d\chi} \right] + \frac{df}{d\chi} \theta(\chi) - f(\chi) \frac{d\theta}{d\chi} - g(\chi) \frac{d\theta}{d\chi} \right] = \frac{d^2\theta}{d\chi^2} + \\
& \frac{k_f Pr Nr}{k_{nf}} \frac{d^2\theta}{d\chi^2} + \frac{k_f Ec Pr}{(1 - \Phi)^{2.5} k_{nf}} \left(\frac{d^2f}{d\chi^2}\right)^2 + \frac{k_f Pr}{k_{nf}} Q \theta(\chi) - \xi \frac{k_f \left[(1 - \Phi) + \Phi \frac{(\rho C_p)_s}{(\rho C_p)_f}\right] Pr}{k_{nf}} \\
& \left[\left(\frac{df}{d\chi}\right)^2 \theta(\chi) - f(\chi) \frac{d^2f}{d\chi^2} \theta(\chi) - g(\chi) \frac{d^2f}{d\chi^2} \theta(\chi) + [f(\chi) + g(\chi)] \left[\frac{df}{d\chi} + \frac{dg}{d\chi} \right] \frac{d\theta}{d\chi} + \right. \\
& \left. [f(\chi) + g(\chi)]^2 \frac{d^2\theta}{d\chi^2} \right] + \frac{k_f Pr \left[1 + \frac{3(\frac{\sigma_s}{\sigma_f} - 1)\Phi}{(\frac{\sigma_s}{\sigma_f} + 2) - (\frac{\sigma_s}{\sigma_f} - 1)\Phi}\right]}{k_{nf}} E_c M \left(\frac{df}{d\chi}\right)^2 \sin^2(\Gamma).
\end{aligned}$$

$$\begin{aligned}
\Rightarrow & \frac{d^2\theta}{d\chi^2} + \frac{k_f Pr Nr}{k_{nf}} \frac{d^2\theta}{d\chi^2} - \frac{k_f \left[(1 - \Phi) + \Phi \frac{(\rho C_p)_s}{(\rho C_p)_f}\right] Pr}{k_{nf}} \left\{ A \left[\theta(\chi) + \frac{\chi}{2} \frac{d\theta}{d\chi} \right] + \frac{df}{d\chi} \theta(\chi) - \right. \\
& \left. f(\chi) \frac{d\theta}{d\chi} - g(\chi) \frac{d\theta}{d\chi} \right\} + \frac{k_f Ec Pr}{(1 - \Phi)^{2.5} k_{nf}} \left(\frac{d^2f}{d\chi^2}\right)^2 + \frac{k_f Pr}{k_{nf}} Q \theta(\chi) - \xi \frac{k_f \left[(1 - \Phi) + \Phi \frac{(\rho C_p)_s}{(\rho C_p)_f}\right] Pr}{k_{nf}} \\
& \left[\left(\frac{df}{d\chi}\right)^2 \theta(\chi) - f(\chi) \frac{d^2f}{d\chi^2} \theta(\chi) - g(\chi) \frac{d^2f}{d\chi^2} \theta(\chi) + [f(\chi) + g(\chi)] \left[\frac{df}{d\chi} + \frac{dg}{d\chi} \right] \frac{d\theta}{d\chi} + \right.
\end{aligned}$$

$$\begin{aligned}
& [f(\chi) + g(\chi)]^2 \frac{d^2\theta}{d\chi^2} \Big] + \frac{k_f Pr \left[1 + \frac{3(\frac{\sigma_s}{\sigma_f} - 1)\Phi}{(\frac{\sigma_s}{\sigma_f} + 2) - (\frac{\sigma_s}{\sigma_f} - 1)\Phi} \right]}{k_{nf}} E_c M \left(\frac{df}{d\chi} \right)^2 \sin^2(\Gamma) = 0. \\
\Rightarrow & \left(1 + \frac{k_f Pr Nr}{k_{nf}} \right) \frac{d^2\theta}{d\chi^2} - \frac{k_f \left[(1 - \Phi) + \Phi \frac{(\rho C_p)_s}{(\rho C_p)_f} \right] Pr}{k_{nf}} \left\{ A \left[\theta(\chi) + \frac{\chi}{2} \frac{d\theta}{d\chi} \right] + \frac{df}{d\chi} \theta(\chi) - \right. \\
& f(\chi) \frac{d\theta}{d\chi} - g(\chi) \frac{d\theta}{d\chi} - \frac{E_c}{(1 - \Phi)^{2.5} \left[(1 - \Phi) + \Phi \frac{(\rho C_p)_s}{(\rho C_p)_f} \right]} \left(\frac{d^2 f}{d\chi^2} \right)^2 - \frac{Q}{\left[(1 - \Phi) + \Phi \frac{(\rho C_p)_s}{(\rho C_p)_f} \right]} \\
& \theta(\chi) + \xi \left[\left(\frac{df}{d\chi} \right)^2 \theta(\chi) - f(\chi) \frac{d^2 f}{d\chi^2} \theta(\chi) - g(\chi) \frac{d^2 f}{d\chi^2} \theta(\chi) + [f(\chi) + g(\chi)] \left[\frac{df}{d\chi} + \right. \right. \\
& \left. \left. \frac{dg}{d\chi} \right] \frac{d\theta}{d\chi} + [f(\chi) + g(\chi)]^2 \frac{d^2\theta}{d\chi^2} \right] - \frac{\left[1 + \frac{3(\frac{\sigma_s}{\sigma_f} - 1)\Phi}{(\frac{\sigma_s}{\sigma_f} + 2) - (\frac{\sigma_s}{\sigma_f} - 1)\Phi} \right]}{\left[(1 - \Phi) + \Phi \frac{(\rho C_p)_s}{(\rho C_p)_f} \right]} E_c M \left(\frac{df}{d\chi} \right)^2 \sin^2(\Gamma) \Big\} = 0. \\
\Rightarrow & \left(1 + \frac{k_f Pr Nr}{k_{nf}} - \frac{k_f \left[(1 - \Phi) + \Phi \frac{(\rho C_p)_s}{(\rho C_p)_f} \right] Pr}{k_{nf}} \xi (f+g)^2 \right) \frac{d^2\theta}{d\chi^2} - \frac{k_f \left[(1 - \Phi) + \Phi \frac{(\rho C_p)_s}{(\rho C_p)_f} \right] Pr}{k_{nf}} \\
& \left\{ A \left[\theta + \frac{\chi}{2} \frac{d\theta}{d\chi} \right] + \frac{df}{d\chi} \theta - f \frac{d\theta}{d\chi} - g \frac{d\theta}{d\chi} - \frac{E_c}{(1 - \Phi)^{2.5} \left[(1 - \Phi) + \Phi \frac{(\rho C_p)_s}{(\rho C_p)_f} \right]} \left(\frac{d^2 f}{d\chi^2} \right)^2 - \right. \\
& \frac{Q}{\left[(1 - \Phi) + \Phi \frac{(\rho C_p)_s}{(\rho C_p)_f} \right]} \theta + \xi \left[\left(\frac{df}{d\chi} \right)^2 \theta - f \frac{d^2 f}{d\chi^2} \theta - g \frac{d^2 f}{d\chi^2} \theta + [f + g] \left[\frac{df}{d\chi} + \frac{dg}{d\chi} \right] \frac{d\theta}{d\chi} \right] \\
& \left. - \frac{\left[1 + \frac{3(\frac{\sigma_s}{\sigma_f} - 1)\Phi}{(\frac{\sigma_s}{\sigma_f} + 2) - (\frac{\sigma_s}{\sigma_f} - 1)\Phi} \right]}{\left[(1 - \Phi) + \Phi \frac{(\rho C_p)_s}{(\rho C_p)_f} \right]} E_c M \left(\frac{df}{d\chi} \right)^2 \sin^2(\Gamma) \right\} = 0.
\end{aligned}$$

The boundary conditions corresponding to PDEs at $\bar{z} = 0$ are transformed into the dimensionless form through the following procedure. [100]

$$\begin{aligned}
& \bar{f}_3(\bar{x}, \bar{y}, \bar{z}) = \bar{W}_{\bar{w}}, & \text{at } \bar{z} = 0. \\
\Rightarrow & \bar{W}_{\bar{w}} = -\sqrt{\frac{c^* \nu_f}{1 - \bar{\xi} \bar{t}}} [f(\chi) + g(\chi)], & \text{at } \chi = 0. \\
\Rightarrow & [f(\chi) + g(\chi)] = -\bar{W}_{\bar{w}} \sqrt{\frac{1 - \bar{\xi} \bar{t}}{c^* \nu_f}}, & \text{at } \chi = 0. \\
\Rightarrow & f(0) = S_1, \quad g(0) = S_2. \\
& \bar{f}_1(\bar{x}, \bar{y}, \bar{z}) = \bar{U}_w(\bar{x}) + \mu_{nf} \left(\frac{\partial \bar{f}_1}{\partial \bar{z}} \right), & \text{at } \bar{z} = 0. \\
\Rightarrow & \frac{c^* \bar{x}}{1 - \bar{\xi} \bar{t}} \frac{df}{d\chi} = \frac{c^* \bar{x}}{1 - \bar{\xi} \bar{t}} + \frac{c^* \bar{x}}{1 - \bar{\xi} \bar{t}} \sqrt{\frac{c^*}{\nu_f (1 - \bar{\xi} \bar{t})}} \frac{\mu_f}{(1 - \Phi)^{2.5}} \frac{d^2 f}{d\chi^2}, & \text{at } \chi = 0.
\end{aligned}$$

$$\begin{aligned}
&\Rightarrow \frac{c^*\bar{x}}{1-\xi\bar{t}} \frac{df}{d\chi} = \frac{c^*\bar{x}}{1-\xi\bar{t}} \left(1 + \sqrt{\frac{c^*}{\nu_f(1-\xi\bar{t})}} \frac{\mu_f}{(1-\Phi)^{2.5}} \frac{d^2f}{d\chi^2} \right), & \text{at } \chi = 0. \\
&\Rightarrow \frac{df}{d\chi} = 1 + \frac{\Lambda_1}{(1-\Phi)^{2.5}} \frac{d^2f}{d\chi^2}, & \text{at } \chi = 0. \\
&\Rightarrow \frac{df}{d\chi}(0) = 1 + \frac{\Lambda_1}{(1-\Phi)^{2.5}} \frac{d^2f}{d\chi^2}(0). \\
&\quad \bar{f}_2(\bar{x}, \bar{y}, \bar{z}) = \bar{V}_w(\bar{y}) + \mu_{nf} \left(\frac{\partial \bar{f}_2}{\partial \bar{z}} \right), & \text{at } \bar{z} = 0. \\
&\Rightarrow \frac{c^*\bar{y}}{1-\xi\bar{t}} \frac{dg}{d\chi} = \frac{c^*\bar{y}}{1-\xi\bar{t}} + \frac{c^*\bar{y}}{1-\xi\bar{t}} \sqrt{\frac{c^*}{\nu_f(1-\xi\bar{t})}} \frac{\mu_f}{(1-\Phi)^{2.5}} \frac{d^2g}{d\chi^2}, & \text{at } \chi = 0. \\
&\Rightarrow \frac{c^*\bar{y}}{1-\xi\bar{t}} \frac{dg}{d\chi} = \frac{c^*\bar{y}}{1-\xi\bar{t}} \left(1 + \sqrt{\frac{c^*}{\nu_f(1-\xi\bar{t})}} \frac{\mu_f}{(1-\Phi)^{2.5}} \frac{d^2g}{d\chi^2} \right), & \text{at } \chi = 0. \\
&\Rightarrow \frac{dg}{d\chi}(0) = 1 + \frac{\Lambda_2}{(1-\Phi)^{2.5}} \frac{d^2g}{d\chi^2}, & \text{at } \chi = 0. \\
&\Rightarrow \frac{dg}{d\chi}(0) = 1 + \frac{\Lambda_2}{(1-\Phi)^{2.5}} \frac{d^2g}{d\chi^2}(0). \\
&\quad -k \left(\frac{\partial \Theta}{\partial \bar{z}} \right) = h_f(\Theta_f - \Theta), & \text{at } \bar{z} = 0. \\
&\Rightarrow -k \left[\frac{c^*\bar{x}}{1-\xi\bar{t}} \right] \frac{d\theta}{d\chi} \sqrt{\frac{c^*}{\nu_f(1-\xi\bar{t})}} = h_f \left(\Theta_\infty + \frac{c^*\bar{x}}{1-\xi\bar{t}} - \Theta \right), & \text{at } \chi = 0. \\
&\Rightarrow \frac{c^*\bar{x}}{1-\xi\bar{t}} \frac{d\theta}{d\chi} = \frac{-h_f}{k} \sqrt{\frac{\nu_f(1-\xi\bar{t})}{c^*}} \left(\Theta_\infty + \frac{c^*\bar{x}}{1-\xi\bar{t}} - \left(\frac{c^*\bar{x}}{1-\xi\bar{t}} \right) \theta(\chi) - \Theta_\infty \right), & \text{at } \chi = 0. \\
&\Rightarrow \frac{c^*\bar{x}}{1-\xi\bar{t}} \frac{d\theta}{d\chi} = -\frac{h_f}{k} \sqrt{\frac{\nu_f(1-\xi\bar{t})}{c^*}} \left(\frac{c^*\bar{x}}{1-\xi\bar{t}} - \frac{c^*\bar{x}}{1-\xi\bar{t}} \theta(\chi) \right), & \text{at } \chi = 0. \\
&\Rightarrow \frac{c^*\bar{x}}{1-\xi\bar{t}} \frac{d\theta}{d\chi} = -\frac{h_f}{k} \sqrt{\frac{\nu_f(1-\xi\bar{t})}{c^*}} \frac{c^*\bar{x}}{1-\xi\bar{t}} (1 - \theta(\chi)), & \text{at } \chi = 0. \\
&\Rightarrow \frac{d\theta}{d\chi}(0) = -Bi(1 - \theta(\chi)), & \text{at } \chi = 0. \\
&\Rightarrow \frac{d\theta}{d\chi}(0) = -Bi(1 - \theta(0)). \\
&\quad \bar{f}_1 \rightarrow 0, & \text{as } \bar{z} \rightarrow \infty. \\
&\Rightarrow \frac{c^*\bar{x}}{1-\xi\bar{t}} \frac{df}{d\chi} \rightarrow 0, & \text{as } \bar{z} \rightarrow \infty. \\
&\Rightarrow \frac{df}{d\chi} \rightarrow 0, & \text{as } \chi \rightarrow \infty. \\
&\quad \bar{f}_2 \rightarrow 0, & \text{as } \bar{z} \rightarrow \infty. \\
&\Rightarrow \frac{c^*\bar{y}}{1-\xi\bar{t}} \frac{dg}{d\chi} \rightarrow 0, & \text{as } \bar{z} \rightarrow \infty. \\
&\Rightarrow \frac{dg}{d\chi} \rightarrow 0, & \text{as } \chi \rightarrow \infty. \\
&\quad \Theta \rightarrow \Theta_\infty, & \text{as } \bar{z} \rightarrow \infty.
\end{aligned}$$

$$\Rightarrow \Theta_\infty + \frac{c^* \bar{x}}{1 - \bar{\xi} \bar{t}} \theta(\chi) \rightarrow \Theta_\infty, \quad \text{as } \bar{z} \rightarrow \infty.$$

$$\Rightarrow \theta(\chi) \rightarrow 0 \quad \text{as } \chi \rightarrow \infty.$$

Moreover, $A = \frac{\bar{\xi}}{c^*}$ is the unsteady flow parameter, $\omega = \frac{1}{\mu_f \hat{\beta} h^*}$ and $\Delta_1 = \frac{\bar{U}_w^3 \bar{x}}{2h^{*2} \nu_f}$, $\Delta_2 = \frac{\bar{U}_w^3 \bar{y}}{2h^{*2} \nu_f}$ are the material parameters, $M = \frac{\sigma_f B_0^2}{c^* \rho_f}$ is the magnetic parameter, and $Pr = \frac{\nu_f}{\alpha_f}$ is the Prandtl number, $\alpha_f = \frac{k_f}{(\rho C_p)_f}$ is the thermal diffusivity parameter, $N_r = \frac{16}{3} \frac{\Theta_\infty^3 \sigma^*}{k^* \nu_f (\rho C_p)_f}$ is the thermal radiation parameter, $Q = \frac{Q_0}{(\rho C_p)_f} (\Theta_f - \Theta_\infty)$ is the heat generation parameter, $S_1 = -\bar{W}_w \sqrt{\frac{1 - \bar{\xi} \bar{t}}{c^* \nu_f}}$, $S_2 = -\bar{W}_w \sqrt{\frac{1 - \bar{\xi} \bar{t}}{c^* \nu_f}}$, are the mass transfer parameters, $\Lambda_1 = \sqrt{\frac{c^*}{\nu_f (1 - \bar{\xi} \bar{t})}} \mu_f$, $\Lambda_2 = \sqrt{\frac{c^*}{\nu_f (1 - \bar{\xi} \bar{t})}} \mu_f$ are the velocity slip parameters, $E_c = \frac{\bar{U}_w}{(C_p)_f}$ is the Eckert number, $\lambda = \lambda_0 (1 - \bar{\xi} \bar{t})$ is the Thermal relaxation time and $B_i = \frac{h_f}{k} \sqrt{\frac{\nu_f (1 - \bar{\xi} \bar{t})}{c^*}}$ is the Biot number. By using (3.34), (3.35), (3.36), (3.37) and (3.38) in the dimensionless form of the governing model is given below.

$$\left(\frac{1}{N_1 N_2} + \frac{w}{N_2} \right) \frac{d^3 f}{d\chi^3} - A \left[\frac{df}{d\chi} + \frac{\chi}{2} \frac{d^2 f}{d\chi^2} \right] - \left(\frac{df}{d\chi} \right)^2 + f \frac{d^2 f}{d\chi^2} + g \frac{d^2 f}{d\chi^2} - \left[\frac{\Delta_1 w}{N_2} \right] \left(\frac{d^2 f}{d\chi^2} \right)^2 - \frac{d^3 f}{d\chi^3} - \frac{N_5}{N_2} M \frac{df}{d\chi} \sin^2(\Gamma) = 0, \quad (4.55)$$

$$\left(\frac{1}{N_1 N_2} + \frac{w}{N_2} \right) \frac{d^3 g}{d\chi^3} - A \left[\frac{dg}{d\chi} + \frac{\chi}{2} \frac{d^2 g}{d\chi^2} \right] - \left(\frac{dg}{d\chi} \right)^2 + f \frac{d^2 g}{d\chi^2} + g \frac{d^2 g}{d\chi^2} - \left[\frac{\Delta_2 w}{N_2} \right] \left(\frac{d^2 g}{d\chi^2} \right)^2 - \frac{d^3 g}{d\chi^3} - \frac{N_5}{N_2} M \frac{dg}{d\chi} \sin^2(\Gamma) = 0, \quad (4.56)$$

$$\left(1 + \frac{k_f Pr N_r}{k_{nf}} - \frac{k_f N_3 Pr}{k_{nf}} \xi (f + g)^2 \right) \frac{d^2 \theta}{d\chi^2} - \frac{k_f N_3 Pr}{k_{nf}} \left\{ A \left[\theta + \frac{\chi}{2} \frac{d\theta}{d\chi} \right] + \frac{df}{d\chi} \theta - f \frac{d\theta}{d\chi} - g \frac{d\theta}{d\chi} - \frac{E_c}{N_1 N_3} \left(\frac{d^2 f}{d\chi^2} \right)^2 - \frac{Q}{N_3} \theta + \xi \left[\left(\frac{df}{d\chi} \right)^2 \theta - f \frac{d^2 f}{d\chi^2} \theta - g \frac{d^2 f}{d\chi^2} \theta + [f + g] \left[\frac{df}{d\chi} + \frac{dg}{d\chi} \right] \frac{d\theta}{d\chi} - \frac{N_5}{N_3} E_c M \left(\frac{df}{d\chi} \right)^2 \sin^2(\Gamma) \right\} = 0. \quad (4.57)$$

The dimensionless form of BCs corresponding to (4.8), are given below.

$$\left. \begin{aligned} f(\chi) = S_1, \quad g(\chi) = S_2, \quad \frac{df}{d\chi} = 1 + \frac{\Lambda_1}{N_1} \frac{d^2 f}{d\chi^2}, \\ \frac{dg}{d\chi} = 1 + \frac{\Lambda_2}{N_1} \frac{d^2 g}{d\chi^2}, \quad \frac{d\theta}{d\chi} = -Bi(1 - \theta(\chi)), \\ \frac{df}{d\chi} \rightarrow 0, \quad \frac{dg}{d\chi} \rightarrow 0, \quad \theta(\chi) \rightarrow 0, \quad as \quad \chi \rightarrow \infty. \end{aligned} \right\} at \chi = 0, \quad (4.58)$$

4.3.2 Non-dimensional Quantities of Interest

The non-dimensionalization of the local Nusselt number $Nu_{\bar{x}}$ and the skin friction coefficients $C_{f_{\bar{x}}}$, $C_{f_{\bar{y}}}$ have particular significance for our purposes at this point.

4.3.2.1 Skin Friction Coefficient

The dimensional form of coefficient of skin friction is given as:

$$C_{f_{\bar{x}}} = \frac{\tau_w}{\rho_f \bar{U}_w^2}. \quad (4.59)$$

In order to obtain the dimensionless form of $C_{f_{\bar{x}}}$, the following procedure will be adopted:

$$\tau_w = \left[\left(\mu_{nf} + \frac{1}{\hat{\beta}h^*} \right) \left(\frac{\partial \bar{f}_1}{\partial \bar{z}} \right) - \frac{1}{6\hat{\beta}h^{*3}} \left(\frac{\partial \bar{f}_1}{\partial \bar{z}} \right)^3 \right] \Big|_{\bar{z}=0}. \quad (4.60)$$

By using (4.23) in (4.60), we get

$$\tau_w = - \left[\left(\mu_{nf} + \frac{1}{\hat{\beta}h^*} \right) \frac{c^*}{1 - \xi \bar{t}} \sqrt{\frac{c^*}{\nu_f(1 - \xi \bar{t})}} \bar{x} \frac{d^2 f}{d\chi^2} - \frac{1}{6\hat{\beta}h^{*3}} \left(\frac{c^*}{1 - \xi \bar{t}} \sqrt{\frac{c^*}{\nu_f(1 - \xi \bar{t})}} \bar{x} \frac{d^2 f}{d\chi^2} \right)^3 \right] \Big|_{\bar{z}=0}.$$

Putting τ_w in (4.59), we get

$$\begin{aligned} C_f &= \frac{- \left[\left(\mu_{nf} + \frac{1}{\hat{\beta}h^*} \right) \frac{c^*}{1 - \xi \bar{t}} \sqrt{\frac{c^*}{\nu_f(1 - \xi \bar{t})}} \bar{x} \frac{d^2 f}{d\chi^2} - \frac{1}{6\hat{\beta}h^{*3}} \left(\frac{c^*}{1 - \xi \bar{t}} \sqrt{\frac{c^*}{\nu_f(1 - \xi \bar{t})}} \bar{x} \frac{d^2 f}{d\chi^2} \right)^3 \right] \Big|_{\bar{z}=0}}{\rho_f \bar{U}_w^2} \\ &= \frac{- \left[\left(\frac{\mu_f}{(1 - \Phi)^{2.5}} + \frac{1}{\hat{\beta}h^*} \right) \frac{c^*}{1 - \xi \bar{t}} \sqrt{\frac{c^*}{\nu_f(1 - \xi \bar{t})}} \bar{x} \frac{d^2 f}{d\chi^2} - \frac{1}{6\hat{\beta}h^{*3}} \frac{c^{*3}}{(1 - \xi \bar{t})^3} \left(\sqrt{\frac{c^*}{\nu_f(1 - \xi \bar{t})}} \bar{x} \frac{d^2 f}{d\chi^2} \right)^3 \right] \Big|_{\bar{z}=0}}{\rho_f \bar{U}_w^2} \end{aligned}$$

$$\begin{aligned}
&= \frac{- \left[\left(\frac{\mu_f}{(1-\Phi)^{2.5}} + \frac{1}{\hat{\beta}h^*} \right) \bar{U}_w \sqrt{\frac{c^*}{\nu_f(1-\xi t)}} \bar{x} \frac{d^2 f}{d\chi^2} - \frac{1}{6\hat{\beta}h^{*3}} \bar{U}_w^3 \left(\sqrt{\frac{c^*}{\nu_f(1-\xi t)}} \bar{x} \frac{d^2 f}{d\chi^2} \right)^3 \right] \Big|_{\bar{z}=0}}{\rho_f \bar{U}_w^2} \\
&= \frac{- \left[\left(\frac{\mu_f}{(1-\Phi)^{2.5}\mu_f} + \frac{1}{\hat{\beta}h^*\mu_f} \right) \bar{U}_w \sqrt{\frac{c^*}{\nu_f(1-\xi t)}} \bar{x} \frac{d^2 f}{d\chi^2} - \frac{1}{6\hat{\beta}h^{*3}\mu_f} \bar{U}_w^3 \left(\sqrt{\frac{c^*}{\nu_f(1-\xi t)}} \bar{x} \frac{d^2 f}{d\chi^2} \right)^3 \right] \Big|_{\bar{z}=0}}{\frac{\rho_f \bar{U}_w^2}{\mu_f}} \\
&= \frac{- \left[\left(\frac{1}{(1-\Phi)^{2.5}} + \frac{1}{\hat{\beta}h^*\mu_f} \right) \frac{d^2 f}{d\chi^2}(0) - \frac{1}{6\hat{\beta}h^{*3}\mu_f} \bar{U}_w^2 \frac{c^* \bar{x}^2}{\nu_f(1-\xi t)} \left(\frac{d^2 f}{d\chi^2} \right)^3(0) \right] \sqrt{\frac{c^*}{\nu_f(1-\xi t)}} \bar{x}}{\frac{\bar{U}_w \bar{x}}{\nu_f}} \\
&= \frac{- \left[\left(\frac{1}{(1-\Phi)^{2.5}} + \frac{1}{\hat{\beta}h^*\mu_f} \right) \frac{d^2 f}{d\chi^2}(0) - \frac{1}{6\hat{\beta}h^{*3}\mu_f} \bar{U}_w^2 \frac{c^* \bar{x} \cdot \bar{x}}{\nu_f(1-\xi t)} \left(\frac{d^2 f}{d\chi^2} \right)^3(0) \right] \sqrt{\frac{c^*}{\nu_f(1-\xi t)}} \bar{x}}{\frac{\bar{U}_w \bar{x}}{\nu_f}} \\
&= \frac{- \left[\left(\frac{1}{(1-\Phi)^{2.5}} + \frac{1}{\hat{\beta}h^*\mu_f} \right) \frac{d^2 f}{d\chi^2}(0) - \frac{1}{3} \frac{1}{\hat{\beta}h^*\mu_f} \frac{\bar{U}_w^3 \bar{x}}{2h^{*2}\nu_f} \left(\frac{d^2 f}{d\chi^2} \right)^3(0) \right] \sqrt{\frac{c^* \bar{x}}{\nu_f \bar{x}(1-\xi t)}} \bar{x}}{\frac{\bar{U}_w \bar{x}}{\nu_f}} \\
&= \frac{- \left[\left(\frac{1}{(1-\Phi)^{2.5}} + \frac{1}{\hat{\beta}h^*\mu_f} \right) \frac{d^2 f}{d\chi^2}(0) - \frac{1}{3} \frac{1}{\hat{\beta}h^*\mu_f} \frac{\bar{U}_w^3 \bar{x}}{2h^{*2}\nu_f} \left(\frac{d^2 f}{d\chi^2} \right)^3(0) \right] \sqrt{\frac{\bar{U}_w \bar{x}^2}{\nu_f \bar{x}}}}{\frac{\bar{U}_w \bar{x}}{\nu_f}} \\
&= \frac{- \left[\left(\frac{1}{(1-\Phi)^{2.5}} + \omega \right) \frac{d^2 f}{d\chi^2}(0) - \frac{1}{3} \omega \Delta_1 \left(\frac{d^2 f}{d\chi^2} \right)^3(0) \right] \sqrt{\frac{\bar{U}_w \bar{x}}{\nu_f}}}{Re_{\bar{x}}} \\
&= \frac{- \left[\left(\frac{1}{(1-\Phi)^{2.5}} + \omega \right) \frac{d^2 f}{d\chi^2}(0) - \frac{\omega \Delta_1}{3} \left(\frac{d^2 f}{d\chi^2} \right)^3(0) \right] \sqrt{Re_{\bar{x}}}}{Re_{\bar{x}}} \\
&= \frac{- \left[\left(\frac{1}{(1-\Phi)^{2.5}} + \omega \right) \frac{d^2 f}{d\chi^2}(0) - \frac{\omega \Delta_1}{3} \left(\frac{d^2 f}{d\chi^2} \right)^3(0) \right]}{\sqrt{Re_{\bar{x}}}}.
\end{aligned}$$

Hence, the dimensionless form of the coefficient of skin friction is

$$C_f Re_{\bar{x}}^{\frac{1}{2}} = - \left[\left(\frac{1}{(1-\Phi)^{2.5}} + \omega \right) \frac{d^2 f}{d\chi^2}(0) - \frac{\omega \Delta_1}{3} \left(\frac{d^2 f}{d\chi^2} \right)^3(0) \right], \quad (4.61)$$

where $Re_{\bar{x}}$ represents the Reynolds number defined as $Re_{\bar{x}} = \frac{\bar{U}_w \bar{x}}{\nu_f}$.

The dimensional form of coefficient of skin friction is given as:

$$C_{f_{\bar{y}}} = \frac{\tau_w}{\rho_f \bar{U}_w^2}. \quad (4.62)$$

In order to obtain the dimensionless form of $C_{f_{\bar{y}}}$, the following procedure will be adopted:

$$\tau_w = \left[\left(\mu_{nf} + \frac{1}{\hat{\beta}h^*} \right) \left(\frac{\partial \bar{f}_2}{\partial \bar{z}} \right) - \frac{1}{6\hat{\beta}h^{*3}} \left(\frac{\partial \bar{f}_2}{\partial \bar{z}} \right)^3 \right] \Big|_{\bar{z}=0}. \quad (4.63)$$

By using (4.30) in (4.63), we get

$$\tau_w = - \left[\left(\mu_{nf} + \frac{1}{\hat{\beta}h^*} \right) \frac{c^*}{1 - \bar{\xi}\bar{t}} \sqrt{\frac{c^*}{\nu_f(1-\bar{\xi}\bar{t})}} \bar{y} \frac{d^2g}{d\chi^2} - \frac{1}{6\hat{\beta}h^{*3}} \left(\frac{c^*}{1 - \bar{\xi}\bar{t}} \sqrt{\frac{c^*}{\nu_f(1-\bar{\xi}\bar{t})}} \bar{y} \frac{d^2g}{d\chi^2} \right)^3 \right] \Big|_{\bar{z}=0}.$$

Putting τ_w in (4.62), we get

$$\begin{aligned} C_f &= \frac{- \left[\left(\mu_{nf} + \frac{1}{\hat{\beta}h^*} \right) \frac{c^*}{1 - \bar{\xi}\bar{t}} \sqrt{\frac{c^*}{\nu_f(1-\bar{\xi}\bar{t})}} \bar{y} \frac{d^2g}{d\chi^2} - \frac{1}{6\hat{\beta}h^{*3}} \left(\frac{c^*}{1 - \bar{\xi}\bar{t}} \sqrt{\frac{c^*}{\nu_f(1-\bar{\xi}\bar{t})}} \bar{y} \frac{d^2g}{d\chi^2} \right)^3 \right] \Big|_{\bar{z}=0}}{\rho_f \bar{U}_w^2} \\ &= \frac{- \left[\left(\frac{\mu_f}{(1-\Phi)^{2.5}} + \frac{1}{\hat{\beta}h^*} \right) \frac{c^*}{1 - \bar{\xi}\bar{t}} \sqrt{\frac{c^*}{\nu_f(1-\bar{\xi}\bar{t})}} \bar{y} \frac{d^2g}{d\chi^2} - \frac{1}{6\hat{\beta}h^{*3}} \frac{c^{*3}}{(1-\bar{\xi}\bar{t})^3} \left(\sqrt{\frac{c^*}{\nu_f(1-\bar{\xi}\bar{t})}} \bar{y} \frac{d^2g}{d\chi^2} \right)^3 \right] \Big|_{\bar{z}=0}}{\rho_f \bar{U}_w^2} \\ &= \frac{- \left[\left(\frac{\mu_f}{(1-\Phi)^{2.5}} + \frac{1}{\hat{\beta}h^*} \right) \bar{U}_w \sqrt{\frac{c^*}{\nu_f(1-\bar{\xi}\bar{t})}} \bar{y} \frac{d^2g}{d\chi^2} - \frac{1}{6\hat{\beta}h^{*3}} \bar{U}_w^3 \left(\sqrt{\frac{c^*}{\nu_f(1-\bar{\xi}\bar{t})}} \bar{y} \frac{d^2g}{d\chi^2} \right)^3 \right] \Big|_{\bar{z}=0}}{\rho_f \bar{U}_w^2} \\ &= \frac{- \left[\left(\frac{\mu_f}{(1-\Phi)^{2.5}\mu_f} + \frac{1}{\hat{\beta}h^*\mu_f} \right) \bar{U}_w \sqrt{\frac{c^*}{\nu_f(1-\bar{\xi}\bar{t})}} \bar{y} \frac{d^2g}{d\chi^2} - \frac{1}{6\hat{\beta}h^{*3}\mu_f} \bar{U}_w^3 \left(\sqrt{\frac{c^*}{\nu_f(1-\bar{\xi}\bar{t})}} \bar{y} \frac{d^2g}{d\chi^2} \right)^3 \right] \Big|_{\bar{z}=0}}{\frac{\rho_f}{\mu_f} \bar{U}_w^2} \\ &= \frac{- \left[\left(\frac{1}{(1-\Phi)^{2.5}} + \frac{1}{\hat{\beta}h^*\mu_f} \right) \frac{d^2g}{d\chi^2}(0) - \frac{1}{6\hat{\beta}h^{*3}\mu_f} \bar{U}_w^2 \frac{c^*\bar{y}^2}{\nu_f(1-\bar{\xi}\bar{t})} \left(\frac{d^2g}{d\chi^2} \right)^3(0) \right] \sqrt{\frac{c^*}{\nu_f(1-\bar{\xi}\bar{t})}} \bar{y}}{\frac{\bar{U}_w \bar{y}}{\nu_f}} \\ &= \frac{- \left[\left(\frac{1}{(1-\Phi)^{2.5}} + \frac{1}{\hat{\beta}h^*\mu_f} \right) \frac{d^2g}{d\chi^2}(0) - \frac{1}{6\hat{\beta}h^{*3}\mu_f} \bar{U}_w^2 \frac{c^*\bar{y} \cdot \bar{y}}{\nu_f(1-\bar{\xi}\bar{t})} \left(\frac{d^2g}{d\chi^2} \right)^3(0) \right] \sqrt{\frac{c^*}{\nu_f(1-\bar{\xi}\bar{t})}} \bar{y}}{\frac{\bar{U}_w \bar{y}}{\nu_f}} \\ &= \frac{- \left[\left(\frac{1}{(1-\Phi)^{2.5}} + \frac{1}{\hat{\beta}h^*\mu_f} \right) \frac{d^2g}{d\chi^2}(0) - \frac{1}{3} \frac{1}{\hat{\beta}h^*\mu_f} \frac{\bar{U}_w^3 \bar{y}}{2h^{*2}\nu_f} \left(\frac{d^2g}{d\chi^2} \right)^3(0) \right] \sqrt{\frac{c^*\bar{y}}{\nu_f\bar{y}(1-\bar{\xi}\bar{t})}} \bar{y}}{\frac{\bar{U}_w \bar{y}}{\nu_f}} \end{aligned}$$

$$\begin{aligned}
&= \frac{-\left[\left(\frac{1}{(1-\Phi)^{2.5}} + \frac{1}{\hat{\beta}h^*\mu_f}\right)\frac{d^2g}{d\chi^2}(0) - \frac{1}{3}\frac{1}{\hat{\beta}h^*\mu_f}\frac{\bar{U}_w^3\bar{y}}{2h^{*2}\nu_f}\left(\frac{d^2g}{d\chi^2}\right)^3(0)\right]\sqrt{\frac{\bar{U}_w\bar{y}^2}{\nu_f\bar{y}}}}{\frac{\bar{U}_w\bar{y}}{\nu_f}} \\
&= \frac{-\left[\left(\frac{1}{(1-\Phi)^{2.5}} + \omega\right)\frac{d^2g}{d\chi^2}(0) - \frac{1}{3}\omega\Delta_2\left(\frac{d^2g}{d\chi^2}\right)^3(0)\right]\sqrt{\frac{\bar{U}_w\bar{y}}{\nu_f}}}{Re_{\bar{y}}} \\
&= \frac{-\left[\left(\frac{1}{(1-\Phi)^{2.5}} + \omega\right)\frac{d^2g}{d\chi^2}(0) - \frac{\omega\Delta_2}{3}\left(\frac{d^2g}{d\chi^2}\right)^3(0)\right]\sqrt{Re_{\bar{y}}}}{Re_{\bar{y}}} \\
&= \frac{-\left[\left(\frac{1}{(1-\Phi)^{2.5}} + \omega\right)\frac{d^2g}{d\chi^2}(0) - \frac{\omega\Delta_2}{3}\left(\frac{d^2g}{d\chi^2}\right)^3(0)\right]}{\sqrt{Re_{\bar{y}}}}.
\end{aligned}$$

Hence, the dimensionless form of the coefficient of skin friction is

$$C_f Re_{\bar{y}}^{\frac{1}{2}} = -\left[\left(\frac{1}{(1-\Phi)^{2.5}} + \omega\right)\frac{d^2g}{d\chi^2}(0) - \frac{\omega\Delta_2}{3}\left(\frac{d^2g}{d\chi^2}\right)^3(0)\right], \quad (4.64)$$

where $Re_{\bar{y}}$ represents the Reynolds number defined as $Re_{\bar{y}} = \frac{\bar{U}_w\bar{y}}{\nu_f}$.

4.3.2.2 Nusselt Number

The dimensional form of the local Nusselt number is defined as:

$$Nu_{\bar{x}} = \frac{\bar{x}q_w}{k_f(\Theta_w - \Theta_\infty)}, \quad (4.65)$$

where q_w is formulated as

$$q_w = -k_{nf}\left(1 + \frac{16}{3}\frac{\sigma^*\Theta_\infty^3}{k^*\nu_f(\rho C_p)_f}\right)\left(\frac{\partial\Theta}{\partial\bar{z}}\right)\Bigg|_{\bar{z}=0}. \quad (4.66)$$

Using (4.36) in (4.66) we get

$$q_w = -k_{nf}\left(1 + \frac{4(4)}{3}\frac{\sigma^*\Theta_\infty^3}{k^*\nu_f(\rho C_p)_f}\right)\left(\frac{c^*\bar{x}}{1-\tilde{\xi}\tilde{t}}\frac{d\theta}{d\chi}\sqrt{\frac{c^*}{\nu_f(1-\tilde{\xi}\tilde{t})}}\right)\Bigg|_{\bar{z}=0}.$$

Putting q_w in (4.65), we get

$$\begin{aligned}
Nu_{\bar{x}} &= - \frac{\bar{x}k_{nf} \left(1 + \frac{16}{3} \frac{\sigma^* \Theta_{\infty}^3}{k^* \nu_f (\rho C_p)_f} \right) \left(\frac{c^* \bar{x}}{1 - \xi \bar{t}} \frac{d\theta}{d\chi} \sqrt{\frac{c^*}{\nu_f (1 - \xi \bar{t})}} \right) \Big|_{\bar{z}=0}}{k_f (\Theta_f - \Theta_{\infty})} \\
&= - \frac{\bar{x}k_{nf} \left(1 + \frac{16}{3} \frac{\sigma^* \Theta_{\infty}^3}{k^* \nu_f (\rho C_p)_f} \right) \left(\frac{c^* \bar{x}}{1 - \xi \bar{t}} \frac{d\theta}{d\chi} (0) \sqrt{\frac{c^*}{\nu_f (1 - \xi \bar{t})}} \right)}{k_f \frac{c^* \bar{x}}{1 - \xi \bar{t}}} \\
&= - \frac{\bar{x}k_{nf} \left(1 + \frac{16}{3} \frac{\sigma^* \Theta_{\infty}^3}{k^* \nu_f (\rho C_p)_f} \right) \frac{d\theta}{d\chi} (0) \sqrt{\frac{c^*}{\nu_f (1 - \xi \bar{t})}}}{k_f} \\
&= - \frac{k_{nf}}{k_f} \left(1 + \frac{16}{3} \frac{\sigma^* \Theta_{\infty}^3}{k^* \nu_f (\rho C_p)_f} \right) \frac{d\theta}{d\chi} (0) \sqrt{\frac{c^* \bar{x}}{\nu_f \bar{x} (1 - \xi \bar{t})}} \bar{x} \\
&= - \frac{k_{nf}}{k_f} (1 + Nr) \frac{d\theta}{d\chi} (0) \sqrt{\frac{\bar{U}_w \bar{x}^2}{\nu_f \bar{x}}} \\
&= - \frac{k_{nf}}{k_f} (1 + Nr) \frac{d\theta}{d\chi} (0) \sqrt{Re_{\bar{x}}}. \\
\Rightarrow \frac{Nu_{\bar{x}}}{Re_{\bar{x}}^{\frac{1}{2}}} &= - \frac{k_{nf}}{k_f} (1 + Nr) \frac{d\theta}{d\chi} (0). \\
\Rightarrow Nu_{\bar{x}} Re_{\bar{x}}^{-\frac{1}{2}} &= - \frac{k_{nf}}{k_f} (1 + Nr) \frac{d\theta}{d\chi} (0). \tag{4.67}
\end{aligned}$$

Finally,

$$\left. \begin{aligned}
C_f Re_{\bar{x}}^{\frac{1}{2}} &= - \left[\left(\frac{1}{(1 - \Phi)^{2.5}} + \omega \right) \frac{d^2 f}{d\chi^2} (0) - \frac{\omega \Delta_1}{3} \left(\frac{d^2 f}{d\chi^2} \right)^3 (0) \right], \\
C_f Re_{\bar{y}}^{\frac{1}{2}} &= - \left[\left(\frac{1}{(1 - \Phi)^{2.5}} + \omega \right) \frac{d^2 g}{d\chi^2} (0) - \frac{\omega \Delta_2}{3} \left(\frac{d^2 g}{d\chi^2} \right)^3 (0) \right], \\
Nu_{\bar{x}} Re_{\bar{x}}^{-\frac{1}{2}} &= - \frac{k_{nf}}{k_f} (1 + Nr) \frac{d\theta}{d\chi} (0).
\end{aligned} \right\} \tag{4.68}$$

4.3.3 Entropy Generation

Now, using (4.26), (3.34), (3.37), and (3.38), the dimensionless form of E_G , is:

$$\begin{aligned}
E_G &= \frac{k_{nf}}{\Theta_{\infty}^2} \left[(1 + Nr) \frac{c^* \bar{x}^2}{\nu_f (1 - \xi \bar{t})^3} \left(\frac{d\theta}{d\chi} \right)^2 \right] + \frac{\mu_{nf}}{\Theta_{\infty}} \frac{c^* \bar{x}^2}{\nu_f (1 - \xi \bar{t})^3} \left(\frac{d^2 f}{d\chi^2} \right)^2 + \frac{\sigma_{nf}^* B_0^2}{\Theta_{\infty}} \\
&\quad \frac{\sin^2(\Gamma)}{(\sqrt{(1 - \xi \bar{t})})^2} \left[\frac{c^* \bar{x}}{(1 - \xi \bar{t})} \frac{df}{d\chi} \right]^2.
\end{aligned}$$

$$\begin{aligned} \Rightarrow E_G &= \frac{N_4 k_f}{\Theta_\infty^2} \left[(1 + Nr) \frac{c^{*2} \bar{x}^2}{(1 - \bar{\xi} \bar{t})^2} \left(\frac{d\theta}{d\chi} \right)^2 \right] \frac{c^* \bar{x}}{\nu_f \bar{x} (1 - \bar{\xi} \bar{t})} + \frac{\mu_{nf}}{\Theta_\infty} \frac{c^{*2} \bar{x}^2}{(1 - \bar{\xi} \bar{t})^2} \frac{c^* \bar{x}}{\nu_f \bar{x} (1 - \bar{\xi} \bar{t})} \\ &\quad \left(\frac{d^2 f}{d\chi^2} \right)^2 + \frac{N_5 \sigma_f B_0^2 \sin^2(\Gamma)}{\Theta_\infty (1 - \bar{\xi} \bar{t})} \frac{c^{*2} \bar{x}^2}{(1 - \bar{\xi} \bar{t})^2} \left(\frac{df}{d\chi} \right)^2. \\ \Rightarrow E_G &= \frac{N_4 k_f}{\Theta_\infty^2} \left[(1 + Nr) (\Theta_f - \Theta_\infty)^2 \left(\frac{d\theta}{d\chi} \right)^2 \right] \frac{\bar{U}_w}{\nu_f \bar{x}} + \frac{\mu_{nf}}{\Theta_\infty} \bar{U}_w^2 \frac{\bar{U}_w}{\nu_f \bar{x}} \left(\frac{d^2 f}{d\chi^2} \right)^2 + \frac{N_5 \sigma_f B_0^2}{\Theta_\infty} \\ &\quad \frac{\sin^2(\Gamma)}{(1 - \bar{\xi} \bar{t})} \bar{U}_w^2 \left(\frac{df}{d\chi} \right)^2. \\ \Rightarrow E_G &= \frac{N_4 k_f}{\Theta_\infty^2} \left[(1 + Nr) (\Theta_f - \Theta_\infty)^2 \left(\frac{d\theta}{d\chi} \right)^2 \right] \frac{\bar{U}_w}{\nu_f \bar{x}} + \frac{\frac{\mu_f}{N_1} \bar{U}_w^2 \bar{U}_w}{\Theta_\infty \nu_f \bar{x}} \left(\frac{d^2 f}{d\chi^2} \right)^2 + \frac{N_5 \sigma_f B_0^2}{\Theta_\infty} \\ &\quad \frac{\sin^2(\Gamma)}{(1 - \bar{\xi} \bar{t})} \bar{U}_w^2 \left(\frac{df}{d\chi} \right)^2. \end{aligned}$$

The dimensionless entropy generation is denoted by NG and is defined as:

$$NG = \frac{\Theta_\infty^2 c^{*2} E_G}{k_f (\Theta_f - \Theta_\infty)^2}. \quad (4.69)$$

The dimensionless form of N_G can be produced through the following procedure:

$$\begin{aligned} NG &= \frac{\Theta_\infty^2 c^{*2}}{k_f (\Theta_f - \Theta_\infty)^2} \left[\frac{N_4 k_f}{\Theta_\infty^2} \left[(1 + Nr) (\Theta_f - \Theta_\infty)^2 \left(\frac{d\theta}{d\chi} \right)^2 \right] \frac{\bar{U}_w}{\nu_f \bar{x}} + \frac{\frac{\mu_f}{N_1} \bar{U}_w^2 \bar{U}_w}{\Theta_\infty \nu_f \bar{x}} \left(\frac{d^2 f}{d\chi^2} \right)^2 \right. \\ &\quad \left. + \frac{N_5 \sigma_f B_0^2 \sin^2(\Gamma)}{\Theta_\infty (1 - \bar{\xi} \bar{t})} \bar{U}_w^2 \left(\frac{df}{d\chi} \right)^2 \right] \\ &= \left[N_4 (1 + Nr) \left(\frac{d\theta}{d\chi} \right)^2 + \frac{1}{N_1} \frac{\Theta_\infty}{(\Theta_f - \Theta_\infty)} \frac{\mu_f \bar{U}_w^2}{k_f (\Theta_f - \Theta_\infty)} \left(\frac{d^2 f}{d\chi^2} \right)^2 \right] \frac{\bar{U}_w c^{*2}}{\nu_f \bar{x}} + \\ &\quad \frac{\Theta_\infty \bar{U}_w^2}{k_f (\Theta_f - \Theta_\infty)^2} \frac{N_5 \sigma_f B_0^2 \sin^2(\Gamma) c^{*2}}{(1 - \bar{\xi} \bar{t})} \left(\frac{df}{d\chi} \right)^2 \\ &= \left[N_4 (1 + Nr) \left(\frac{d\theta}{d\chi} \right)^2 + \frac{1}{N_1} \frac{Br}{\Omega} \left(\frac{d^2 f}{d\chi^2} \right)^2 \right] Re + \frac{\Theta_\infty N_5}{(\Theta_f - \Theta_\infty)} \frac{\bar{U}_w^2}{k_f (\Theta_f - \Theta_\infty)} \frac{\sigma_f B_0^2}{\rho_f c^*} \rho_f c^* \\ &\quad \frac{\sin^2(\Gamma) c^{*2} \bar{x}}{(1 - \bar{\xi} \bar{t}) \bar{x}} \left(\frac{df}{d\chi} \right)^2 \\ &= \left[N_4 (1 + Nr) \left(\frac{d\theta}{d\chi} \right)^2 + \frac{1}{N_1} \frac{Br}{\Omega} \left(\frac{d^2 f}{d\chi^2} \right)^2 \right] Re + \frac{N_5}{\Omega} \frac{\bar{U}_w^2 \mu_f}{k_f (\Theta_f - \Theta_\infty)} \frac{\sigma_f B_0^2}{c^* \rho_f} \frac{c^* \bar{x}}{(1 - \bar{\xi} \bar{t})} \\ &\quad \sin^2(\Gamma) \frac{c^{*2}}{\nu_f \bar{x}} \left(\frac{df}{d\chi} \right)^2 \\ &= \left[N_4 (1 + Nr) \left(\frac{d\theta}{d\chi} \right)^2 + \frac{1}{N_1} \frac{Br}{\Omega} \left(\frac{d^2 f}{d\chi^2} \right)^2 \right] Re + \frac{N_5}{\Omega} Br M \frac{\bar{U}_w c^{*2}}{\nu_f \bar{x}} \sin^2(\Gamma) \left(\frac{df}{d\chi} \right)^2 \\ &= \left[N_4 (1 + Nr) \left(\frac{d\theta}{d\chi} \right)^2 + \frac{1}{N_1} \frac{Br}{\Omega} \left(\frac{d^2 f}{d\chi^2} \right)^2 \right] Re + \frac{N_5 Br M Re \sin^2(\Gamma)}{\Omega} \left(\frac{df}{d\chi} \right)^2 \end{aligned}$$

$$= Re \left[N_4(1 + Nr) \left(\frac{d\theta}{d\chi} \right)^2 + \frac{1}{N_1} \frac{Br}{\Omega} \left(\left(\frac{d^2 f}{d\zeta^2} \right)^2 + N_1 N_5 M \sin^2(\Gamma) \left(\frac{df}{d\chi} \right)^2 \right) \right].$$

4.4 Solution Methodology

In order to acquire the numerical solution for the ordinary differential equation system (4.55), (4.56) and (4.57) subject to the boundary conditions (4.58), the shooting method has been used. From (4.55), (4.56) and (4.57),

$$\begin{aligned} \frac{d^3 f}{d\chi^3} = & \frac{1}{\left(\frac{1}{N_1 N_2} + \frac{w}{N_2} - \left[\frac{\Delta_1 w}{N_2} \right] \left(\frac{d^2 f}{d\chi^2} \right)^2 \right)} \left\{ A \left[\frac{df}{d\chi} + \frac{\chi}{2} \frac{d^2 f}{d\chi^2} \right] + \left(\frac{df}{d\chi} \right)^2 - f \frac{d^2 f}{d\chi^2} \right. \\ & \left. - g \frac{d^2 f}{d\chi^2} + \frac{N_5}{N_2} M \frac{df}{d\chi} \sin^2(\Gamma) \right\} \end{aligned} \quad (4.70)$$

$$\begin{aligned} \frac{d^3 g}{d\chi^3} = & \frac{1}{\left(\frac{1}{N_1 N_2} + \frac{w}{N_2} - \left[\frac{\Delta_2 w}{N_2} \right] \left(\frac{d^2 g}{d\chi^2} \right)^2 \right)} \left\{ A \left[\frac{dg}{d\chi} + \frac{\chi}{2} \frac{d^2 g}{d\chi^2} \right] + \left(\frac{dg}{d\chi} \right)^2 - f \frac{d^2 g}{d\chi^2} \right. \\ & \left. - g \frac{d^2 g}{d\chi^2} + \frac{N_5}{N_2} M \frac{dg}{d\chi} \sin^2(\Gamma) \right\} \end{aligned} \quad (4.71)$$

$$\begin{aligned} \frac{d^2 \theta}{d\chi^2} = & \frac{1}{\left(1 + \frac{k_f Pr Nr}{k_{nf}} - \frac{k_f N_3 Pr}{k_{nf}} \xi (f + g)^2 \right)} \left\{ \frac{k_f N_3 Pr}{k_{nf}} \left\{ A \left[\theta + \frac{\chi}{2} \frac{d\theta}{d\chi} \right] + \frac{df}{d\chi} \theta - f \frac{d\theta}{d\chi} \right. \right. \\ & - g \frac{d\theta}{d\chi} + \frac{E_c}{N_1 N_3} \left(\frac{d^2 f}{d\chi^2} \right)^2 - \frac{Q}{N_3} \theta + \xi \left[\left(\frac{df}{d\chi} \right)^2 \theta - f \frac{d^2 f}{d\chi^2} \theta - g \frac{d^2 f}{d\chi^2} \theta + [f + g] \right. \\ & \left. \left. \left[\frac{df}{d\chi} + \frac{dg}{d\chi} \right] \frac{d\theta}{d\chi} \right] - \frac{N_5}{N_3} E_c M \left(\frac{df}{d\chi} \right)^2 \sin^2(\Gamma) \right\} \end{aligned} \quad (4.72)$$

The ordinary differential equations (4.70) and (4.71), are coupled in f and g. For numerical solution of these coupled ODEs, we will use the shooting method by assuming

that the values of f and g is known. For this, we utilize the following notations:

$$\begin{aligned} f = Y_1, \quad \frac{df}{d\chi} = Y_1' = Y_2, \quad \frac{d^2f}{d\chi^2} = Y_1'' = Y_2' = Y_3, \quad \frac{d^3f}{d\chi^3} = Y_1''' = Y_2'' = Y_3', \\ g = Y_4, \quad \frac{dg}{d\chi} = Y_4' = Y_5, \quad \frac{d^2g}{d\chi^2} = Y_4'' = Y_5' = Y_6, \quad \frac{d^3g}{d\chi^3} = Y_4''' = Y_5'' = Y_6', \end{aligned}$$

As a result, the coupled ODEs (4.70) and (4.71), are converted into the following system of 1st order ODEs.

$$Y_1' = Y_2, \quad Y_1(0) = S_1,$$

$$Y_2' = Y_3, \quad Y_2(0) = 1 + \frac{\Lambda_1}{N_1} Y_3,$$

$$Y_3' = \frac{1}{\frac{1}{N_1 N_2} + \frac{w}{N_2} - \frac{\Delta_1 w}{N_2} Y_3^2} \left\{ A \left[Y_2 + \frac{\chi}{2} Y_3 \right] + Y_2^2 - Y_1 Y_3 - Y_3 Y_4 + \frac{N_5}{N_2} M Y_2 \sin^2(\Gamma) \right\},$$

$$Y_3(0) = s_1,$$

$$Y_4' = Y_5, \quad Y_4(0) = S_2,$$

$$Y_5' = Y_6, \quad Y_5(0) = 1 + \frac{\Lambda_2}{N_1} Y_6,$$

$$Y_6' = \frac{1}{\frac{1}{N_1 N_2} + \frac{w}{N_2} - \frac{\Delta_2 w}{N_2} Y_6^2} \left\{ A \left[Y_5 + \frac{\chi}{2} Y_6 \right] + Y_5^2 - Y_1 Y_6 - Y_4 Y_6 + \frac{N_5}{N_2} M Y_5 \sin^2(\Gamma) \right\},$$

$$Y_6(0) = s_2.$$

where s_1 and s_2 are the missing conditions which will initially be guessed. To solve the initial value problem above, we use the fourth-order Runge-Kutta method. An approximate solution of (55) and (56) transforms the unbounded domain $[0, \infty)$ into the bounded domain $[0, \chi_\infty]$, where χ_∞ is a suitable finite positive real number that should be chosen such that there is no large variation in the solution of $\chi > \chi_\infty$.

The updation of the missing conditions s_1 and s_2 is made such that the following conditions must be verified:

$$(Y_2(s_1, s_2))_{\chi_\infty} = 0, \quad (Y_5(s_1, s_2))_{\chi_\infty} = 0.$$

In order to solve the above two algebraic equations for the missing conditions s_1 and

s_2 in a systematic way, the Newton's iterative method will be used. The method used the following iterative scheme for finding missing conditions.

$$\begin{bmatrix} s_1^{(n+1)} \\ s_2^{(n+1)} \end{bmatrix} = \begin{bmatrix} s_1^{(n)} \\ s_2^{(n)} \end{bmatrix} - \begin{bmatrix} \frac{\partial Y_2(s_1, s_2)}{\partial s_1} & \frac{\partial Y_2(s_1, s_2)}{\partial s_2} \\ \frac{\partial Y_5(s_1, s_2)}{\partial s_1} & \frac{\partial Y_5(s_1, s_2)}{\partial s_2} \end{bmatrix}_{(s_1=s_1^{(n)}, s_2=s_2^{(n)})}^{-1} \begin{bmatrix} Y_2(s_1, s_2) \\ Y_5(s_1, s_2) \end{bmatrix} \quad (4.73)$$

Let us further introduce the new notations that will be helpful for finding the numerical solution of ODEs.

$$\begin{aligned} \frac{\partial Y_1}{\partial s_1} &= Y_7, & \frac{\partial Y_2}{\partial s_1} &= Y_8, & \frac{\partial Y_3}{\partial s_1} &= Y_9, & \frac{\partial Y_4}{\partial s_1} &= Y_{10}, & \frac{\partial Y_5}{\partial s_1} &= Y_{11}, & \frac{\partial Y_6}{\partial s_1} &= Y_{12}, \\ \frac{\partial Y_1}{\partial s_2} &= Y_{13}, & \frac{\partial Y_2}{\partial s_2} &= Y_{14}, & \frac{\partial Y_3}{\partial s_2} &= Y_{15}, & \frac{\partial Y_4}{\partial s_2} &= Y_{16}, & \frac{\partial Y_5}{\partial s_2} &= Y_{17}, & \frac{\partial Y_6}{\partial s_2} &= Y_{18}. \end{aligned}$$

The above mentioned notations will change the form of Newton's iterative scheme as follows:

$$\begin{bmatrix} s_1^{(n+1)} \\ s_2^{(n+1)} \end{bmatrix} = \begin{bmatrix} s_1^{(n)} \\ s_2^{(n)} \end{bmatrix} - \begin{bmatrix} Y_8 & Y_{14} \\ Y_{11} & Y_{17} \end{bmatrix}_{(s_1=s_1^{(n)}, s_2=s_2^{(n)})}^{-1} \begin{bmatrix} Y_2(s_1, s_2) \\ Y_5(s_1, s_2) \end{bmatrix} \quad (4.74)$$

Now, differentiating the system of Six first ODEs w.r.t. to the missing conditions s_1 and s_2 respectively. We will get another system of Twelve first order ODEs as follows:

$$Y_7' = Y_8, \quad Y_7(0) = 0,$$

$$Y_8' = Y_9, \quad Y_8(0) = \frac{\Lambda_1}{N_1},$$

$$\begin{aligned} Y_9' &= \frac{1}{\left(\frac{1}{N_1 N_2} + \frac{w}{N_2} - \left[\frac{\Delta_1 w}{N_2}\right] Y_3^2\right)^2} \left\{ \left(\frac{1}{N_1 N_2} + \frac{w}{N_2} - \left[\frac{\Delta_1 w}{N_2}\right] Y_3^2\right) \left[A \left[Y_8 + \frac{\chi}{2} Y_9\right]\right. \right. \\ &\quad \left. \left. + 2Y_2 Y_8 - Y_1 Y_9 - Y_7 Y_3 - Y_3 Y_{10} - Y_9 Y_4 + \frac{N_5}{N_2} M Y_8 \sin^2(\Gamma)\right] - \left[A \left[Y_2 + \frac{\chi}{2} Y_3\right]\right. \right. \\ &\quad \left. \left. + Y_2^2 - Y_1 Y_3 - Y_3 Y_4 + \frac{N_5}{N_2} M Y_2 \sin^2(\Gamma)\right] \left(\frac{1}{N_1 N_2} + \frac{w}{N_2} - \left[\frac{\Delta_1 w}{N_2}\right] 2Y_3 Y_9\right) \right\}, \\ & \quad Y_9(0) = 1, \end{aligned}$$

$$Y'_{10} = Y_{11}, \quad Y_{10}(0) = 0,$$

$$Y'_{11} = Y_{12}, \quad Y_{11}(0) = 0,$$

$$Y'_{12} = \frac{1}{\left(\frac{1}{N_1 N_2} + \frac{w}{N_2} - \left[\frac{\Delta_2 w}{N_2}\right] Y_6^2\right)^2} \left\{ \left(\frac{1}{N_1 N_2} + \frac{w}{N_2} - \left[\frac{\Delta_2 w}{N_2}\right] Y_6^2\right) \left[A \left[Y_{11} + \frac{\chi}{2} Y_{12}\right] + 2Y_5 Y_{11} - Y_1 Y_{12} - Y_7 Y_6 - Y_4 Y_{12} - Y_{10} Y_6 + \frac{N_5}{N_2} M Y_{11} \sin^2(\Gamma)\right] - \left[A \left[Y_5 + \frac{\chi}{2} Y_6\right] + Y_5^2 - Y_1 Y_6 - Y_4 Y_6 + \frac{N_5}{N_2} M Y_5 \sin^2(\Gamma)\right] \left(\frac{1}{N_1 N_2} + \frac{w}{N_2} - \frac{\Delta_2 w}{N_2} 2Y_6 Y_{12}\right) \right\},$$

$$Y_{12}(0) = 0,$$

$$Y'_{13} = Y_{14}, \quad Y_{13}(0) = 0,$$

$$Y'_{14} = Y_{15}, \quad Y_{14}(0) = 0,$$

$$Y'_{15} = \frac{1}{\left(\frac{1}{N_1 N_2} + \frac{w}{N_2} - \left[\frac{\Delta_1 w}{N_2}\right] Y_3^2\right)^2} \left\{ \left(\frac{1}{N_1 N_2} + \frac{w}{N_2} - \left[\frac{\Delta_1 w}{N_2}\right] Y_3^2\right) \left[A \left[Y_{14} + \frac{\chi}{2} Y_{15}\right] + 2Y_2 Y_{14} - Y_1 Y_{15} - Y_{13} Y_3 - Y_3 Y_{16} - Y_{15} Y_4 + \frac{N_5}{N_2} M Y_{14} \sin^2(\Gamma)\right] - \left[A \left[Y_2 + \frac{\chi}{2} Y_3\right] + Y_2^2 - Y_1 Y_3 - Y_3 Y_4 + \frac{N_5}{N_2} M Y_2 \sin^2(\Gamma)\right] \left(\frac{1}{N_1 N_2} + \frac{w}{N_2} - \left[\frac{\Delta_1 w}{N_2}\right] 2Y_3 Y_{15}\right) \right\},$$

$$Y_{15}(0) = 0,$$

$$Y'_{16} = Y_{17}, \quad Y_{16}(0) = 0,$$

$$Y'_{17} = Y_{18}, \quad Y_{17}(0) = \frac{\Lambda_2}{N_1},$$

$$Y'_{18} = \frac{1}{\left(\frac{1}{N_1 N_2} + \frac{w}{N_2} - \left[\frac{\Delta_2 w}{N_2}\right] Y_6^2\right)^2} \left\{ \left(\frac{1}{N_1 N_2} + \frac{w}{N_2} - \left[\frac{\Delta_2 w}{N_2}\right] Y_6^2\right) \left[A \left[Y_{17} + \frac{\chi}{2} Y_{18}\right] + 2Y_5 Y_{17} - Y_1 Y_{18} - Y_{13} Y_6 - Y_4 Y_{18} - Y_{16} Y_6 + \frac{N_5}{N_2} M Y_{17} \sin^2(\Gamma)\right] - \left[A \left[Y_5 + \frac{\chi}{2} Y_6\right] + Y_5^2 - Y_1 Y_6 - Y_4 Y_6 + \frac{N_5}{N_2} M Y_5 \sin^2(\Gamma)\right] \left(\frac{1}{N_1 N_2} + \frac{w}{N_2} - \left[\frac{\Delta_2 w}{N_2}\right] 2Y_6 Y_{18}\right) \right\},$$

$$Y_{18}(0) = 1.$$

The stopping criteria for shooting method is given below:

$$\max\{|Y_2(\chi_\infty, s_1, s_2)|, |Y_5(\chi_\infty, s_1, s_2)|\} < \epsilon,$$

where $\epsilon > 0$ is an arbitrarily small positive number. The value of ϵ has been taken as 10^{-9} . Equation (4.72), will be treated in a similar way, by considering f and g as the known functions calculated through the above procedure.

4.5 Numerical Results and Discussions

In this section, the numerical results for momentum and energy equations for the physical quantities for unsteady three-dimensional Powell-Eyring magneto-nanofluid flow by utilizing Cattaneo-Christov heat flux model have been discussed through tables and graphs. The numerical data that has been shown through tables and graphs is produced by varying the influence of different physical quantities used in the ODEs. The effect of the dimensionless parameters of interest on the skin friction coefficient $C_{f_x} Re_x^{\frac{1}{2}}$, $C_{f_y} Re_y^{\frac{1}{2}}$, Nusselt number $Nu_x Re_x^{-\frac{1}{2}}$ and Entropy generation NG has been thoroughly discussed through different graphs and tables.

In Table 4.1, 4.3 shows that I_{f_1} and I_{f_2} are the intervals for the choice of missing conditions s_1 and s_2 while computing the Skin friction coefficient for nanofluid respectively. It is observed that for the computation of Nusselt number, there is a great flexibility in the choice of the missing initial condition.

Tables 4.2, 4.4 and 4.6 explain the effect of the material parameters ω , Δ_1 and Δ_2 , unsteady parameter A , magnetic parameter M , nanoparticle volume fraction Φ , velocity slip parameters Λ_1 and Λ_2 , thermal radiation parameter Nr , Eckert number Ec , Biot number Bi and mass transfer parameters S_1 and S_2 with fixed Prandtl number $Pr = 6.2$ and $q = 3$ on the fluid motion, temperature variation and the total volumetric entropy generation of Powell-Eyring nanofluid. The obtained results are relevant for the non-Newtonian Powell-Eyring nanofluids Cu-MeOH and SiC-MeOH.

Standard values of physical parameters have been set as $\omega = 0.1$, $A = 0.2$, $\Delta_1 = 0.2$, $\Delta_2 = 0.2$, $\Gamma = \pi/2$, $M = 0.1$, $\Phi = 0.2$, $\Lambda_1 = 0.1$, $\Lambda_2 = 0.2$, $Nr = 0.3$, $Ec = 0.2$,

$Bi = 0.2$, $S_1 = 0.1$, $S_2 = 0.3$, $Re = 5$, $Br = 5$, and $q = 3$ unless otherwise mentioned. At the end of this section, the phenomenon of entropy generation corresponding is explained through graphs for numerous dimensionless parameters.

4.5.1 Velocity Profile

Here, through the analysis of different graphs of the velocity profile, the dynamics of the fluid motion, will be observed.

- Figures 4.2-4.3 represent the impact of ω on the velocity profile of the Powell-Eyring nanofluid. For $\omega = 0.0, 0.1, 0.2, 0.21$, computations are carried out with nanoparticles' volume fraction $\Phi = 0.2$. The velocity profile in Figures 4.2 and 4.3 increases with the increasing values of ω and hence augments the thickness of the momentum boundary layer. The SiC–MeOH nanofluid's boundary layer thickness is comparatively greater than the Cu–MeOH nanofluid's, as seen by these two pictures.
- The influence of nanofluid motion with increasing material fluid parameter Δ_1 is shown in Figures 4.4-4.5. In contrast to the influence of ω , Δ_1 affects fluid velocity and the extent of boundary layer thickening. The velocity profiles depicted in Figures 4.4-4.5 exhibit a reduction in thickness due to increasing values of Δ_1 .
- Figures 4.6-4.7 depict the impact of the velocity profile due to variation in the non-Newtonian fluid Δ_2 . For the increasing values of Δ_2 , Figures 4.6-4.7 shows an increasing trend in the velocity profile.
- The effects of the inclination angle Γ of the magnetic field on the velocity profile is illustrated in Figures 4.8-4.9. It is found that higher values of the inclination Γ tend to decrease the velocity profile. These two figures demonstrate that the SiC–MeOH nanofluid's boundary layer thickness is comparatively higher than the Cu–MeOH nanofluid's.
- Figures 4.10-4.11 show the effect of the magnetic parameter M on the velocity profile. The velocity of the nanofluids decreases as the magnitude of the

magnetic parameter M increases gradually. The applied inclined magnetic field produces a resistive force called the Lorentz force which offers resistance to the flow. These two figures demonstrate that the boundary layer thickness of SiC–MeOH nanofluid is greater higher than that of the Cu–MeOH nanofluid.

- Figures 4.12-4.13 display the nature of fluid motion within boundary layer for Powell-Eyring nanofluid due to variations in the nanoparticle volume concentration parameter Φ . The parameter Φ corresponds to the volume of solid particles in the basefluid. As per expectations, an increase in Φ reduces the fluid velocity as observed from Figures 4.12-4.13. These two figures reflect that the boundary layer thickness of SiC–MeOH nanofluid is relatively greater than that of the Cu–MeOH nanofluid.
- Figures 4.14-4.15 illustrated that the positive values of slip parameter Λ_1 reduces fluid movement. In Figures 4.14-4.15 the decrease in velocity is consistent with the fact that slip velocity retards the motion of the boundary surface. In other words, velocity slip act opposite to stretching pull of the surface and resists its transmission to the fluid. As a result, momentum boundary layer decreases with rise in parameter Λ_1 .
- Figures 4.16-4.17 depict the impact of the velocity profile due to variation in the non-Newtonian fluid velocity slip parameter Λ_2 . For the increasing values of velocity slip parameter Λ_2 , Figures 4.16-4.17 shows an increasing trend in the velocity profile.

TABLE 4.1: Results of $\frac{d^2f}{d\chi^2}$ and $\frac{d^2g}{d\chi^2}$ at $\chi = 0$ for $Pr = 6.2$ and $q = 3$.

(Cu-MeOH)												
ω	A	Δ_1	Δ_2	Γ	M	Φ	Λ_1	Λ_2	S_1	S_2	I_{f_1}	I_{f_2}
0.1	0.2	0.2	0.2	$\pi/2$	0.1	0.2	0.1	0.2	0.1	0.3	[-1.42, -1.12]	[-0.93, -0.30]
0.0											[-1.58, -1.00]	[0.68, 2.00]
0.2											[-1.48, -1.00]	[-0.66, -0.13]
0.21											[-1.47, -1.00]	[-0.83, -0.84]
	0.0										[-1.46, -1.02]	[-0.50, 0.19]
	0.1										[-1.48, -1.03]	[-0.66, -0.00]
	0.3										[-1.47, -1.01]	[-0.91, -0.89]
		0.3									[-1.52, -1.00]	[-0.79, -0.18]
		0.5									[-1.53, -1.00]	[-0.80, -0.20]
		0.9									[-1.55, -1.00]	[-0.90, -0.18]
		4									[-1.44, -0.88]	[-0.60, -0.29]
		7									[-1.39, -0.99]	[-0.58, -0.44]
		9									[-1.35, -1.05]	[-0.66, -0.43]
			$\pi/4$								[-1.50, -1.00]	[-0.73, -0.99]
			$\pi/6$								[-1.49, -1.01]	[-0.76, -0.10]
			$\pi/8$								[-1.49, -0.89]	[-0.59, -0.01]
				0.0							[-1.48, -0.92]	[-0.57, 0.20]
				0.2							[-1.52, -0.98]	[-0.70, -0.14]
				0.4							[-1.50, -0.97]	[-0.84, -0.86]

TABLE 4.1: Results of $\frac{d^2f}{d\chi^2}$ and $\frac{d^2g}{d\chi^2}$ at $\chi = 0$ for $Pr = 6.2$ and $q = 3$.

(Cu-MeOH)

ω	A	Δ_1	Δ_2	Γ	M	Φ	Λ_1	Λ_2	S_1	S_2	I_{f_1}	I_{f_2}
0.1	0.2	0.2	0.2	$\pi/2$	0.1	0.2	0.1	0.2	0.1	0.3	[-1.42, -1.12]	[-0.93, -0.30]
						0.1					[-1.59, -1.00]	[-0.68, -0.08]
						0.15					[-1.58, -1.00]	[-0.74, -0.14]
						0.17					[-1.57, -0.98]	[-0.74, -0.14]
							0.0				[-2.00, -1.14]	[-1.00, -0.71]
							0.2				[-1.18, -1.12]	[-0.75, -0.40]
							0.11				[-1.48, -0.98]	[-0.69, -0.02]
								0.0			[-1.28, -1.00]	[-0.08, 0.79]
								0.1			[-1.51, -1.00]	[-0.34, 0.30]
								0.11			[-1.52, -1.00]	[-0.47, 0.11]
									0.2		[-1.62, -0.95]	[-0.65, 0.11]
									0.4		[-1.81, -0.99]	[-0.60, 0.11]
									0.5		[-1.91, -1.08]	[-0.54, 0.22]
										0.6	[-1.83, -1.05]	[-0.57, 0.12]
										0.8	[-2.00, -1.00]	[-0.29, 0.48]
										0.9	[-2.20, -1.02]	[-0.34, 0.49]

TABLE 4.2: Results of $\frac{d^2f}{d\chi^2}$ and $\frac{d^2g}{d\chi^2}$ at $\chi = 0$ for $Pr = 6.2$ and $q = 3$.

(Cu-MeOH)												
ω	A	Δ_1	Δ_2	Γ	M	Φ	Λ_1	Λ_2	S_1	S_2	$C_{f_x} Re_x^{\frac{1}{2}}$	$C_{f_y} Re_y^{\frac{1}{2}}$
0.1	0.2	0.2	0.2	$\pi/2$	0.1	0.2	0.1	0.2	0.1	0.3	2.5007	1.9868
0.0											2.4299	1.9207
0.2											2.5705	2.0519
0.21											2.5774	2.0583
	0.0										2.4300	1.9388
	0.1										2.4655	1.9629
	0.3										2.5357	2.0105
		0.3									2.4971	1.9867
		0.5									2.4899	1.9864
		0.9									2.4749	1.9857
			4								2.4946	1.8919
			7								2.4884	1.7972
			9								2.4830	1.7152
				$\pi/4$							2.4848	1.9760
				$\pi/6$							2.4768	1.9705
				$\pi/8$							2.4735	1.9682
					0.0						2.4687	1.9649
					0.2						2.5319	2.0081
					0.4						2.5921	2.0487

TABLE 4.2: Results of $\frac{d^2f}{d\chi^2}$ and $\frac{d^2g}{d\chi^2}$ at $\chi = 0$ for $Pr = 6.2$ and $q = 3$.

(Cu-MeOH)												
ω	A	Δ_1	Δ_2	Γ	M	Φ	Λ_1	Λ_2	S_1	S_2	$C_{f_x} Re_x^{\frac{1}{2}}$	$C_{f_y} Re_y^{\frac{1}{2}}$
0.1	0.2	0.2	0.2	$\pi/2$	0.1	0.2	0.1	0.2	0.1	0.3	2.5007	1.9868
						0.1					1.9346	1.6131
						0.15					2.2226	1.8079
						0.17					2.3347	1.8811
							0.0				3.5165	2.0214
							0.2				1.9660	1.9600
							0.11				2.4332	1.9843
								0.0			2.5817	3.5682
								0.1			2.5309	2.5309
								0.11			2.5273	2.4622
									0.2		2.6027	2.0546
									0.4		2.8110	2.1899
									0.5		2.9166	2.2570
										0.6	2.8110	2.1899
										0.8	3.0227	2.3234
										0.9	3.1290	2.3889

TABLE 4.3: Results of $\frac{d^2f}{d\chi^2}$ and $\frac{d^2g}{d\chi^2}$ at $\chi = 0$ for $Pr = 6.2$ and $q = 3$.

(SiC-MeOH)												
ω	A	Δ_1	Δ_2	Γ	M	Φ	Λ_1	Λ_2	S_1	S_2	I_{f_1}	I_{f_2}
0.1	0.2	0.2	0.2	$\pi/2$	0.1	0.2	0.1	0.2	0.1	0.3	[-0.94, -1.00]	[-0.65, -0.02]
0.0											[-0.99, -1.00]	[1.74, 1.76]
0.2											[-1.02, -1.11]	[-0.96, -1.00]
0.21											[-1.02, -1.11]	[-0.96, -1.00]
	0.0										[-1.01, -1.26]	[-0.94, -1.00]
	0.1										[-1.03, -1.19]	[-0.96, -1.00]
	0.3										[-0.97, -1.00]	[-0.88, -0.20]
		0.3									[-1.05, -1.10]	[-1.00, -1.00]
		0.5									[-1.05, -1.10]	[-1.00, -1.00]
		0.9									[-1.05, -1.11]	[-1.00, -1.00]
			4								[-0.97, -1.00]	[-0.65, -0.31]
			7								[-1.01, -0.96]	[-0.56, -0.31]
			9								[-1.09, -0.89]	[-0.45, -0.25]
				$\pi/4$							[-1.07, -1.16]	[-0.96, -1.00]
				$\pi/6$							[-1.05, -1.16]	[-0.95, -1.00]
				$\pi/8$							[-1.03, -1.18]	[-0.94, -1.00]
					0.0						[-1.02, -1.20]	[-0.93, -1.00]
					0.2						[-1.00, -1.01]	[-0.75, -1.00]
					0.4						[-1.10, -1.02]	[-0.96, -0.83]

TABLE 4.3: Results of $\frac{d^2f}{d\chi^2}$ and $\frac{d^2g}{d\chi^2}$ at $\chi = 0$ for $Pr = 6.2$ and $q = 3$.

(SiC-MeOH)

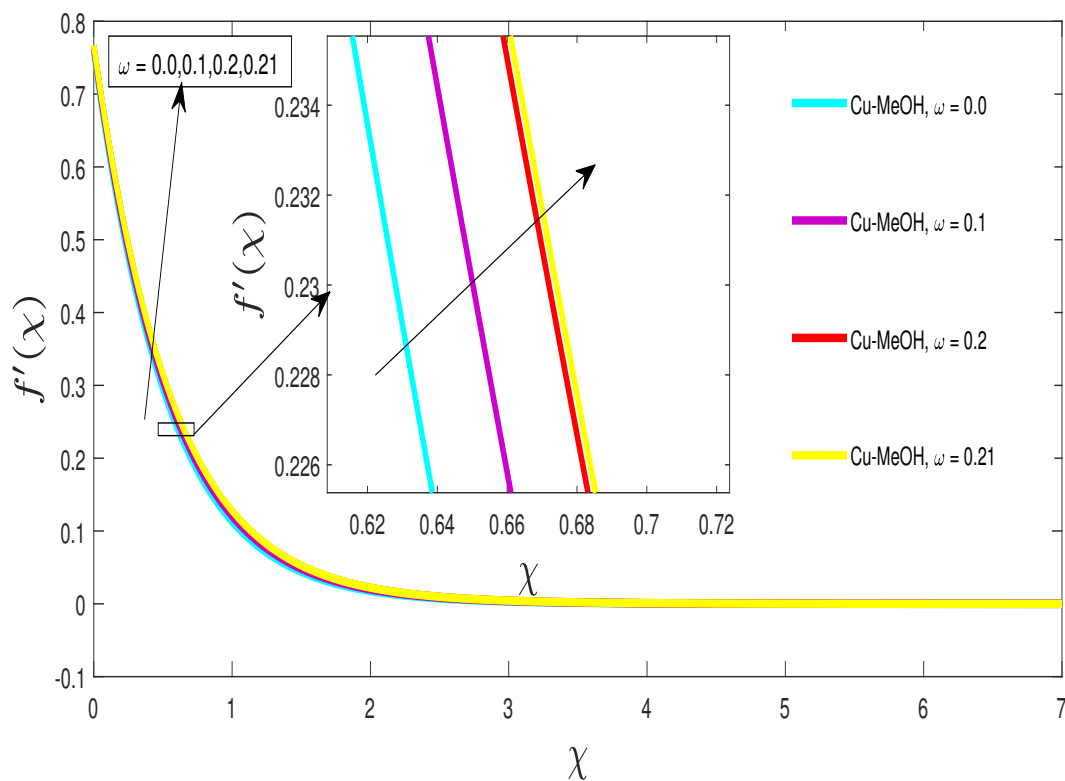
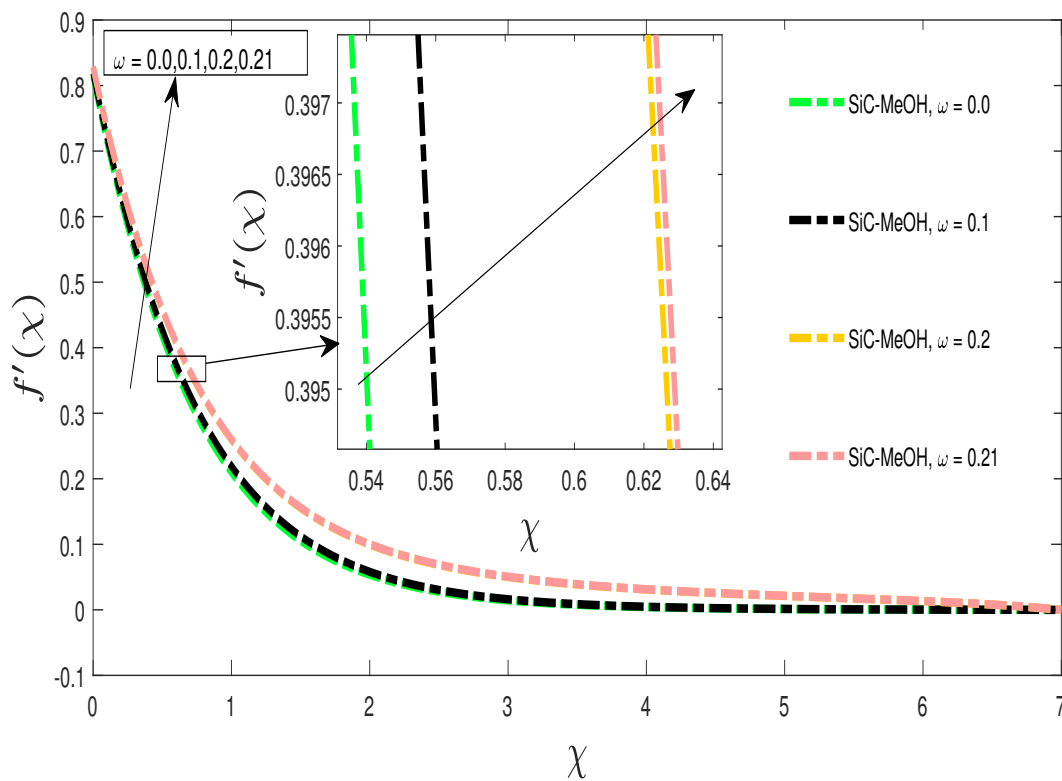
ω	A	Δ_1	Δ_2	Γ	M	Φ	Λ_1	Λ_2	S_1	S_2	I_{f_1}	I_{f_2}
0.1	0.2	0.2	0.2	$\pi/2$	0.1	0.2	0.1	0.2	0.1	0.3	[-0.94, -1.00]	[-0.65, -0.02]
						0.1					[-1.20, -1.03]	[-0.63, 0.00]
						0.15					[-1.08, -1.00]	[-0.61, 0.07]
						0.17					[-1.03, -1.10]	[-0.65, 0.02]
							0.0				[-1.24, -1.13]	[-0.81, 0.08]
							0.2				[-0.76, -1.09]	[-0.62, -0.12]
							0.11				[-1.03, -1.11]	[-0.97, -1.00]
								0.0			[-1.31, -1.09]	[-0.10, -1.00]
								0.1			[-1.16, -1.02]	[-0.41, 0.29]
								0.11			[-1.15, -1.09]	[-0.44, 0.29]
									0.2		[-1.01, -1.00]	[-0.60, 0.12]
									0.4		[-1.24, -1.00]	[-0.39, 0.32]
									0.5		[-1.25, -1.00]	[-0.23, 0.49]
										0.6	[-1.24, -1.01]	[-0.54, 0.20]
										0.8	[-1.31, -1.05]	[-0.42, 0.38]
										0.9	[-1.38, -1.09]	[-0.29, 0.58]

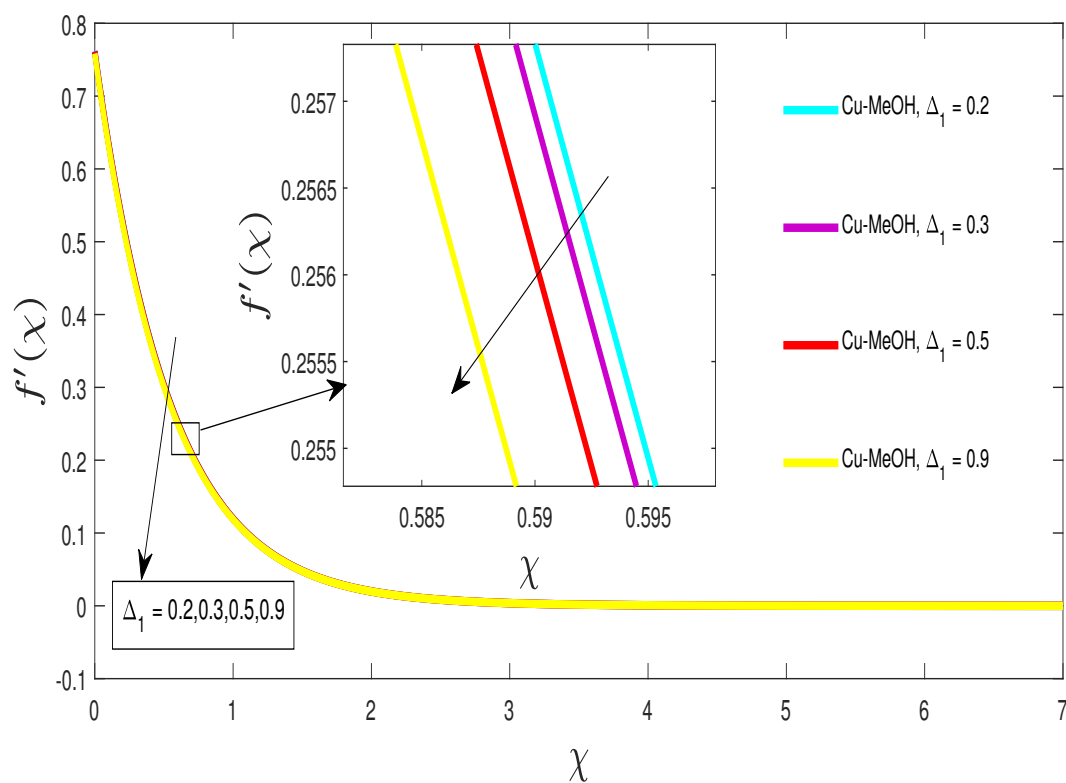
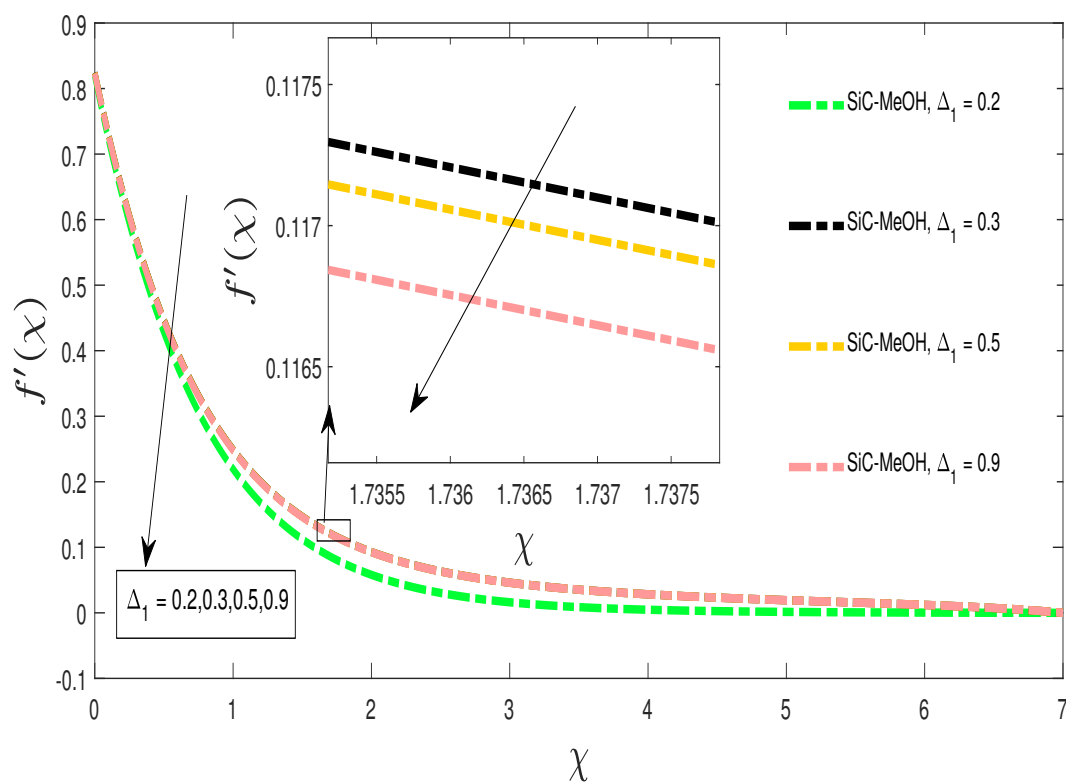
TABLE 4.4: Results of $\frac{d^2f}{d\chi^2}$ and $\frac{d^2g}{d\chi^2}$ at $\chi = 0$ for $Pr = 6.2$ and $q = 3$.

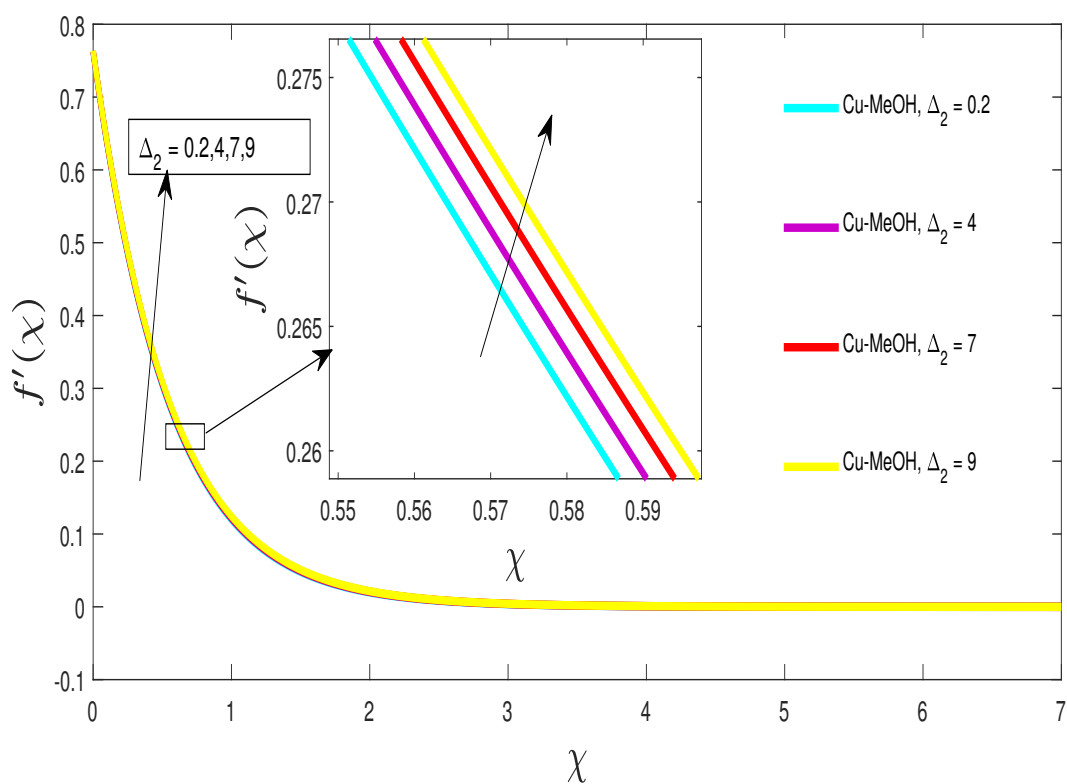
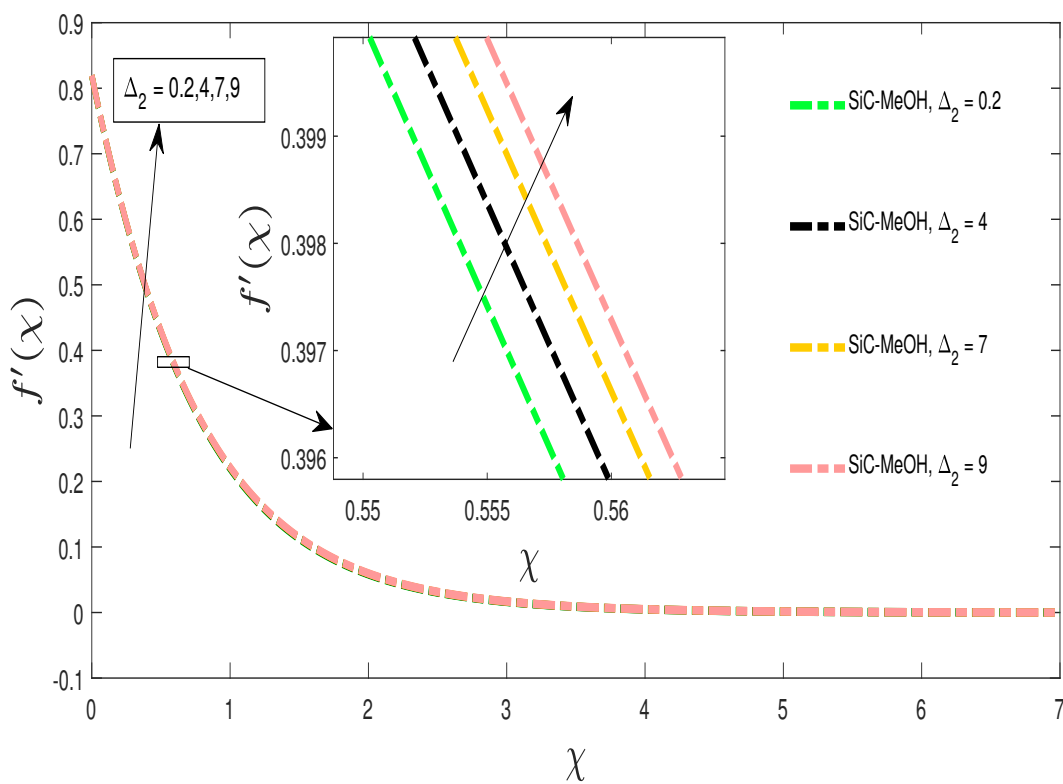
(SiC-MeOH)												
ω	A	Δ_1	Δ_2	Γ	M	Φ	Λ_1	Λ_2	S_1	S_2	$C_{f_x} Re_x^{\frac{1}{2}}$	$C_{f_y} Re_y^{\frac{1}{2}}$
0.1	0.2	0.2	0.2	$\pi/2$	0.1	0.2	0.1	0.2	0.1	0.3	1.9078	1.5887
0.0											1.8525	1.5364
0.2											1.9006	1.9550
0.21											1.9055	1.9624
	0.0										1.7665	1.9200
	0.1										1.8104	1.8943
	0.3										1.9371	1.6102
		0.3									1.8494	1.8810
		0.5									1.8468	1.8807
		0.9									1.8415	1.8801
			4								1.9049	1.5462
			7								1.9023	1.5078
			9								1.9003	1.4787
				$\pi/4$							1.8229	1.8608
				$\pi/6$							1.8088	1.8502
				$\pi/8$							1.8029	1.8458
					0.0						1.7945	1.8394
					0.2						1.9561	1.6242
					0.4						2.0472	1.6903

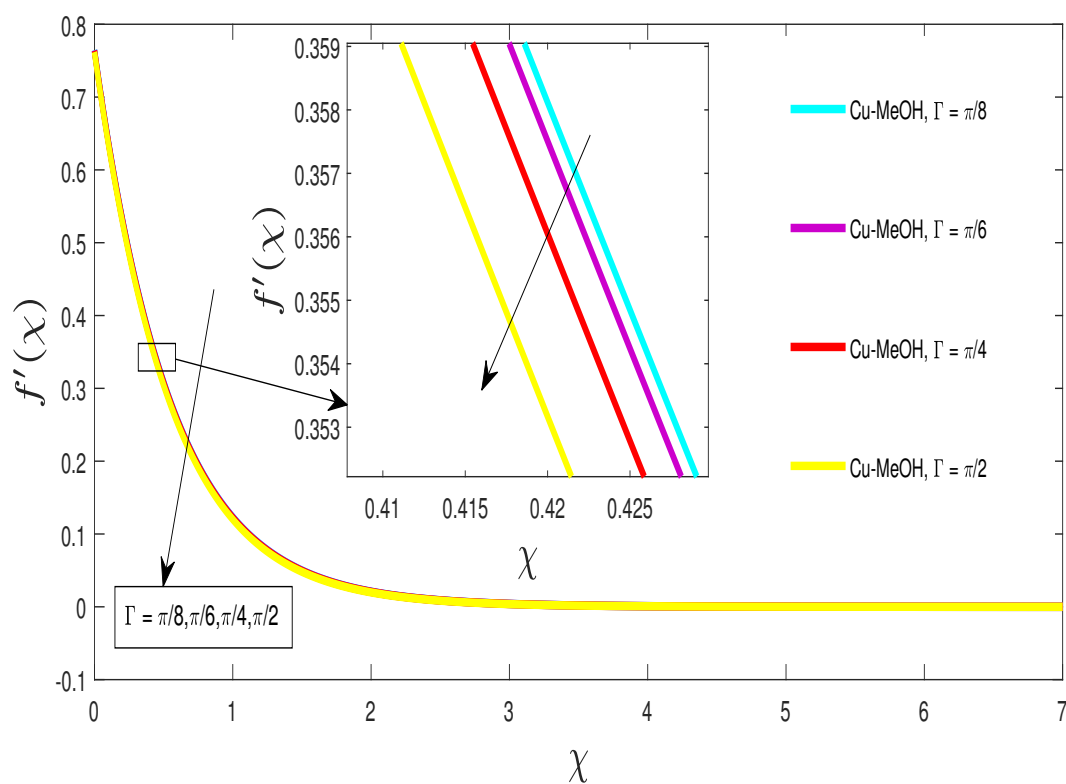
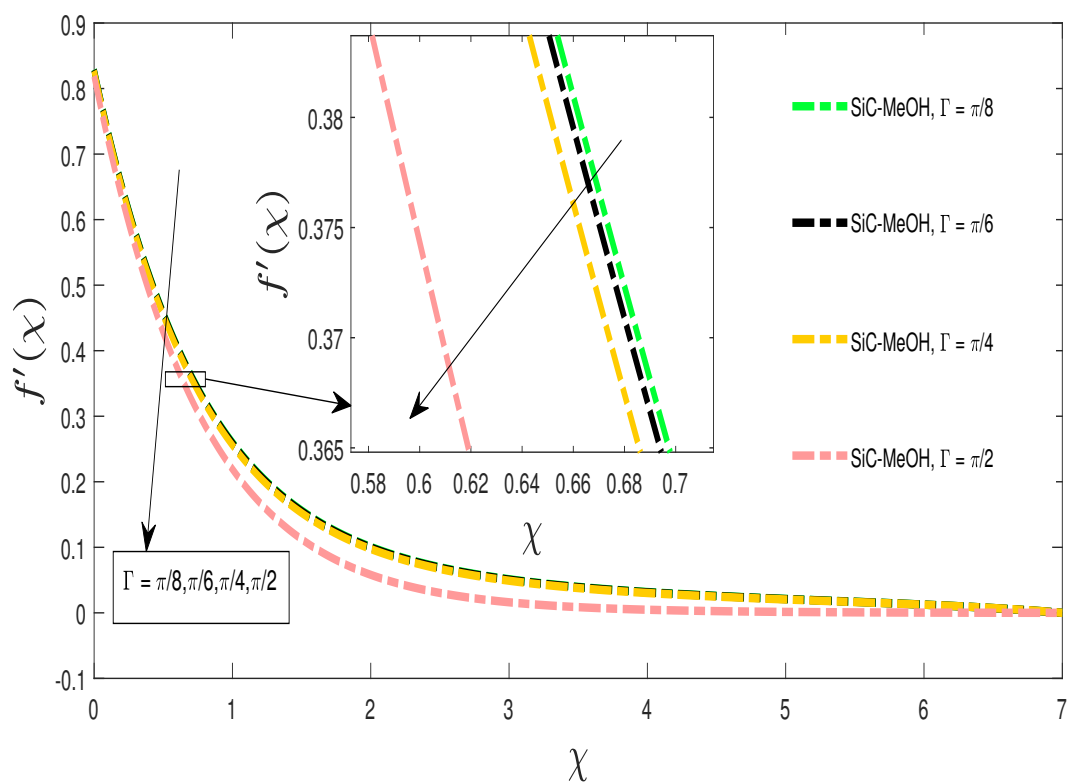
TABLE 4.4: Results of $\frac{d^2f}{d\chi^2}$ and $\frac{d^2g}{d\chi^2}$ at $\chi = 0$ for $Pr = 6.2$ and $q = 3$.

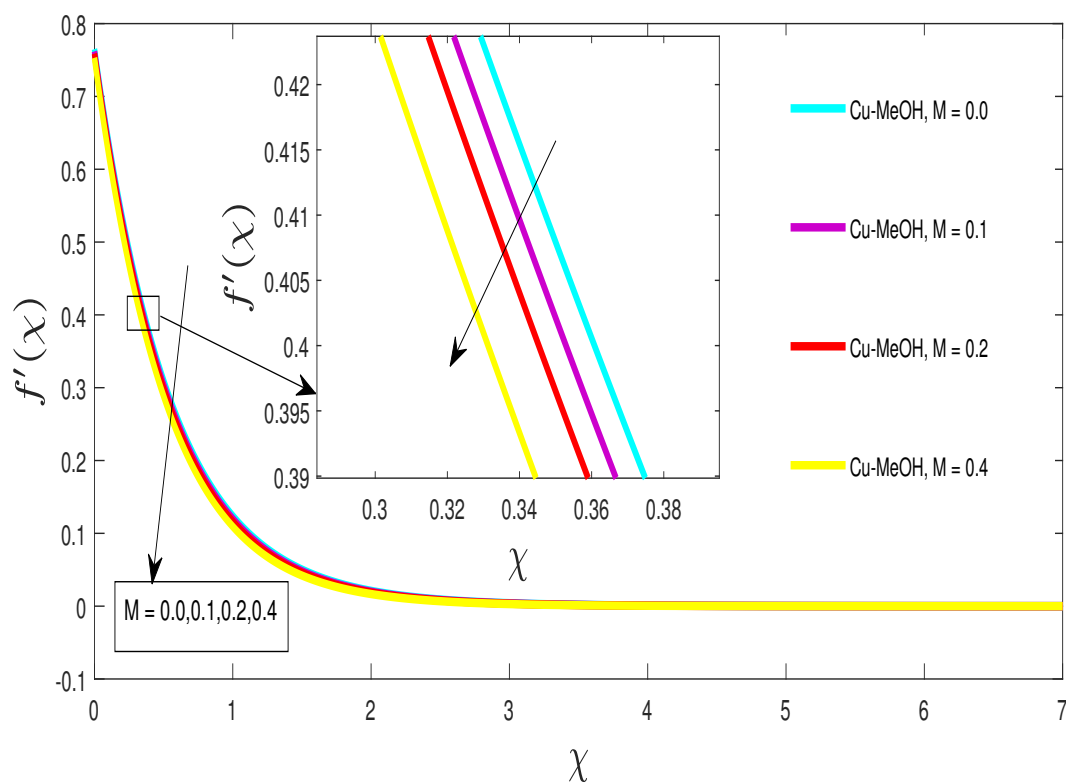
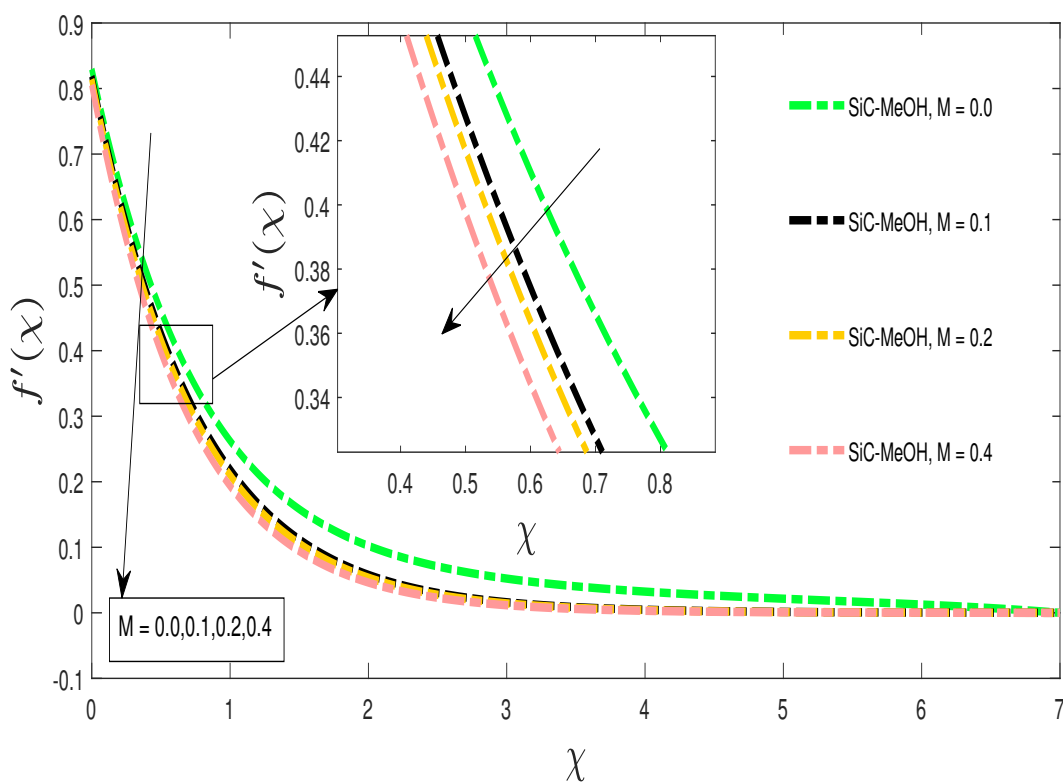
(SiC-MeOH)												
ω	A	Δ_1	Δ_2	Γ	M	Φ	Λ_1	Λ_2	S_1	S_2	$C_{f_x} Re_x^{\frac{1}{2}}$	$C_{f_y} Re_y^{\frac{1}{2}}$
0.1	0.2	0.2	0.2	$\pi/2$	0.1	0.2	0.1	0.2	0.1	0.3	1.9078	1.5887
						0.1					1.5879	1.3625
						0.15					1.7439	1.4745
						0.17					1.8084	1.5199
							0.0				2.4570	1.6115
							0.2				1.5733	1.5733
							0.11				1.8122	1.8774
								0.0			1.9597	2.4882
								0.1			1.9286	1.9286
								0.11			1.9262	1.8875
									0.2		1.9673	1.6317
									0.4		2.0892	1.7187
									0.5		2.1514	1.7625
										0.6	2.0892	1.7187
										0.8	2.2144	1.8064
										0.9	2.2780	1.8504

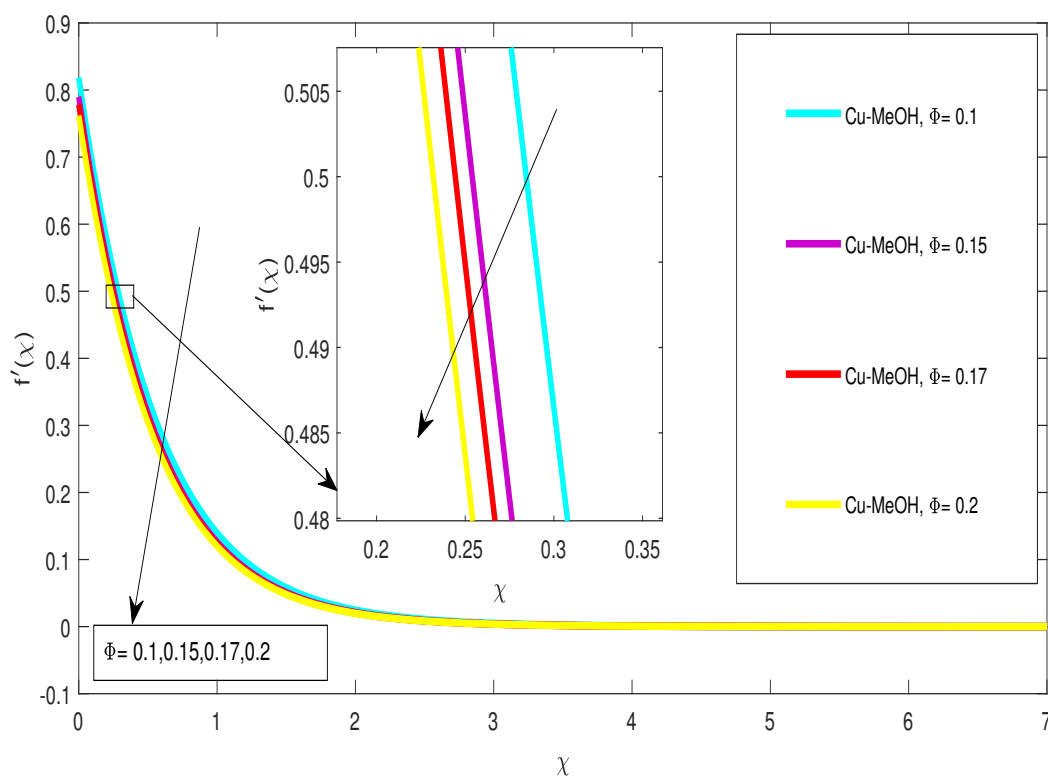
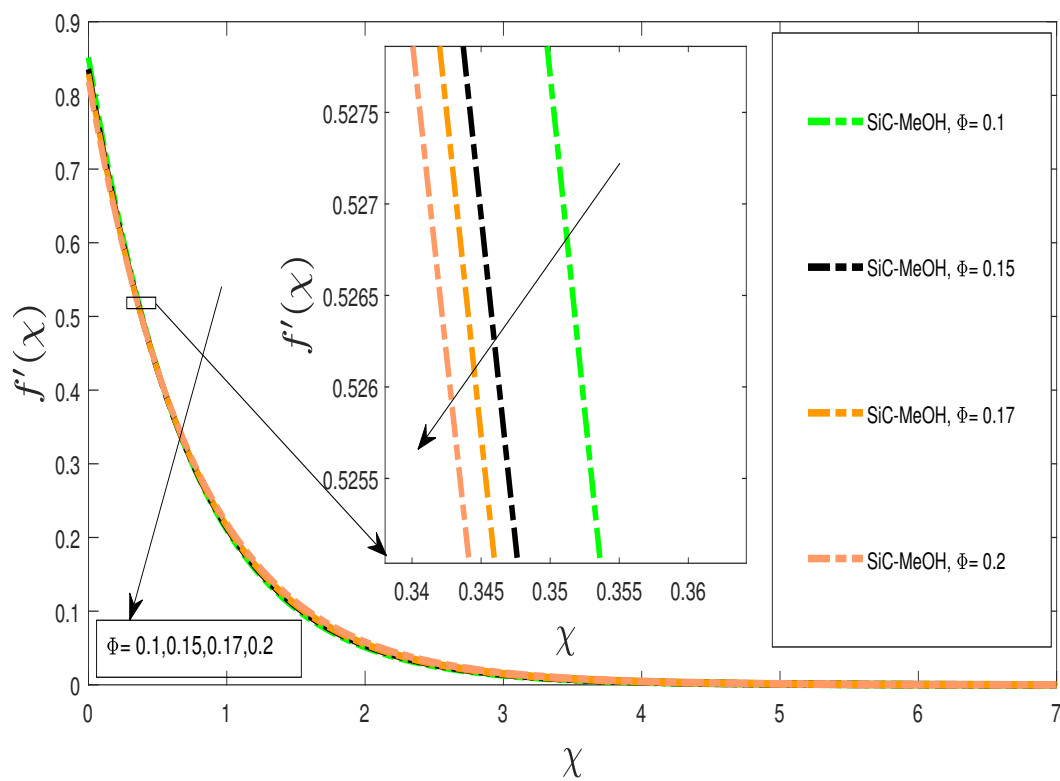
FIGURE 4.2: Velocity profile against ω FIGURE 4.3: Velocity profile against ω

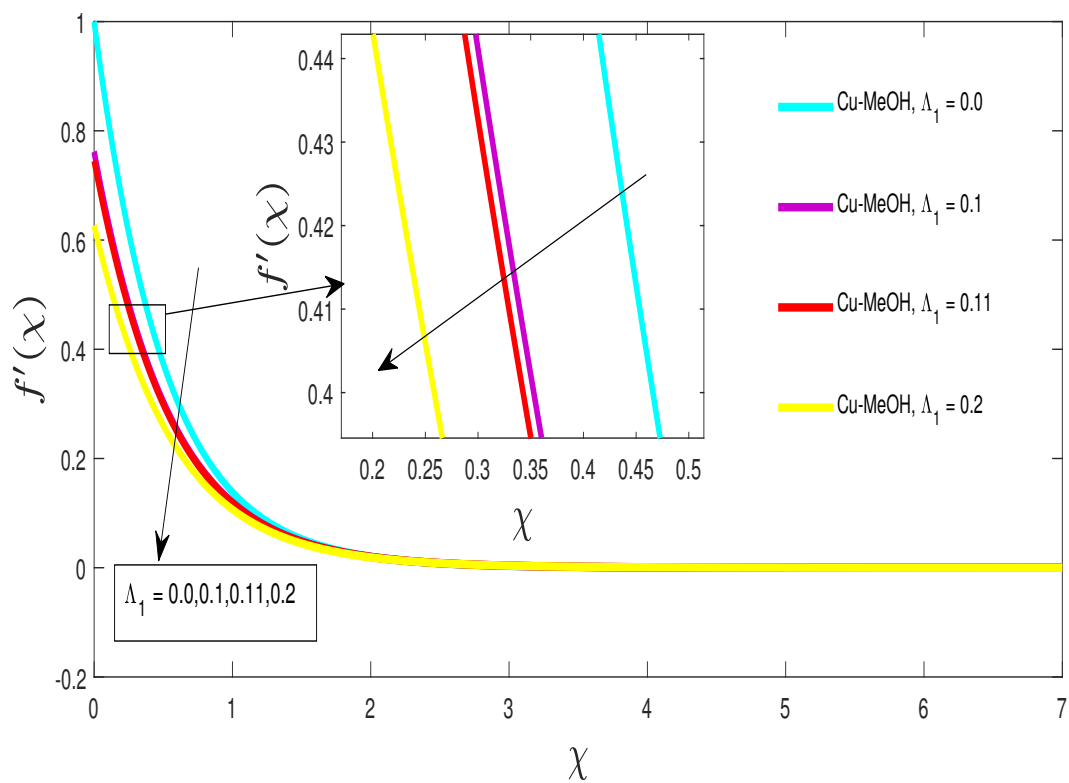
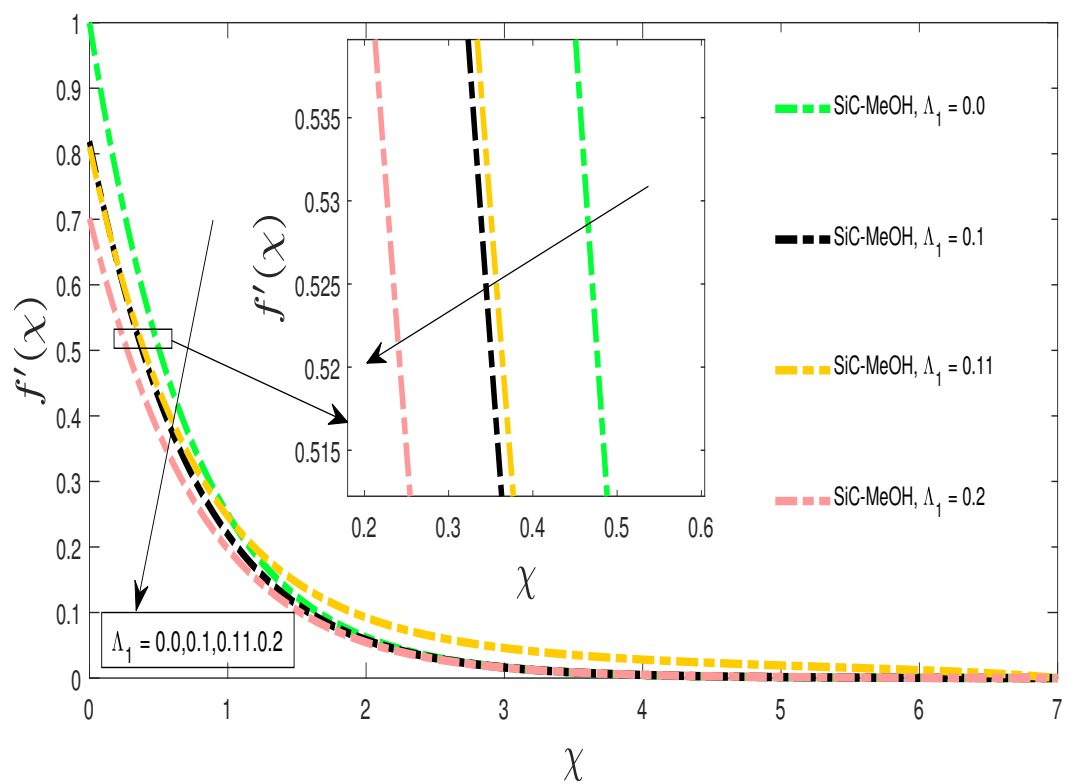
FIGURE 4.4: Velocity profile against Δ_1 FIGURE 4.5: Velocity profile against Δ_1

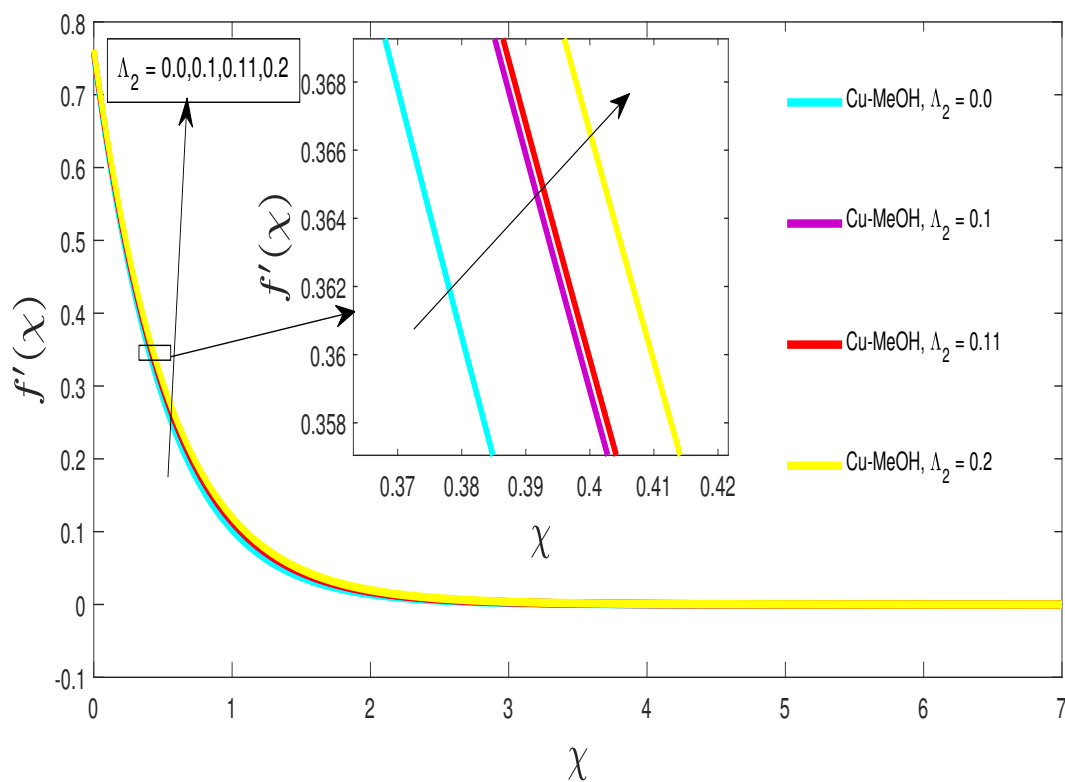
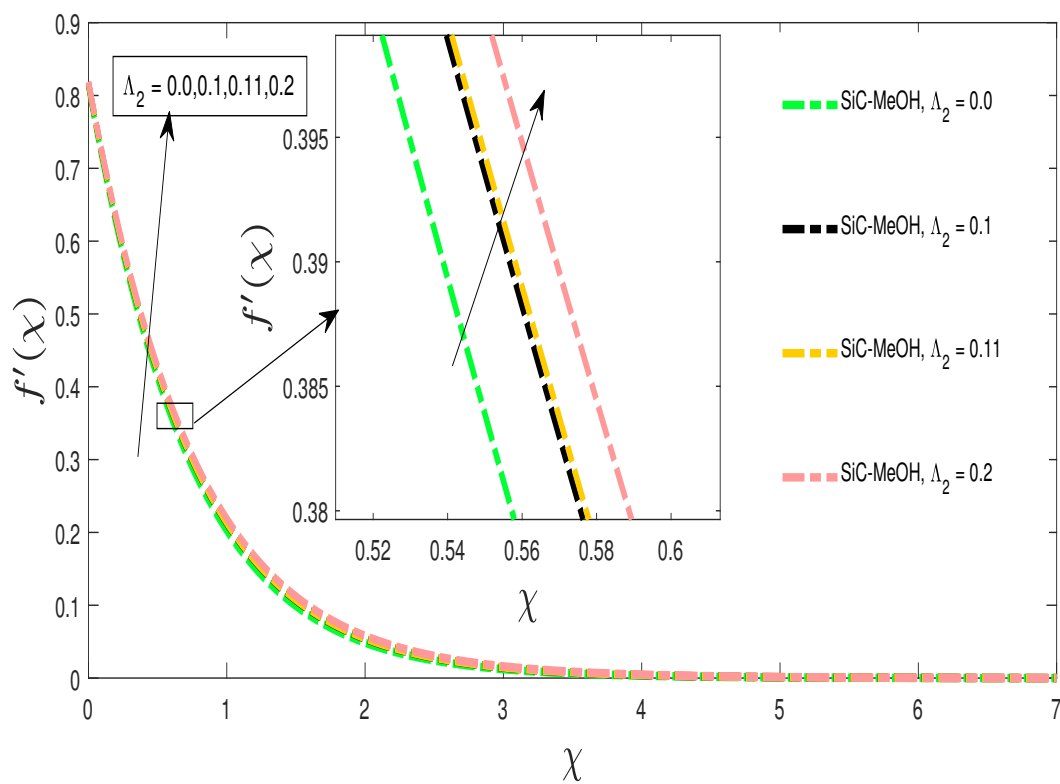
FIGURE 4.6: Velocity profile against Δ_2 FIGURE 4.7: Velocity profile against Δ_2

FIGURE 4.8: Velocity profile against Γ FIGURE 4.9: Velocity profile against Γ

FIGURE 4.10: Velocity profile against M FIGURE 4.11: Velocity profile against M

FIGURE 4.12: Velocity profile against Φ FIGURE 4.13: Velocity profile against Φ

FIGURE 4.14: Velocity profile against Λ_1 FIGURE 4.15: Velocity profile against Λ_1

FIGURE 4.16: Velocity profile against Λ_2 FIGURE 4.17: Velocity profile against Λ_2

4.5.2 Temperature Profile

In this subsection, the temperature distribution will be discussed through the graphs for different values of certain parameters of interest.

- The influence of the material-fluid parameter ω on the temperature profile of the non-Newtonian Powell-Eyring Cu-MeOH and SiC-MeOH is shown in Fig. 4.18-4.19. Calculations were performed with $\omega = 0.0, 0.1, 0.2, 0.21$, at a uniform nanoparticle concentration of 0.2. From the Figures 4.18-4.19, it can be seen that the temperature of the nanofluids decreases as the value of the parameter ω increases. This decreasing trend indicates a decrease in the thickness of the thermal boundary layer and an improved heat transfer rate. The reason behind this behaviour of the temperature profile is due to the reduced elastic stress parameter. Heat transfer rate (Nusselt number) increases for both Cu and SiC-MeOH based nanofluids Table 4.6.
- Figures 4.20-4.21 depicted the impact of unsteady parameter A on temperature profiles of Powell-Eyring nanofluid. The temperature in the boundary layer decreases as the value of parameter A is increased. This due to the fact that unsteadiness parameter A is inversely proportional to stretching rate, so increasing A reduces the stretching of the surface. The effect of increasing the parameter A value is to reduce the thickness of the thermal boundary layer.
- It can be seen in the Figures 4.22-4.25 that the temperature of the nanofluid increases with the values of the fluid parameters Δ_1 and Δ_2 ascending. This upward trend shows that the thickness of the thermal boundary layer increases and the heat transfer rate decreases.
- For increasing values of Φ , Figures 4.26-4.27 show an increased temperature profile $\theta(\chi)$ due to higher thermal conductivity of solid particles, which increases the overall thermal conductivity of nanofluids. These two figures reflect that the boundary layer thickness of SiC-MeOH nanofluid is relatively larger than that of the Cu-MeOH nanofluid.

- The Figures 4.28-4.29 represent the temperature profile of Λ_1 . Figure 4.28-4.29 shows that profiles gradually decrease near the surface and show the opposite effect, then reaching zero asymptote for sufficiently large boundary conditions.
- Figure 4.30-4.31 shows the temperature distribution in the boundary layer for parameter Λ_2 . The velocity slip is inversely proportional to the temperature distribution and increasing the parameter Λ_2 will increase the thickness of the thermal boundary layer and decrease the Nusselt number. Table 4.6 shows that a positive increase in velocity slip leads to a decrease in velocity gradient and heat transfer rate for Cu-MeOH and SiC-MeOH nanofluids. This expected behavior is due to the fact that the boundary slip reduces friction at the solid-fluid interface and thus reduces the rate of heat transfer.
- Figures 4.32-4.33 demonstrate that the temperature profile and the thickness of the thermal boundary layer are lower for the larger unsteady parameter ξ . To increase the values of ξ , the temperature configuration $\theta(\chi)$ will decrease. These two figures reflect that the boundary layer thickness of SiC-MeOH nanofluid is relatively larger than that of the Cu-MeOH nanofluid.
- Figures 4.34-4.35 illustrate the effect of heat generation Q on $\theta(\chi)$. It is observed that increasing the values of Q , more heat is generated, so $\theta(\chi)$ and the thickness of the boundary layer increase. These two figures reflect that the boundary layer thickness of the Cu-MeOH nanofluid is relatively larger than that of the SiC-MeOH nanofluid.
- Figures 4.36-4.37 illustrate the influence of different shapes of nanoparticles (sphere, hexahedron, tetrahedron, column, and lamina) on the heat transfer characteristics of the boundary layer flow in Cu-MeOH and SiC-MeOH nanofluids at nanoparticle concentration $\Phi = 0.2$. The graphical view shows that the dimensionless temperature of the nanofluid increases as the shape factor q increases. The geometrical shapes for different values of q have been mentioned in Table 4.5. The dimensionless temperature is lowest for the spherical nanoparticles, followed by hexahedron, tetrahedron, column and lamina. Spherical shape particles tend to draw more heat from the boundary layer due to their larger surface area,

while this effect is less pronounced for particles of other shapes. Therefore, the temperature drop in the boundary layer is more visible for spherical particles.

TABLE 4.5: Empirical shape factors for different particle shapes

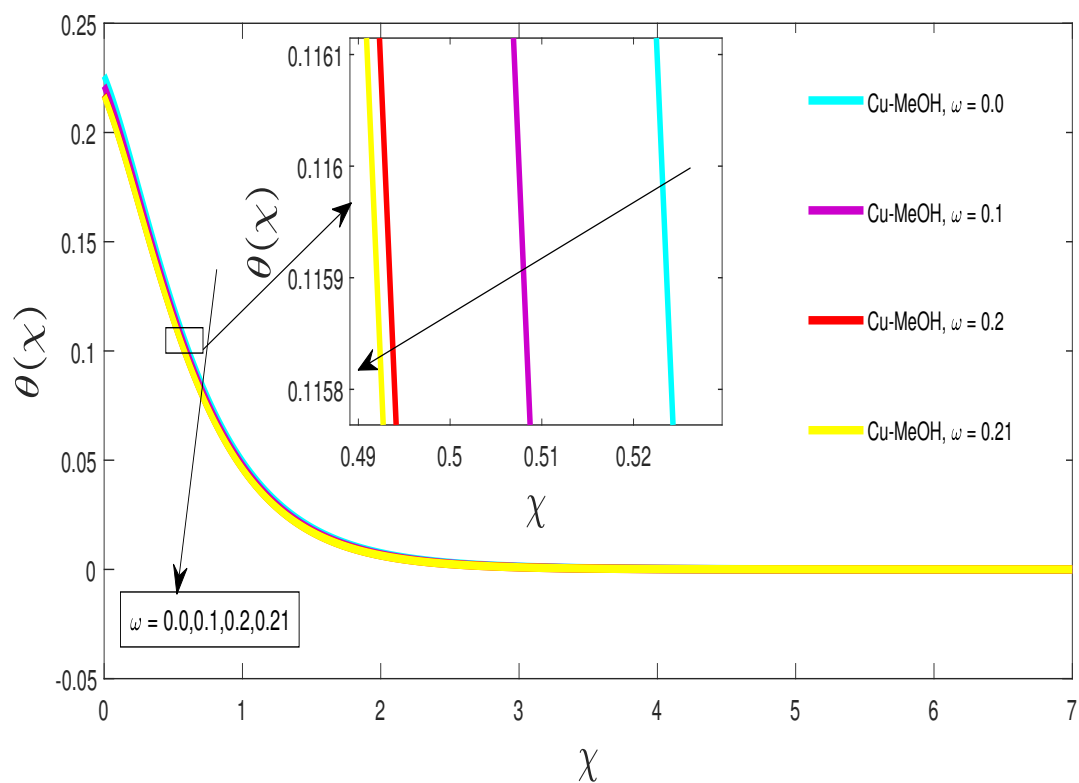
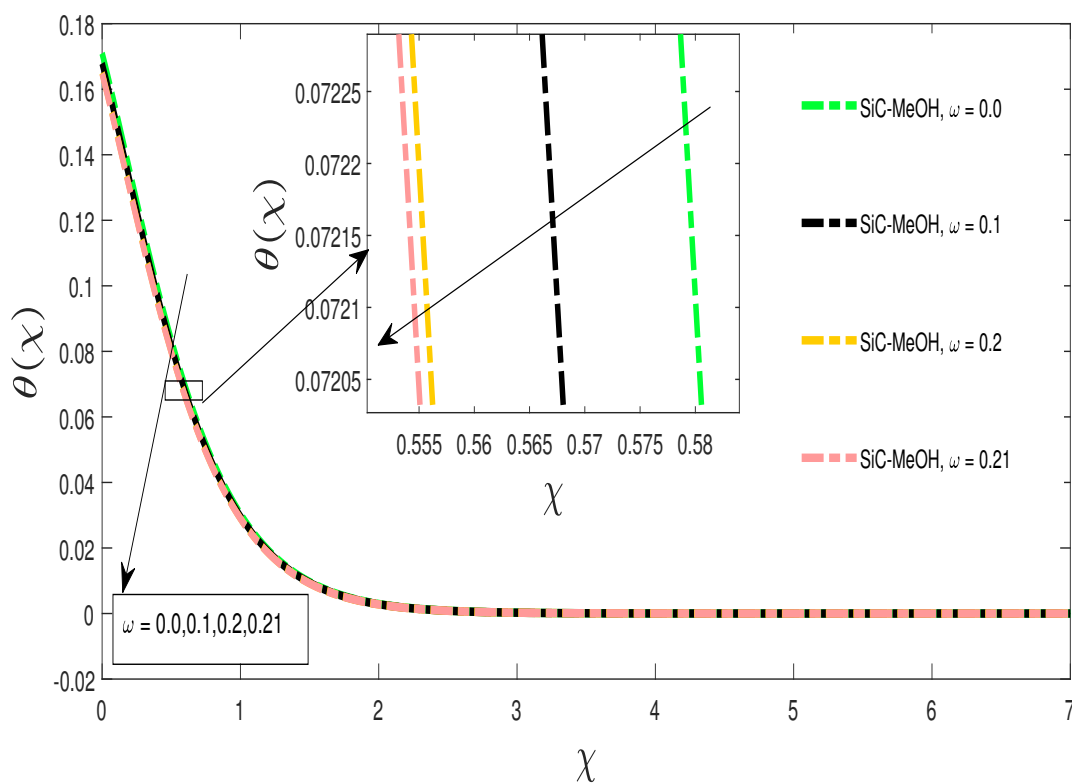
Nanoparticles type	Shape Factor
Sphere	3.0
Hexahedron	3.7221
Tetrahedron	4.0613
Column	6.3698
Lamina	16.1576

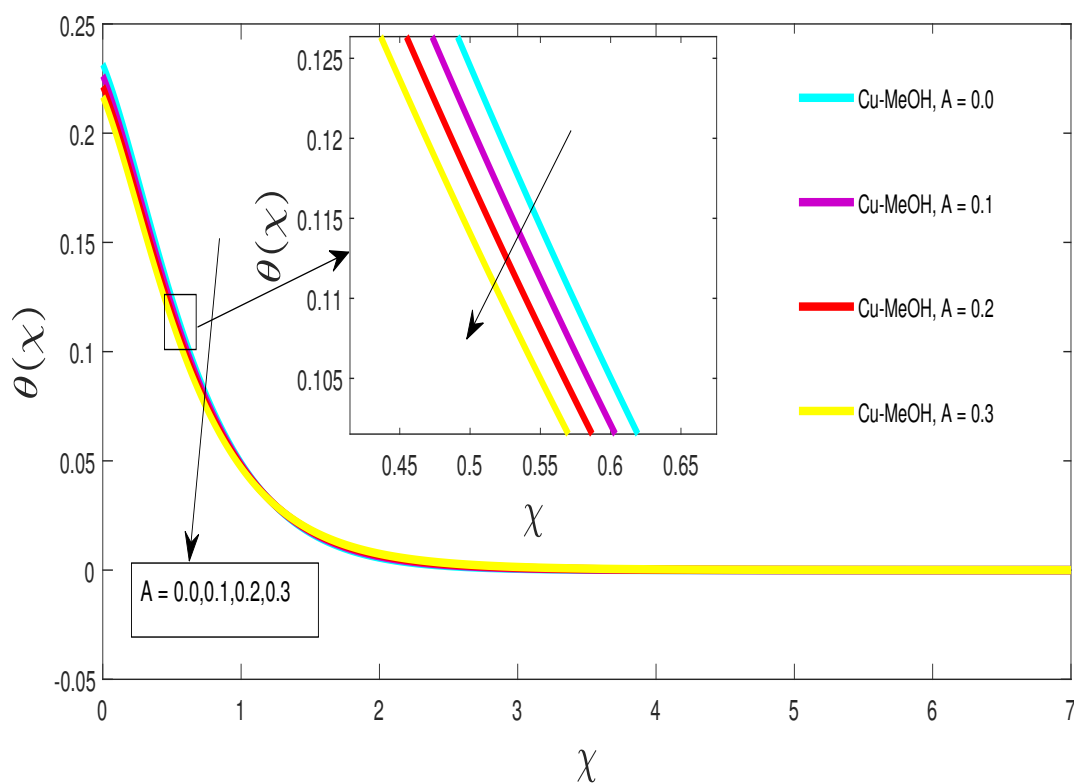
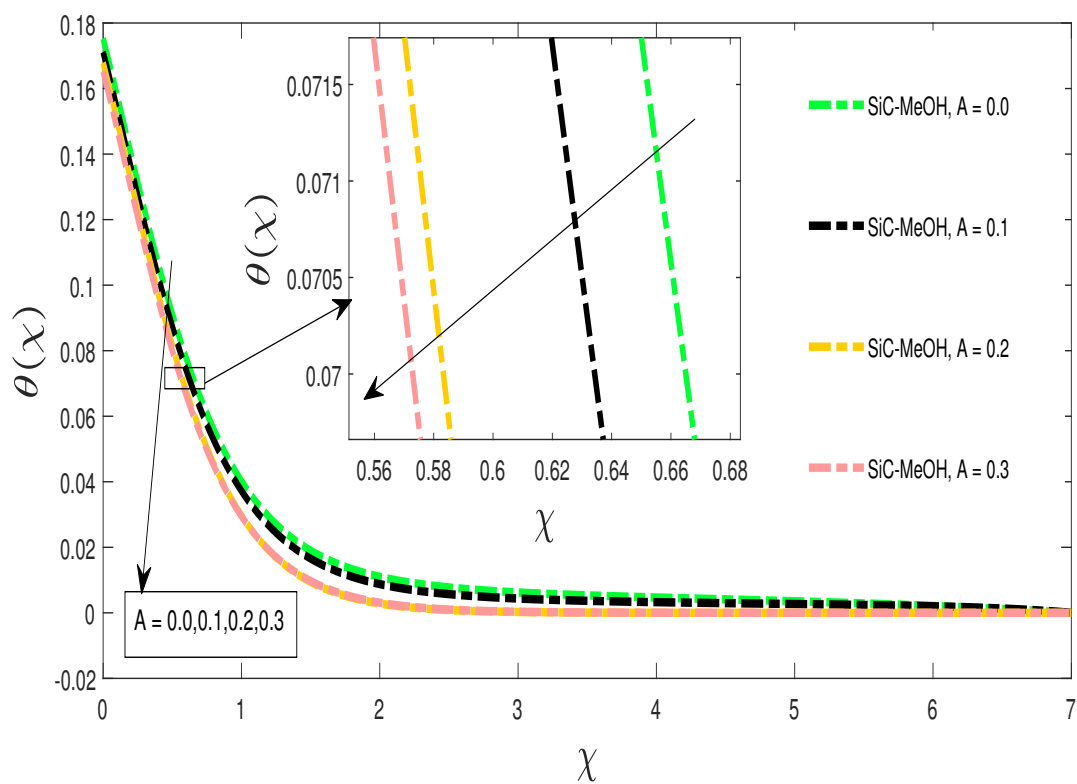
TABLE 4.6: Results of $\theta(0)$ for $Pr = 6.2$, $q = 3$

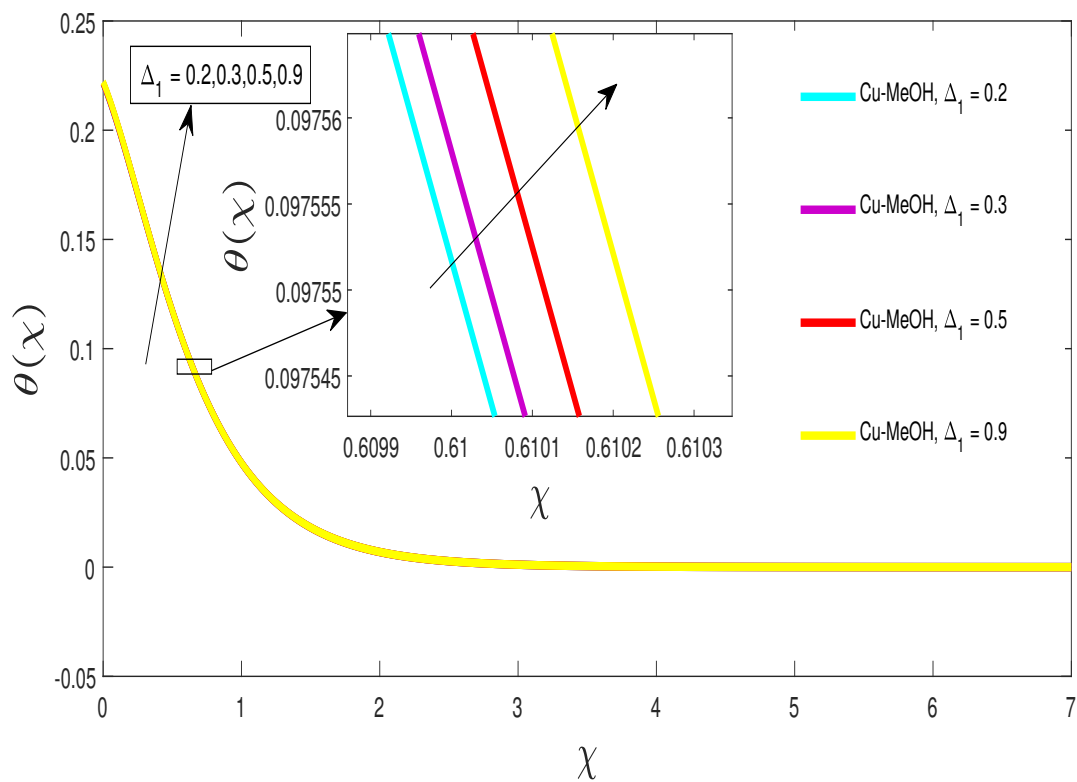
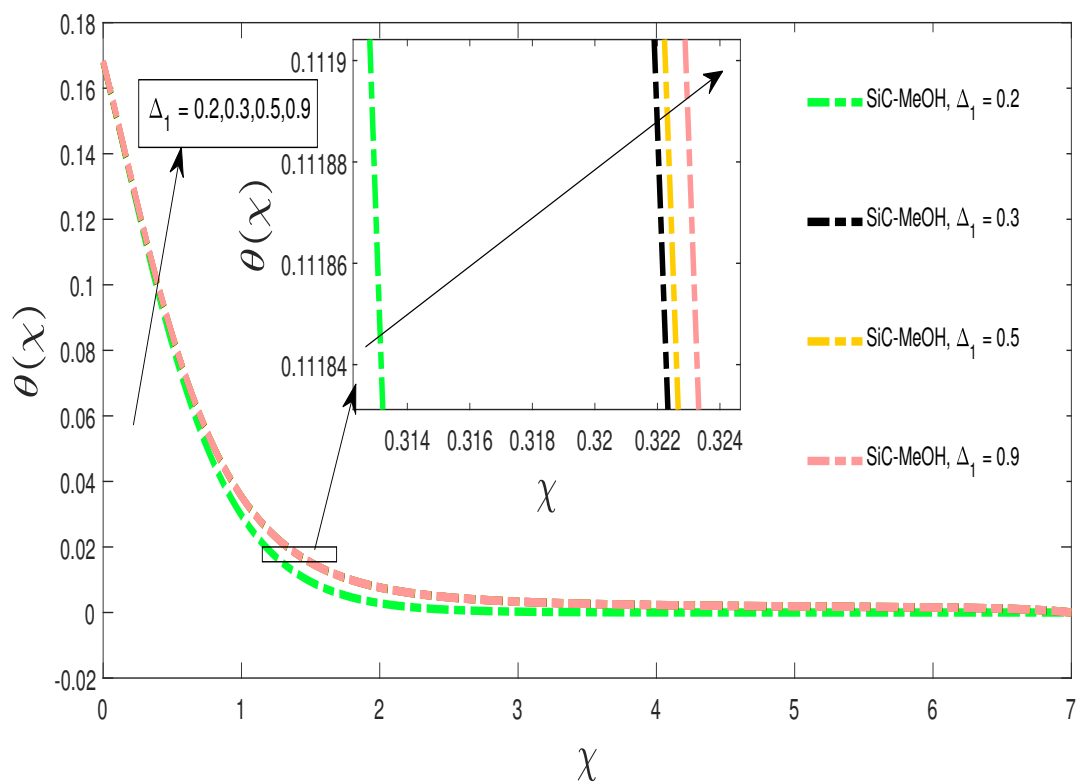
ω	A	$\Delta_1 \Delta_2 \Gamma$	$M \Phi$	Λ_1	Λ_2	S_1	S_2	$NrBi$	$Ec\xi$	Q	Cu-MeOH	SiC-MeOH
0.1	0.20	20.2	$\pi/20$	10.2	0.1	0.20	10.30	30.20	20.0	10.1	0.3539	0.3783
0.0											0.3519	0.3769
0.2											0.3559	0.3796
0.21											0.3561	0.3798
	0.0										0.3493	0.3749
	0.1										0.3517	0.3768
	0.3										0.3561	0.3795
		0.3									0.3539	0.3782
		0.5									0.3538	0.3782
		0.9									0.3536	0.3781
		4									0.3538	0.3782
		7									0.3536	0.3781
		9									0.3534	0.3781
		$\pi/4$									0.3553	0.3805
		$\pi/6$									0.3561	0.3817
		$\pi/8$									0.3563	0.3822
		0.0									0.3568	0.3828
		0.2									0.3512	0.3747
		0.4									0.3459	0.3681
		0.1									0.2794	0.2909
		0.15									0.3143	0.3320
		0.17									0.3296	0.3499
		0.0									0.3166	0.3622
		0.2									0.3702	0.3867
		0.11									0.3561	0.3792

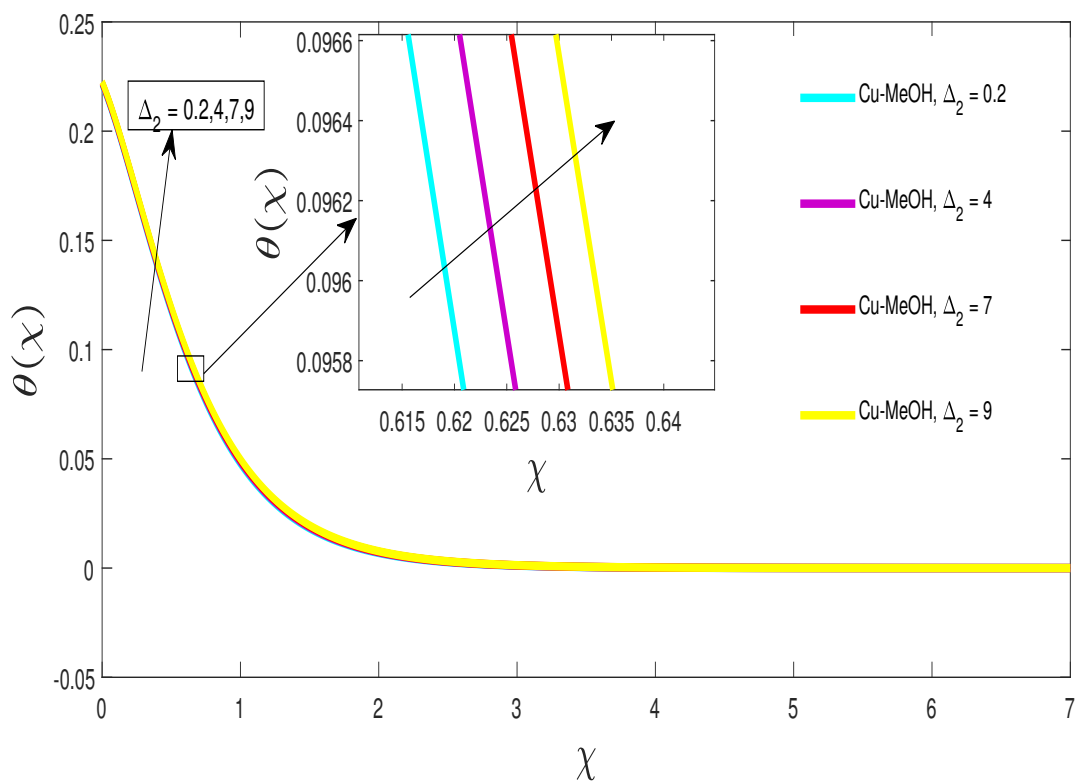
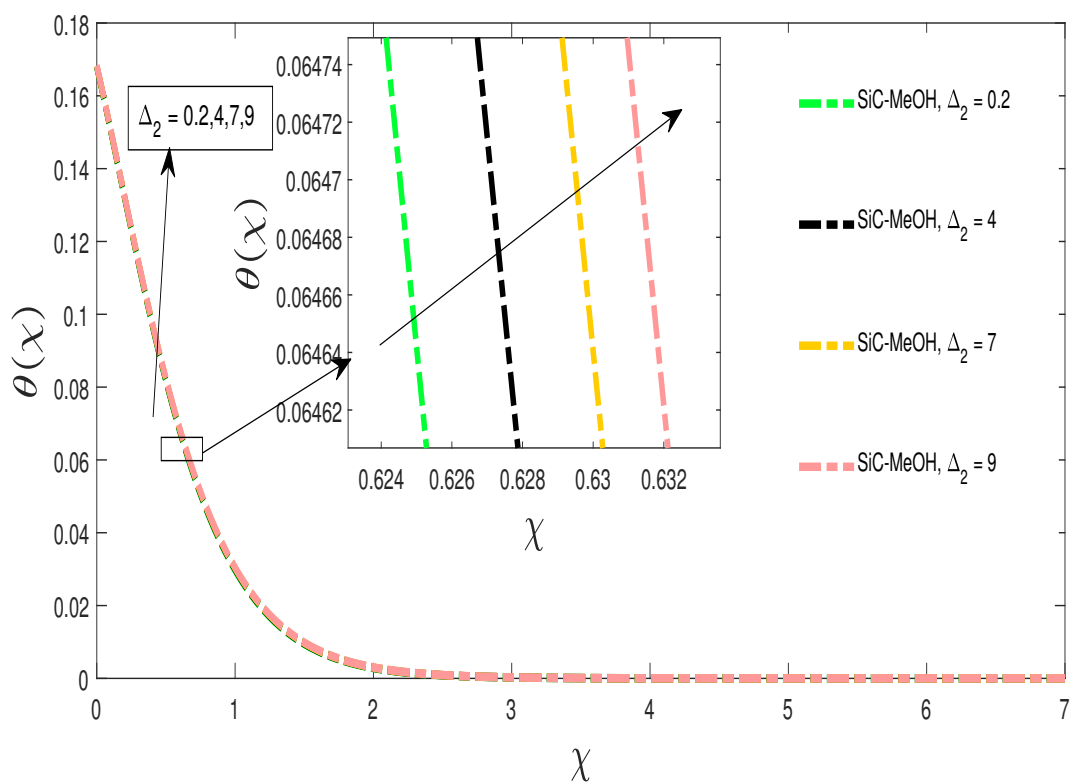
TABLE 4.6: Results of $\theta(0)$ for $Pr = 6.2$, $q = 3$

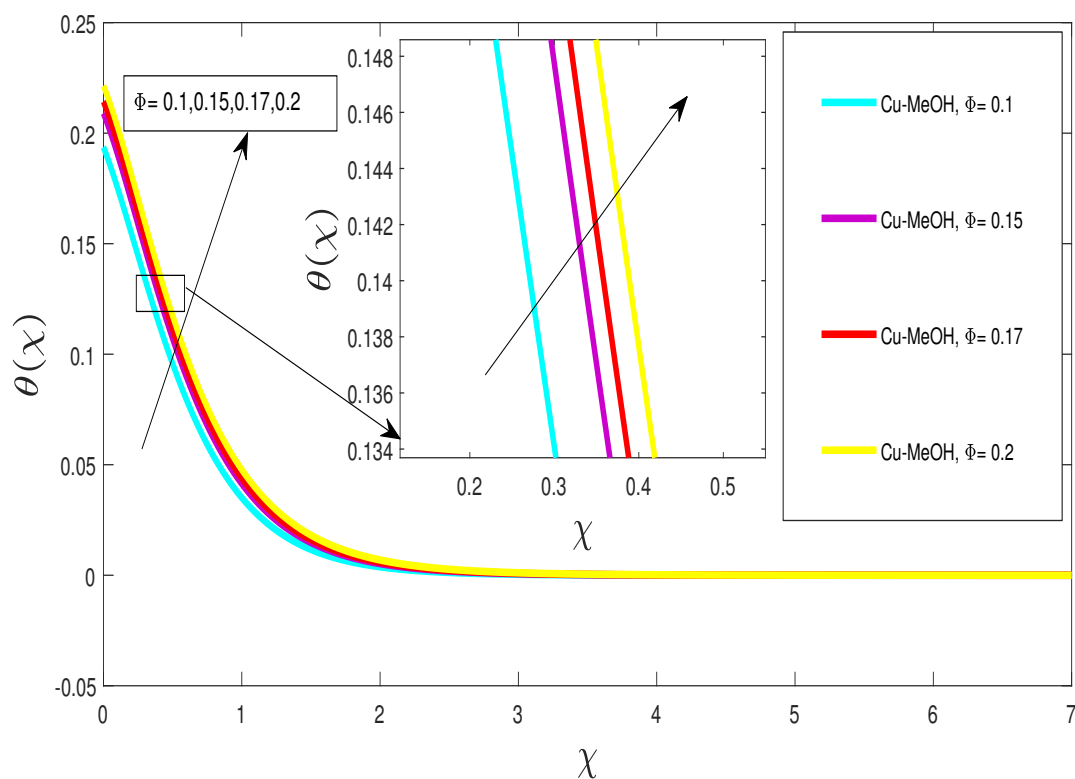
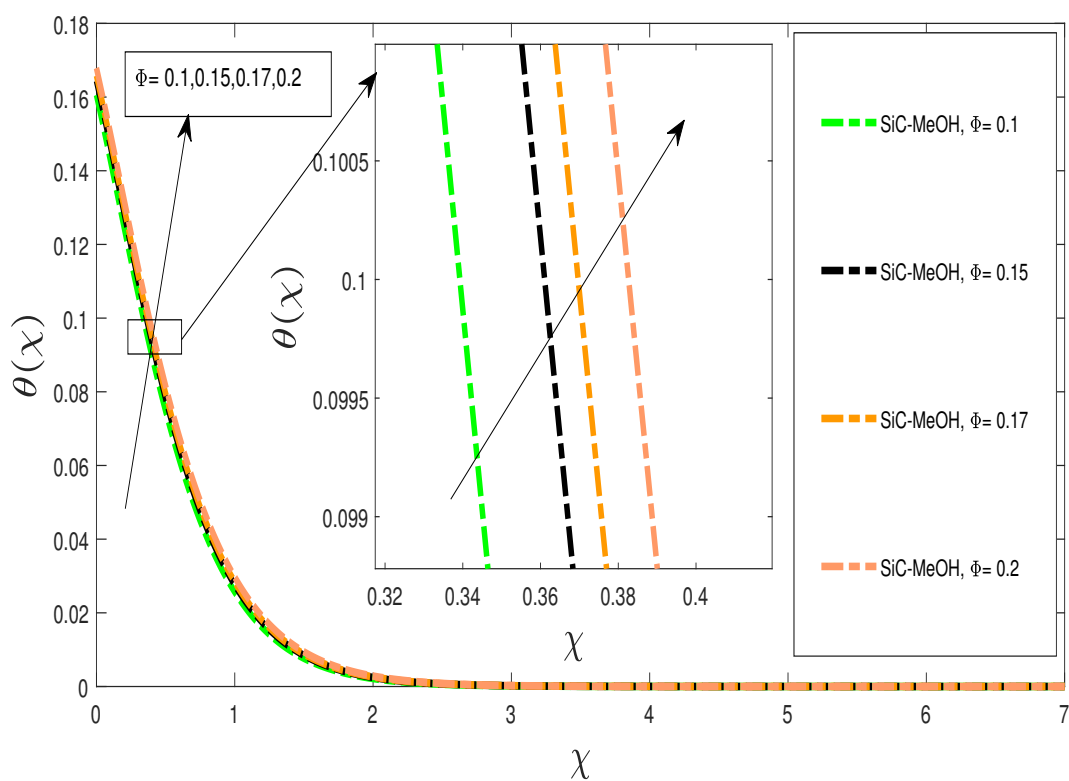
ω	A	Δ_1	Δ_2	Γ	M	Φ	Λ_1	Λ_2	S_1	S_2	Nr	Bi	Ec	ξ	Q	Cu-MeOH	SiC-MeOH
0.1	0.1	0.2	0.2	$2\pi/20$	0.1	0.1	0.2	0.1	0.2	0.1	0.3	0.3	0.2	0.2	0.1	0.3539	0.3783
																0.3563	0.3798
																0.3548	0.3789
																0.3547	0.3788
																0.3571	0.3809
																0.3633	0.3857
																0.3663	0.3880
																0.3633	0.3857
																0.3693	0.3901
																0.3722	0.3922
																0.4018	0.4303
																0.4703	0.5059
																0.4923	0.5305
																0.1857	0.1973
																0.8934	0.9729
																1.1977	1.3183
																0.2961	0.3398
																0.2672	0.3205
																0.2383	0.3012
																0.3555	0.3795
																0.3581	0.3815
																0.3586	0.3819
																0.3445	0.3733
																0.3301	0.3673
																0.2612	0.3495

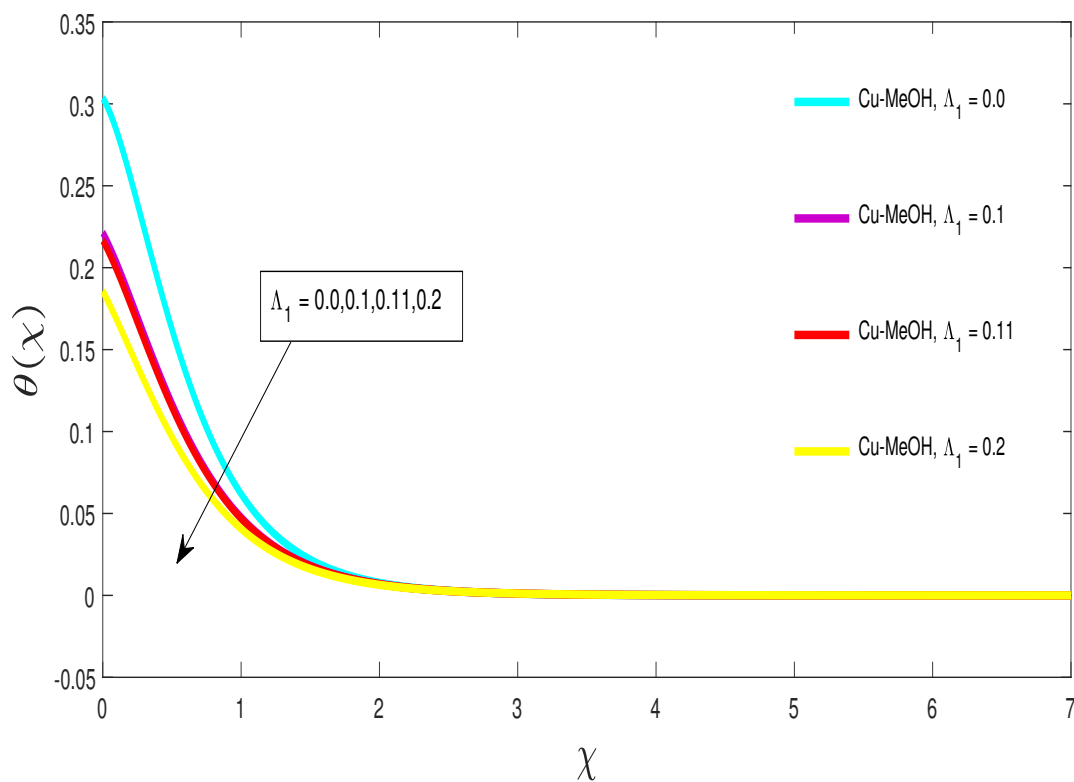
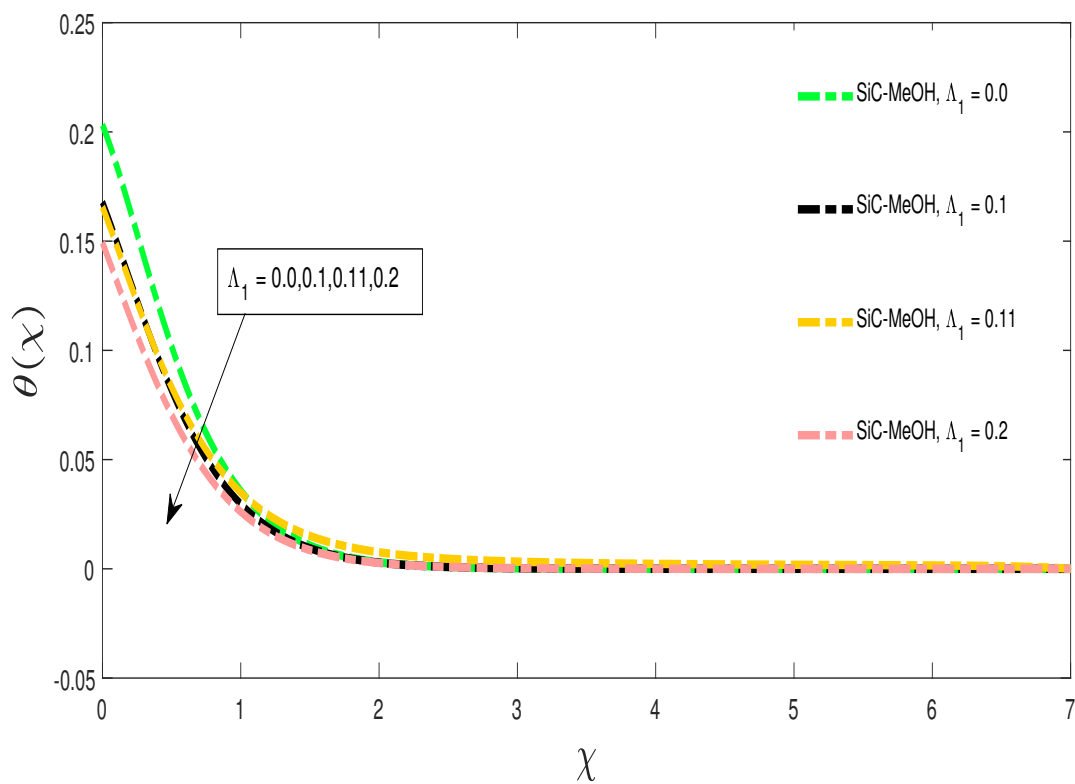
FIGURE 4.18: Temperature profile against ω FIGURE 4.19: Temperature profile against ω

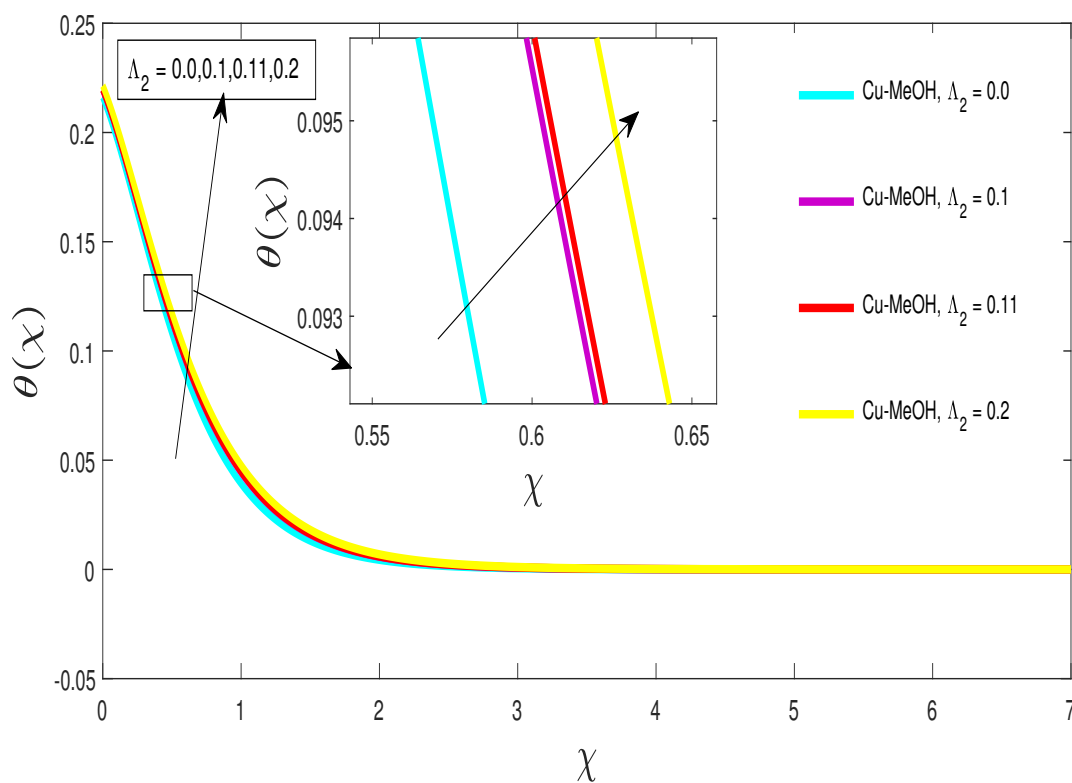
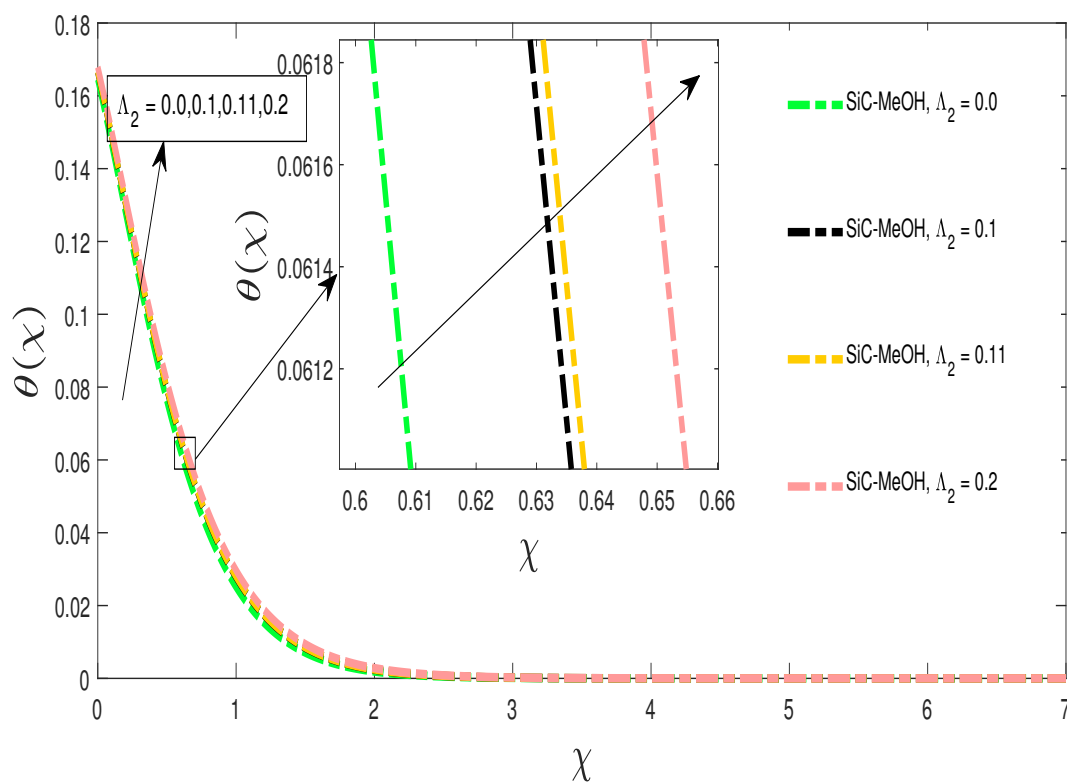
FIGURE 4.20: Temperature profile against A FIGURE 4.21: Temperature profile against A

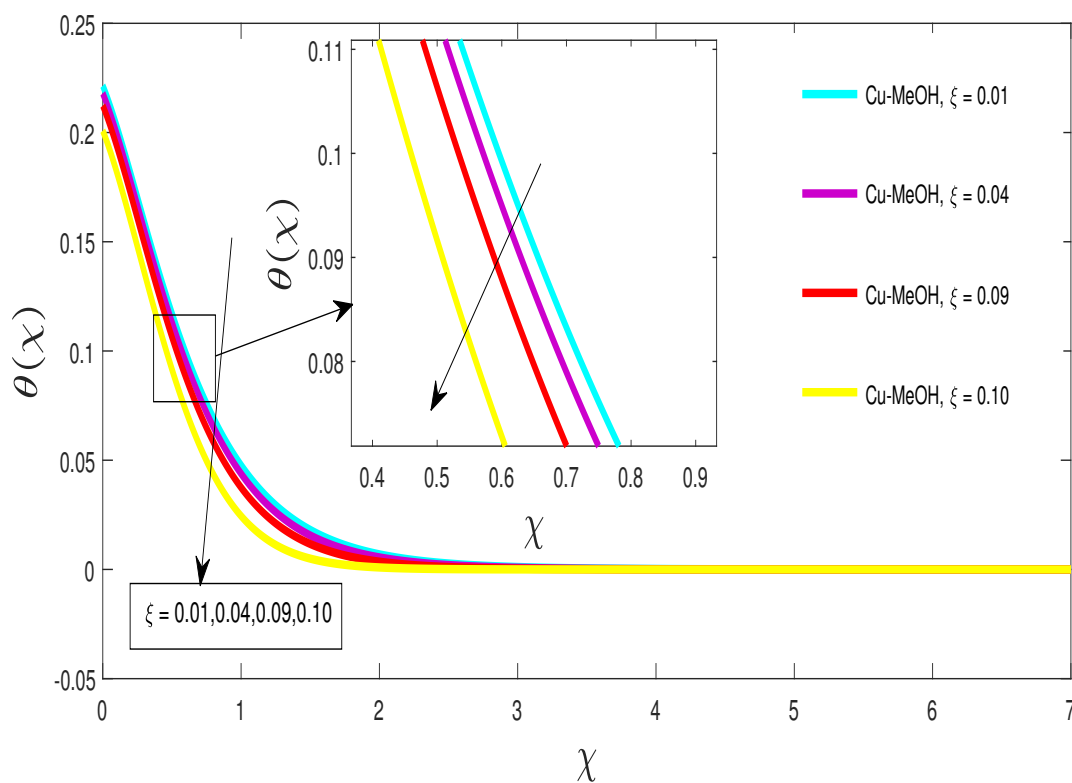
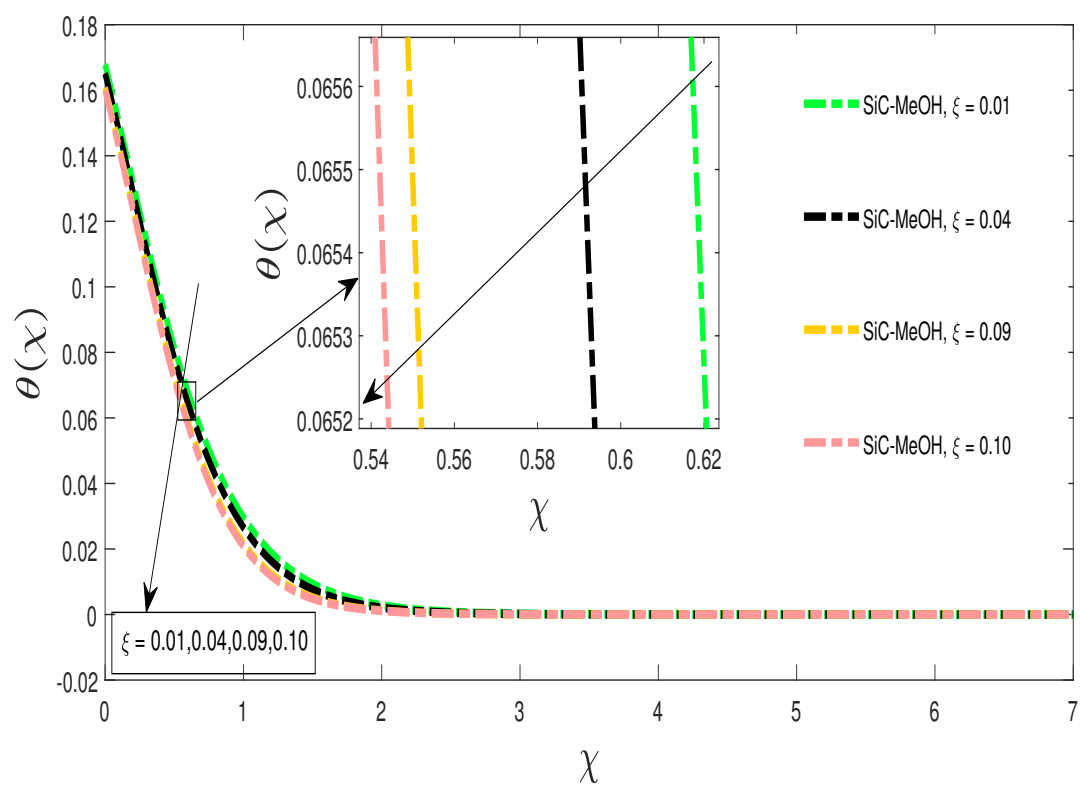
FIGURE 4.22: Temperature profile against Δ_1 FIGURE 4.23: Temperature profile against Δ_1

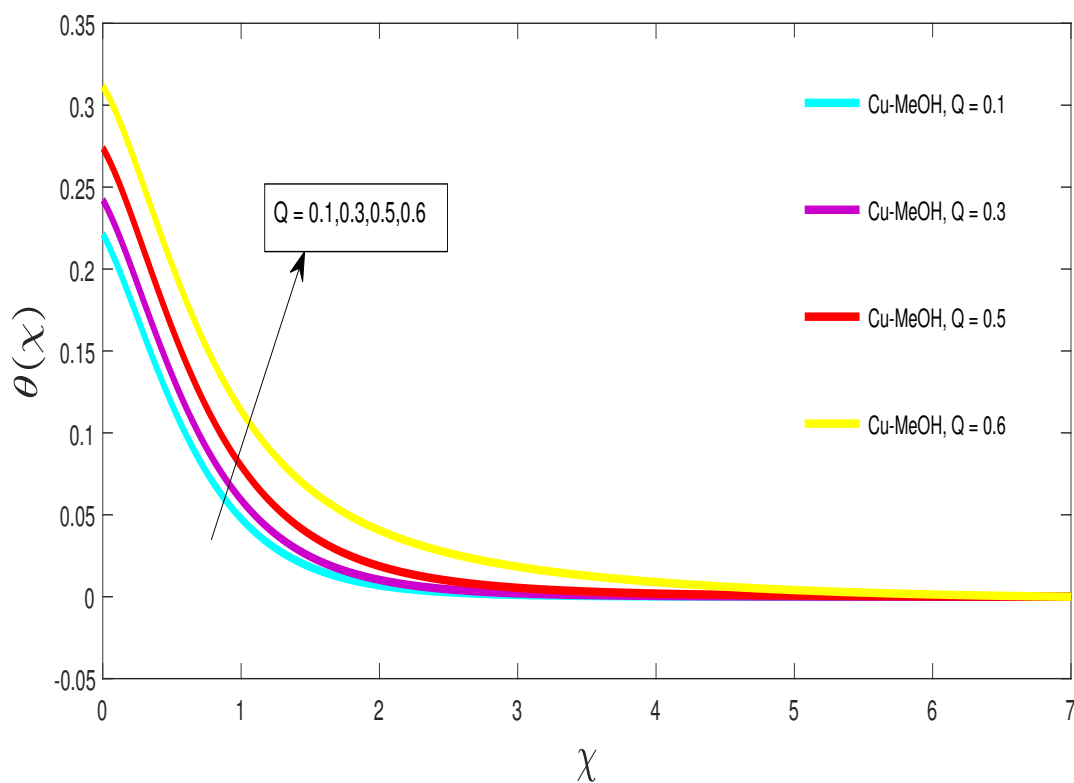
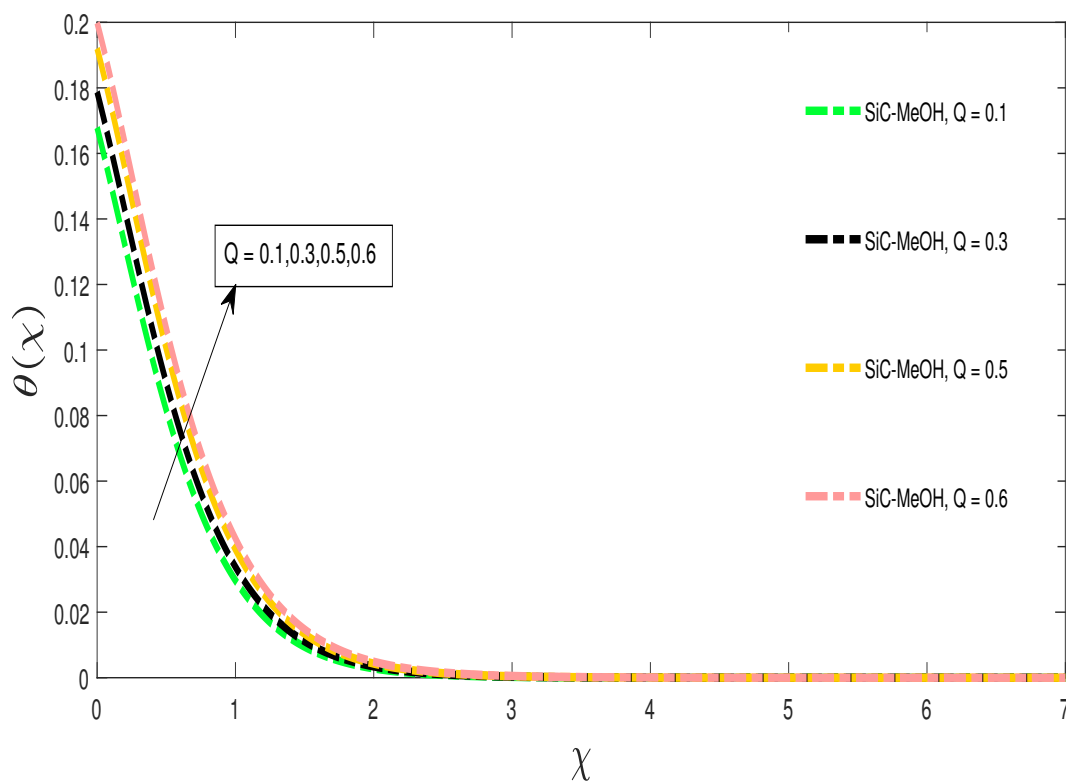
FIGURE 4.24: Temperature profile against Δ_2 FIGURE 4.25: Temperature profile against Δ_2

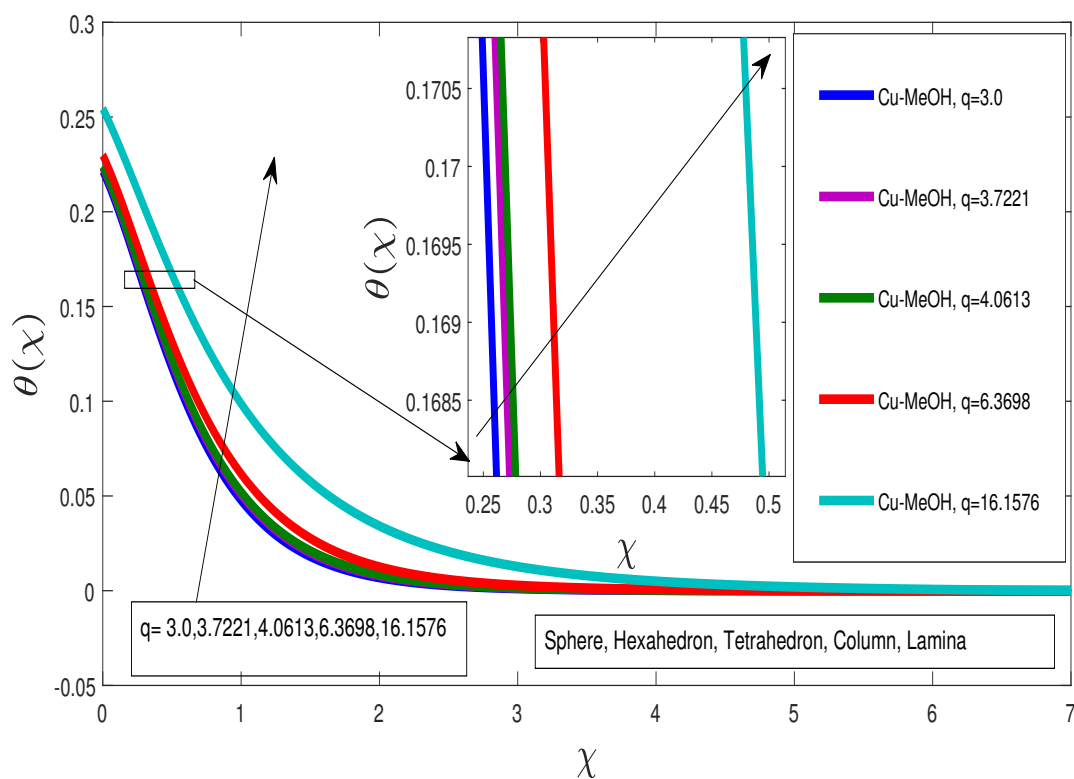
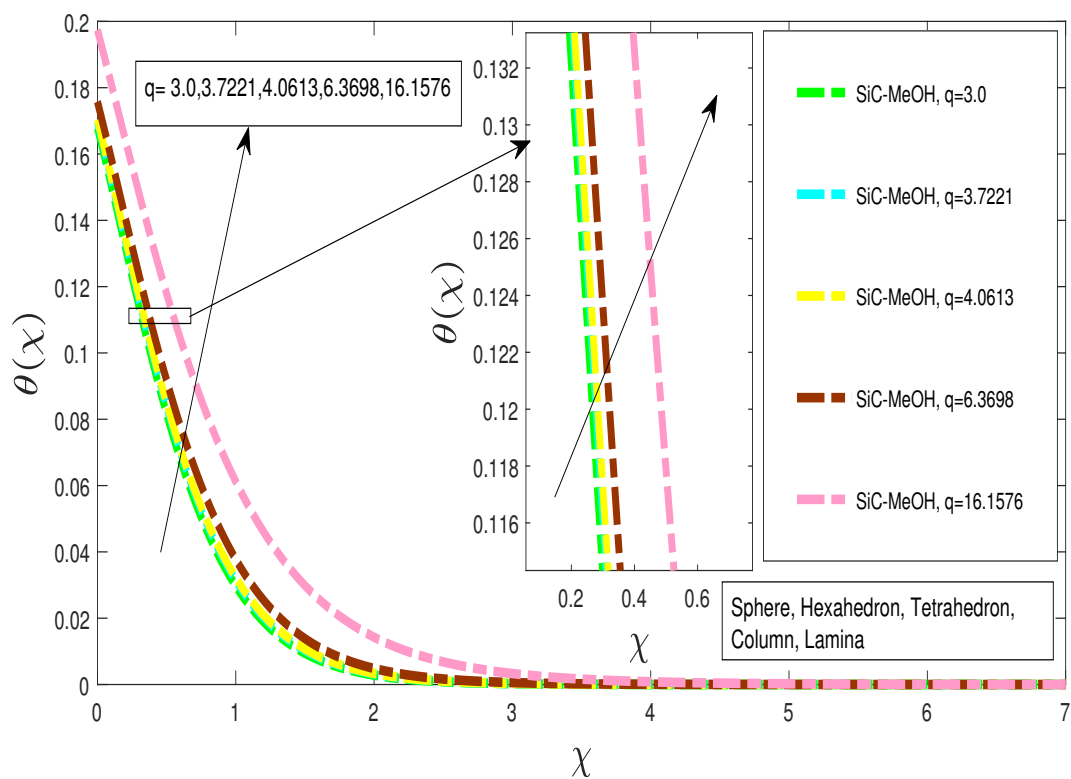
FIGURE 4.26: Temperature profile against Φ FIGURE 4.27: Temperature profile against Φ

FIGURE 4.28: Temperature profile against Λ_1 FIGURE 4.29: Temperature profile against Λ_1

FIGURE 4.30: Temperature profile against Λ_2 FIGURE 4.31: Temperature profile against Λ_2

FIGURE 4.32: Temperature profile against ξ FIGURE 4.33: Temperature profile against ξ

FIGURE 4.34: Temperature profile against Q FIGURE 4.35: Temperature profile against Q

FIGURE 4.36: Temperature profile against q FIGURE 4.37: Temperature profile against q

4.5.3 Entropy Profile

Entropy is a disorder of a system and its surroundings from a physical perspective and is also known as the number of irreversibilities. As a result of entropy, heat cannot entirely be converted into work. Entropy often arises in a number of systems, particularly those involving fluid viscous force, Joule heating, and flow-driven force. The dimensional form of entropy generation is expressed as follows [91]:

$$E_G = \frac{k_{nf}}{\Theta_\infty^2} \left[\left(\frac{\partial \Theta}{\partial \bar{z}} \right)^2 + \frac{16}{3} \frac{\sigma^* \Theta_\infty^3}{k^* \nu_f (\rho C_p)_f} \left(\frac{\partial \Theta}{\partial \bar{z}} \right)^2 \right] + \frac{\mu_{nf}}{\Theta_\infty} \left(\frac{\partial \bar{f}_1}{\partial \bar{z}} \right)^2 + \frac{\sigma_{nf}^* B^2(\bar{t}) \sin^2(\Gamma) \bar{f}_1^2}{\Theta_\infty}.$$

The dimensionless entropy generation after applying the similarity transformation, is denoted by NG and formulated as:

$$NG = Re \left[N_4(1 + Nr) \left(\frac{d\theta}{d\chi} \right)^2 + \frac{1}{N_1} \frac{Br}{\Omega} \left(\left(\frac{d^2 f}{d\zeta^2} \right)^2 + N_1 N_5 M \sin^2(\Gamma) \left(\frac{df}{d\chi} \right)^2 \right) \right].$$

- Figures 4.38-4.41 depict the entropy generation behavior due to the variation of the non-Newtonian fluid material parameters Δ_1 and Δ_2 . As an illustration, random values are taken for $\Delta_1 = 0.2, 0.3, 0.5, 0.9$ and $\Delta_2 = 0.2, 4, 7, 9$ at $\Phi = 0.2$. To increase the values of Δ_1 and Δ_2 , Figures 4.38-4.41 show a decreasing trend in the entropy generation NG .
- Figures 4.42-4.43 exhibit the influence of Cattaneo-Christov parameter ξ on the entropy profile, respectively. For the increasing values of the Cattaneo-Christov parameter ξ , the entropy profile NG is observed to increase. These two figures reflect that the entropy for Cu-MeOH near the surface is higher than that of SiC-MeOH but the other way round, away from the surface.
- The influence of heat generation parameter Q on NG is elaborated through Figures 4.44-4.45. It is evident that NG gets enhanced for increasing the values of the heat generation parameter Q . These two figures reflect that the entropy for Cu-MeOH near the surface is higher than that of SiC-MeOH but away from the surface, an different behavior can also be seen.
- In Figures 4.46-4.47, it has been shown that for the increasing values of Re , the entropy generation NG increases. Through Figures 4.48-4.49, the effect of

the Brinkman number on the entropy generation is depicted. According to the definition of the Brinkman number, molecular absorption causes viscous heating, which slows down the rate of heat transfer. The generation of large quantity of heat between the layers of the non-Newtonian fluid is the real cause of the increased entropy generation.

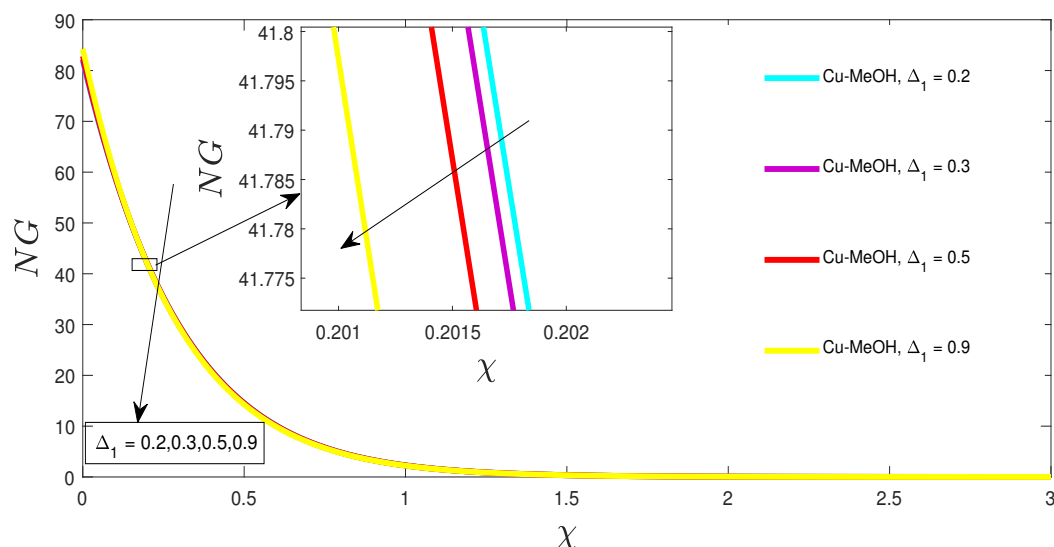


FIGURE 4.38: Entropy profile against Δ_1

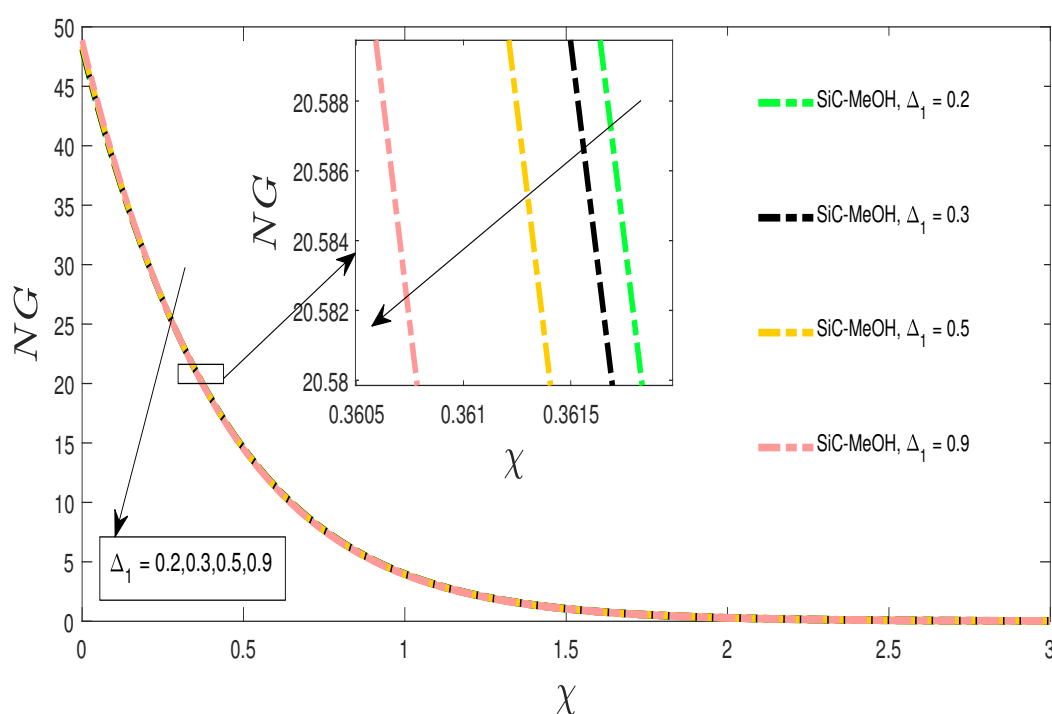
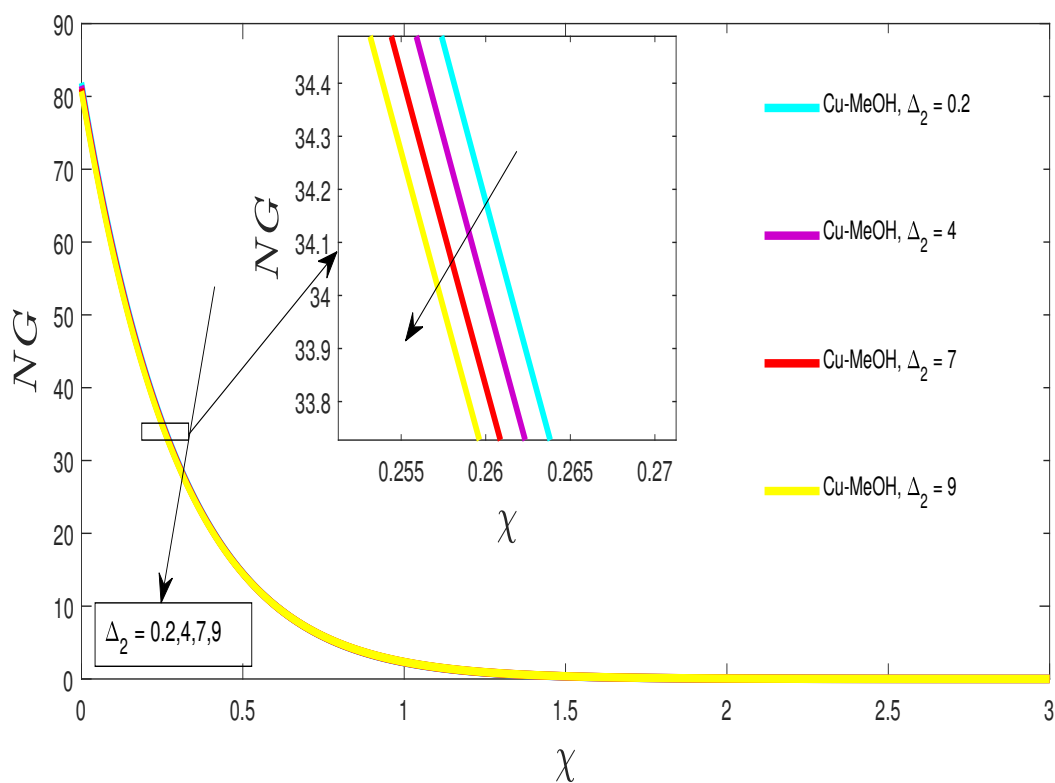
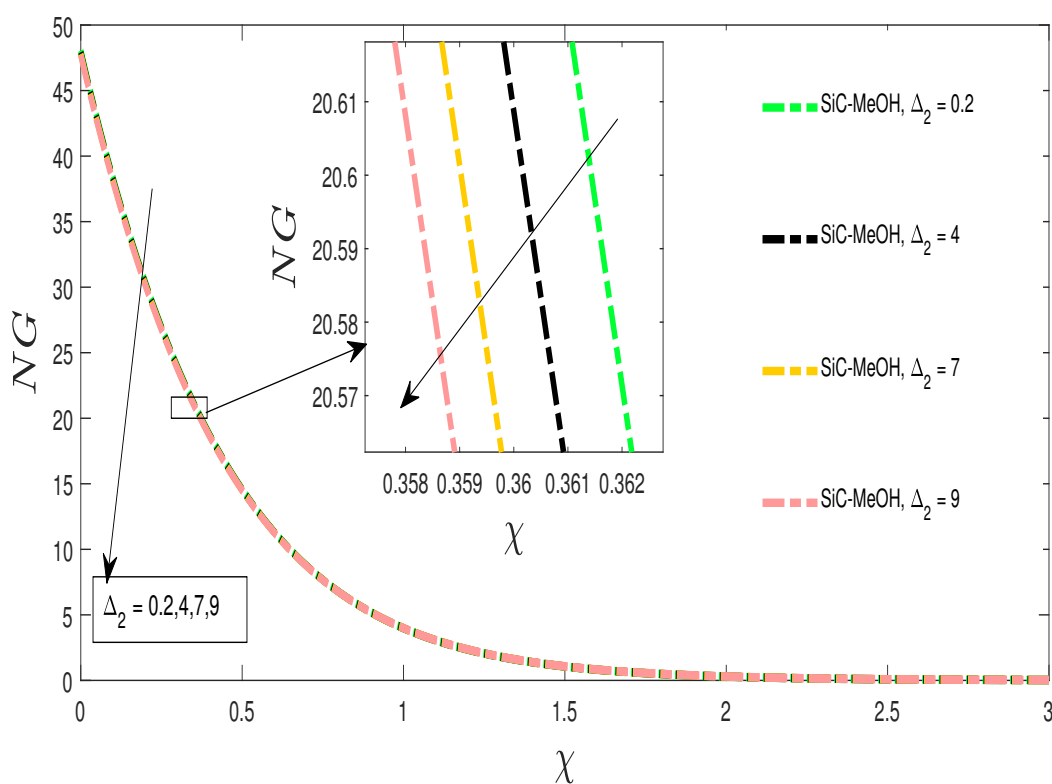
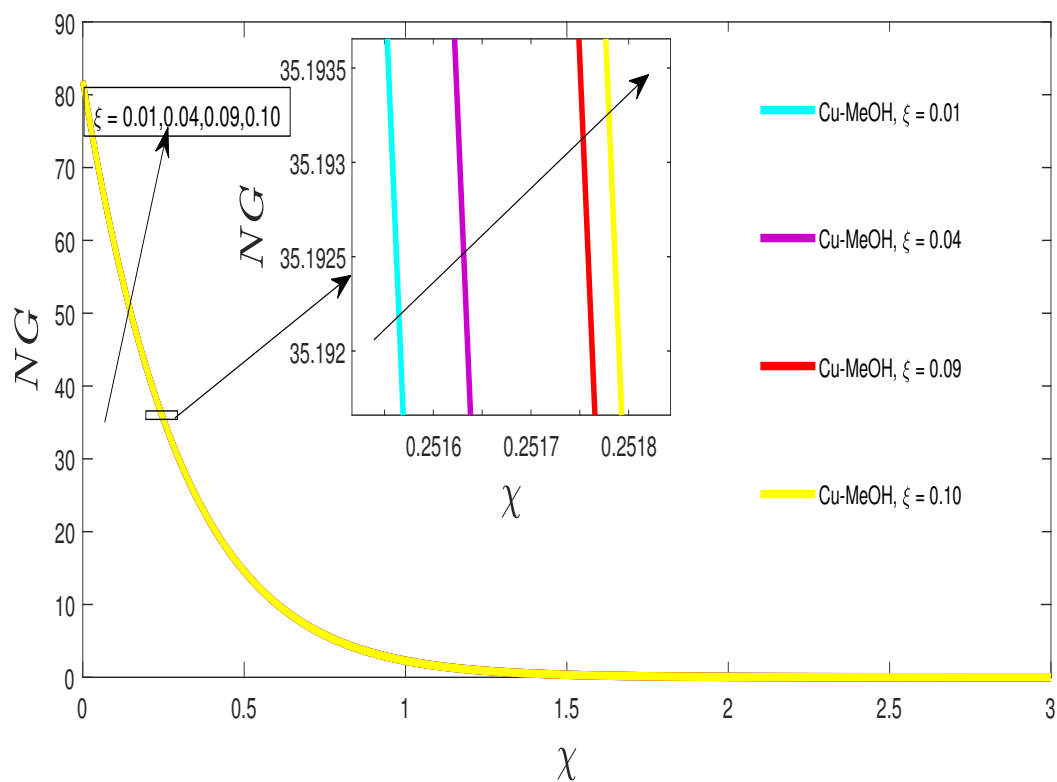
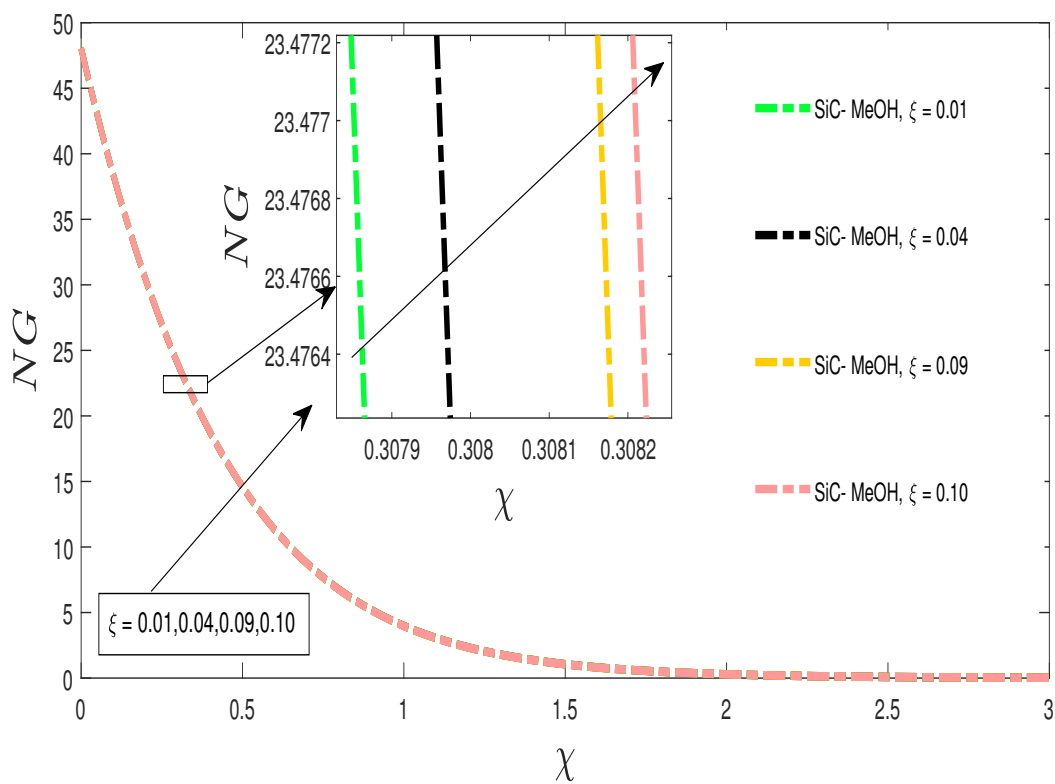
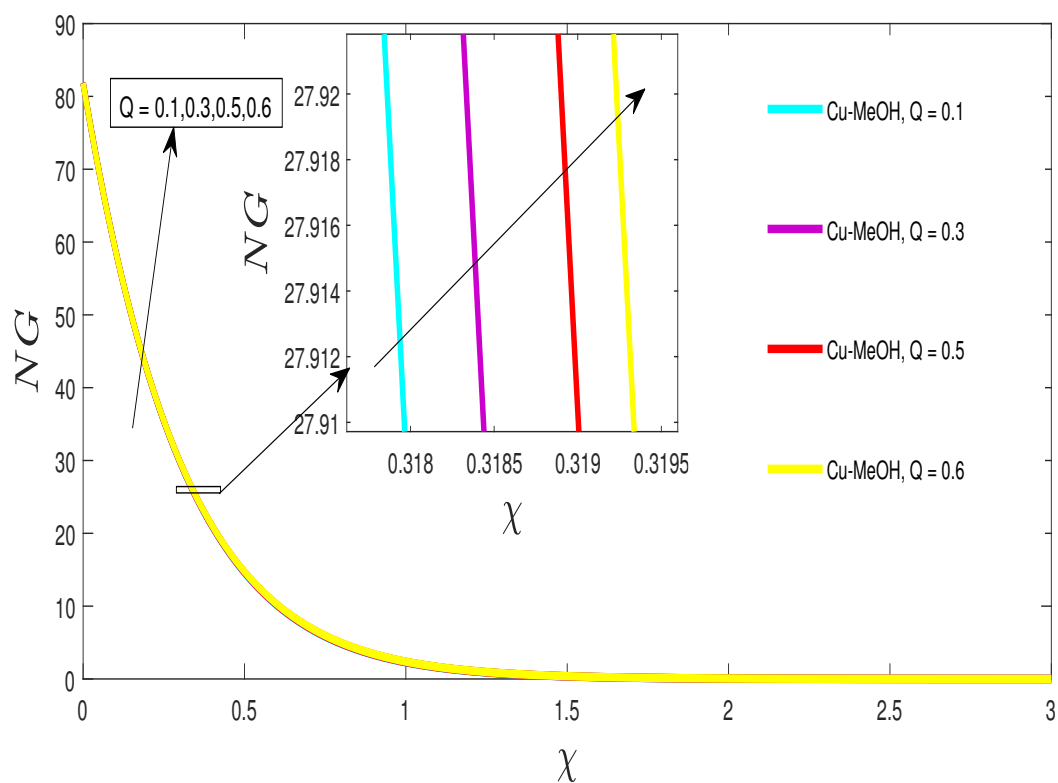
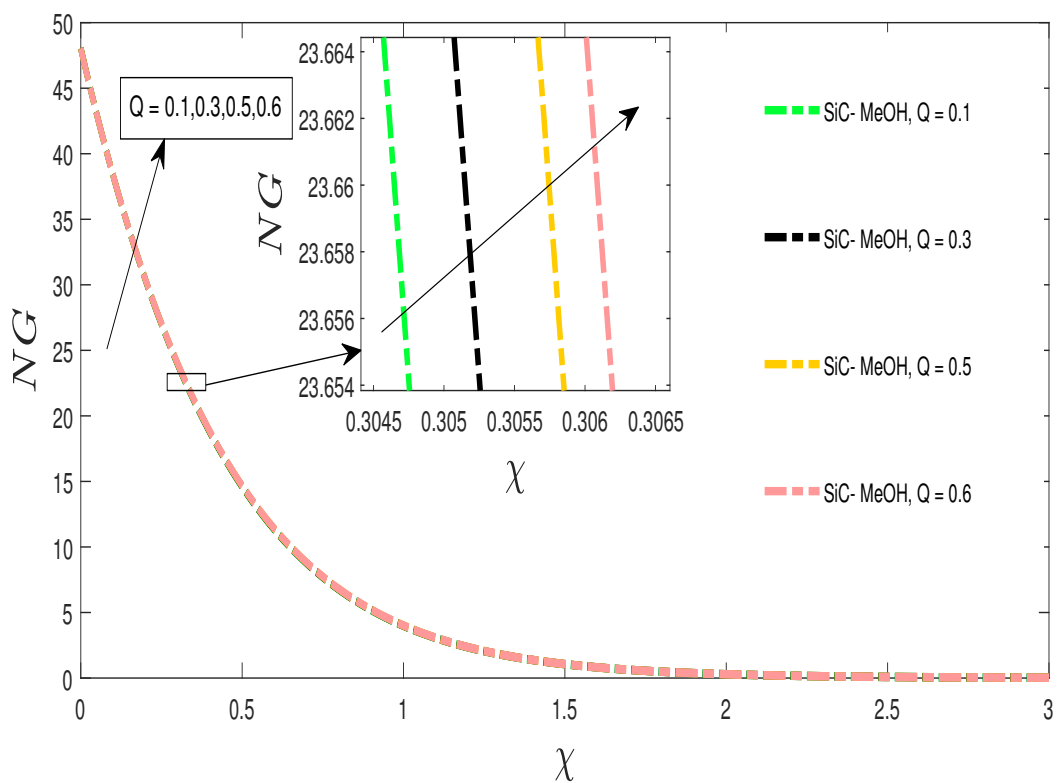
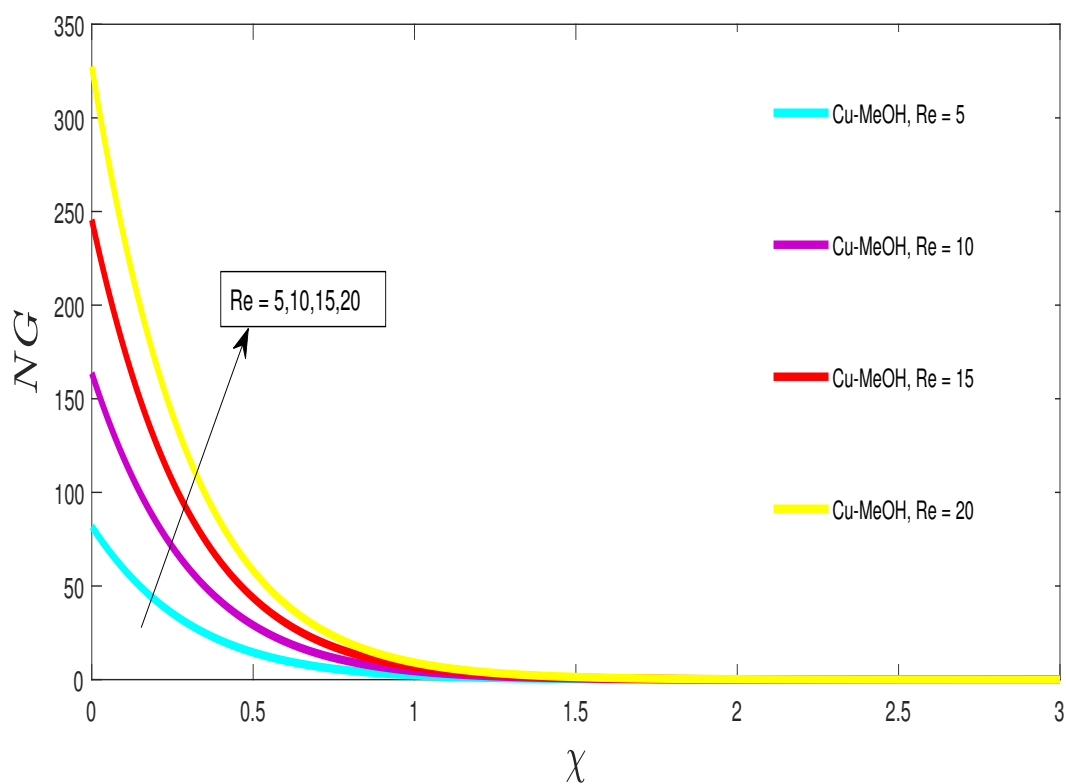
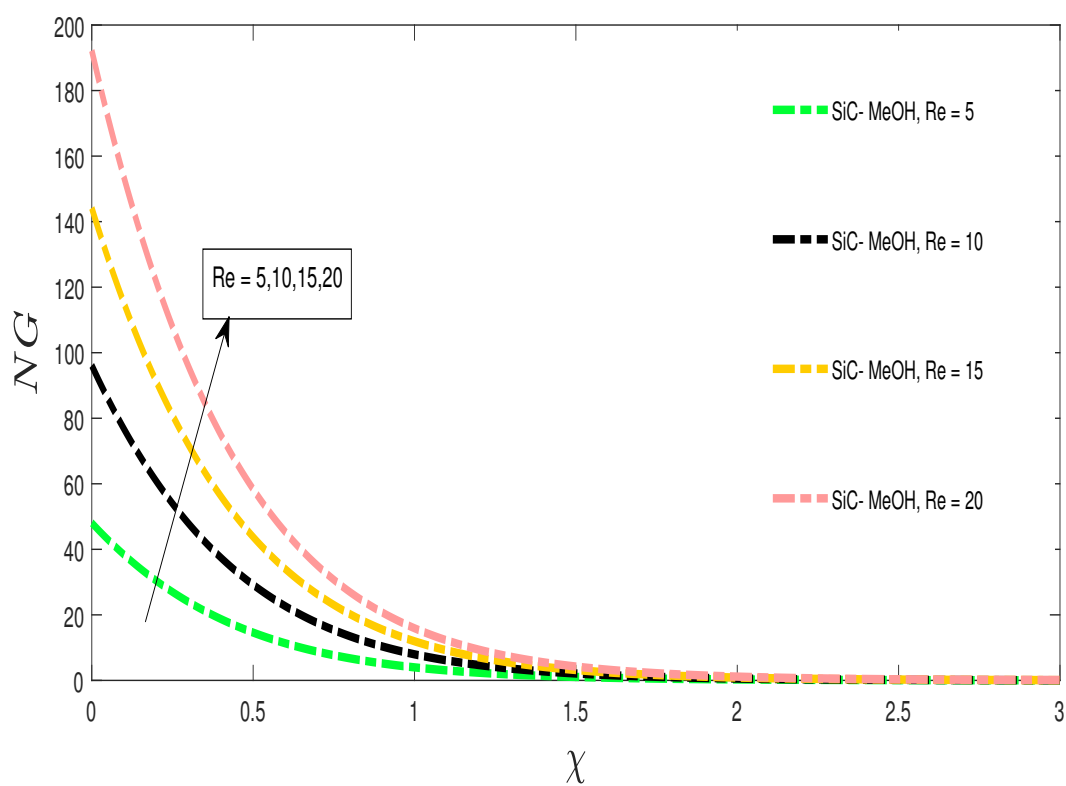


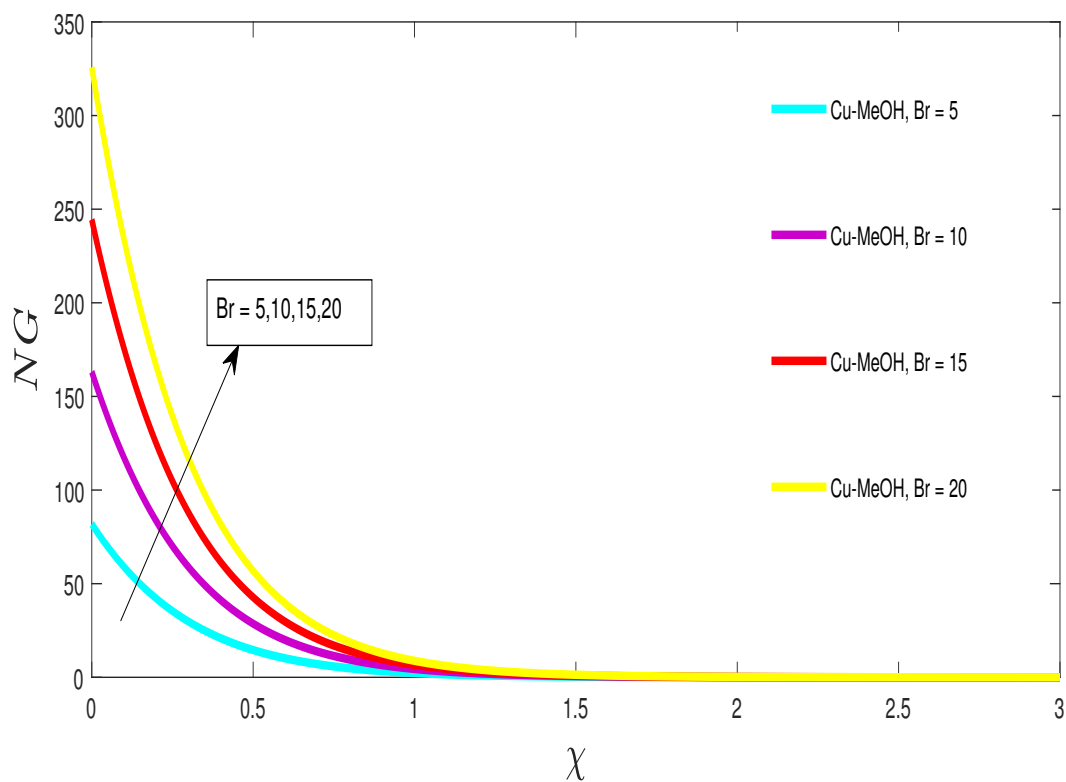
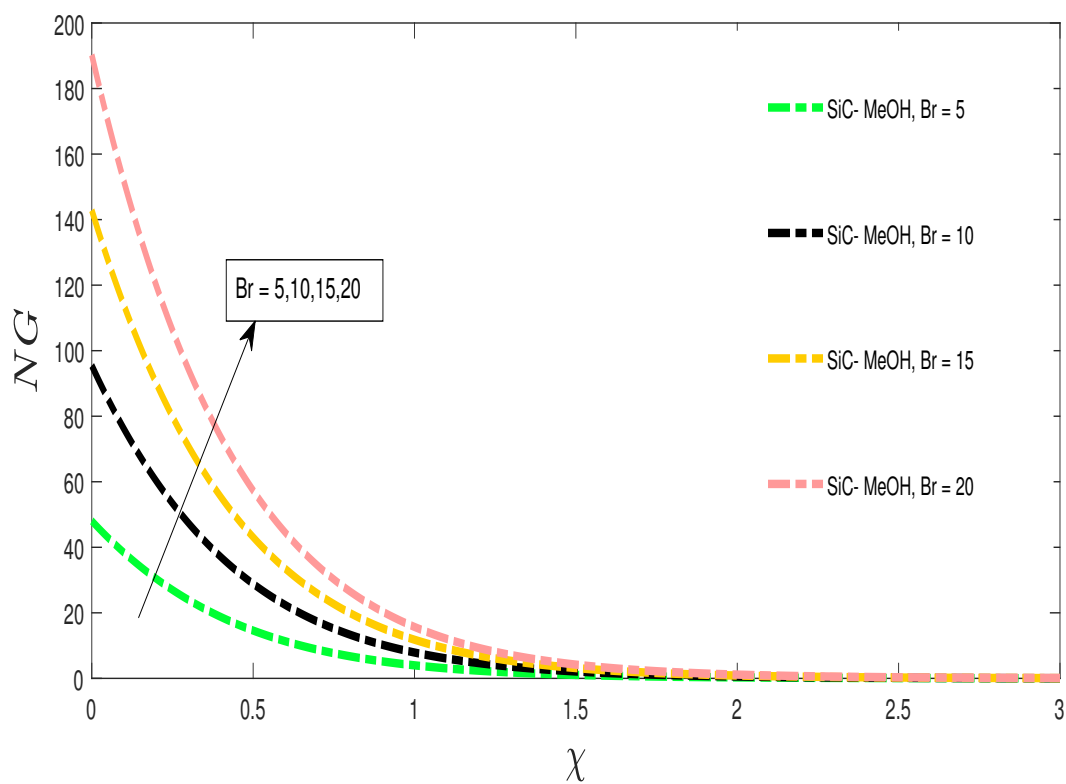
FIGURE 4.39: Entropy profile against Δ_1

FIGURE 4.40: Entropy profile against Δ_2 FIGURE 4.41: Entropy profile against Δ_2

FIGURE 4.42: Entropy profile against ξ FIGURE 4.43: Entropy profile against ξ

FIGURE 4.44: Entropy profile against Q FIGURE 4.45: Entropy profile against Q

FIGURE 4.46: Entropy profile against Re FIGURE 4.47: Entropy profile against Re

FIGURE 4.48: Entropy profile against Br FIGURE 4.49: Entropy profile against Br

Chapter 5

Conclusion

In this thesis, we studied the flow, heat transfer and entropy generation for containing non-Newtonian nanofluids. Nanofluids have countless applications in fields like biomedical devices, tumor treatment, solar collectors, nuclear reactor, crystal growth, heat exchangers and cooling radiators etc. When nanoparticles are added to a base fluid that is Newtonian in nature, the fluid's behavior often changes to one that is not Newtonian. However, the amount of nanoparticles in the base fluid, their size, shape, and interactions with one another all play a role in this. As a result, heat transfer and nanofluid flow are better understood using non-Newtonian models. Keeping above in view this thesis aims to understand the non-Newtonian nanofluids flow, heat transfer and entropy generation along with variable thermophysical properties. The most significant fundamental equations are derived from the conservation laws of mass, momentum, and energy. By applying the proper similarity transformations, these equations are converted into a system of associated nonlinear ordinary differential equations. The shooting method, an effective numerical technique, is then used to solve the ODE. Numerical results are also presented in the form of graphs and tables showing the influence of physical parameters such as non-Newtonian parameters, thermal radiation parameter, mass transfer parameter, Biot number, Reynolds number and Brinkman number, nanoparticle volume concentration parameter, velocity slip parameters, etc. The study of the physical behavior of dimensionless quantities such as velocity, temperature, and entropy generation. The entire study can be concluded with the following observations.

- When M is increased, the temperature profile rises and the velocity profile falls.
- As the Prandtl number values rise, the temperature profile suffers a reduction.
- As the Cattaneo-Christov temperature parameter ξ increases, the temperature profile decreases.
- As the value of the Eckert number Ec rises, the temperature profile also rises.
- As unsteady parameter A increases, the temperature profile decreases.
- As the Brinkman number Br rises, correspondingly rises the rate at which entropy is generated.
- The increasing values of the magnetic parameter M lead to a rise in the entropy generation rate.
- It is shown that velocity profiles progressively diminish as the value of A rises.
- Each parameter, M , Br and Bi , individually increase the irreversibility of thermal energy.
- Increasing the values of Φ , the velocity profile decreases while the temperature profile increases.
- On increment of physical parameter ω , there is increases in velocity profile.
- Temperature profile rises while extending the radiation parameter.
- The fluid energy accelerates effectively with an increase in the Biot number.

Bibliography

- [1] L. Prandtl, “On movement of fluids with very small friction,” *International Mathematics Kongr Heidelberg*, pp. 484–491, 1904.
- [2] O. D. Makinde and O. Onyejekwe, “A numerical study of MHD generalized Couette flow and heat transfer with variable viscosity and electrical conductivity,” *Journal of Magnetism and Magnetic Materials*, vol. 323, no. 22, pp. 2757–2763, 2011.
- [3] S. Ibrahim and O. D. Makinde, “Chemically reacting magnetohydrodynamics (MHD) boundary layer flow of heat and mass transfer past a low-heat-resistant sheet moving vertically downwards,” 2011.
- [4] O. Makinde, “Entropy analysis for MHD boundary layer flow and heat transfer over a flat plate with a convective surface boundary condition,” *International Journal of Energy*, vol. 10, no. 2, pp. 142–154, 2012.
- [5] S.-J. Liao, “On the analytic solution of magnetohydrodynamic flows of non-Newtonian fluids over a stretching sheet,” *Journal of Fluid Mechanics*, vol. 488, pp. 189–212, 2003.
- [6] H. Xu and S.-J. Liao, “Series solutions of unsteady magnetohydrodynamic flows of non-Newtonian fluids caused by an impulsively stretching plate,” *Journal of Non-Newtonian Fluid Mechanics*, vol. 129, no. 1, pp. 46–55, 2005.
- [7] S. Liao, “A new branch of solutions of boundary-layer flows over an impermeable stretched plate,” *International Journal of Heat and Mass Transfer*, vol. 48, no. 12, pp. 2529–2539, 2005.

- [8] M. Guedda and Z. Hammouch, “Similarity flow solutions of a non-Newtonian power-law fluid,” *arXiv preprint arXiv:0904.0315*, 2009.
- [9] M. S. Abel, P. Siddheshwar, and M. M. Nandeppanavar, “Heat transfer in a viscoelastic boundary layer flow over a stretching sheet with viscous dissipation and non-uniform heat source,” *International Journal of Heat and Mass Transfer*, vol. 50, no. 5-6, pp. 960–966, 2007.
- [10] M. Sajid and T. Hayat, “Influence of thermal radiation on the boundary layer flow due to an exponentially stretching sheet,” *International Communications in Heat and Mass Transfer*, vol. 35, no. 3, pp. 347–356, 2008.
- [11] R. Cortell, “Effects of viscous dissipation and radiation on the thermal boundary layer over a nonlinearly stretching sheet,” *Physics Letters A*, vol. 372, no. 5, pp. 631–636, 2008.
- [12] C.-H. Chen, “Effects of magnetic field and suction/injection on convection heat transfer of non-Newtonian power-law fluids past a power-law stretched sheet with surface heat flux,” *International Journal of Thermal Sciences*, vol. 47, no. 7, pp. 954–961, 2008.
- [13] A. Postelnicu and I. Pop, “Falkner–skan boundary layer flow of a power-law fluid past a stretching wedge,” *Applied Mathematics and Computation*, vol. 217, no. 9, pp. 4359–4368, 2011.
- [14] T. Hayat, R. S. Saif, R. Ellahi, T. Muhammad, and A. Alsaedi, “Simultaneous effects of melting heat and internal heat generation in stagnation point flow of Jeffrey fluid towards a nonlinear stretching surface with variable thickness,” *International Journal of Thermal Sciences*, vol. 132, pp. 344–354, 2018.
- [15] R. K. Kumar, G. V. Kumar, C. Raju, S. Shehzad, and S. Varma, “Analysis of arrhenius activation energy in magnetohydrodynamic Carreau fluid flow through improved theory of heat diffusion and binary chemical reaction,” *Journal of Physics Communications*, vol. 2, no. 3, p. 035004, 2018.
- [16] E. Elbashbeshy, “Heat transfer over an exponentially stretching continuous surface with suction,” *Archives of Mechanics*, vol. 53, no. 6, pp. 643–651, 2001.

- [17] E. Sanjayanand and S. K. Khan, “On heat and mass transfer in a viscoelastic boundary layer flow over an exponentially stretching sheet,” *International Journal of Thermal Sciences*, vol. 45, no. 8, pp. 819–828, 2006.
- [18] H. Maiti and S. Mukhopadhyay, “Existence of mhd boundary layer hybrid nanofluid flow through a divergent channel with mass suction and injection,” *Chemical Engineering Journal Advances*, vol. 14, p. 100475, 2023.
- [19] E. M. Elbashbeshy, H. G. Asker, and B. Nagy, “The effects of heat generation absorption on boundary layer flow of a nanofluid containing gyrotactic microorganisms over an inclined stretching cylinder,” *Ain Shams Engineering Journal*, vol. 13, no. 5, p. 101690, 2022.
- [20] B. Ali, S. Jubair, L. A. Al-Essa, Z. Mahmood, A. Al-Bossly, and F. S. Alduais, “Boundary layer and heat transfer analysis of mixed convective nanofluid flow capturing the aspects of nanoparticles over a needle,” *Materials Today Communications*, vol. 35, p. 106253, 2023.
- [21] N. Hafez, E. N. Thabet, Z. Khan, A. Abd-Alla, and S. Elhag, “Electroosmosis-modulated darcy–forchheimer flow of casson nanofluid over stretching sheets in the presence of newtonian heating,” *Case Studies in Thermal Engineering*, p. 103806, 2023.
- [22] A. M. Ajeena, I. Farkas, and P. Víg, “Energy and exergy assessment of a flat plate solar thermal collector by examine silicon carbide nanofluid: An experimental study for sustainable energy,” *Applied Thermal Engineering*, vol. 236, p. 121844, 2024.
- [23] S. U. Choi and J. A. Eastman, “Enhancing thermal conductivity of fluids with nanoparticles,” tech. rep., Argonne National Lab.(ANL), Argonne, IL (United States), 1995.
- [24] H. Gupta, G. Agrawal, and J. Mathur, “An overview of nanofluids: A new media towards green environment,” *International Journal of Environmental Sciences*, vol. 3, no. 1, pp. 433–440, 2012.

- [25] K. Sreelakshmy, A. S. Nair, K. Vidhya, T. Saranya, and S. C. Nair, "An overview of recent nanofluid research," *International Research Journal of Pharmacy*, vol. 5, no. 4, pp. 239–243, 2014.
- [26] W. Chamsa-Ard, S. Brundavanam, C. C. Fung, D. Fawcett, and G. Poinern, "Nanofluid types, their synthesis, properties and incorporation in direct solar thermal collectors: A review," *Nanomaterials*, vol. 7, no. 6, p. 131, 2017.
- [27] J. A. Eastman, S. Choi, S. Li, W. Yu, and L. Thompson, "Anomalously increased effective thermal conductivities of ethylene glycol-based nanofluids containing copper nanoparticles," *Applied Physics Letters*, vol. 78, no. 6, pp. 718–720, 2001.
- [28] X. Wang, X. Xu, and S. U. Choi, "Thermal conductivity of nanoparticle-fluid mixture," *Journal of Thermophysics and Heat Transfer*, vol. 13, no. 4, pp. 474–480, 1999.
- [29] P. Keblinski, S. Phillpot, S. Choi, and J. Eastman, "Mechanisms of heat flow in suspensions of nano-sized particles (nanofluids)," *International Journal of Heat and Mass Transfer*, vol. 45, no. 4, pp. 855–863, 2002.
- [30] J. Buongiorno, "Convective transport in nanofluids," 2006.
- [31] A. R. Rahmati, O. A. Akbari, A. Marzban, D. Toghraie, R. Karimi, and F. Pourfattah, "Simultaneous investigations the effects of non-Newtonian nanofluid flow in different volume fractions of solid nanoparticles with slip and no-slip boundary conditions," *Thermal Science and Engineering Progress*, vol. 5, pp. 263–277, 2018.
- [32] A. Arabpour, A. Karimipour, D. Toghraie, and O. A. Akbari, "Investigation into the effects of slip boundary condition on nanofluid flow in a double-layer microchannel," *Journal of Thermal Analysis and Calorimetry*, vol. 131, no. 3, pp. 2975–2991, 2018.
- [33] O. Koriko, I. Animasaun, M. G. Reddy, and N. Sandeep, "Scrutinization of thermal stratification, nonlinear thermal radiation and quartic autocatalytic chemical reaction effects on the flow of three-dimensional Eyring-Powell alumina-water

- nanofluid,” *Multidiscipline Modeling in Materials and Structures*, vol. 14, no. 2, pp. 261–283, 2018.
- [34] I. Tlili, W. Khan, and I. Khan, “Multiple slips effects on MHD $SA - Al_2O_3$ and SA-Cu non-Newtonian nanofluids flow over a stretching cylinder in porous medium with radiation and chemical reaction,” *Results in Physics*, vol. 8, pp. 213–222, 2018.
- [35] P. Barnoon and D. Toghraie, “Numerical investigation of laminar flow and heat transfer of non-Newtonian nanofluid within a porous medium,” *Powder Technology*, vol. 325, pp. 78–91, 2018.
- [36] M. Sheikholeslami, “CuO-water nanofluid flow due to magnetic field inside a porous media considering Brownian motion,” *Journal of Molecular Liquids*, vol. 249, pp. 921–929, 2018.
- [37] A. A. Hakeem, N. V. Ganesh, and B. Ganga, “Magnetic field effect on second order slip flow of nanofluid over a stretching/shrinking sheet with thermal radiation effect,” *Journal of Magnetism and Magnetic Materials*, vol. 381, pp. 243–257, 2015.
- [38] K.-L. Hsiao, “Micropolar nanofluid flow with MHD and viscous dissipation effects towards a stretching sheet with multimedia feature,” *International Journal of Heat and Mass Transfer*, vol. 112, pp. 983–990, 2017.
- [39] S. Qayyum, T. Hayat, and A. Alsaedi, “Thermal radiation and heat generation/absorption aspects in third grade magneto-nanofluid over a slendering stretching sheet with Newtonian conditions,” *Physica B: Condensed Matter*, vol. 537, pp. 139–149, 2018.
- [40] M. Khan, M. Malik, T. Salahuddin, and A. Hussian, “Heat and mass transfer of Williamson nanofluid flow yield by an inclined Lorentz force over a nonlinear stretching sheet,” *Results in Physics*, vol. 8, pp. 862–868, 2018.
- [41] M. R. Eid, K. L. Mahny, T. Muhammad, and M. Sheikholeslami, “Numerical treatment for Carreau nanofluid flow over a porous nonlinear stretching surface,” *Results in Physics*, vol. 8, pp. 1185–1193, 2018.

- [42] Y. B. Kho, A. Hussanan, N. M. Sarif, Z. Ismail, and M. Z. Salleh, “Thermal radiation effects on MHD with flow heat and mass transfer in Casson nanofluid over a stretching sheet,” in *MATEC Web of Conferences*, vol. 150, p. 06036, EDP Sciences, 2018.
- [43] M. Elias, M. Miqdad, I. Mahbubul, R. Saidur, M. Kamalifarvestani, M. Sohel, A. Hepbasli, N. Rahim, and M. Amalina, “Effect of nanoparticle shape on the heat transfer and thermodynamic performance of a shell and tube heat exchanger,” *International Communications in Heat and Mass Transfer*, vol. 44, pp. 93–99, 2013.
- [44] O. Mahian, A. Kianifar, S. Z. Heris, and S. Wongwises, “First and second laws analysis of a minichannel-based solar collector using boehmite alumina nanofluids: effects of nanoparticle shape and tube materials,” *International Journal of Heat and Mass Transfer*, vol. 78, pp. 1166–1176, 2014.
- [45] X. Xu and S. Chen, “Cattaneo-Christov heat flux model for heat transfer of Marangoni boundary layer flow in a copper–water nanofluid,” *Heat Transfer—Asian Research*, vol. 46, no. 8, pp. 1281–1293, 2017.
- [46] M. Sheikholeslami, “Magnetic field influence on $Cu - H_2O$ nanofluid convective flow in a permeable cavity considering various shapes for nanoparticles,” *International Journal of Hydrogen Energy*, vol. 42, no. 31, pp. 19611–19621, 2017.
- [47] M. Shen, S. Chen, and F. Liu, “Unsteady mhd flow and heat transfer of fractional Maxwell viscoelastic nanofluid with Cattaneo heat flux and different particle shapes,” *Chinese Journal of Physics*, vol. 56, no. 3, pp. 1199–1211, 2018.
- [48] M. Hatami, M. Jafaryar, J. Zhou, and D. Jing, “Investigation of engines radiator heat recovery using different shapes of nanoparticles in $H_2O/(CH_2OH)_2$ based nanofluids,” *International Journal of Hydrogen Energy*, vol. 42, no. 16, pp. 10891–10900, 2017.
- [49] U. Khan, N. Ahmed, and S. T. Mohyud-Din, “Analysis of magnetohydrodynamic flow and heat transfer of Cu-water nanofluid between parallel plates for different

- shapes of nanoparticles,” *Neural Computing and Applications*, vol. 29, pp. 695–703, 2018.
- [50] M. Sheikholeslami and D. Ganji, “Influence of electric field on Fe_3O_4 – water nanofluid radiative and convective heat transfer in a permeable enclosure,” *Journal of Molecular Liquids*, vol. 250, pp. 404–412, 2018.
- [51] V. Mikkola, S. Puupponen, H. Granbohm, K. Saari, T. Ala-Nissila, and A. Seppälä, “Influence of particle properties on convective heat transfer of nanofluids,” *International Journal of Thermal Sciences*, vol. 124, pp. 187–195, 2018.
- [52] F. Selimefendgil, “Natural convection in a trapezoidal cavity with an inner conductive object of different shapes and filled with nanofluids of different nanoparticle shapes,” *Iranian Journal of Science and Technology, Transactions of Mechanical Engineering*, vol. 42, pp. 169–184, 2018.
- [53] A. Dogonchi, F. Selimefendgil, and D. Ganji, “Magneto-hydrodynamic natural convection of CuO-water nanofluid in complex shaped enclosure considering various nanoparticle shapes,” *International Journal of Numerical Methods for Heat & Fluid Flow*, vol. 29, no. 5, pp. 1663–1679, 2019.
- [54] A. Bejan, *Entropy generation minimization: the method of thermodynamic optimization of finite-size systems and finite-time processes*. CRC press, 1995.
- [55] J. Qing, M. M. Bhatti, M. A. Abbas, M. M. Rashidi, and M. E.-S. Ali, “Entropy generation on MHD Casson nanofluid flow over a porous stretching/shrinking surface,” *Entropy*, vol. 18, no. 4, p. 123, 2016.
- [56] M. M. Bhatti, T. Abbas, M. M. Rashidi, M. E.-S. Ali, and Z. Yang, “Entropy generation on MHD Eyring-Powell nanofluid through a permeable stretching surface,” *Entropy*, vol. 18, no. 6, p. 224, 2016.
- [57] A. Shahzad, R. Ali, M. Hussain, and M. Kamran, “Unsteady axisymmetric flow and heat transfer over time-dependent radially stretching sheet,” *Alexandria Engineering Journal*, vol. 56, no. 1, pp. 35–41, 2017.

- [58] H. Sithole, H. Mondal, and P. Sibanda, “Entropy generation in a second grade magnetohydrodynamic nanofluid flow over a convectively heated stretching sheet with nonlinear thermal radiation and viscous dissipation,” *Results in Physics*, vol. 9, pp. 1077–1085, 2018.
- [59] J. B. J. Fourier, *Théorie analytique de la chaleur*. Gauthier-Villars et fils, 1888.
- [60] C. Cattaneo, “On heat conduction,” *Proceedings Sem. Mat.Phys.University of Modena*, vol. 3, pp. 83–101, 1948.
- [61] C. Christov, “On frame indifferent formulation of the Maxwell-Cattaneo model of finite-speed heat conduction,” *Mechanics Research Communications*, vol. 36, no. 4, pp. 481–486, 2009.
- [62] J. Sui, L. Zheng, and X. Zhang, “Boundary layer heat and mass transfer with Cattaneo-Christov double-diffusion in upper-convected Maxwell nanofluid past a stretching sheet with slip velocity,” *International Journal of Thermal Sciences*, vol. 104, pp. 461–468, 2016.
- [63] T. Hayat, T. Muhammad, A. Alsaedi, and B. Ahmad, “Three-dimensional flow of nanofluid with Cattaneo-Christov double diffusion,” *Results in Physics*, vol. 6, pp. 897–903, 2016.
- [64] N. Muhammad, S. Nadeem, and T. Mustafa, “Squeezed flow of a nanofluid with Cattaneo-Christov heat and mass fluxes,” *Results in Physics*, vol. 7, pp. 862–869, 2017.
- [65] A. Dogonchi and D. Ganji, “Impact of Cattaneo-Christov heat flux on mhd nanofluid flow and heat transfer between parallel plates considering thermal radiation effect,” *Journal of the Taiwan Institute of Chemical Engineers*, vol. 80, pp. 52–63, 2017.
- [66] N. Akmal, M. Sagheer, and S. Hussain, “Numerical study focusing on the entropy analysis of mhd squeezing flow of a nanofluid model using Cattaneo-Christov theory,” *AIP Advances*, vol. 8, no. 5, 2018.

- [67] A. Dogonchi, A. J. Chamkha, S. Seyyedi, and D. Ganji, “Radiative nanofluid flow and heat transfer between parallel disks with penetrable and stretchable walls considering cattaneo–christov heat flux model,” *Heat Transfer—Asian Research*, vol. 47, no. 5, pp. 735–753, 2018.
- [68] D. Lu, Z. Li, M. Ramzan, A. Shafee, and J. D. Chung, “Unsteady squeezing carbon nanotubes based nano-liquid flow with Cattaneo-Christov heat flux and homogeneous–heterogeneous reactions,” *Applied Nanoscience*, vol. 9, pp. 169–178, 2019.
- [69] M. Zubair, Z. Shah, S. Islam, W. Khan, and A. Dawar, “Study of three dimensional Darcy-Forchheimer squeezing nanofluid flow with Cattaneo-Christov heat flux based on four different types of nanoparticles through entropy generation analysis,” *Advances in Mechanical Engineering*, vol. 11, no. 5, p. 1687814019851308, 2019.
- [70] B. Ramadevi, V. Sugunamma, A. Kumar, and R. R. JV, “MHD flow of Carreau fluid over a variable thickness melting surface subject to Cattaneo-Christov heat flux,” *Multidiscipline Modeling in Materials and Structures*, vol. 15, no. 1, pp. 2–25, 2018.
- [71] U. Shankar and N. Naduvinamani, “Magnetized impacts of Cattaneo-Christov double-diffusion models on the time-dependent squeezing flow of Casson fluid: A generalized perspective of Fourier and Fick’s laws,” *The European Physical Journal Plus*, vol. 134, pp. 1–24, 2019.
- [72] R. Ellahi, M. Hassan, and A. Zeeshan, “A study of heat transfer in power law nanofluid,” *Thermal Science*, vol. 20, no. 6, pp. 2015–2026, 2016.
- [73] C. Sravanthi and R. S. R. Gorla, “Effects of heat source/sink and chemical reaction on MHD Maxwell nanofluid flow over a convectively heated exponentially stretching sheet using homotopy analysis method,” *International Journal of Applied Mechanics and Engineering*, vol. 23, no. 1, 2018.

- [74] I. Khan, S. Fatima, M. Malik, and T. Salahuddin, “Exponentially varying viscosity of magnetohydrodynamic mixed convection Eyring-Powell nanofluid flow over an inclined surface,” *Results in Physics*, vol. 8, pp. 1194–1203, 2018.
- [75] M. Irfan, M. Khan, and W. Khan, “Numerical analysis of unsteady 3D flow of Carreau nanofluid with variable thermal conductivity and heat source/sink,” *Results in physics*, vol. 7, pp. 3315–3324, 2017.
- [76] S. Reddy, K. Naikoti, and M. M. Rashidi, “MHD flow and heat transfer characteristics of Williamson nanofluid over a stretching sheet with variable thickness and variable thermal conductivity,” *Transactions of A. Razmadze Mathematical Institute*, vol. 171, no. 2, pp. 195–211, 2017.
- [77] M. Khan, L. Ahmad, and M. M. Gulzar, “Unsteady sisko magneto-nanofluid flow with heat absorption and temperature dependent thermal conductivity: a 3D numerical study,” *Results in physics*, vol. 8, pp. 1092–1103, 2018.
- [78] R. K. Tiwari and M. K. Das, “Heat transfer augmentation in a two-sided lid-driven differentially heated square cavity utilizing nanofluids,” *International Journal of Heat and Mass transfer*, vol. 50, no. 9-10, pp. 2002–2018, 2007.
- [79] R. Rajput, *A Textbook of Fluid Mechanics and Hydraulic Machines*. S. Chand Publishing, 2004.
- [80] R. Bansal, “A Textbook of Fluid Mechanics and Hydraulic Machines (revised,” 2010.
- [81] J. N. Reddy and D. K. Gartling, *The finite element method in heat transfer and fluid dynamics*. CRC press, 2010.
- [82] Y. Cengel, J. Cimbala, and C. C. Solutions, “Mechanics: Fundamentals and applications cengel...,” *MECHANICS*, vol. 11, p. 22, 2004.
- [83] P. C. Barman, R. R. Kairi, A. Das, and R. Islam, “An overview of non-Newtonian fluid,” *International Journal of Applied Science and Engineering*, vol. 4, no. 2, pp. 97–101, 2016.

- [84] C. Kothandaraman, *Fundamentals of Heat and Mass Transfer*. New Age International, 2006.
- [85] W. M. Rohsenow, J. P. Hartnett, Y. I. Cho, *et al.*, *Handbook of Heat Transfer*, vol. 3. Mcgraw-Hill New York, 1998.
- [86] J. Kunes, *Dimensionless Physical Quantities in Science and Engineering*. Elsevier, 2012.
- [87] L. Prandtl, “On fluid motions with very small friction,” *Verhldg*, vol. 3, pp. 484–491, 1904.
- [88] O. Mahian, L. Kolsi, M. Amani, P. Estellé, G. Ahmadi, C. Kleinstreuer, J. S. Marshall, M. Siavashi, R. A. Taylor, H. Niazmand, *et al.*, “Recent advances in modeling and simulation of nanofluid flows-part i: Fundamentals and Theory,” *Physics Reports*, vol. 790, pp. 1–48, 2019.
- [89] N. B. Reddy, T. Poornima, and P. Sreenivasulu, “Influence of variable thermal conductivity on MHD boundary layer slip flow of ethylene-glycol based Cu nanofluids over a stretching sheet with convective boundary condition,” *Int J Eng Math*, vol. 2014, p. 905158, 2014.
- [90] Y. Taki, M. Kitiwan, H. Katsui, and T. Goto, “Electrical and thermal properties of off-stoichiometric SiC prepared by spark plasma sintering,” *Journal of Asian Ceramic Societies*, vol. 6, no. 1, pp. 95–101, 2018.
- [91] W. Jamshed, W. Al-Kouz, and N. A. Mohd Nasir, “Computational single phase comparative study of inclined MHD in a Powell-Eyring nanofluid,” *Heat Transfer*, vol. 50, no. 4, pp. 3879–3912, 2021.
- [92] S. Nadeem and S. Hussain, “Flow and heat transfer analysis of Williamson nanofluid,” *Applied Nanoscience*, vol. 4, pp. 1005–1012, 2014.
- [93] B. Kumar and S. Srinivas, “Unsteady hydromagnetic flow of Eyring-Powell nanofluid over an inclined permeable stretching sheet with Joule heating and thermal radiation,” *Journal of Applied and Computational Mechanics*, vol. 6, no. 2, pp. 259–270, 2020.

- [94] T. Hayat, M. Qasim, and S. Mesloub, "MHD flow and heat transfer over permeable stretching sheet with slip conditions," *International Journal for Numerical Methods in Fluids*, vol. 66, no. 8, pp. 963–975, 2011.
- [95] I. Khan, M. Malik, T. Salahuddin, M. Khan, and K. U. Rehman, "Homogenous–heterogeneous reactions in MHD flow of Powell-Eyring fluid over a stretching sheet with Newtonian heating," *Neural Computing and Applications*, vol. 30, pp. 3581–3588, 2018.
- [96] W. Jamshed and A. Aziz, "A comparative entropy based analysis of Cu and Fe_3O_4 /methanol Powell-Eyring nanofluid in solar thermal collectors subjected to thermal radiation, variable thermal conductivity and impact of different nanoparticles shape," *Results in Physics*, vol. 9, pp. 195–205, 2018.
- [97] T. Thumma and S. Mishra, "Effect of nonuniform heat source/sink, and viscous and Joule dissipation on 3D Eyring-Powell nanofluid flow over a stretching sheet," *Journal of Computational Design and Engineering*, vol. 7, no. 4, pp. 412–426, 2020.
- [98] A. Alshomrani, M. Z. Ullah, S. Capizzano, W. Khan, and M. Khan, "Interpretation of chemical reactions and activation energy for unsteady 3D flow of Eyring–Powell magneto-nanofluid," *Arabian Journal for Science and Engineering*, vol. 44, pp. 579–589, 2019.
- [99] M. Ramzan, M. Bilal, and J. D. Chung, "Influence of homogeneous-heterogeneous reactions on MHD 3D Maxwell fluid flow with Cattaneo-Christov heat flux and convective boundary condition," *Journal of Molecular Liquids*, vol. 230, pp. 415–422, 2017.
- [100] M. Azam, W. A. Khan, and M. K. Nayak, "Three dimensional flow of cross nanofluid over bidirectional moving surface in Darcy-Forchheimer medium with Cattaneo-Christov heat flux," *Case Studies in Thermal Engineering*, vol. 49, p. 103250, 2023.

Turnitin Originality Report

Unsteady 3D Powell-Eyring Flow of Copper and Silicon-Carbide/Methanol for a Boundary Layer Using Cattaneo-Christov Model with Entropy Analysis by ATIF ALI ZAFAR

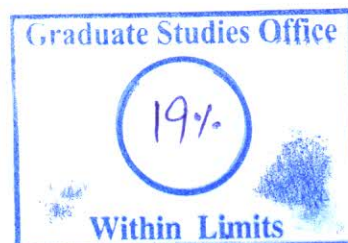


From CUST Library (Ms Theses)

- Processed on 28-Nov-2023 16:52 PKT
- ID: 2240491582
- Word Count: 41227

Similarity Index
19%
Similarity by Source

Internet Sources:
13%
Publications:
16%
Student Papers:
4%

**sources:**

- 1 1% match (Wasim Jamshed, Wael Al-Kouz, Nor A. A. Mohd Nasir. "Computational single phase comparative study of inclined MHD in a Powell-Eyring nanofluid", Heat Transfer, 2021)
Wasim Jamshed, Wael Al-Kouz, Nor A. A. Mohd Nasir. "Computational single phase comparative study of inclined MHD in a Powell-Eyring nanofluid", Heat Transfer, 2021
- 2 1% match (Internet from 14-Dec-2022)
<https://cust.edu.pk/static/uploads/2021/02/PhD-Thesis-Maleeha-Atlas.pdf>
- 3 1% match (Asif Mahmood, Wasim Jamshed, Asim Aziz. "Entropy and Heat Transfer Analysis Using Cattaneo-Christov Heat Flux Model for a Boundary Layer Flow of Casson Nanofluid", Results in Physics, 2018)
Asif Mahmood, Wasim Jamshed, Asim Aziz. "Entropy and Heat Transfer Analysis Using Cattaneo-Christov Heat Flux Model for a Boundary Layer Flow of Casson Nanofluid", Results in Physics, 2018
- 4 1% match (Wasim Jamshed, Asim Aziz. "A Comparative Entropy Based Analysis of and /methanol Powell-Eyring Nanofluid in Solar Thermal Collectors Subjected to Thermal Radiation, Variable Thermal Conductivity and Impact of Different Nanoparticles Shape ", Results in Physics, 2018)
Wasim Jamshed, Asim Aziz. "A Comparative Entropy Based Analysis of and /methanol Powell-Eyring Nanofluid in Solar Thermal Collectors Subjected to Thermal Radiation, Variable Thermal Conductivity and Impact of Different Nanoparticles Shape ", Results in Physics, 2018
- 5 1% match (Wasim Jamshed. "Numerical investigation of MHD impact on Maxwell nanofluid", International Communications in Heat and Mass Transfer, 2021)
Wasim Jamshed. "Numerical investigation of MHD impact on Maxwell nanofluid", International Communications in Heat and Mass Transfer, 2021
- 6 1% match (student papers from 28-Feb-2021)
Submitted to RMIT University on 2021-02-28
- 7 1% match (Internet from 10-Sep-2021)
<https://www.degruyter.com/document/doi/10.1515/phys-2018-0020/html>
- 8 1% match (Asim Aziz, Wasim Jamshed, Yasir Ali, Moniba Shams. "Heat transfer and entropy analysis of Maxwell hybrid nanofluid including effects of inclined magnetic field, Joule heating and thermal radiation", Discrete & Continuous Dynamical Systems - S, 2020)
Asim Aziz, Wasim Jamshed, Yasir Ali, Moniba Shams. "Heat transfer and entropy analysis of Maxwell hybrid nanofluid including effects of inclined magnetic field, Joule heating and thermal radiation", Discrete & Continuous Dynamical Systems - S, 2020
- 9 1% match (Internet from 25-Dec-2022)
<https://coek.info/pdf-a-comparative-entropy-based-analysis-of-cu-and-fe3o4-methanol-powell-eyring-nano.html>
- 10 < 1% match (Internet from 09-Jan-2023)
<https://thesis.cust.edu.pk/UploadedFiles/Ayesha%20Maqbool-MMT183019.pdf>
- 11 < 1% match (Internet from 02-Feb-2023)
<https://thesis.cust.edu.pk/UploadedFiles/MMT183011-Muhammad%20Asif%20Khan.pdf>
- 12 < 1% match (Internet from 04-Feb-2023)